Discovery and Characterisation of Novel Protein Interactions with Death Associated Protein Kinase

Benjamin J Harrison

For the Degree of Doctor of Philosophy

The University of Edinburgh

2007

To My Wife, Angela

I maintain that the cosmic religious feeling is the single strongest and noblest motive for scientific research.

- Albert Einstein, Ideas and Opinions

She was a wonder junkie. In her mind, she was a hill tribesman standing slack-jawed before the real Ishtar Gate of ancient Babylon; Dorothy catching her first glimpse of the vaulted spires of the Emerald City of Oz; a small boy from darkest Brooklyn plunked down in the Corridor of Nations of the 1939 world's Fair, the Trylon and Perisphere beckoning in the distance; she was Pocahontas sailing up the Thames estuary with London spread out before her from horizon to horizon. … Her heart sang with anticipation. ... Advocate and practitioner of romance, she was off to see the Wizard.

- Carl Sagan, Contact

Scepticism is the chastity of the intellect, and it is shameful to surrender it too soon or to the first comer: there is nobility in preserving it coolly and proudly through long youth, until at last, in the ripeness of instinct and discretion, it can be safely exchanged for fidelity and happiness.

- George Santayana, Scepticism and Animal Faith, IX

Declaration

I declare that thesis has been composed by myself the undersigned Benjamin J Harrison and that the work herein is entirely my own unless otherwise clearly acknowledged. This work has been submitted for the degree Doctor of philosophy and has not been submitted for any other qualification, professional or otherwise.

13 JAN 2008

Abstract

Death Associated Protein Kinase (DAPK) has a wide-ranging role in cell death signaling and growth control. Over the past decade the importance of DAPK as a tumour suppressor has been highlighted by numerous studies that show its expression is ablated in many cancer types by epigenetic silencing. However the mechanisms by which this multi-domain protein exerts death-inducing effects have not been well defined, given that very few substrates or interaction partners have been discovered. Many protein-protein interactions involving cell signaling processes are driven by linear interaction motifs. Therefore combinatorial peptide libraries displayed on M13 filamentous bacteriophage were used to identify peptide consensus binding sites for the kinase domain of DAPK. Peptides that bound to the DAPKcore kinase domain were then isolated and sequenced leading to the discovery of binding peptides with striking homology to the SH1-4 family of transcription factors, the Promyelocytic Leukemia protein (PML) and the microtubule associating protein MAP1B. Immunobinding assays, immunofluorescent cell staining studies and biochemical fractionations demonstrated that DAPK can interact with human MAP1B via an N-terminal interface *in-vitro* and in cells and so this interaction was subject to further study. DAPK has been shown to integrate death inducing signals through a number of pathways including the p53 tumour suppression pathway and apoptotic and autophagic cell death inducing pathways. Therefore a range of assays were developed to characterise the biological significance of DAPK interaction with MAP1B in the context of each pathway. Cell growth and viability assays demonstrated that MAP1B co-operates with DAPK to reduce cell proliferation. This co-operative cell growth inhibition was independent of the p53 pathway and

apoptotic (Type I) cell death, but induced autophagic (Type II) cell death. MAP1B co-operation with DAPK was marked by a striking increase in the number of cells with membrane blebbing morphology, an effect previously shown to involve DAPK interaction with the actin cytoskeleton leading to actin-myosin contraction. This was in contrast to the known role of MAP1B that is primarily thought of as a tubulin associating protein that modifies microtubule dynamics. Therefore the role of the cytoskeleton in DAPK co-operation with MAP1B was studied in detail using immunofluorescent cytoskeleton staining and microtubule purification assays. During DAPK transfection induced membrane blebbing, a pool of DAPK and MAP1B co-localise and co-purify with tubulin whereas a separate pool is co-located to cortical actin. Thus DAPK and MAP1B cooperation-induced membrane blebbing involves a novel interaction with both microtubules and microfilaments. These studies highlight the utility of peptide combinatorial libraries to identify novel binding interfaces and highlight a positive role for MAP1B in DAPK dependent cytoskeletal rearrangement and the autophagic cell death program.

Chapter 1

Introduction

1.1 The DAPK Family Members, Structural and Functional Homology

DAPK was discovered using a technical knock out (TNO) screen designed to target genes involved in cell death (Deiss et al., 1995). The TNO screen worked on the basis of random inactivation of genes in HeLa cells with antisense cDNA expression libraries. Interferon gamma (IFN-γ) was used as a killing agent so that IFN- γ signaling genes sequences could be isolated from transformants with increased resistance. This approach was based on the assumption that a specific anti-sense RNA-mediated inactivation of a rate limiting death-promoting gene would confer a growth advantage to treated cells. In this way genes of interest could be isolated and cloned by virtue of a specific phonotypic change, in this case reduced susceptibility to death inducing signaling by IFN- γ. Using this forward selection approach to rescue death promoting cDNAs, seven novel genes were isolated including five novel genes and two previously characterised genes, thioredoxin and cathespin D (Levy-Strumpf and Kimchi, 1998). The five novel genes were termed Death Associated Proteins (DAPs) DAP-1 through DAP-5. Subsequently DAP-2 was renamed DAP-kinase (DAPK1 simply referred to as DAPK in this thesis).

Amino acid sequence analysis comparison lead to the discovery of five family members that share a high level of sequence similarity to DAPK in their respective kinase domains (Kawai et al., 1998; Kawai et al., 1999; Sanjo et al., 1998). These

five members include three closely related kinases; DAPK1 (DAPK), DAPK2 (Also known as DRP-1 (DAPK Related Protein 1)) and DAPK3 (Also known as ZIPK (ZIP Kinase) or (Dlk) (DAPK-Like Kinase)) that share 80% and 83% amino acid sequence homology in their kinase domains. More distantly related are the DRAKs (DAPK-related apoptosis inducing protein kinases); DRAK1 and DRAK2 that share 48% and 51% respective kinase domain sequence homology (Figure 1.1). The DAPK family is phylogeneticaly placed in the Ca2+/CaM-regulated serene/threonine kinase family which includes Myosin Light Chain Kinase (MLCK) (Figure 1.2). Homologous DAPK proteins are present in vertebrate species through rodents to *C.elegans* but not in *drosophila* or lower organisms. However, this is only the case with DAPK. In contrast DAPK2 and ZIPK orthologues are only present in mammals and DRAK-1 only in rodents. No DRAK-2 orthologues have been discovered (For review see (Bialik and Kimchi, 2006)). Whereas the function and mechanism of action of the DRAK proteins is virtually unknown, functions for the DAPK family members have been discovered, and the mechanisms by which they regulate death-inducing stimuli are beginning to be uncovered. DAPK is by far the better characterised and is a prototypical representative of the three closest family members DAPK1-3.

1.2 The Modular Structure of DAPK

DAPK is a structurally unique 160 kDa modular multidomain protein with an N-terminal catalytic kinase domain negatively regulated by a calmodulin (CaM) binding region. Adjacent to this are 8 ankryn repeats followed by two P-loop motifs and a cytoskeleton binding domain. Towards the carboxyl end of the protein is a

death domain. The C-terminus contains a threonine and serine rich regulatory tail module (Raveh et al., 2000).

1.2.1 The DAPK *Kinase Domain*

The kinase domain of DAPK spans 255 amino acids from position 13 to 267 and consists of the 11 subdomains archetypical of serine/threonine kinases. The crystal structure of the DAPK kinase domain has been resolved to 1.5Å resolution providing invaluable information indicative of its function and its mechanism of substrate recognition. The structures of the kinase domain in its apo (inactive) form and its binary and tertiary active intermediate forms have been resolved (Tereshko et al., 2001) permitting analysis of the conformational changes that take place during substrate binding, phosphorylation and release. Comparison between these intermediate structures and crystals from 5 other kinases' sharing close sequence homologies (twitchin kinase (TDB), titin kinase (TK), Ca2+/CaM-dependent protein kinase 1 (CaMK1), phosphorylase kinase (PHK) and cAMP-dependent kinase (cAPK)) has disclosed unique features of the DAPK catalytic domain. Comparisons of conserved and unique substructures within the domains lead to the discovery of a basic loop structure found above the cleft of the kinase domain. This loop, unique to the DAPK family termed the 'DAPK family fingerprint region' consists of mainly basic residues (7 of arginine or lysine), from Lys45 to Val 56 inclusively and maps to the surface of the kinase domain, protruding from it as a 'lid' above the putative peptide binding ledge. The exact function of the basic loop remains unknown. It has been perturbed by site directed mutagenesis (Velentza et al., 2001) with no effect on Km values suggesting that it does not play a role in classic CaM kinase autoinhibition. In addition, this loop is present on ZIPK which does not posses a

calmodulin regulatory region also indicating that it is not involved in CaM kinase autoinhibition. The position of the loop in proximity to the substrate binding interface suggests that it may interact with regulatory proteins to keep its activity in check. This is an attractive possibility because the corresponding amino acids are conserved across the death promoting kinases where death promoting effects must be negatively regulated in order to allow normal cell growth conditions.

1.2.2 The Calmodulin-Binding Regulatory Domain

The autoinhibitory region of DAPK is a calmodulin binding region directly C-terminal to the kinase domain. Numerous studies have shown that the activity of DAPK is dependant on available Ca2+ and binding of CaM to this domain (Cohen et al., 1997) Methods of regulation of DAPK kinase activity are discussed in more detail below.

1.2.3 The Ankyrin Repeats

Adjacent to the CaM regulatory domain are a series of 8 ankyrin repeat motifs running from residues 373 to 637. The ankyrin repeat a common protein-protein interaction motif. Deletion of this domain results in miss localised ectopically expressed protein (Bialik et al., 2004). In addition, disruption of the ankyrin repeats on endogenous protein with interfering-peptide fragments reduces DAPK death promoting activity (Raveh et al., 2000). This suggests that this domain could function by mediating interaction with as yet unknown factors that are required for correct localisation and function.

1.2.4 The p-loop Motifs and the Cytoskeletal Binding Domain

C-terminal to the ankyrin repeats are two phosphate binding loop (p-loop) motifs (Ala/Gly-X-X-X-X-Gly-Lys-Ser/Thr) located at regions 639-646 and 695-702, the second within the cytoskeletal binding domain which runs from position 649 to 844. P-loop motifs are wide spread among nucleotide binding proteins that undergo conformational changes upon GTP/ATP binding and hydrolysis (Walker et al., 1982). Because these lie within the cytoskeletal binding domain, this suggests that DAPK may have a role in regulation of cytoskeletal dynamis. Subsequent studies have provided evidence that DAPK is primarily an actin-associated kinase, where it controls microfilament dynamics by positively regulating myosin contraction (Bialik et al., 2004). The role of DAPK in the regulation of cytoskeletal dynamics is discussed in section 4.5.

1.2.5 The Death Domain

Death domains are homeotypic protein interaction modules composed of a bundle of six alpha-helices. They are evolutionarily related to death effecter domains and the caspase recruitment domains, have analogous properties and function in similar pathways (Reed et al., 2004). Death domains bind each other facilitating homeotypic interactions with other proteins (Reed et al., 2004). Death domain-containing proteins are involved in the regulation of cell death programs and inflammation often through activation of caspases and NF-kappaB. This typically involves interactions with the tumour necrosis factor (TNF) cytokine receptors (Baker and Reddy, 1998).

Cohen et. al. (1999) observed that Tumour Necrosis Factor alpha (TNFα) and Fas signaling activated DAPK resulting in apoptosis in transfected cells. This activity required an intact death domain, providing the first evidence that this region is a

positive regulator of DAPK activity. Subsequent studies have shown that a death domain deleted mutant of DAPK (DAPK-ΔDD) has reduced ability to kill cells (Kuo et al., 2003) (Cohen et al., 1999). Also, transfection of this mutant protein protects against cell death triggered by death receptors, even when the kinase is constitutively active suggesting it is able to act as a dominant negative. Multiple studies have demonstrated that the death domain is an integral positive regulator of DAPK activity, directing protein-protein interactions that are critical fur its killing ability (Chen et al., 2005; Llambi et al., 2005).

The death domain of DAPK harbors a germ-line mutation, N1347S that prevents death domain binding to extracellular regulated kinase (ERK), a positive regulator of DAPK activity (Stevens et al., 2007). 1347S mutation fundamentally disrupts the higher order structure of purified recombinant death domain miniprotein, and accordingly, is defective in directing protein-protein interactions *in-vivo* as determined by protein cross-linking experiments. In human genomic DNA, this SNP is present in 41 to 47% of heterozygotes, and 12 to 15% of homozygotes.

1.2.6 The C-terminal Serine-Rich Tail

At the C-terminus of DAPK is a serine rich tail thought to function as a negative regulator of DAPK activity (Raveh et al., 2000). However, the mechanisms where by this region imparts negative regulation remain unknown. Given its linear and serine rich structure it is likely modified by inhibitory kinases, possibly to alostericaly block interactions with the adjacent death domain (see section 1.7.2).

1.3 DAPK is a Tumour Suppressor

In 1995, initial genomic studies using rodent-human cell hybrids probed by FISH with labeled DAPK cDNA mapped DAPK to position 9q34.1 (Feinstein et al., 1995a). Loss of heterozygosity studies in tumor samples have shown that this region is often lost in tumours (Feinstein et al., 1995a), providing an early indication that DAPK could be a tumour suppressor gene. An important study relating to DAPK action as a tumour suppressor was then published by Inbal *et. al.* 1997 who were investigating the levels of DAPK in cancer cell lines. They observed that DAPK mRNA and protein expression was undetectable in highly-metastatic cell lines from murine Lewis and lung carcinomas. When transformed with ectopic DAPK and injected into mice, the growth of highly-metastatic cell lines was delayed accompanied by a marked reduction in the number of lung metastases compared to DAPK null cells. The number of metastases in recipients was inversely proportional to DAPK expression and examination of the intra-foot-pad recipient's lung metastases revealed loss of DAPK expression in 55% of cases. This could be rectified by treatment with 5-aza-2'-deoxcytidine, an inhibitor of DNA methylation. These results indicated that loss of DAPK expression provided a positive selective advantage during the formation of lung metastases and furthermore that DAPK expression was attenuated by methylation. This was ascribed to the apoptosis inducing activity of DAPK, because cells retrieved from DAPK expressing tumors had a higher apoptotic index and were more amenable to apoptotic stimuli such as TNF, in contrast to the DAPK-methylated tumors which were much less responsive to TNF. Loss of DAPK expression, resulted in resistance to apoptotic stimuli particularly in metastastases, thus supporting the proposal that loss of apoptotic

control is an important factor in metastasis and providing a link between DAPK and metastasis.

1.3.1 Epigenetic Silencing and loss of DAPK Expression by Promoter Methylation

DAPK has been comprehensively shown to be inactivated by promoter methylation in a verity of solid tumours and leukiemias including B-cell malignancies, thyroid lymphomas, non-small cell lung cancer, T- and natural killer T-cell malignancies and gastric cancers (Brakensiek et al., 2004; Cohen and Kimchi, 2001; Gonzalez-Gomez et al., 2003; Katzenellenbogen et al., 1999; Nakatsuka et al., 2001; Nakatsuka et al., 2000; Schneider-Stock et al., 2005; Waki et al., 2003). B-cell chronic lymphocytic leukemia (CLL) is associated with loss of expression of DAPK caused by promoter hypermethylation in nearly all sporadic cases. However, CLL also has a relatively high degree is a heritability, and heritable tumours are also hypermethylated in most cases (Raval et al., 2007). This is caused by decreased DAPK expression by 75% in cells from CLL patients due to increased HOXB7 binding in the DAPK promoter (Raval et al., 2007). This then increases susceptibility to CLL by further promoter methylation resulting in additional loss of DAPK expression.

1.4 Methods of DAPK Tumour Suppression

DAPK can be downregulated by epigenetic silencing during the natural history of a tumour or by germ line mutation resulting in increased HOXB7 binding to the DAPK promoter (Raval et al., 2007). This loss of DAPK expression provides a selective advantage to cells, increasing the likelihood of subsequent clonal expansion and tumour growth. DAPK loss then provides resistance to death inducing stimuli and resistance to cell detachment increasing the chance of tumour metastasis. DAPK-

induced tumour suppression results from cell death activated by multiple stimuli including, IFN-γ, TNF-α, Fas, cyclohexamide, amino acid depletion, steroid withdrawal, and detachment from the extracellular matrix. During apoptosis, DAPK acts upstream of the terminator caspases and the apoptosome and above mitochondrial events involving BAX/bcl2. DAPK is downsteam of the initiator caspases and in the case of cytokine signalling, downstream of death receptor complexes (Cohen et al., 1999; Jang et al., 2002; Pelled et al., 2002).

1.4.1 DAPK *Activation by Death Receptors*

DAPK is implicated in apoptotic signaling from death receptors. Death receptors are cell surface receptors that transmit apoptosis signals initiated by specific ligands though activation of the caspase cascade. They belong to the tumor necrosis factor (TNF) gene superfamily, of which CD95 (or Fas), TNFR1 (TNF receptor-1) and the TRAIL (TNF-related apoptosis inducing ligand) receptors DR4 and DR5 have been well characterised (Figure 1.3). TNF is produced by T-cells and activated macrophages in response to infection. By ligating TNFR1, TNF can initiate apoptosis and can also activate NF-kB and AP-1 leading to the induction of proinflammatory and immunomodulatory genes (For review of death receptors see (Baud and Karin, 2001)) (Figure 1.4).

Binding of TNFα ligand to TNFR1 results in receptor trimerisation and clustering of its intracellular death domains. This induces binding of an intracellular adapter molecule called TRADD (TNFR-associated death domain) via homeotypic death domain interaction. TRADD then recruits a number of different proteins to the activated receptor. Apoptosis is induced by subsequent association of FADD, after recruitment and cleavage of pro-caspase 8. TNFR1 is also able to mediate apoptosis

through the recruitment of an adapter molecule called RAIDD (RIP-associated ICH-1 / CED-3 homologous protein with a death domain). RAIDD associates with RIP through interactions between death domains and can recruit caspase 2 through an interaction with a motif, similar to the death effector domain, known as CARD (caspase recruitment domain). Recruitment of caspase 2 then leads to induction of apoptosis.

Roles for fas include cytotoxic T-cell mediated cell killing, removal of activated T-cells after an immune response and destruction of inflammatory and immune cells in immune-privileged sites. Fas mediated activation of apoptosis is induced by fas ligand (FasL). A trimer that, on association with the receptor, promotes receptor trimerisation in turn resulting in intracellular clustering of the receptor at death domains. This allows the FADD adapter protein (Fas-associated death domain) to associate with the receptor through homologous death domains on the receptor and on FADD. As well as containing a death domain, FADD also contains a death effector domain (DED). The death effecter domain allows binding of pro-caspase 8 to the ras-FADD complex. Pro-caspase 8 then associates with FADD though its own death effector domain, and is cleaved to produce caspase 8. This then triggers activation of execution caspases (such as caspase 9). The Fas, FADD and pro-caspase 8 complex that triggers apoptosis is termed the Death Inducing Signaling Complex (DISC).

Ectopic expression of TNFR or presentation with agonistic anti-fas antibody results in oligomerisation of receptor and apoptosis in HeLa cells. Expression of DAPK antisense RNA or DAPK-ΔDD (dominant negative, death domain deleted DAPK)

results in reduction of cell death as measured by cell membrane blebbing (Cohen et al., 1999). Co-transfection of dominant negative DAPK and FADD resulted in rescue from cell death, whereas cotransfection of dominant negative FADD or dominant negative caspase-8 with DAPK-ΔCaM (constitutively active DAPK) results in cell death. Also, transfection of DAPK-ΔCaM with bcl-2 or treatment with terminator caspase inhibitors reduces cell death. These results suggest that DAPK is involved in TNF-α and Fas-induced cell death and that DAPK is down stream of the DISK (containing FADD and Caspase 8) and upstream of bcl-2 and the apoptosome in this pathway. However the role of DAPK in TNF signaling is controversial and research has been published contradicting this, raising the possibility that DAPK can inhibit cell death caused by death receptors in some circumstances (see section 1.8).

Supporting evidence showing that DAPK positively mediates death receptor signaling through another pathway was published by Jang et. al. 2002 (Jang et al., 2002). Using a complementary microarray approach they observed DAPK upregulation after treatment of HEP3B hepatoma cells with transforming growth factor beta (TGF-β). This was then confirmed by northern blot analysis of mRNA levels and western blot analysis of protein levels, where DAPK expression was increased at both levels. An 8-fold induction of DAPK was recorded after 8 hours treatment and proceeding apoptosis. Apoptosis could be blocked by expression of DAPK-ΔDD or DAPK antisense RNA.

Like TNFα signaling TGF-β signaling is implicated both in the regulation of growth and proliferation and in oncogenesis . The TGF-β receptor includes Type I and Type II subunits that are serine-threonine kinases that signal through the Smad family of

transcription factors. Binding of TGF-β ligand to Type II receptor leads to phosphorylation of the Type I receptor. Type I receptor then phosphorylates and activates Smad2. Smad2, in combination with Smad4, is translocated to the nucleus where the activated Smad complex recruits other transcription factors activating the expression of target genes (Figure 1.5). Paradoxically, some of the activated target genes stimulate tumorigenesis, while others have tumor suppressor functions (for review see (Liu, 2003). Jangs' group observed that upregulation of DAPK was blocked after treatment with the transcription inhibitor actinomycin suggesting that regulation of DAPK by TGF-β was at transcriptional level. Using cloned 5' fragments of DAPK in a luciferase reporter promoter deletion experiment, they saw that the region –705 to –352 was responsive to TGF-β. Cotransfection of this region with Smad 2, 3 and 4 resulted in a 4-fold increase in mRNA levels suggesting that DAPK is a transcriptional target for Smads. The Smad proteins initiate transcription of DAPK by binding to 4 consensus Smad binding elements on the DAPK promoter region. Bcl-2 and cyotochrome-c protein levels were reduced by cotransfection of DAPK with DAPK-ΔDD, consistent with other studies placing DAPK upstream of mitochondrial events after stimulation with apoptotic factors.

1.4.2 DAPK *Activation by Ceramide*

Ceramide is a pleiotropic lipid second messenger generated by sphingomyelin hydrolysis or produced by the binding of nerve growth factor (NGF) to the p75 neurotrophin receptor. Ceramide is also a second messenger in the TNF pathway (Figure 1.4). Ceramide plays a key role in cell fate decisions making, regulating cell cycle arrest, differentiation and apoptosis during different stages of neuronal development (Warzocha et al., 1995). Exposure to cell-permeable ceramide analogs

(C2/C6-ceramide) induces apoptosis in a wide range of cells including many types of neuronal cells. DAPK expression is increased after exposure to ceramide (Pelled et al., 2002) and DAPK null cells are resistant to its effects. Also, transfection of DAPK-ΔDD conferres a protective effect from ceramide treatment. Cell death induced by C2-ceramide is independent of Calmodulin and treatment does not induce an increase in cellular Ca2+ levels, suggesting that the DAPK response to ceramide is regulated by other means as yet unknown (Yamamoto et al., 2002).

1.4.3 DAPK *and Extracellular Signal-Regulated Kinase (ERK)*

The extracellular signal-regulated kinase (ERK) family of mitogen-activated kinases (MAPK) is activated by mitogens through Ras, Raf and MEK (Cobb, 1999; Schaeffer and Weber, 1999; Chang and Karin, 2001). ERK translocates from the cytoplasm to the nucleus and signals the upregulation of specific gene transcription influencing cell fate decisions by inducing cell proliferation, differentiation or apoptosis depending on the situation (Howe et al, 2002). ERK's sub-cellular compartmentalisation is regulated by interactions within the MAPK cascade or with nuclear and cytoplasmic retention proteins.

ERK binds to DAPK via a death domain interaction and phosphorylates Ser735 increasing DAPK kinase activity both *in-vitro* and in cells (Chen et al., 2005). Also, DAPK promotes cytoplasmic retention of ERK, inhibiting nuclear ERK signaling (Chen et al., 2005). This 2-way regulation between DAPK and ERK comprises a positive feedback loop promoting the apoptotic activity of DAPK, and inhibiting the anti-apoptotic or proliferative role of ERK. Co-transfection of ERK with DAPK results in increased DAPK-induced apoptosis as determined by caspase activity. Also, induction of cell death by physiological stimuli can be blocked by siRNA to

both ERK and DAPK (Chen et al., 2005). DAPK harboring the N1347S death domain mutation (see section 1.2.5) was unable to interact with ERK and was deficient in induction of apoptosis as defined by poly(ADP-ribose) polymerase (PARP) cleavage, Annexin V staining, and terminal deoxynucleotidyl transferase-mediated dUTP nick end labeling (TUNEL) imaging (Stevens et al., 2007). These independent studies show that bidirectional signals between DAPK and ERK contribute to the apoptosis-promoting function of DAPK.

1.4.4 DAPK *and the p53 Pathway*

In mouse embryonic fibroblasts, p53 is required for DAPK mediated cell death (Raveh et al., 2001). Coexpression of Myc, Ras or E1a oncogenes with DAPK into MEFs lead to decreased oncogenic transformation in foci assays as compared to transfection of oncogene without DAPK. Co-expression of large-T antigen or dominant negative p53 mutants with DAPK blocks inhibition of transformation. Also, knock-out of p53 or ARF from MEFs blocks apoptosis induced by DAPK. Whereas in wild-type cells expression DAPK death inducing effects are retained. These results suggest that DAPK induced apoptosis and suppression of oncogene transformation in MEFS executes through an apoptotic p53/ARF dependent mechanism. It should be noted that DAPK is active in both p53 null / inactive cell lines (such as HeLa cells that express viral T-antigen), and also in p53 active cell lines, sugesting that DAPK may act through p53 dependent and independent pathways (Bialik and Kimchi, 2006) (see section 4.33).

DAPK is a transcriptional target of p53. p53 transfection can induce expression of DAPK in various cell lines by interaction with p53 consensus binding sites present on both the human and mouse DAPK promoters (Martoriati et al., 2005). For

example, DAPK expression induces p53 and its target genes in both transformed and primary fibroblasts (Raveh et al., 2001). In the absence of DAPK, p53 is only partially upregulated in response to proliferative signals induced by oncogene expression (Raveh et al., 2001). Thus DAPK is an activator of p53 in addition to p53 being an activator of DAPK. This strongly suggests that there is a positive feedback loop in which DAPK and p53 can activate one another.

The downstream targets of p53; MDM2, p19ARF and p21 are also implicated in regulating DAPK-induced apoptotic signaling. Upregulation of p53 and commensurate induction of Type I cell death require the expression of p19ARF (Raveh et al., 2001), which is a positive regulator of the p53 pathway. p19ARF inhibits the p53 E3 ubiquitin ligase MDM2, a promoter of ubiquitin-dependent degradation of p53 (Sherr and Weber, 2000). Using a phage peptide interaction screen, ZIPK was found to interact directly with MDM2 and was subsequently shown to phosphorylate Mdm2 on Ser166 (Burch et al., 2004a; Burch et al., 2004b). This is interesting because ZIPK is a positive regulator of DAPK, and this provides a mechanism to link MDM2 to the DAPK pathway. p53 is regulated by posttranslational modification at multiple sites to control its specific activity as a transcription factor. For example, the phosphoaccepter Ser20 is within the N-terminal transactivation domain and mediates p300-catalyzed DNA-dependent p53 acetylation (Dornan et al., 2003b). A host of candidate Ser20 kinases have been proposed including HK2, CHK1, DAPK1, DAPK3, DRAK-1, and AMPK that are able to phosphorylate this site in cell free kinase assays. Of these possible Ser20 kinases, CHK1 and DAPK1 have been shown to stimulate p53 transactivation in conjunction with Ser20 phosphorylation in cells (Craig et al., 2007). Interestingly,

peptides derived from the MDM2 ubiquitination signal of p53 are able to enhance DAPK and CHK1 induced Ser20 phosphorylation in *trans.* suggesting that DAPK interaction with p53 is regulated by an allosteric mechanism. These results provide further evidence that DAPK plays a major role in signaling to p53 and reveal yet another layer of complexity to the regulation of DAPK interplay with p53. The cyclin dependent kinase inhibitor p21/Waf1 is a well characterised transcriptional target of p53. This protein has a highly conserved DAPK consensus phosphorylation site, consisting of the basic and hydrophobic cores. Phosporylation of p21 by DAPK is highly efficient *in-vitro* (Figure 3.10 a), and also in cells (Fraser and Hupp, 2007). Synthesised overlapping fragments of p21 have been used as peptide ligands for characterisation in phosphorylation assays and for manipulation of DAPK interactions in trans. Strikingly, three distinct p21-derived peptides bind to the DAPKcore kinase domain and stimulate DAPK activity specifically toward p53 and not toward the well characterised *in-vivo* substrate MLC or to p21 itself (Fraser and Hupp, 2007). These data provide yet more evidence that DAPK is a regulator of the p53 pathway showing that DAPK interacts with p21 and p53 in concert, where by the former allostericaly enhances interaction with the latter, this in addition to allosteric regulation by the MDM2 signal region of p53.

1.5 Autophagy and Autophagic Cell Death

It is widely accepted that caspase dependent apoptosis is one of many programs of cell death. Programmed cell death (PCD) is classified based on morphological criteria into several categories. Apoptosis or type I cell death is the most extensively studied and is characterised by cell rounding and cytoplasmic condensation,

membrane blebbing, cytoskeletal collapse, chromatin condensation and fragmentation, and formation of apoptotic bodies that are phagocytosed by macrophages or neighboring cells (Kerr et al., 1972; Wyllie et al., 1980). Autophagic or type II cell death is characterised by the formation of autophagic vesicles in the cytoplasm accompanied by mitochondrial dilation, enlargement of the ER and the Golgi, nuclear condensation without fragmentation and membrane blebbing (Clarke, 1990). Type II cell death has been observed both in whole organisms during development (for review see Clarke, 1990; Zakeri et al., 1995), in pathological situations, during neurodegeneration such during as Alzheimer's (Cataldo et al., 1994)and Parkinson's diseases (Anglade et al., 1997), and in cell culture (Paglin et al., 2001). Type I and type II cell death programs are in no way mutually exclusive and can coincide *in-vivo* in certain tissues (Clarke, 1990), and in cell culture (Xue et al., 1999).

The very existence of autophagic cell death remains a topic for debate because autophagy is also a mechanism to maintain homeostasis. Controlled breakdown of intracellular components provides a nutrient supply during starvation and other stresses where removal of damaged organelles, such as mitochondria with reduced membrane potential, can protect cells from damage (Gozuacik and Kimchi, 2004; Mills et al., 2004). The mechanism of how autophagy contributes to cell death is largely unknown. Both apoptotic and autophagic processes may be regulated by the same pathways, although one form of cell death can be enhanced when the other is blocked (for reviews see (Bursch, 2004; Yoshimori, 2007). For example, autophagy inhibition can enhance apoptotic signaling. As such, activation of autophagy during death may be a cause of lethality or may actually be a futile attempt at rescue.

1.6 The DAPK Family and Induction of Autophagic Cell Death

Autophagy has a dualistic nature, able to provide support or to cause cell death in stressed cells. The decision of whether to live or die presumably depends on the type and severity of damage, and is under tight regulation by death promoting and inhibitory proteins. The DAPK family proteins are the first molecules described to directly regulate autophagic cell death.

Autophagic cell death induced by transfection of DAPK family members is independent of caspase activity and is characterised by striking extensive formation of autophagic vesicles and cell- membrane blebs and nuclear condensation without DNA degradation accompanied by no measurable loss of mitochondrial membrane potential or release of cytochrome c (Inbal et al., 2002). Knockdown of DAPK by antisense RNA blocks autophagic cell death induced by serum withdrawal or amino acid starvation in MCF7 cells, providing strong evidence that it is necessary for autophagic cell death in this system (Inbal et al., 2002).

DAPK is capable of initiating both Type I apoptotic and Type II autophagic cell death programs, depending on the cell system and specific stimulus. The extent to which DAPK contributes to Type I apoptotic death often depends on p53 status, but p53 does not impact on regulation of type II cell death induced by DAPK (see sections 1.4.4 and 4.3.4.4). The proposed 2 modes of action of DAPK add to the notion that it is a central player in cell death activated by a diverse array of different stimuli.

It has been proposed that autophagic cell death is a more ancient-based type of cell death program (Wada et al., 1990), because many of the autophagy associated genes

are evolutionary conserved between yeast and mammalian organisms. However the DAPK family does not have related paralogues in yeast and so probably evolved afterward to link the basic evolutionary conserved autophagic machinery and the apoptotic machinery.

1.7 Regulation of DAPK Activity

DAPK is expressed in healthy cells non-cycling cells and in actively dividing cells during development. As a result, its catalytic activity needs to be tightly regulated to ensure a response only upon the correct apoptotic triggers. Multiple layers of regulation of DAPK death-inducing activity have been discovered.

1.7.1 Regulation of Kinase Activity by the CaM domain and by Autophosphorylation

Adjacent to the kinase domain of DAPK is the CaM binding autoregulatory domain, which suppresses activity by physical association with the catalytic cleft (Tereshko et al., 2001; Yamakawa et al., 2004). The kinase domain is also autophosphorylated at Ser308, resulting in increased binding to the CaM-binding domain and reduced affinity to calmodulin. This reduces the stimulatory ability of calmodulin after autophosphorylation and conversely, dephosphorylation results in increased propensity to activation by calmodulin. Activation of DAPK catalytic activity then requires binding of Ca2+ activated CaM, releasing this domain out from the catalytic cleft and dephosphorylation of Ser308 increasing the affinity for CaM. As a result, two factors are thought to activate DAPK: elevation of intracellular Ca2+ levels and an as yet unknown phosphatase that would dephosphorylate Ser308. Dephosphorylation of DAPK at Ser308 has been observed in response to ceramide, TNF-α, UNC5H2 signaling and IFN-γ (Bialik and Kimchi, 2006). However, the

physiological consequence of Ser308 dephosphorylation is disputed, with reports showing it can activate DAPK activity in response to TNF in certain circumstance ((see section 1.8).

1.7.2 Regulation by the Serine-rich C-terminal Tail

The discovery of a peptide fragment that binds to the C-terminus of DAPK and that can inhibit its function in *trans*, suggests that this region confers another level of regulation (Raveh et al., 2000). Subsequent deletion of this region and ectopic expression of the resulting protein results in an increase in death inducing ability.

This region is homologous to serine rich tails present on other death domain containing proteins (Feinstein et al., 1995a; Feinstein et al., 1995b). Deletion of this region from other death domain containing proteins such as fas, has also been shown to increase their cell killing potency. In the case of fas, deletion of this region increases its affinity to bind to the death domain on FADD, and dephosphorylation by phosphotase activity reduces binding. It is therefore feasible that the C-terminal region of DAPK could play a similar role, inhibiting interactions with death domain binding proteins and this effect could be regulated by its phosphorylation state.

1.7.3 Regulation of DAPK *Activity by the MAPK ERK Pathway*

As already discussed, ERK phosphorylation of DAPK at Ser735 correlates with enhanced DAPK killing activity (section 1.4.3). This is attributed to a direct enhancement of *in-vitro* catalytic activity which is surprising because Ser735 is within the cytoskeletal interacting domain. How this post-translational modification effects DAPK kinase activity is unknown. Also, a downstream effecter of the ERK pathway, the p90 ribosomal S6 kinase (RSK), inhibits transfected DAPK kinase

activity by phosphorylation at Ser289. This residue is within the autoregulatory CaM binding domain, suggesting that modification at this site either increases affinity for calmodulin or increases its inhibitory interaction with the adjacent kinase domain (Anjum et al., 2005). These studies suggest that activation of the ERK pathway can regulate DAPK by either activation or inhibition of DAPK activity (Figure 1.6).

The duel nature of the ERK pathway's interaction with DAPK may serve to differentially regulate DAPK activity depending upon variations in upstream signaling events which require alternative cellular responses. This may involve simultaneous phosphorylation or sequential modifications acting to transiently enhance or reduce DAPK activity. However, it is not known how ERK signaling and modification of Ser289 or Ser735 effect DAPK cell fate decision making in response to physiological stimuli

1.7.4 Regulation of DAPK *Protein Levels*

IFNγ, C6-ceramide, and oncogene expression stabilise DAPK protein levels (Pelled et al., 2002; Raveh et al., 2001). The mechanisms of DAPK stabilisation by physiological stimuli have not been defined, but it is known that DAPK is regulated at the transcriptional level and by protein degradation. DAPK regulatory motifs within the DAPK gene promoter include a TGFβ-response element with Smad binding motifs (Jang et al., 2002) and a p53 consensus binding site (Martoriati et al., 2005)as discussed above. Accordingly, DAPK gene expression increases in response to TGFβ and to p53 activating stimuli, such as DNA damaging agents and oncogene expression (Raveh et al., 2001).

DAPK protein has a long half-life, and its protein levels are uncoupled from mRNA levels after viral RNA treatment suggesting that its activity is regulated at the protein level (Lin et al., 2007). There is growing evidence showing that changes in DAPK protein levels are regulated by a cathepsin B-dependent dependent mechanism (Henshall et al., 2003). The binding region on DAPK for cathepsin-B maps to amino acids 836-947, and. transfection of DAPK(836-947) miniprotein disrupts cathepsin-B binding to DAPK. DAPK(836-947) miniprotein acts in a dominant negative manner to induce endogenous DAPK protein degradation, suggesting that cathepsin-B is a negative regulator of DAPK degradation (Lin et al., 2007).

1.8 A Role for DAPK in Cell Survival Signalling

Although it is widely accepted that DAPK is a cell death promoting protein thought to primarily initiate type I apoptotic cell death programs, a series of papers have been published by P. Gallagher's group and others challenging this paradigm (Jin et al., 2001; Jin et al., 2002; Jin et al., 2006; Jin and Gallagher, 2003; Zhang et al., 2007). P. Gallagher's group found that over expression of mouse DAPK in human HeLa and in canine MDCK cells protected them from TNF-induced apoptosis. Expression of a kinase-dead mutant of mouse DAPK (K42AmDAPK) resulted in increased levels of apoptosis. Apoptosis levels were determined by measurement of DNA fragmentation by FACS analysis, and by levels of caspase 3, 9 and 8 cleavage (Jin et al., 2001). Using a yeast 2 hybrid screen they isolated a novel binding partner of wild-type mouse DAPK (mDAPK) called DIP-1. DIP-1 is a ring finger domain containing protein and is a homologue of drosophila mind bomb (MIB). Co-transfection of mDAPK with DIP-1 in HeLa cells resulted in reduction of mDAPK

levels. This was presumably due to the activity of DIP-1 which was shown to have ubiquitin ligase activity. Reduction of exogenous mDAPK levels by transfected DIP-1 protected cells from TNF-induced apoptosis (Jin et al., 2002).

The above results seemed a direct contradiction to the previously published A. Kimchi report suggesting that DAPK is a positive regulator of TNF-induced apoptosis (Cohen et al., 1999). A. Kimchi suggested that the mouse form of DAPK used in these studies could have a different function to the Human DAPK used in her studies and suggested that mouse DAPK could have acted as a dominant negative in the canine and human cells used in P. Gallagher's studies (Shohat et al., 2002). However, Gallagher's group subsequently showed that antisense depletion of endogenous DAPK in HeLa and in primary human aortic smooth muscle cells (HASMC) also protected from TNF-induced apoptosis as determined by quantitation of DNA fragmentation and caspase cleavage. Thus demonstrating that this effect was not limited to mouse DAPK (Jin and Gallagher., 2003). Importantly and in contrast to this, data is presented showing that depletion of DAPK levels enhanced survival of cells treated with INFγ. Additionally, treatment with INFγ resulted in caspase independent cell death where DNA was not fragmented, both of which are hallmarks of autophagic cell death. This suggested that DAPK was a positive regulator of type II cell death induced by INFγ and a negative regulator of type I cell induced by TNF. Subsequent studies by A. Kimchi's group have shown that DAPK and ZIPK do indeed protect cells from a type II cell death program initiated by INFγ {Shani, 2004 #133).

Further data is presented by Gallagher's group suggesting that phosphorylation of DAPK Ser308 results in decreased CaM binding and increased DAPK kinase activity towards MLC in response to TNF (Jin et al., 2006). Which is a direct contradiction to previous findings suggesting the opposite (Shani et al., 2001) (see section 1.7.1), where DAPK autophosphorylation decreases its activity in hippocampal neurons treated with ceramide (Pelled et al., 2002). However, Ser308 phosphorylation by TNF signaling has been shown to increase DAPK activity in hippocampal neurons (Henshall et al., 2003) (see section 4.4.1.7.2) in agreement with the Gallagher study (Jin et al., 2006).

Transfection of the TNR receptor; TNFR1 (p55) into A549 cells induces complex formation between DAPK and cathepsin B. Depletion of cathepsin B using siRNA stimulates TNFR1 dependent apoptosis. Transfection of DAPK(836-947) miniprotein (Lin et al., 2007) acts in a dominant negative manner to induce endogenous DAPK protein degradation in a TNFR1-dependent manner. These data suggest that DAPK forms a multiprotein complex with cathepsin B, increasing cell survival by countering the rate of TNFR1-dependent apoptosis. Thus providing a mechanism to explain the suggested role of DAPK in protection from TNF-induced death.

Although contradictory data is presented in the published literature, it is clear that DAPK has an important and direct role in TNF signaling. It is well known that the TNF signaling pathway has two functional arms that can result in promoting apoptosis or alternatively promoting cell growth and proliferation, and this could go some way to explaining the discrepancies between published studies. Also, given that

DAPK can induce type I and type II cell death, this may suggest that some studies failed to see DAPK induced death if relying on assays for activation of caspases and apoptotic dependent events, such as DNA fragmentation that would have missed the autophagic component. Rather, during autophagy nuclei undergo pyknosis and DNA is randomly fragmented (Figure 1.7). These nuclei can easily be mistaken for apoptotic nuclei. Therefore assays that measure nuclear fragmentation should be used to determine that extent of apoptosis in response to DAPK activity (Jin et al., 2003).

1.9 The DAPK Interactome, Discovery of New Binding Partners

Given that DAPK is a multi-domain protein involved in the regulation of multiple cell death programs induced by multiple signals, it is highly likely that it interacts with multiple different proteins. Various studies have been conducted to find new binding partners for DAPK including yeast 2-hybrid assays using the death domain (Cohen et al., 1999) and using whole protein (Jin et al., 2002).

1.9.1 Linear Interaction Motifs in Signal Transduction

A proteome is defined as the complete set of proteins and protein networks encoded by a given organisms genome. It is estimated that the human genome encodes around 30000 to 50000 genes (Lander et al., 2001; Venter et al., 2001). The number of proteins in the human proteome is expected to be many fold greater than this due to variations such as splice variants, post-translational modifications (such as phosphorylation, glycosylation, lipidadation, etc.) and combinatorial changes such as domain shuffling (Bogarad and Deem, 1999; Riechmann and Winter, 2000). Each of these individual peptide moieties is expected to bind with many other partners creating the network of protein interactions that control diverse biological activity.

These networks and their constituent protein-protein interactions are critical for all cellular processes, and so their perturbation can lead to disease states such as cancer.

The study and mapping of protein interactions is fundamental to understanding biochemical pathways. Protein interaction networks can be visualised as protein interaction maps (PIMs) that represent a snapshot of a given set of protein-protein interactions ranging from whole proteome maps to signal transduction pathways and smaller interaction groups. Classically, studies in model organisms such as yeast that are easily manipulated and genetically tractable, have been used to expand on protein interaction maps and characterise biochemical pathways. Conserved networks can then be extrapolated from yeast to higher organisms leading to identification of biochemical pathways in humans. However, many elements involved in cancer growth control are not present in model organisms and so classical genetics cannot always be relied upon to identify novel cancer regulators. Therefore novel approaches are required to expand protein-interaction maps in humans due to our genetic intractability. For example, although DAPK has homologues in vertabrate species it is not expressed in yeast (Bialik and Kimchi, 2006). Also, mouse DAPK (mDAPK) has been shown to act differently to human DAPK (hDAPK), where mDAPK has alternate splice verients that play a more prominent cell survival role than hDAPK (Jin et al., 2001).

Throughout evolution, proteins have diverged and have been extensively duplicated allowing them to be grouped into families where clusters share a similar function. This process of divergent evolution has given rise to protein modular structure, each module being a discrete region assigned a discrete function. There are currently over

7000 known protein globular domains, modular elements typically more that 30 amino acids in length that form folded independent compact structures (Bateman et al., 2002). Globular domains perform a vastly diverse set of functions ranging from death signaling to catalysis during metabolism.

Studies have shown that globular protein domains cover only a fraction of an organism's total amino-acid sequence (McEntyre and Gibson, 2004). The remaining peptide sequence is either of low-complexity or is intrinsically disordered (McEntyre and Gibson, 2004). Although a proportion of these regions are designated linker regions dividing globular domains, the majority are known to have critical functional roles in signaling pathways (Dyson and Wright, 2005). For example, protein interaction regions such as phosporylation motifs and binding sites are often located in linear disordered regions of proteins. These very short functional regions are on average only 4 amino acids in length and like globular domains conform to evolutionarily conserved sequence patterns (Puntervoll et al., 2003).

Linear motifs evolve in a fundamentally different way from globular domains. Linear motifs are short sequences, of which only a few amino acids are critical to their function, and so have a much higher probability of evolving by chance. This is apposed to globular domains that are highly constrained due a requirement to conserve elements involved in correct folding. Therefore linear motifs have a higher degree of evolutionary plasticity than globular domains. Whereas globular domains are often conserved down to lower eukaryotes, as far as humans are concerned it is estimated that only 65% of linear motifs are conserved outside the vertebrates (McEntyre and Gibson, 2004).

Globular domains and linear motifs differ greatly in affinity for binding partners. Whereas globular domains bind partners relatively strongly, down to picomolar affinities, linear motifs have weaker binding kinetics often as high as the 10μM range (Neduva and Russell, 2005). Thus, linear motifs are often involved in transient interactions such as those in signaling networks (e.g., at phophorylation sites or through the SH3 domain or 14-3-3 domain etc.). Sensitive regulation of cellular processes requires transient signals from many weakly interacting components interacting in synergy. Useful information could not be provided by strong and long-term interactions between only pairs of proteins. Therefore signal transduction among many components interacting via linear motifs with weaker binding kinetics can provide specific and sensitive regulation of cellular processes.

1.9.2 Signal Transduction Through the Intrinsically Unstructured N-Terminus of p53

p53 is a protein with characterised regions of unstructured and globular domains and serves as a good example. Even though p53 is one of the most well characterised proteins associated with cancer, establishing a structure function relationship for its entire amino acid sequence has proven difficult.. This is in part due to the fact that only 30% of its residues are present in well defined structured globular domains; the highly conserved DNA binding domain and the tetramerisation domain. Because the remaining sequence is not folded into secondary or tertiary structure, p53 can be designated an intrinsically unstructured protein (IUP). Under physiological conditions the entire N-terminal region of p53 (amino acid residues1-93) is not only devoid of tertiary structure it is also largely missing secondary structure elements (Dawson et al., 2003). However, this region is the site for multiple linear motif-driven interactions with a series of acetyltransferases, ubiquitin ligases and protein

kinases that are critical for signaling through the p53 pathway. Characterised linear interaction motifs within the N terminal activation domain of p53 include the highly conserved 15 amino acid Box I linear domain which harbors multiple interaction sites including; an LXXLL-type p300 cofactor interaction site (Avantaggiati et al., 1997), an FXXWXXXL consensus MDM2 interaction site and multiple phosphoaccepter residues with their adjacent consensus motifs. Outside the box I domain, within the N-terminus are five proline-rich SH3 binding PXXP motif domains and a secondary proline-repeat domain required for allosteric control of DNA dependent acetylation. It is not surprising therefore that many signal transduction cascades converge at the N-terminal region of p53. For example, DNA damage activated kinases like CHK1 and CHK2 modify Thr18 and Ser20 by means of an allosteric mechanism (Craig et al., 2003; Shieh et al., 2000). These modifications differentially modulate positive interactions involving the p300 acetyltransferase or inhibitory interactions via the ubiquitin E3 ligase MDM2. Whereas phosporylation at Thr18 blocks MDM2 binding, phosphorylation of Ser20 has no effect on MDM2 interaction (Craig et al., 1999b; Schon et al., 2002). but creates a p300 phospoacceptor LXXLL concensus motif (Dornan and Hupp, 2001). N-terminal binding of MDM2 sterically suppresses p53 dependent transcription by competing with binding of positive adapters like p300. In this way p300 stabalises the p53-DNA complex and blocks its degradation via the MDM2 ubiquitin degradation pathway. In addition, interaction with p300 via the LXXLL motif promotes DNA-dependent acetylation of p53 and recruitment of chromatin-remodeling enzymes to co-operate in transcription activation (Barlev et al., 2001; Dornan et al., 2004; Espinosa and Emerson, 2001). DAPK has been recently

identified as a p53 Ser20 kinase (Craig et al., 2007). Ser20 kinase activity from cell lysates co-elutes with DAPK, and recombinant DAPK is able to phosphorylate Ser20 in a cell free kinase assay. DAPK and p53 complexes can be isolated by co-immunoprecipitation, and DAPK protein depletion by siRNA attenuates basal p53 Ser20 phosphorylation in cells. This Ser20 kinase activity directed by DAPK correlates with p53 dependent transactivation. That the action of multiple kinases such as ATM, DAPK and CHK1/CHK2 can be activated by multiple stress pathways, this provides a mechanism for linking specific stresses to p53 activation and resultant tumour suppression via its intrinsically unstructured N-terminal domain.

The importance of the linear motifs within the N-terminal region of p53 to cancer development is highlighted by studies showing that their mutation *in-vivo* increases cancer incidence. Transgenic animals with an alanine substituted CHK2 phosphoacceptor site have attenuated levels of UV-induced p53-dependent transcription in mouse skin and are sensitive to UV-induced skin cancer development (Hoogervorst et al., 2003; MacPherson et al., 2004). Also, a separate study shows that mutation of Ser20 in mice stimulates spontaneous B-cell lymphoma in transgenic mice models (Craig et al., 1999a). Knowledge of multiple linear interaction motifs in transduction pathways is therefore required to develop a full appreciation of signaling events in cancer development.

1.9.3 Using Phage Display to Discover Protein-Protein Interactions

Linear motifs have a much lower affinity for binding partners and interact transiently making them ideal candidates for study with regards to signaling pathways. It is predicted that there are far more instances of linear motif modules involved in

signaling-pathway regulation than there are globular domain modules in the entire proteome. However, current online search resources contain around 7000 globular domains and yet only 200 linear motifs (elm.eu.org). This is because the experimental procedures employed to discover new protein interactions often rely on fishing methods that select for globular domains. For example, tagged-protein complex immunoprecipitation selects for higher affinity interactions and so is unable to pull down lower affinity transiently binding proteins. Also, homogenisation of cell lysates, employed during protein purification enriches globular domains because disordered proteins are more likely to be disrupted by proteases (Dyson and Wright, 2005). Likewise, yeast 2-hybrid technologies have difficulty resolving transient interactions when presented with library protein that binds a with lower Km. In addition to this, bait or prey may be miss folded and full length proteins may obscure smaller interaction sites so they are only transiently exposed. Finally, expression of exogenous protein in host species can obscure interaction surfaces due to aberrant post translational modification. Therefore standard proteomics involving epitope-tagging, yeast 2-hybrid and mass spectrometry are sub optimal tools for discovering protein-protein interactions involving linear intrinsically disordered peptides that are critical to signal transduction pathways.

In-vitro phage peptide display technology can be used to identify novel protein-protein contact sites driven by small linear interaction motifs. Phage display allows the antigenic presentation of extensive combinatorial peptide libraries to purified recombinant bait protein. Peptide libraries are expressed as fusions on the coat protein of the filamentous phage M13 and allowed to interact with isolated target protein. This is followed by removal of non-reacting phage so specifically bound

phage can then be eluted using either a co-factor, such as ATP or metal ions, or by denaturing conditions such as concentrated acid. After binding phage have been eluted, higher affinity peptide interactions can be selected for by a biopanning to isolate a few highly specific reacting phage. Panning involves elution of bound phage, enrichment and amplification of phage in *E.coli* and then subsequent reintroduction of purified phage particles onto the isolated bait protein. After the desired number of pans, enriched and isolated phage DNA from individual plaques is sequenced to allow identification of the primary structure of the specifically binding peptides. Using this method of sequential biopanning, lower affinity interacting peptides can be identified during the first binding through to higher binding interactions isolated during later subsequent pans.

Use of phage peptide display technology methodology has classically been geared towards characterising contact sites for known binding partners. For example, a second MDM2-binding site in the DNA binding domain of p53 and a second p300-docking site in p53 have both been identified in this manner (Dornan et al., 2003a; Shimizu et al., 2002). Also, because the purified bait can be manipulated relatively easily *in-vitro*, phage display has often been used to determine binding affinity changes upon alteration of the target proteins conformation. However, broader use of phage display to identify truly novel interaction partners has only recently been developed. Expansion of putative protein interaction maps has been achieved using MDM2 as prototypical bait target (Burch et al., 2004a; Burch et al., 2004b). Unsurprisingly, the majority of MDM2 associating phage had significant homology to the p53 box I domain, a known interaction interface between MDM2 and p53. But 10% of isolated phage did not display peptide with homology to any previously

known binding partner. These peptide sequences were then used to define novel binding partners for MDM2, including the DAPK family member ZIP kinase, the ubiquitin ligase NEDD4 and the HSP90 heat shock protein. These novel MDM2 binding partners were then subject to further phage display in order to develop an interaction map. Using this tandem approach to phage display, the MDM2 interacting ZIP-kianse was in turn found to interact with p21. This is especially striking because using this method ZIP kinase was identified as a novel modifier of 2 key components of the p53 pathway; MDM2 and p21. These studies demonstrate that phage display technology can be used to rapidly discover novel binding partners and expand on protein interaction maps involving signal transduction pathways.

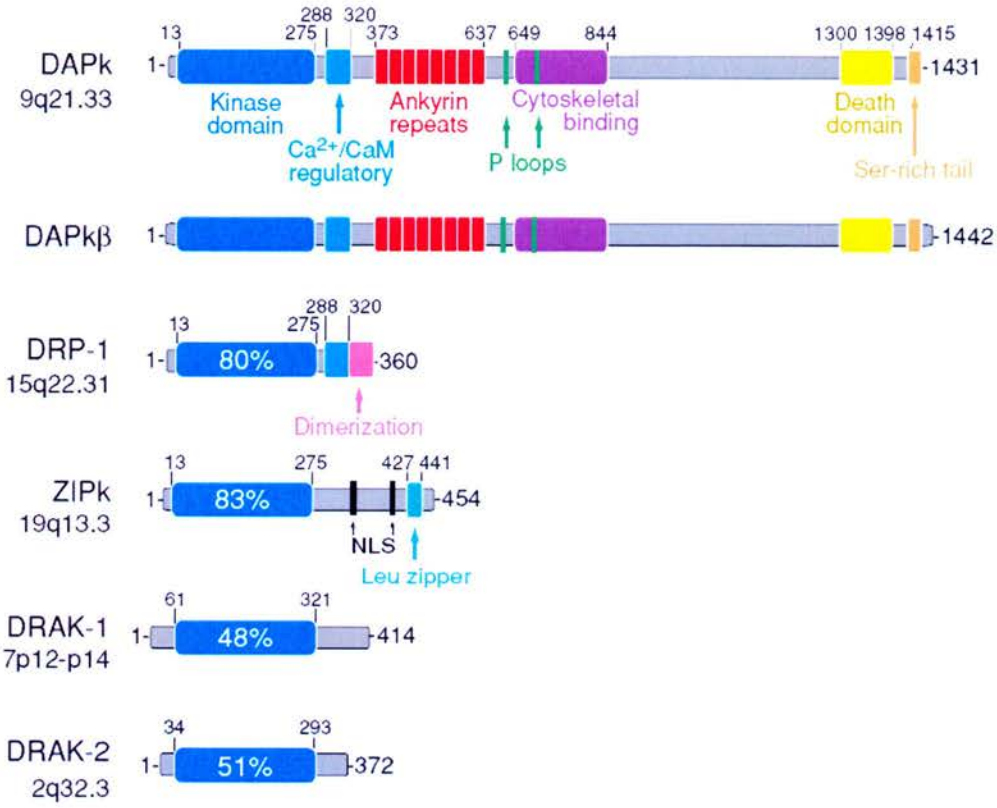

Figure 1.1 The Death Associated Protein Kinase (DAPK) Family of Calcium Calmodulin Serine/Threoine Protein Kinases. Numbers define the amino acid position of protein domains. Percentage homology within kinase domains and chromosomal locations are shown. NLS = nuclear localization signal.

Figure from S Bialik and A Kimchi, Annu. Rev. Biochem. (2006).

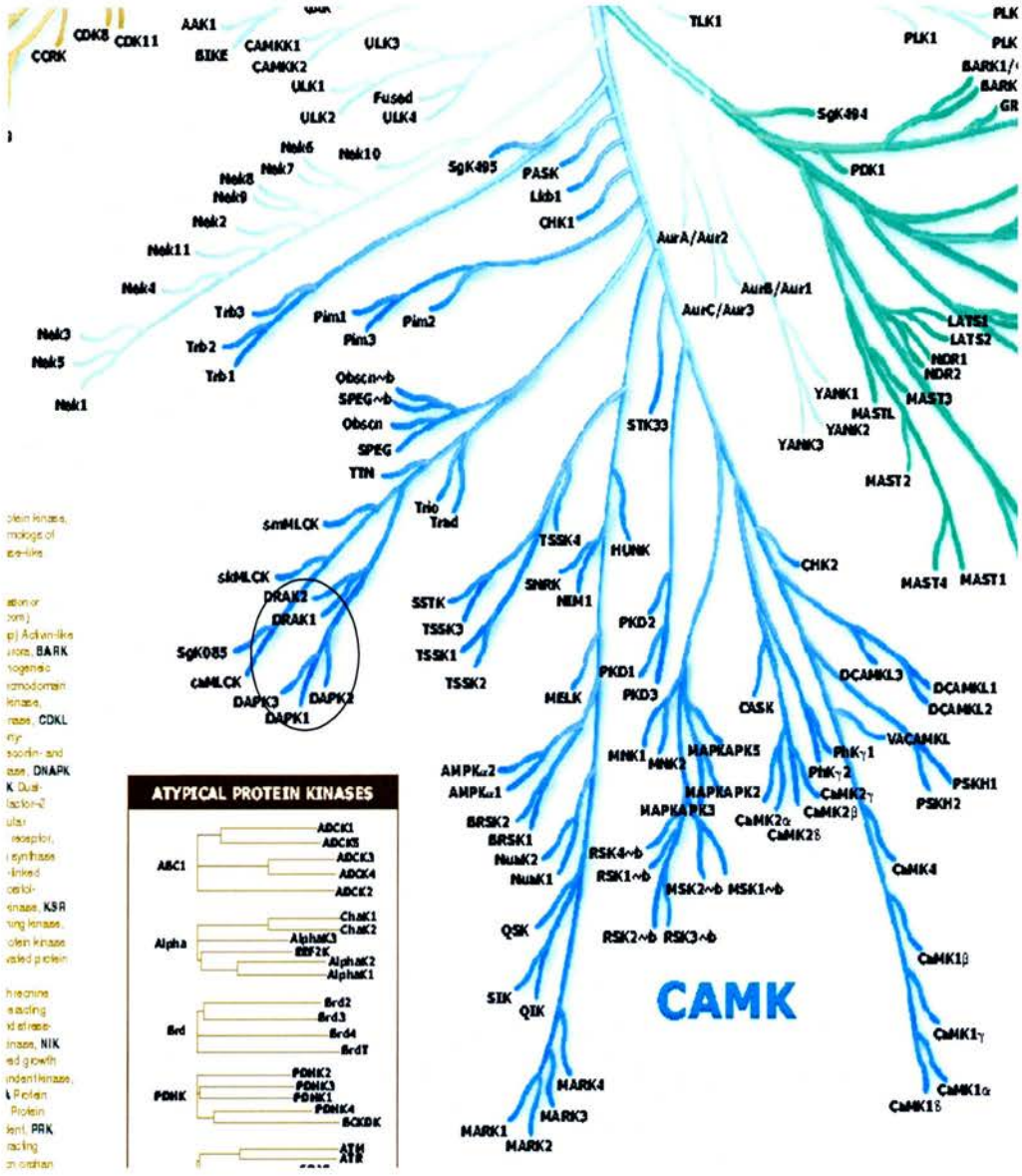

Figure 1.2 The Calcium/Calmodulin Kinase (CAMK) Superfamily. DAPK family members are highlighted.

Figure adapted from G Manning, DB Whyte, R Martinez, T Hunter and S Sudarsanam Science (2002).

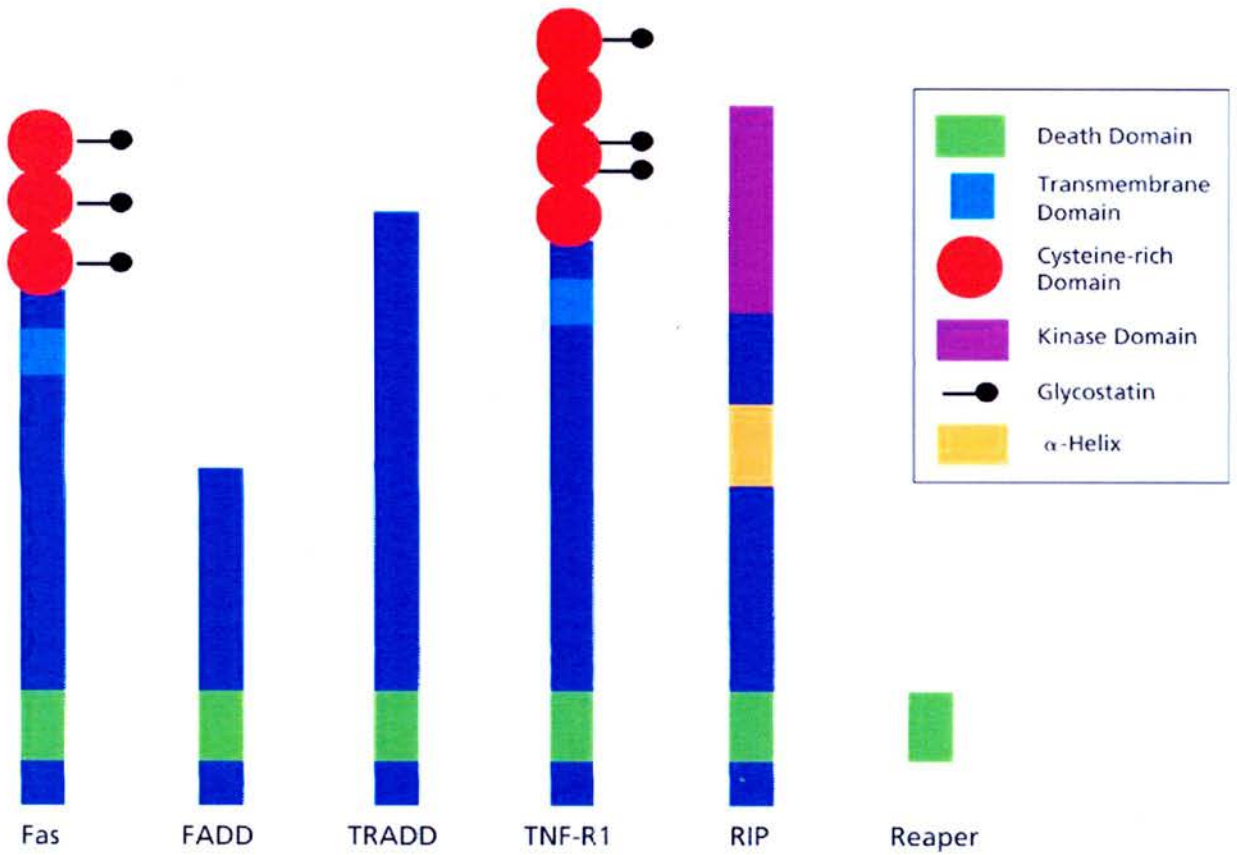

Figure 1.3 The Tumour Necrosis Factor (TNF) Family of Death Receptors.
Figure from sigma pathways:
http://www.sigmaaldrich.com/Area_of_Interest/Life_Science/Cell_Signaling/Scientific_Resources/Pathway_Slides___Charts.html

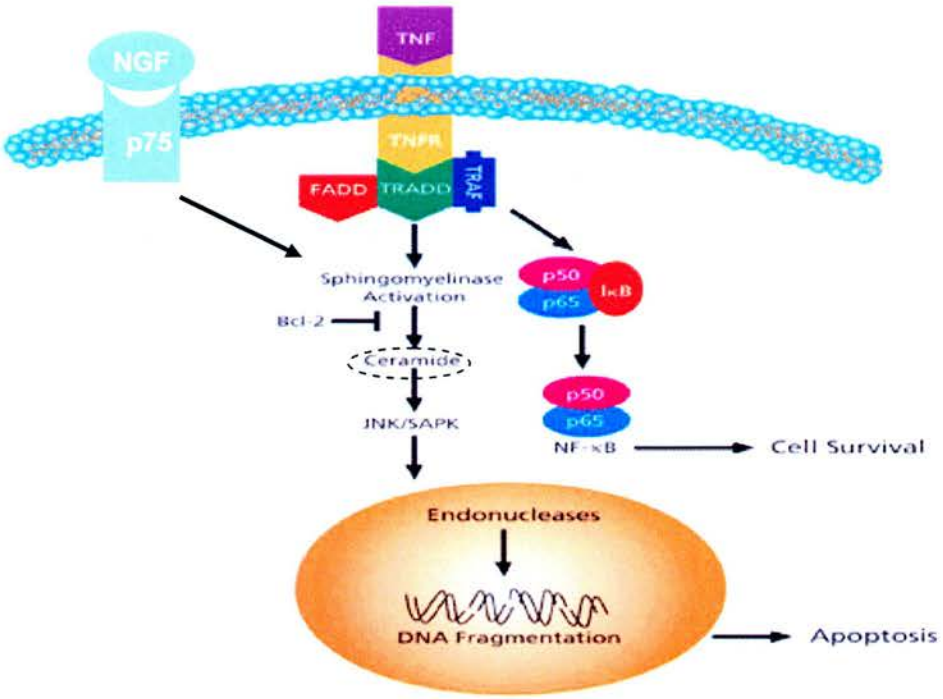

Figure 1.4 Nerve growth factor (NGF) and TNF Cell Fate Signalling. The ceramide second messenger molecule is highlighted by dashed circle. NGF engagement with neurotopin receptor (p75) initiates sphingomyelin hydrolysis also resulting in ceramide production.

Figure adapted from sigma pathways:
http://www.sigmaaldrich.com/Area_of_Interest/Life_Science/Cell_Signaling/Scientific_Resources/Pathway_Slides___Charts.html

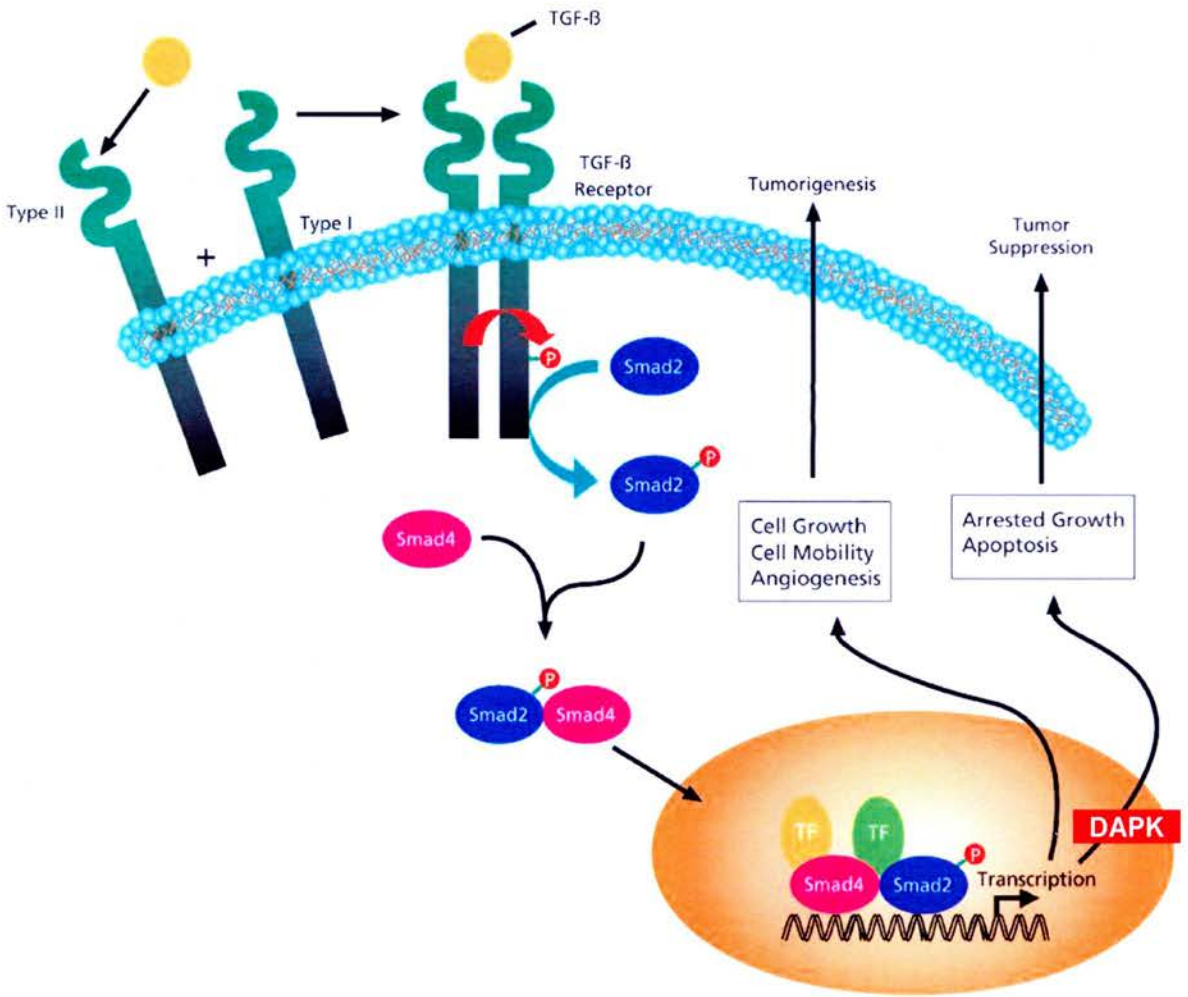

Figure 1.5 Transforming Grown Factor β (TFG-β) Signalling Through SMADs Initiates Transcription of DAPK. Activation of DAPK transcription by TGF-β is associated with cell death

Figure adapted from sigma pathways: http://www.sigmaaldrich.com/Area_of_Interest/Life_Science/Cell_Signaling/Scientific_Resources/Pathway_Slides___Charts.html

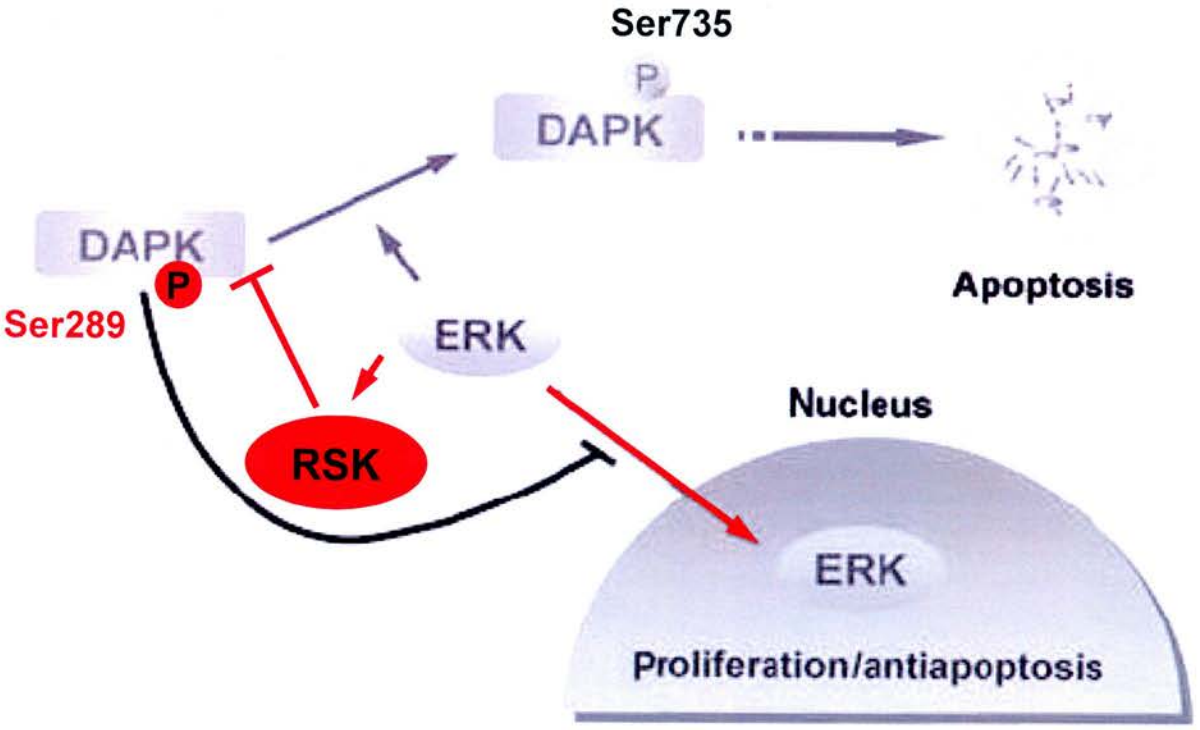

Figure 1.6: Regulation of DAPK by Extra Cellular Regulated Kinase (ERK). Positive regulation in black and gray, negative regulation in red.

Figure adapted from: C Chen, W Wang, J Kuo, H Tsai, J Lin, Z Chang and R Chen, EMBO (2005) (highlighted in black and grey). With additional data from R Anjum, P Roux, B Ballif, S Gygi and J Blenis, Current Biology (2005) (highlighted in red).

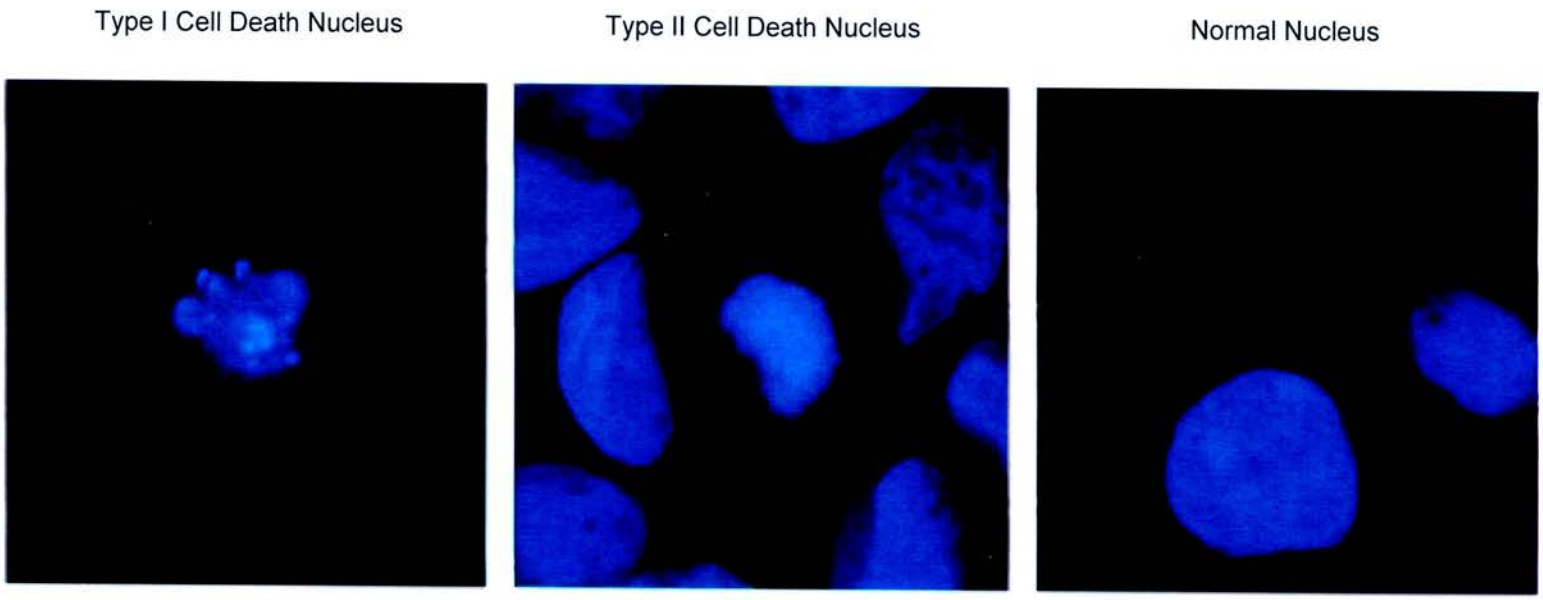

Figure 1.7 Nuclear Morphologies During Type I and Type II Cell Death. Type I cell death nuclei contain orderly fragmented DNA. Type II cell death nuclei appear condensed and DNA is randomly fragmented.

Figure adapted from G Shani, L Marash, D Gozuacik, S Bialik, L Teitelbaum, G Shohat, and A Kimchi, MCB (2004).

Chapter 2

Materials and Methods

2.1 Reagents

All chemicals were obtained from Sigma- Aldrich or Merk-BDH unless stated otherwise.

2.1.1 Purified Proteins

Purified p53 tetramers (Expressed in Sf9 insect cells), His-tagged CHK2 (Expressed in *E.coli*) and His-tagged and GST tagged DAPKcore (Expressed in *E.coli*) were provided by Dr A Craig. GST-DAPKcore (amino acids 1-264) in destination vector pDEST20 was obtained from Dr L. Burch.

2.1.2 Plasmids

Full length native DAPK in Gateway entry vector was obtained from Dr L Pohler. Full length human native transcript variant 1 (NM 005909) of MAP1B was purchased from Origene (USA). HA-tagged DAPK (NM 004938), kinase activity attenuated (K42A) and calmodulin domain deleted (ΔCaM) DAPK constructs were a gift from Adi Kimchi (Weizmann Institute, Israel).

2.1.3 Antibodies

The suppliers and dilution factors used for western blotting and immunofluorescent studies are detailed in Figure 2.1.

2.2 Chromatographic Separation of Protein Samples by SDS Polyacrylamide Gel Electrophoresis

Protein samples were dissolved in SDS loading buffer (5% SDS, 20% Glycerol, 20 mM Tris, 10 mM EDTA, 200 mM DTT, pH 6.8) and incubated at 85C for 5 minuets to reduce. Samples were then loaded into 4-12% NuPAGE Tris-Glycine gels unless stated otherwise in the figure legend, before separation using MOPS-SDS buffer at 150 V for 2 hours.

2.3 In-Gel Coomassie Staining of Separated Proteins

Gels were stained using coomassie blue (R-250) solution in 45% methalol, 10% acetic acid for 1 hour and washed until background staining was reduced.

2.4 Western Immunoblotting

Gels were assembled into electroblotting apparatus for transfer onto Hybond-C nitrocellulose membranes using transfer buffer (0.192 M glycine and 25 mM Tris) supplemented with 20% methanol. Proteins were transferred using 200A current for 2 hours at 4C.

For separation of MAP1B; 1.5X transfer buffer was used (0.288 M glycine and 37.5 mM Tris) and was supplemented with only 10% methanol. Proteins were transferred using 400A current for 2 hours at 4C. These optimised conditions allowed efficient transfer of proteins with molecular weights above 200 kDa.

Even transfer of proteins onto membranes was verified by Indian ink-staining, before blocking with 5% non-fat milk in blot wash buffer (PBS with 0.05% Tween 20). Primary antibodies were then incubated at room temperature for 2 hours at diluted in blocking buffer at the concentrations indicated in the figure legend. After primary antibody binding, membranes were washed 3 times for 5 minuets with blot wash buffer, before incubation with the appropriate HRP-conjugated secondary antibody (DAKO) at 1:1000 dilution. Protein bands were detected using enhanced chemiluminescence (ECL). ECL solution was incubated on blots for 1 minuet and then removed with blotting paper. Blots were then covered with cling film and exposed to ECL hyperfilm.

2.5 Purification of GST-DAPKcore

GST-tagged DAPK kinase domain corresponding to amino acids 1-274 (GST-DAPK-core) was cloned into destination insect cell expression vector pDEST20 using the invitrogen gateway cloning system.. Sf9 insect cells were infected with plasmid allowing expression of GST-DAPKcore using the baculovirus expression system (Invitrogen).

Cells were grown in suspension in serum-free 900II medium until needed, and the plated at 4x107 cells per 175cm2 flask for use. Once adhered media was removed and replaced before infection with GST-DAPKcore in pDEST20 expression vector. 72 hours post-infection, cells were scraped, pelleted and snap frozen in liquid nitrogen. Frozen pellet was then resuspended in gentle lysis buffer (10mM HEPES, 10 mM NaCl, 2 mM DTT and protease inhibitors at pH 7.4), incubated on ice for 5

minuets and centrifuged at 13000g for 15 minutes at 4C. Supernatent was then removed and lysate was snap frozen for later purification of protein.

After gentle lysis, GST fusion proteins were purified using glutathione-sepharose 4B beads (Amersham).

2.6 Non-radioactive DAPK Kinase Assay Using p53 Tetramers as a Substrate

The activity of purified kinase fractions was determined by a non-radioactive kinase assay using tetrameric p53 as a substrate. Tetrameric p53 was obtained from Dr A Craig. 100ng p53 was mixed into kinase buffer (10mM ATP, 50mM HEPES, 50mM KCl, 10mM MgCl2, 0.2mM EDTA 1mM DTT at pH 7.5) containing purified kinase fractions. Kinase reactions were allowed to proceed for 30 minuets at 30C. The extent of p53 Ser20 phosphorylation was visualised by immunoblotting using phosphospecific monoclonal antibody FPS20.

2.7 Development of DAPK Binding Ligands Using Peptide Combinatorial Libraries

The phage peptide interaction screen was jointly performed by Dr L. Burch and myself.

A Peptide Display Library of random 12- mer peptides (New England Biolabs) was used as a source of combinatorial peptides. 96-well flat bottom plate wells (Microlite 2 - Dynatech laboratories) were coated with 1 μg/ml anti-GST mouse monoclonal antibody (Sigma) to capture purified GST-DAPKcore. After capture and washing, wells were incubated for one hour with 2×1011 phages in PBS containing

0.1% Tween20. The phage particles were eluted by acid incubation and neutralised with 15 µl of 1 M Tris– HCl (pH 9.1). Eluted phage particles were then amplified by infection of ER2378 cells and then PEG-precipitated. This procedure was repeated three times with approximately 2×1011 pfu of the first or second round amplified eluate used as input phage. In addition, the concentration of Tween20 in the binding and wash buffers was increased stepwise, from 0.1% to 0.5%, with each successive round of biopanning in order to reduce non-specific binding of the amplified phage-peptide particles. The third round PEG-precipitated phage were titrated and individual plaques were regrown and tested for GST-DAPKcore binding activity. DNA from 10 binding phage plaques was then amplified and prepared according to the manufacturer's protocol (New England Biolabs). The Abi Prism 377 automated DNA sequencer was used to sequence the DNA with the -96gIII primer.

After phage display biopanning, the ability of purified DAPK to bind isolated phage 12-mers was further assessed using synthesised biotinylated peptides (Cambridge Peptides) by ELISA. Peptide association was detected using HRP-conjugated streptavidin.

2.8 Bioinformatics

2.8.1 Determination of Homology between Isolated Phage Display Peptide Sequences and Human Proteins.

Sequence data from the 12-mer peptides was inputted into E-motif (http://brutlag.stanford.edu/emotif-search/) or BLAST search programs of the NCBI (http://www.ncbi.nlm.nih.gov/BLAST/) genbanc human protein database to identify

consensus or individual peptide motifs with homology to known or uncharacterised proteins.

The BLAST search program was optimised to find short nearly exact hits. Hits that consisted of 5 or more identical amino acids were considered for further analysis. The E-motif search used to identify any consensus motifs arising from more than one isolated peptide that had significant homology to proteins in the genbanc database.

2.8.2 Analysis of Evolutionary Conservation within the N-terminus of MAP1B

MAP1B paralogue sequences were obtained by blast searching of the emble whole genome databases ranging from vertebrates to insects. Sequences were then aligned using ClustalW (www.ebi.ac.uk/clustalw/), and color coded according to amino acid chemistry.

2.8.3 Mining the Cancer Genome Anatomy Databaser to Determine MAP1B and DAPK *Expression Levels in Cancer Cell Lines*

The NCBI cancer genome anatomy database consists of data from microarray analysis of RNA from the NCI60 panel of cancer cell lines (http://cgap.nci.nih.gov/). The level of expression of DAPK and MAP1B was determined from representative arrays in the database.

2.9 Evaluation of Protein Binding Using Enzyme-Linked Immunosorbant Assay (ELISA)

ELISA assays were conducted in 96 well Dynex microtitre plates. For direct adsorption onto the solid phase, purified GST-DAPKcore or p53 tetramer proteins were diluted in high pH buffer (0.1M NaB4 at pH9) over night at 4C. For antibody capture or capture by glutathione, proteins were dissolved in PBS and incubated for 1

hour at room temperature. Wells were washed with PBS-T 3 times, before blocking with PBS supplemented with 3% BSA for 1 hour at room temperature. After blocking, the indicated proteins and/or peptides were incubated for 2 hours at room temperature before washing 3 times with PBS-T.

For antibody detection of bound proteins, primary antibody was incubated for 1 hour at room temperature before washing 3 times with PBS-T. The appropriate HRP-conjugated secondary antibody was incubated for 1 hour at room temperature before washing 3 times with PBS-T. Binding was detected after addition of ECL solution using a luminometer (Labsystems, Fluoroscan Ascent FL). For detection of bound biotinylated peptides, HRP conjugated streptavidin was used.

2.10 Propagation of Exogenous Plasmid DNA in Bacteria

2.10.1 Preparation of Transformation-Competent Bacteria

E.coli DH5α bacteria grown in LB broth were used to propagate plamid DNA. Heat shock competent cells were created by incubation with TFBI buffer (30 mM Potasium Acetate, 100 mM RbCl2, 10mM CaCl2, 50 mM MnCl2 at pH 5.8) for 10 minuets at 4C. Then after pelleting the bacteria were resuspended in TFBII (10 mM MOPS, 75 mM CaCl2, 10 mM RbCl2, 15% Glycerol at pH 6.5) at 4C for 15 minuets before aliquoting and snap freezing on dry ice-methanol for storage at -80C.

2.10.2 Transformation of Competent Bacteria

50µl competent *E.coli* DH5α bacteria aliquots were thawed before addition of 100ng of the required plasmid DNA and mixed, before allowing to stand in ice for 1 hour. Bacteria were then heat shocked for 45 seconds at 42C before retuning to ice for a

further 5 mins. Before plating, samples were incubated at 37C for 1 hour with agitation to allow expression of resistance markers. Cells were then streaked on LB plates containing the appropriate antibiotic resistance marker and allowed to grow overnight at 37C.

2.10.3 Preservation of Transformed E-Coli Stocks by Freezing in Glycerol

800µl 80% sterile glycerol was added to 200µl of transformed *E.coli* in log phase growth before snap freezing and storage at -80C.

2.10.4 Purification of Plasmid DNA from Transformed Bacteria

Plasmid DNA was amplified in transformed bacteria over night before purification using Qiagen plasmid purification kits as per manufacturer's protocol. DNA concentration was determined using 260nm UV spectroscopy.

2.11 Analysis of DNA by Agarose Gel Electrophoresis

DNA samples were diluted in loading buffer (0.04% bromophenol blue, 0.04% xylene cyanol FF, 2.5% Ficoll) and chromatographically separated in 0.8% agarose gels using TBE buffer (90 mM tris, 90 mM barate, 300 mM EDTA at pH 8.0) unless otherwise stated. After electrophoresis, gels were stained using ethidium bromide to visualise the DNA banding pattern.

2.12 Gene Cloning

MAP1B fragments V1, V2 and N126 were created using the Gateway recombinase system. DAPK, DAPK2 and ZIPK genes were cloned into donor vectors in house by

Dr L. Pohler or Dr L. Burch. HA-tagged DAPK constructs were obtained from Adi Kimchi. All DNA primers were purchased from Sigma Genesis.

2.12.1 Using the Gateway System for Gene Cloning

Recombination cloning vectors and recombinase reagents were obtained from Invitrogen for use in the Gateway cloning system. Cloning into donor vectors was facilitated by DNA recombination between att sites using DNA recombinase. Forward and reverse primers were designed to contain the att sites; attB1 (ggggacaagtttgtacaaaaaagcaggctgg) and attB2 (ggggaccactttgtacaagaaagctgggtg) respectively for incorporation into the donor vector pDONR201 using the BP reaction as per the manufatorers protocol. This resulted in DNA cloned into plasmid with flanking recombination sites for further subcloning into destination vectors. Cloned genes were sequenced to ensure that they were in the correct reading frame and to verify sequence integrity.

Genes cloned into pDONR221 constructs were then recombined using the LR reaction into the required destination vector as per manufacturers protocol. This system allowed multiple expression vectors to be created from a single gene clone for use as required. DAPK, MAP1B V1, MAP1B V2 and N126 Genes were subcloned into destination vectors containing promoters designed for bacterial, insect cell or mammalian expression. Native, His tagged, GST tagged, V5 tagged and GFP tagged genes were created. Empty vector constructs contained 1kb of non-specific DNA preceded by 2 stop codons incorporated by Gateway recombination cloning.

2.13 Cloning of MAP1B Gene Fragments from Human Foetal Brain RNA

MAP1B gene fragments were cloned from human foetal brain total RNA (Ambion) into pDONR221 using the gateway system. ≈ 4kb fragments of transcript variants 1 (V1) and 2 (V2) (corresponding to the rat constructs cloned by Y. Uchida (Uchida, 2003)) were cloned using forward primers: atggcgaccgtggtggtgg and atgatcactgatgctgccc respectively. For both of these constructs the reverse primer: actgaattcaaaactcactg was used. The N terminus of variant 1 (N126) was cloned using the reverse primer: taagcgcacctcggtg. All primers were optimised to have annealing temperatures above 60C. See section 3.3.4.

2.13.1 RT-PCR of MAP1B Fragments from Brain RNA

1µg of human foetal brain total RNA was denatured with 50 picomoles of oligodT primer for 10 minuets at 65C before immediate cooling on ice. Reverse transcription buffer, 100mM DDT, 10 mM dNTPs, RNase inhibitor and reverse transcriptase (Roche long template system) were then added and incubated at 43C for 60 minuets in a thermocycler with heated lid.

After the reaction, the RT mix was immediately used for PCR to reduce the possibility of denaturing the long MAP1B cDNAs. 1 µl RT buffer was used with 300nmoles of each primer in PCR buffer and 1 µl DNA polymerase (Roche long template system) per 50µl PCR reaction. PCR was performed in a thermocycler for 30 cycles using a 58.5C annealing temperature.

2.14 Tissue Culture

2.14.1 Growth media

HCT116 cells were cultured in McCoys 5A medium, MC7 cells in RPMI medium and primary fibroblasts in primary fibroblast media, all supplemented with 10% FBS. All other cell lines were cultured in DMEM supplemented with 10% FBS. Cells were grown in a humidified incubator in 5% CO2 at 37oC.

2.14.2 Subculturing

Cultures were grown to 80% confluency before subculturing. Cells were washed with sterile PBS and removed from the culture vessel by trypsination at room temperature until visibly dislodged. Pre-warmed media was then used to stop the trypsin before replating at $1/6^{th}$ cell concentration.

2.14.3 Cryogenic Storage of Cell Lines

After suspension by trypsinisation, pelleting and washing cell pellets were resuspended in growth FBS supplemented with 10% DMSO. Cells were then slowly frozen over night to -80C before transfer into liquid nitrogen for long term storage.

Cryogenically frozen stocks were recovered by fast warming to 37C in a water bath before quick addition into 10 ml growth media. Cell suspension was then pelleted and resuspended in fresh media to remove DMSO before plating and culturing.

2.15 Transfection of Expression Plasmid DNA into Cell Lines

For transfections, cells were seeded into six-well plates at a density of 2X105 per well 1 day prior to transfection unless otherwise stated. Transient transfections were performed using 3µl of Lipofectamine2000 reagent per microgram DNA in Optimem

(Invitrogen) according to the manufacturer's instruction. Cells were harvested 24 h after transfection unless otherwise stated. After washing, cells were harvested into PBS using a rubber policeman at 4C.

2.15.1 Preparation of Transfected Cell Lysates

For direct immunoblotting to determine protein composition, cells were lysed in denaturing RIPA buffer (10 mM Tris pH 7.5, 150 mM NaCl, 1% NP40, 1% deoxycholic acid, 0.1% SDS and 1 mM EDTA with 1x protease inhibitor cocktail (Roche). Lysates were reduced in sample buffer containing 0.2 M DTT at 85°C for 5 min before chromatographic separation by SDS-PAGE.

2.16 Immunoprecipitation

2.16.1 Co-immunoprecipitation of Cotransfected Proteins

HCT116 or A375 cells were co-transfected for 24h with a total of 2μg plasmid DNA consisting of 1 μg DAPK and 1 μg V5-tagged MAP1B V1/V2 construct or control vector as indicated. Cells were lysed with mammalian cell detergent lysis buffer (1% NP40, 50 mM HEPES (pH 7.6), 5 mM DTT, 0.4 M KCl with 1x protease inhibitor cocktail (ROCHE) for 20 min on ice and cleared at 13,000 r.p.m. for 10 min. 2μg Anti-V5 mouse monoclonal antibody (Invitrogen) was immobilised per 20μl Protein G-Agarose beads (Amersham) and washed 3 times in 1 ml PBS-T for immunoprecipitaion. Immunoprecipitations were carried out on a rotor for 2 h at 4°C in binding buffer (25 mM HEPES (pH7.5, 15% glycerol, 0.1% Triton X-100, 1 mM DTT, 100 mM KCl and protease inhibitor) using 20 μl of V5- beads with 200 μg of total protein. After precipitation, the beads were sedimented, washed 3 times with PBS-T and incubated for 5 min at 85OC with sample buffer + 0.2 M DTT. Co-

precipitated DAPK was detected by immunoblotting using mouse monoclonal anti-DAPK antibody (BD Biosciences).

2.16.2 Co-immunoprecipitation of endogenous MAP1B with Transfected HA-tagged DAPK

A375 cells were transfected for 24 hours before lysis with mammalian cell detergent lysis buffer as above. Bi-directional immunoprecipitation was performed as above using 2µg goat polyclonal anti-MAP1B antibody N19 (sigma) or 2µg Anti-HA 3F10 rat monoclonal antibody (Roche) immobilised per 20µl Protein G-Agarose beads. Co-precipitated proteins were detected by immunoblotting using anti- DAPK (BD Biosciences) and anti MAP1B (AA6) antibodies.

2.16.3 Co-immunoprecipitation of Endogenous MAP1B with Endogenous DAPK *form A549 Cells*

A549 cells were grown to 80% confluency before lysis with mammalian cell detergent lysis buffer. Bi-directional immunoprecipitation of MAP1B and DAPK was performed using 2µg goat polyclonal anti-MAP1B antibody N19 (sigma) or 2µg Anti-DAPK (BD Biosciences) mouse monoclonal antibody (Roche) immobilised per 20µl Protein G-Agarose beads. Co-precipitated proteins were detected by immunoblotting using anti- DAPK (BD Biosciences) and anti MAP1B (AA6) antibodies.

2.17 Radioactive GST-DAPKcore Kinase Assay.

100ng of p21 (positive control) or a titration of N126 was mixed into kinase buffer (10mM 32P-ATP, 50mM HEPES, 50mM KCl, 10mM MgCl2, 0.2mM EDTA 1mM DTT at pH 7.5) containing purified kinase fraction E2. Samples were incubated at

30C for 30 mins before separation by SDS-PAGE. The extent of phosphorylation was visualised by autoradiography of gels followed by scanning using a phosphoimager (Amersham) to allow electronic quantitaion of radioactive band intensities.

2.18 Tandem Ion Exchange / Gel Filtration Chromatography

Cell culture, lysis and preparation in addition to ion exchange chromatography experiments were performed by Dr J Fraser. Gel filtration experiments were jointly performed by Dr T. Hupp and myself.

MAP1B and DAPK containing complexes from A549 cells were isolated using Ion exchange chromatography followed by gel filtration. 4 13.7cm tissue culture plates of cells were grown to 80% confluency, harvested, resuspended in 3ml lysis buffer (25mM HEPES pH7.4, 1mM DTT, 500mM ng to Kcl, 10% glycerol and 1% triton X with 1 X protease inhibitor cocktail (Roche)) and lysed by 3 X freeze-thaw cycles followed by passage through a fine gauge needle. The lysate was cleared by gentle centrifugation at 1000rpm for 5 min at 4C and the supernatant diluted with 20 mls buffer A (25mM HEPES pH7.4, 1mM DTT, 10% glycerol with 1 X protease inhibitor cocktail) to achieve a final KCl salt concentration of ≈50mM.

2.18.1 Ion Exchange

Samples were loaded onto a 5 ml column and eluted by 10 column volumes of 0 to 1M linear gradient KCl running buffer at 0.5ml/min into 1ml fractions. The elution profiles of MAP1B and DAPK was determined by immunoblotting.

2.18.2 Size Exclusion

MAP1B and DAPK positive fractions 36 – 41 (inclusive) were pooled and concentrated using a 30KDa spin column Centricon filter devise (Millipore) at 500g for 30 mins. The resulting concentrated sample was loaded onto a column for gel filtration at 0.5ml/min into 1ml fractions. The protein in each fraction was concentrated using TCA-precipitation followed by resuspension of the pellet in 20µl of sample buffer. Fractions were then analysed by immunoblotting.

2.19 Microtubule Polymerisation Cycling

137 mm plates of 80% confluent cells were used to prepare microtubule complexes by temperature dependent polymerisation/depolymerisation cycling. Cells were harvested in 2.5 ml homogenisation buffer HB (0.1 M MES, 0.5 mM MgCl2, 1 mM EGTA) containing phosphatase inhibitor 10 mM β- glycerophosphate and protease inhibitor cocktail (Calbiochem). Cell lysis was achieved by addition of Triton X-100 to a final concentration of 0.1% for 30 min at 4oC on a rotor and then the lysates were cleared by 2 x 20 min 13,000g centrifugation. GTP was added to cleared lysates (final concentration 1 mM) to allow microtubules to form at 37oC for 30 min. Microtubules were then pelleted by centrifugation at 13,000g. for 15 min, the supernatant removed and the microtubules in the pellet depolymerised in 1 ml HB for 40 min at 4oC. Microtubule polymerisation and depolymerisation was performed a further 2 cycles to obtain a purified microtubule preparation.

2.20 2D Differential in-Gel Electrophoresis (DIGE) of Purified microtubules

2.20.1 Creation of Tetracycline DAPK-*inducible A375 cells.*

A375 cells were stably transfected with pCDNA6Tet vector expressing the tet operon (Invitrogen) using the blastocidin resistance marker present in the plasmid. Selection was allowed to proceed for 2 weaks to allow sufficient growth of clones. 10 independent clones were then picked by pipette tip and cultured separately. To test the clones for tet repressor expression, native DAPK was subcloned into pDEST30 expression vector under control of the tet operon. This construct was then used to screen clones for stable expression of tet repressor. To this end 500ng DAPK was transfected into the panel of 10 independent clones in 6 well plates for 24 hours before harvesting, cell lysis and analysis by western blot. Expression of DAPK then indicated that tet repressor was not present in sufficient amounts to block transcription and was therefore discarded. Of the 10 clones tested, 2 clones (Tet3 and Tet3) effectively repressed DAPK expression. Tet4 was isolated for further manipulation (Figure 2.2a).

Clone Tet4 was stably transfected with DAPK pDEST30 using by selection using the geneticin resistant marker. Selection was allowed to proceed for 14 days to allow sufficient growth of clones. 6 independent clones were then picked by pipette tip and screened for DAPK-inducibility using 5μg.ml tetracycline. Of the 6 clones tested 2 expressed DAPK after 24 hours induction (Figure 2.2b Clones TD1 and TD2). DAPK expression can be efficiently induced in both clones by treatment with 5μg/ml tetracycline for 24 hours, with no detectable background DAPK expression (Figure 2.2c). Clone TD2 was isolated for use in DIGE experiments.

2.20.2 Preparation of Microtubules from Tetracycline Induced Cells for DIGE Analysis

10 13.7cm plates of clone TD2 were grown to 50% confluence. 5 plates were induced by 5μg/ml tetracycline for 24 hours and 5 treated with vehicle control to act as a reference sample. Cells were harvested and processed for 3 rounds of microtubule polymerisation.

2.20.3 DIGE Analysis: Isoelectric Focusing, SDS-PAGE separation, Flourescent Dye Labeling and Scanning.

DIGE analysis was conduced by Dr R. Burchmore at the functional genomics department, Glasgow University.

Briefly, Reference and induced samples were acetone precipitated and resuspended in 2D-gel buffer using mass spectrometry grade reagents. Induced sample was labeled by Cy5 die and the reference sample with Cy3 dye. Samples were then pooled and separated by SDS-PAGE in an 8% tris-glycine gel. 2D protein profiles were visualised by fluorescent scanning before automated spot intensity calculation.

2.21 Cell Growth Assay

The required cell lines were grown in 6-well plates and transfected with 2μg of plasmid consisting of; 1μg of the designated DAPK construct, 1μg of the designated MAP1B construct or 1μg of control vector. 48 hours later each well was washed with PBS and the cells trypsinised for 5 min at room temperature. After addition of serum containing media to stop the trypsin, cells were carefully and thoroughly suspended before titration onto 10cm plates in selective media for 7 days, replenishing the media after 3 days. After selection and growth of resistant cells, plates were washed,

fixed in methanol at -20C for 10mins and stained with 1X Giemsa (Sigma) for 30min to visualise colonies. The extent of cell growth was quantified by densitometric analysis of scanned images. Plates were scanned using a flat bed scanner and the mean staining intensity determined by scnimage software.

2.22 Cell Viability Determination by Trypan Blue Exclusion

Cells were transfected for 24 hours before harvesting by trypsinisation. Cells were diluted to approximately 1*10^6 cells/ml in PBS before addition 1:1 to 0.4% trypan blue solution. 20µl of cells were then loaded into the hemocytometer before immediately counting the total number of cells and the number of trypan blue positive cells to calculate percentage cell viability.

2.23 Transient MAP1B Knock-Down Using siRNA

For transient MAP1B knock-down cells were seeded at half density (1X105) per 30mm diameter plate. MAP1B siGENOME SMARTpool siRNA was obtained from Dharmacon. 120 picomoles of siRNA oligos were transfected per 30mm plate with 2µl of Lipofectamine for 48 hours. Non-targeting siCONTROL was used as a negative control in siRNA experiments.

2.24 Cell Cycle Analysis

Cell cycle analysis experiments were jointly performed by Dr K Samuel and myself.

HCT116 cells were co-transfected with the indicated amounts of full length native DAPK and full length native MAP1B expression vectors for the indicated times.

Cells were co-transfected with the cell surface marker CD-20 (at 1:5 DNA ratio) to allow efficient selection of the transfected population using anti CD20-FITC conjugated antibody (Caltag Biotech). After transfection adherent cells were thoroughly resuspended by trypsination and pooled with floating cells, washed stained with FITC-conjugated anti CD20 antibody and fixed with 50% ethanol suplimented with 10% FCS overnight. After anti-CD20 staining and fixation, cells were treated with RNase A and simultaneously stained with propidium iodide for 30 minuets at 37C to stain cell nuclei. CD20 positive cell nuclei were gated and sorted according to FL height using a Becton Dickinson FACSCalibur flow cytometer to visualise cell cycle profiles. Cell Quest and quantfit software was used to determine the percentage of nuclei at each stage of the cell cycle.

2.25 Apoptosis Assays

2.25.1 AnnexinV Assay

Cells were transfected with the indicated amounts of DNA for the indicated times. Following transfection, adherent cells were thoroughly resuspended by trypsinisation and pooled with floating cells before washing and staining with APC-conjugated annexin V and propidium iodide (Bender Medsystems) as per manufacturers instruction. Phosphatidylserine positive cells were visualised using using a Becton Dickinson FACSCalibur flow cytometer on the FL 4 channel

2.25.2 TUNEL Assay

The TUNEL assays were performed by Dr C. Stevens.

HCT116 cells were grown directly on cover slips and transfected with the indicated amounts of expression vectors for 24h. Following transfection cells were fixed in 1% paraformaldehyde for 10min at room temperature. Apoptotic cells were labelled using Apoptag Plus Fluorescein In-Situ Apoptosis Detection Kit S7111 (Chemicon International) according to the manufacturers instruction and viewed by fluorescence microscopy.

2.26 Autophagy Assays

2.26.1 GFP-LC3 Cleavage Assay

Autophagy was detected in a HEK-293 cell line stably expressing the autophagy marker GFP-LC3 (Kochl et al., 2006). HEK293-LC3 cells were a gift from Sharon Tooze (CRUK, London). For LC3 cleavage analysis, cells were transfected with the indicated combination of expression vectors for the indicated times susing 3µl of lipofectamine2000 transfection reagent per total microgram of DNA. Cells were then lysed using RIPA lysis buffer and GFP-LC3 protein was detected by western blot using anti-GFP antibody. The ratio of GFP-LC3-I to lipidated GFP-LC3-II was quantified using scnimage densitometry software.

For assay of autophagy after MAP1B siRNA, HEK-LC3 cells were seeded at half density and 25 picomoles per cm2 of MAP1B siGENOME SMARTpool siRNA oligos were transfected using 0.4µl/cm2 Lipofectamine2000 for 32 hours. After 32 hours siRNA knock-down, growth medium was changed and cells were transfected for a further 32 hours with 100ng/cm2 of each of the indicated expression vectors with 0.8µl/cm2 of Lipofectamin2000. Cell lysates were assayed for LC3 cleavage as above.

2.26.2 GFP-LC3 Foci Assay

Autophagosomes were also counted in fixed and stained GFP-LC3 stably expression HEK-293 cells, providing a separate quantifiable marker of autophagy. Cells were transfected with the indicated combination of expression vectors for 32 hours using 3µl of lipofectamine2000 transfection reagent per total microgram of DNA. Separate cultures were starved by replacement of growth medium with Earle's balanced salt solution for 3 hours.10 random fields were analysed per cover slip. In each field the total number of cells was counted. The total number of autophagosomes in each field was visualised by increasing the fluorescent threshold using Leica SP5 confocal microscope and software. This highlighted the very intense GFP fluorescent foci, facilitating counting. The extent of autophagy induction was determined as the total number of autophagosomes per field per total number of cells per field.

2.27 Membrane Blebbing Assays

2.27.1 Blebbing Assay in Co-Transfected HCT116 Cells

HCT116 or A375 cells were used for blebbing analysis in co-transfected cells where the indicated MAP1B proteins and GFP-tagged DAPK were co-transfected for 24 hours. 200 co-transfected cells were detected by dual imunofluorescent staining and scored for blebbing morphology along transverse sections of cover slips. Cells were fixed with 4% paraformaldehyde in PBS for 10 minuets, washed and blocked with antibody dilution buffer. Fixed cells were simultaneously blocked and membrane-permeabilised using antibody dilution buffer (PBS with 0.1% Triton and 10% horse serum) to allow entry of primary antibodies into the cells. Full length MAP1B was detected using mouse monoclonal AA6 (1:200), V5-tagged MAP1B V1 and V2

proteins were detected using mouse monoclonal anti-V5 antibody (Invitrogen 1:1000), and GFP-tagged DAPK detected with rabbit anti- GFP (Abcam ab290 1:2000). After incubation of primary antibodies for 1 hour cells were washed and stained with Alexa conjugated secondary antibodies alexa568 anti-mouse and alexa488 anti-rabbit before scoring with a standard fluorescent microscope using a 100X objective.

2.27.2 Blebbing Assay in A375 Cells

In A375 cells HA-DAPK WT, HA-DAPK K42A or HADAPK ΔCaM was transfected for 24 hours and cells were scored for membrane blebbing morphology along converse sections of cover slips using a standard fluorescent microscope. Cells were fixed with 4% paraformaldehyde in PBS for 10 mins before simultaneous blocking and membrane permeabilisation. Transfected cells were visualised using anti-HA antibody 3F10 (1:50) and anti-rat alexa488 conjugated secondary antibody (1:100).

2.27.3 Blebbing Assay in after MAP1B siRNA in A375 Cells

For blebbing analysis after transient MAP1B knock-down in A375 cells, cells were seeded at half density and 25 picomoles of MAP1B siGENOME SMARTpool siRNA oligos were transfected per 1cm2 coverslip using 0.4µl of Lipofectamine for 48 hours. After 48 hours knock-down the growth medium was changed and cells were transfected for a further 24 hours with HA-DAPK constructs before fixing and staining. Non-targeting siRNA was used as a negative control.

2.28 Immunofluorescence Staining and Cell Morphology Assessment

2.28.1 Quantification of DAPK-*induced Cell Morphology Changes*

A375 cells were fixed with 3% formaldehyde and 0.2% glutaraldehyde in PBS for 10 min at 37oC before simultaneous blocking and membrane permeabilisation in antibody dilution buffer for 30 mins. Primary antibodies were used at the following concentrations MAP1B (AA6) 1:200 and HA (Rat monoclonal 3F10 Roche) 1:50 in antibody dilution buffer for 1 hour at room temperature. Fluorescent highly cross-adsorbed Alexa dye-conjugated alexa488 anti-rat and alexa568 ant-mouse secondary antibodies were diluted 1:100 in antibody dilution buffer and incubated at room temperature for 45 mins. F-actin was stained with alexa633 conjugated phalloidin. Cells were visualised using a Leica SP1 or SP5 confocal microscope using the 100X or 63X objective lens, respectively.

2.28.2 Imunofluorescent Staining of A375 Cell Cytoskeletons after Partial Cytplasmic Extraction

A375 cell cytoskeletons were visualised by partial cytoplasm extraction using fixative supplemented with detergent (3% paraformaldehyde and 0.01% triton in PHEM Buffer - 60 mM Pipes, 25 mM Hepes, 10 mM EGTA, 2 mM MgC12 – pH 6.9). After transfection HA-DAPK or GFP and full length MAP1B or dsRED for the indicated times cells were fixed for 15 minutes at 37C, washed with PBS and then incubated at room temperature for 30 minutes with antibody dilution buffer (10% normal horse serum and 0.1% triton in PBS) to block. Blocked cells were then incubated for 1 hour at room temperature with the following primary antibodies in antibody dilution buffer: rat anti-HA 1:50 (3F10 Roche), rabbit anti-tubulin 1:100 (Abcam ab6046), and mouse anti-MAP1B 1:200 (Mouse monoclonal AA6 Sigma). After washing with PBS the following highly cross-adsorbed fluorescent Alexa dye

conjugated secondary antibodies (Invitrogen) were diluted 1:100 and bound for 45 mins at room temperature: alexa488 anti-rat, alexa405 anti-tubulin and alexa568 anti-mouse. F-actin was stained with alexa633 conjugated phalloidin. Cells were visualised using a Leica SP5 confocal microscope using the 63X objective lens.

Antibody	Supplier	Western Blot	Immunoflourescence	ELISA
HRP-Anti Mouse	Dako	1:1000		1:1000
HRP-Anti Rabbit	Dako	1:1000		1:1000
p53 Serine20 (7F7)	Dr A Craig	1:2000		1:2000
p53 (DO1)	Borek	1:2000		1:2000
p53 (ICA9)	Borek	1:1000		1:1000
DAPK	BD Biosciences	1:500		1:500
MAP1B (AA6)	Sigma	1:500	1:200	1:500
V5	Invitrogen	1:5000	1:1000	1:5000
HA (3F10)	Roche		1:100	
GST	Sigma	1:5000		1:5000
GFP	Abcam	1:2000	1:1000	
Tubulin	Abcam	1:1000	1:200	
Actin	Sigma	1:5000		
DAPK2	Abcam	1:1000		
DAPK3	Abcam	1:1000		
p21	Oncogene Biosciences	1:1000		
Bax	Santa Cruz	1:1000		
Alexa Flouroflour Conjugated	Invitrogen		1:100	

Figure 2.1 Table of Antibodies including supplier details and dilution factors used for Western blotting, immunoflourescence and ELISA assays.

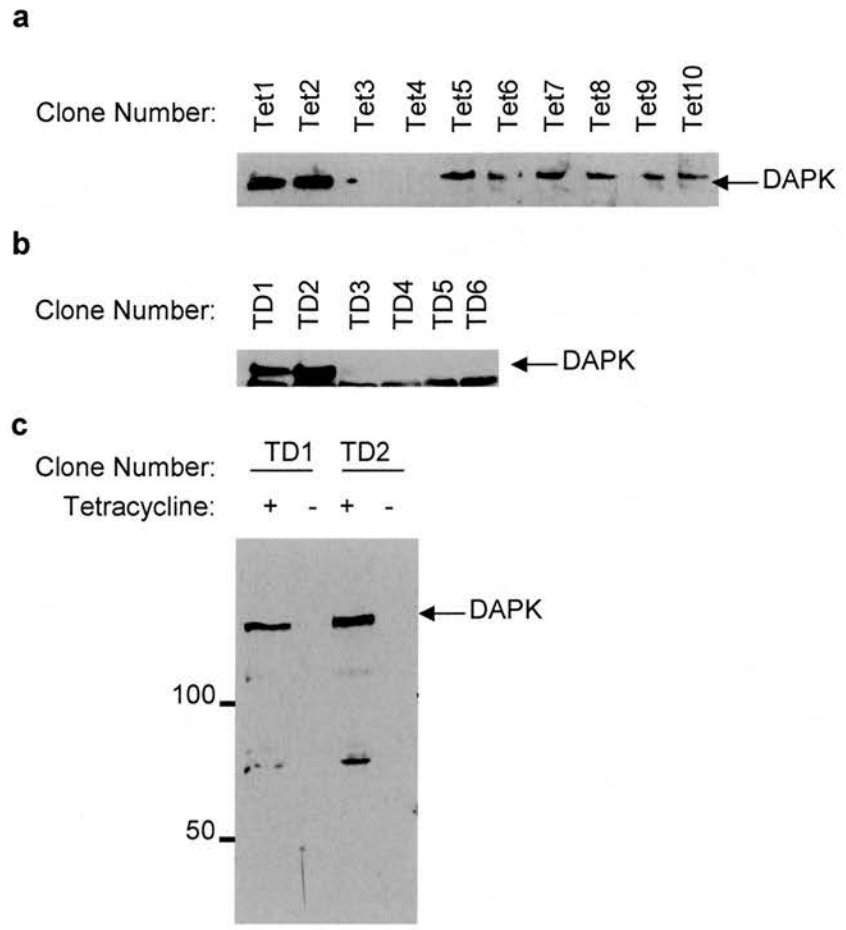

Figure 2.2 Creation of a Stable DAPK-Inducible Cell Line From A375 Cells. (**a**) Screen of clones Tet1 – 10 for stable expression of tet repressor. Clones were transfceted with 500ng of DAPK in 6 well plates. Clones Tet3 and Tet4 efficiently blocked ectopic DAPK expression. (**b**) Screen of subclones derived from Tet 4 for stable inducibility of DAPK. Subclones were treated with 5μg/ml tetracycline for 24 hours. DAPK expression could be induced in subclones TD1 and TD2. (**c**) Subclones TD1 and TD2 did not express background DAPK. Cultures were treated with 5μg/ml tetracycline for 24 hours.

Chapter 3

3.1 Introduction

DAPK is a 160kDa serine/threoine calcium-calmodulin regulated kinase with a multi-domain structure. DAPK is able to reduce cancer growth and metastasis, and is often deactivated by epigenetic silencing during the development of many cancer types. A wide array of signaling pathways can activate DAPK including death receptor pathways, cytokines, ceramide, the ERK/MAPK and JUNK/SAPK pathways, the p53 pathway and physical detachment from the extracellular matrix. Through DAPK, these signals initiate type I and/or type II cell death programs characterised by morphological changes such cell membrane blebbing and nuclear fragmentation and/or nuclear condensation and autophagosome production.

Although DAPK activation by a multitude of signals has been well documented, there is an inadequate understanding of the genetic and biochemical mechanisms that underlie this activity. In order to understand DAPK-induced tumour suppression pathway more fully, it is required to define new interaction partners. The kinase domain of DAPK is elemental for integration of DAPK-mediated tumour suppression where post-translational modification of target substrates by DAPK integrates numerous signaling events with their effective response to aberrant cell growth. Therefore identification of novel DAPK kinase domain binding proteins and

substrates would expand on our understanding of the mechanisms of the diverse functions of DAPK.

3.2 Results

3.2.1 Purification and Characterisation of Active Recombinant DAPK Kinase Domain.

Phage peptide display was chosen as a technology to find novel proteins that interact with the kinase domain of DAPK. This approach leads to enrichment of short linear peptides that interact specifically with their target. The primary structure of these could then be used to deduce *in-vivo* associating proteins and hence draw inferences about the mode of DAPK action in tumors. In order to ensure that the interacting peptides would be representative of proteins that could interact with DAPK *in-vivo*, it was imperative to generate a highly purified, active and hence conformational bait protein. Highly purified protein is required to limit the possibility of phage binding to contaminants and active protein is indicative of conformational and stable protein that is folded identically to how it would be folded *in-vivo*. To achieve this, GST-tagged recombinant DAPK kinase domain amino acids 1-274 (GST-DAPKcore) was subcloned into *E.coli* and Sf9 insect cell expression vectors using the Gateway destination vector system. After host transformation and gene induction, the respective protein was purified from the cell lysates on glutathione beads. A representative purification is shown in Figure 3.1a, GST-DAPKcore protein from lysates derived from Sf9 cells infected with GST-DAPK-core virus (Figure 3a, lanes 1-2) was purified from a Glutathione column (Figure 3a, lanes 4 and 5). Lane 3 is control lysate from non-infected cells and lanes 6-9 show wash and flow through

contaminants. Coomassie gel staining ensured that GST-DAPKcore was of a high concentration and purity.

Next the purified kinase was examined to determine if the conformational integrity of the enzyme was intact. The GST-DAPKcore fractions were tested for both kinase activity and peptide-binding capacity. To assess the activity of the fractions, a p53-tetramer kinase assay was used. Tthis non-radioactive kinase assay was developed based on using phospho-protein specific antibodies that detect phosporylation of p53 at Ser20. DAPK was shown to phopshorylate Ser20 to the same level as classic Ser20 kinases such as CHK2 as p53 has significant homology to the DAPK consensus phosphorylation site(Craig et al., 1999a; Craig et al., 1999b). A titration of GST-DAPKcore fractions (arbitrarily designated fractions E1 and E2) in this assay demonstrated that both fractions could stimulate Ser20-site phosphorylation of p53 (Figure 3.1b, lanes 2-5 and 7-10). The background bands observed without kinase (Figure 3b, lanes 1 and 6) are present because the monoclonal antibody used has a non-phospho-epitope component to its specificity whilst phosphorylation stabilises the antibody binding to its phospho-epitope (34). When various purified DAPKcore fractions were tested, using different N-terminal tags and expression systems, it was found that GST-DAPKcore from insect *Sf9* cells has the highest specific activity (Figure 3.1c, lane 4 vs. lane 1) and it is this fraction that was used for further analysis. The specific activity of purified kinase was higher when prepared form insect cells as compared to the preparation from bacteria (Figure 3.1 c). This is because insect cells have protein folding machinery and chaperones that are more closely related to mammalian cells than bacteria. Thus, protein expressed from insect cells is more likely to be in a native conformation. Also, GST-tagged kinase was

more active than his-tagged. This is because GST is able to recruit folding machinery that recognises GST to the expressed protein.

As it was planned to elute peptides from GST-DAPKcore not only with ATP (to dissociate ATP-binding affected substrates) but also with acid (to dissociate ATP-independent binding substrates), GST-DAPKcore protein was tested for ability to bind to p53 within the ubiquitin signal in the DNA-binding domain of p53 (Craig et al., 2007). This motif forms a docking site for certain calcium-calmodulin kinase superfamily members including DAPK(Craig et al., 2007). When p53 was coated onto a solid phase, there was a dose-dependent binding of GST-DAPKcore to p53 (Figure 3.1a). Further, when GST-DAPKcore was coated onto a solid phase, dose-dependent binding of p53 to the kinase was detected (Figure 3.1b) and glutathione captured GST-DAPKcore also was able to bind to p53 in a dose-dependent manner (Figure 3.1ci). When the *BOX-V* docking site peptide (which binds MDM2 and DAPK/CHK1) from the core domain of p53 was added to reactions, binding of GST-DAPKcore protein to p53 was stimulated (Figure 3.2b). Also, using this system addition of ATP dissociated p53 from the antibody-captured DAPK (Figure 3.2.cii). These data demonstrated that the purified recombinant GST-DAPKcore bound to the solid phase is active in both substrate phosphorylation and in peptide-docking when bound to the solid phase. Therefore this fraction was used as a bait to select for peptide binding ligands.

3.2.2 Elution of different classes of peptide motifs from the DAPK kinase domain.

Active and conformationaly stable GST-DAPKcore was adsorbed onto the solid phase. Random peptides from an extensive combinatorial library were allowed to interact and were then eluted in cycles with either ATP cofactor or removed with acid. Isolated phage were then propagated in *E.coli* and reintroduced onto fresh kinase domain for subsequent biopanning (Figure 3.3). The biopanning process was repeated three times, as previous studies have shown that one or two biopans yield an unmanageable number of peptides ranging from lower binding affinities. Conversely, four or more biopans generates very few peptides with only very high binding affinities (Burch et al., 2004a; Burch et al., 2004b). Therefore threee biopans were used. After selection and sequencing the amino acid sequence from each peptide was input into a BLAST search configured to check for small nearly exact sequences or motifs present in all known human proteins.

Using ATP co-factor elution two independent phage clones were isolated that displayed peptide with significant homology to one protein in the database, transcription factor Sp1 (SP1) which as a sequence specific DNA-binding protein and transcription factor (Figure 3.4a. Peptides 1 and 2, Motif: T/S.PSPLALL). Secondly, two identical phage were isolated displaying peptide SPPSNLIPPTLR (Figure 3.4a. Peptides 3 and 4) that has no significant homology to any known human protein sequence. Lastly, two classess of independent phage with separate sequences were isolated that combined to give the motif TXXHLLXSA (Figure 3.4a Peptides 5 and 6). However, using the Emotif search engine it was not possible to find a human protein in the database containing this motif. The acid eluted phage

displayed peptides with homology to Microtubule Associated Protein 1B (MAP1B), PML (promyelocytic leukaemia protein), and RPL3 (ribosomal protein L3) (Figure 3.4b Peptides 1-3). Also isolated were 3 independent phage with no significant homology to sequences in the NCBI database (Figure 3.4b Peptides 4-6) (see section 2.7).

3.2.3 Characterisation of the GST-DAPKcore to MAP1B Peptide Interaction

The phage display biopanning procedure lead to the isolation of 5 independent phage displaying significant homology to sequences in the NCBI protein database. Two independent phage sequenced had homology to the SP1-4 family of transcription factors eluted with ATP. Three separate peptides were eluted with acid with homology to MAP1B, PML or RPL3. During the course of these studies a report was published showing that DAPK-3 can localise to PML bodies in interferon treated cells (Kawai et al., 2003). Given that there is such a high degree of sequence similarity between the kinase domains of DAPK1 and DAPK3 there is a possibility that this result represents a false positive, or it could be that PML interacts with both DAPK and DAPK3. However, because this is not a novel interaction PML was not evaluated as a potential DAPK binding protein. Ribosomal protein L3 is a very poorly characterised protein with an unknown function and so development of assays to characterise a DAPK to RP3 interaction would be difficult. In hindsight, the possibility of an interaction between DAPK and RPL3 is very interesting because it implies an interface with DAPK and the translational machinery. However, this has only recently been highlighted as important by research papers published late during the course of these studies (Anjum et al., 2005; Schumacher et al., 2006).

The possibility of an interaction between SP1-4 and DAPK is an interesting prospect that warrants further investigation. However, the SP transcription factors are primarily confined to the cell nucleus whereas DAPK1 is confined to the cytoplasmic compartment. This, in addition to the fact that DAPK3 is a nuclear protein that could be a more likely binding partner led us to decide that further study would be confined to the characterisation of a possible interaction with MAP1B. MAP1B is a cytoplasmic protein known to interact with microtubules and microfilaments where it influences cytoskeletal dynamics. This theoretically puts MAP1B in the same cellular compartment with DAPK. In addition to this, MAP1B, like DAPK, is primarily expressed in the brain where it is known to influence cell fate decisions. There were no direct links established between MAP1B and the DAPK family prior to these studies.

The isolated phage peptide with homology to MAP1B maps to the N-terminal region of human MAP1B at position 46-57. This region is conserved throughout higher vertebrates were the amino acid chemistry similarity is EH(L/V)(R/K)X(P/A)(I/V/L), where X is not conserved in *xenopus* or zebrafish (Figure 3.5). However the fact that the protein chemistry of this motif is conserved in vertebrates is unsurprising because the entire MAP1B protein is also highly conserved in these species, with the exception of the N-terminal 30 or so amino acids that are less conserved in *xenopus* and zebrafish. What is interesting is that the four center amino acids in this motif (HLRR) are conserved down to lower invertebrates including fruit flies in an area of otherwise unconserved amino acid sequence at the N-terminus. This gave further confidence that the phage peptide screen had isolated an interaction motif with homology to a conserved interaction site on MAP1B.

An ELISA based assay was used to characterise the interaction of the phage peptide (Φ-peptide) and the corresponding MAP1B homologous peptide with GST-DAPKcore (Figure 1.6). Biotinilated synthetic peptides were obtained for use in an ELISA based assay. First, an optimisation experiment was performed to calculate the optimal peptide concentrations for specific binding (Figure 3.6a). GST-DAPKcore binding to a non-relevant control peptide (NR), phage peptide with homology to MAP1B (Φ; LPFEEHLRRPVG) and the naturally occurring peptide sequence in MAP1B itself (1B, IVTEEHLRRAIG) were titrated and assessed for binding. Using this system it was determined that using 100ng of peptide provided the optimal resolution of differential binding. GST-DAPKcore binding could be detected to Pep Φ and Pep 1B, relative to the control Pep NR (Figure 1.6b, right 3 bars vs GST-only control left three bars). These data confirm that GST-DAPKcore can interact with peptides containing the core EEHLRRx(I/V)G motif, and that this is not due to non-specific interaction with GST or with contaminants.

3.3.4 Cloning MAP1B Constructs into Expression Vectors

Having determined that the MAP1B peptide could bind specifically to GST-DAPKcore it was decided to clone MAP1B protein from human tissue. Cloned MAP1B in a protein expression plasmid would be an invaluable reagent to assess the ability of naturally occurring peptide to bind GST-DAPKcore and to elucidate any functional role that this interaction may have *in-vivo*. MAP1B has two known splice variants expressed in human cells designated transcript variants 1 (V1) and 2 (V2). Protein isoform 1, is derived from transcript variant 1 which has an extra exon designated exon 3A. Variant 1 therefore gives rise to protein that is 126 amino acids

longer than transcript variant 2 that lacks this 5' exon. These 126 amino acids are located at the N-terminus or variant 1 and are designated N126.

A previous research paper indicates that rat transcript variant 1 may play a role in cell fate decisions in developing brain because it induces apoptosis in cultured rat hippocampal neurons. This effect is specific to rat variant 1 because rat variant 2 expression does not induce apoptosis. This is of interest because the putative EEHLRRx(I/V)G interaction site uncovered by the phage display screen is only present in variant 1, being positioned within the N126 region. This would suggest that DAPK interaction would be different with respect to isoform 1 and isoform 2 and therefore fragments of MAP1B were cloned corresponding to both splice variants. Fragments were cloned from 5' position 1 (for V1) and 5' position 378 (for V2) to an arbitrary 3' location 4101. This 3' location was chosen because it corresponds to the position of the rat clones created by Uchida (Uchida, 2003). Also, cloned was a miniprotein corresponding to the N-terminal amino acids (N1-126) of V1. Human fetal brain RNA that has a high abundance of MAP1B was chosen as template using the indicated primers for cloning (Figure 1.7a). Fragments of the indicated sizes were obtained (Figure 1.7b) by RT-PCR and cloned into the Gateway system for characterisation. The full length sequence of each clone was verified (Figure 1.7c).

The full length MAP1B gene encodes a polyprotein precursor that is post-translationaly processed into heavy chain and light chain forms of MAP1B (Figure 3.8). The heavy chain (HC) contains a microtubule binding (MT) domain, whereas the light chain (LC) has an actin binding and oligomerisation domain (A/O) in

addition to an independent microtubule binding domain (MT). An expression vector containing full length human MAP1B gene was obtained from a commercial source because it was difficult to clone in house owing to its large size. This clone is present in an expression vector that leads to production of full length native MAP1B protein when transfected into cells (Figure 3.8 lane 2). Fragments V1, V2 and N126 were sub-cloned into expression vectors that lead to the expression of C-terminal V5 viral epitope-tagged fusion protein when transfected into cells (Figure 3.8 lanes 3-5). Transfected V1 and V2 lead to expression of multiple bands corresponding to the predicted size (approx. 170kDa) and also to a faster migrating band (approx. 100 kDa). This indicated that these constructs were sbject to post translational modification. Also, V1 transfection lead to expression of an additional higher molecular weight band (approx. 250 kDa) indicating that V1 is differentially modified.

3.2.5 Characterisation of DAPK and MAP1B Protein Interaction *In-vitro* and in Cells

The isolated phage peptide and peptide corresponding to the human MAP1B sequnec specifically interacted with purified GST-DAPK$_{core}$ in the solid phase *in-vitro*. MAP1B gene fragments were therefore cloned into expression vectors to produce naturally occurring mini-protein to assess for binding to DAPK proteins. *In-vitro* binding assays were performed using GST-DAPK$_{core}$ and MAP1B protein synthesised in transfected human HCT116 cells including; full-length human MAP1B, V5-tagged MAP1B-V1 (amino acids 1-1367, containing the N-terminal EEHLRRx(I/V)G motif), V5-tagged MAP1B-V2 (without the N terminal EEHLRRx(I/V)G motif), and N126 (containing the N-terminal EEHLRRx(I/V)G

motif). Full length native DAPK was separately expressed in HCT116 cells and precipitated onto the solid phase using anti-DAPK monoclonal antibody. Stable binding to antibody-captured DAPK was detected with full-length MAP1B, MAP1BV1, and N126 (Figure 1.9a). However, less binding was observed to MAP1B-V2, which lacks the N-terminal EEHLRRx(I/V)G motif. The difference in binding affinity between MAP1B-V1 and MAP1B-V2 was also demonstrated using a co-immunoprecipitation assay with lysate from co-transfected human cells. Co-transfection of V5-tagged variants of MAP1B with untagged DAPK was followed by immunoprecipitation of MAP1B with anti-V5 sepharose beads and assay of the resulting precipitate by immunoblotting for DAPK. Relative to empty vector controls, MAP1B-V1 bound to DAPK (Figure 3F, lane 4 vs 3) to a higher extent than MAP1B-V2 (Figure 3F, lane 7 vs 6) again suggesting that the primary interaction site between DAPK and MAP1B is on the N-terminal domain of the MAP1B protein.

Endogenous MAP1B can be isolated in complex with HA-tagged DAPK by immunoprecipitation with an anti-HA antibody (Figure 3.9c). AA6 antibody was used to immunoprecipitate MAP1B from lysates prepared from A375 melanoma cells transfected with HA-DAPK. Immunoblotting of the precipitated MAP1B protein (Figure 3.9c, lanes 9 and 10) showed that most of the HA-DAPK was present in the bound fraction (Figure 3.9c, lane 10 vs 9 compared to lanes 6 and 5). Equally, HA-antibody was used to immunoprecipitate HA-DAPK from lysates (Figure 3.9c, lanes 7 vs 8) and most of the MAP1B was present in the bound fraction (Figure 3.9c, lane 8 vs 7 compared to lanes 3 and 4). Actin was not present in any of the immunoprecipitates (Figure 3.9c, lanes 7-10), which might be surprising given that the documented role for DAPK involves its association with actin. However, a

possible explanation for this is that during gentle lysis conditions used to preserve the protein-protein complexes, some microfilaments are not disrupted and hence any DAPK associated with the actin cytoskeleton will not be present in the centrifuge-cleared soluble lysate. Therefore only cytoplasmic associated pools were available for coimmunoprecipitation. Tubulin levels could not be determined in the precipitated fractions because of interference with IgG heavy chain (both approx. Mr 50 kDa).

3.2.6 Purified Recombinant N126 is Phosphorylated by GST-DAPKcore *In-vitro*

Recombinant DAPKcore was able to bind to the MAP1B peptide deduced from phage isolated during the interaction screen (Figure 3.6). This peptide mapped to the N-terminus of transcript variant 1 (V1) of MAP1B, and subsequent binding assays showed that full length recombinant DAPK was able to bind to this region (Figure 3.9 a and b). During the phage peptide screen, a MAP1B homologous peptide was eluted from GST-DAPKcore by acid and not by ATP suggesting that this interaction site could be a docking area not directly phosphorylated by DAPK. In addition to this there are no serine or threonine phosphoaccepters on the phage peptide or the equivalent area on MAP1B. The N-terminus of MAP1B-V1 is an unordered linear region that is evolving relatively quickly as compared to highly conserved areas further down stream that are conserved from insects (Figure 3.5). This suggests that the N-terminus of MAP1B could be a regulatory region, possibly involved in modifying MAP1B response to signalling events (See Section 1.9). Often, linear regulatory domains of proteins are post-translationaly modified by kinases to effect signal transduction. Therefore, the N-terminus of MAP1B-V1 (N126) was assessed

for ability to be phosphorylated by DAPK. This was facilitated by the fact that N126 had been already cloned in house (Figure 3.8) and so could easily be subcloned into a bacterial expression vector for rapid expression and purification given its small size.

His-tagged N126 was expressed in *E.coli* and purified using nickel beads and incubated with GST-DAPKcore in a kinase assay. Titration of N126 revealed that it was phosphorylated when 50ng was added to the reaction (Figure 3.10 a, lanes 5 and 6 – band highlighted by arrow). 100ng of p21 was used as a positive control that was efficiently phosphorylated by DAPK as previously reported (Craig et al., 2007; Fraser and Hupp, 2007). These data show that N126 can be phosphorlated by GST-DAPKcore *in-vitro* and suggest that MAP1B may be a substrate for post-translational modification by DAPK. However, this does not prove that DAPK can phosphorylate MAP1B-V1 in cells.

3.2.7 Isolation of High Molecular Weight Multiprotein Complexes Containing MAP1B and DAPK Using Ion Exchange and Gel Filtration Chromatography

The immunoprecipitation experiments detailed above involve transfection of either DAPK or both MAP1B with DAPK. Therefore, further experiments were devised in order to determine if endogenous proteins interact. A549 cells co-express large amounts of MAP1B and DAPK and so endogenous co-IP experiments were set up in these cells. Immunoprecipitation using mouse monoclonal anti MAP1B AA6 or mouse monoclonal anti DAPK resulted in efficient purification of the respective endogenous proteins (Figure 3.10 a). However, only a small amount of DAPK was reproducibly co-precipitated with anti-MAP1B and *vica-verca* only a small amount of MAP1B reproducibly with anti-DAPK. This suggests that only a small amount of

the endogenous proteins bind. This could indicate that the interaction between the two could be transient and therefore involve a small pool of the total MAP1B and DAPK. However, the fact that only a weak IP was obtained might be due to experimental reasons associated with co-IP experiments. For example the epitopes could be occluded or antibody binding could disrupt endogenous complex formation or the multi-protein complex might be disrupted from by buffers used for cell lysis. Another possibility is that MAP1B and DAPK complexes could interact with microfilaments that would remain insoluble during lysis. It should be noted that microtubule polymerisation is highly temperature dependent. Therefore this would not be the case with microtubules that are dissolved during lysis and as such any associating proteins are liberated. This could also be a reason for a weak co-IP, because if the endogenous DAPK and MAP1B interaction relies on polymerised tubulin it would be dissociated during lysis.

Because preparing a convincing immunoprecipitate with endogenous MAP1B and DAPK in complex was unsuccessful, it was assessed whether the two proteins could co-purify using chromatography, which would be suggestive that they can assemble into a stable complex. A549 small cell lung carcinoma cell lysate, which contains relatively large amounts of MAP1B and DAPK (Figure 4.2) was applied to an ion exchange column and eluted with an increasing salt gradient. DAPK broadly eluted from the column in fractions 10-21 (Figure 3.11b). In contrast MAP1B elution was confined to a peak in fractions 18-24. Endogenous DAPK and MAP1B proteins are therefore not in a stable complex in A549 cell lysate as they generally co-purify away from each other. This might explain, in part, why is has been difficult to isolate a stable endogenous MAP1B-DAPK protein complex by co-precipitation as the

abundance of interacting protein in lysates is relatively low. The broad elution of DAPK suggests it is heterogeneous with respect to charge or binding proteins. However, a portion of DAPK did co-elute with MAP1B and so fractions 18-21 were pooled based on the assumption that these could contain a stable DAPK-MAP1B complex. This pooled fraction was subsequently applied to a gel filtration column. After gel filtration, DAPK roughly eluted into two pools, the first corresponding to its monomeric molecular weight (3.11c Fraction 14) and the second in a higher molecular weight fraction that co-elutes with MAP1B (Figure 3.11c Fraction 9). MAP1B eluted into fraction 10 and into fraction 9. Interestingly fraction 9 had multiple immunoreactive bands migrating faster than the protein present in both fractions 9 and 10. This suggests that there are multiple forms of MAP1B in A549 cell lysate, however only the slowest migrating form co-eluted with DAPK. These multiple bands could be isoforms, or could be post translationaly modified moieties. Together, these data imply that a proportion DAPK and a slow migrating isoform of MAP1B are present in a high molecular weight complex in A549 cells.

3.2.8 Quantitation of DAPK and MAP1B Association with Microtubules

Co-immunoprecipitation and chromatography assays provided evidence suggesting that only small pool of soluble endogenous MAP1B and DAPK associate in complex in cell lysate. However, the HA tag of transfected HA-DAPK could be used to efficiently pull down MAP1B in complex with DAPK. No actin was detected in the immunoprecipitate, all of which remained in the unbound fraction. Using co-IP it was not possible to assay the level of tubulin in the precipitate because of interference with the heavy chain of IgG which is approximately the same molecular

weight. So experiments were conducted to determine if DAPK, like MAP1B could interact with polymerised tubulin.

In-vitro microtubule polymerisation and depolymerisation cycling is a classic method used to determine if a protein is capable of binding to microtubules. To achieve this, a microtubule preparation was prepared *in-vitro* using lysate that has been thoroughly clarified by centrifugation. During cold lysis, microtubule depolymerisation is spontaneously induced and so any associated proteins are liberated and dissolved. Then GTP is added to the lysate before incubation at 37C to stimulate polymerisation of microtubules. *In-vitro* microtubules and any associated proteins are then separated by centrifugation and can be assayed for protein content by western blot.

Initially, tubulin precipitation was employed to screen multiple cell lines for DAPK and MAP1B co-precipitation with tubulin (Figure 3.12 a). A549 cells and A375 cells that express endogenous MAP1B were transfected with HA-DAPK only, whereas HCT116 colon carcinoma cells that express very little MAP1B were co-transfected with MAP1B and HA-DAPK. Microtubule pellets (p) and supernatants (s) were assayed for MAP1B, DAPK and tubulin content using SDS PAGE and western blotting. Transfected HA-DAPK was enriched in microtubule preparations from all cell lines.

The isolation of bona-fide microtubule associating proteins (MAPs) requires that the prepared microtubules are depolymerised and re-polymerised during three subsequent rounds of cycling. In this way, non-specific interactions are eliminated by dilution so that after the third cycle only specifically interacting proteins are precipitated with tubulin polymers. A375 cells were transfected with HA-DAPK for

24 hours before lysis and 3 rounds of microtubule cycling. DAPK and MAP1B both co-purified with tubulin whereas only a smaller residual amount of each remained soluble in the supernatant. The stoichiometry of binding to microtubules was roughly 3 to 1 for MAP1B and a striking 5 to 1 for DAPK after 3 rounds of cycling. Actin was eliminated form the preparation after 2 cycles, indicating that interaction with actin by either MAP1B or DAPK was not required for their binding to mictotubules. In addition, this provided confidence that only specifically bound protein was present in the preparation and that non interacting proteins were removed with the supernatant fraction. These data provide compelling evidence that DAPK is able to strongly interact either with microtubules directly or with microtubule associated proteins. This is a remarkable result because previous published work has concentrated on DAPK as an actin associating protein. This proposed interaction of DAPK with the microtubule network is entirely novel.

3.2.9 Proteomic Analysis of Microtubule Preparations Using Fluorescence 2-D Difference in-Gel Electrophoresis (DIGE)

If DAPK interacts strongly with microtubules, it is highly likely that this will induce changes in the total microtubule associated proteome. Given DAPK's role in the regulation of cell death it is therefore also likely that these proteomic changes will effect DAPK induced tumour regulation. As a consequence, study of DAPK's effect on the microtubule network could shed light of DAPK-induced tumour suppression. A proteomic study was set up to determine the effect of DAPK interaction with microtubules on the microtubule associated proteome.

Differential in Gel Electrophoresis (DIGE) is used to monitor the difference between proteomic profiles of biological samples. Protein preparations are tagged with different fluorescent dyes and then separated on the same 2D-gel. After separation the two fluorescent images are superimposed to visualise protein moieties at similar concentrations in both samples and protein moieties that are present at different concentrations. The main advantage of using this technology is that it allows for simultaneous comparison of multiple samples on one gel, thereby negating inter-gel variation.

A375 cells were used to create a DAPK stabile-inducible cell line. DAPK expression was under regulation by tet operon, and could be induced by addition of tetracycline into the growth medium. This cell line expressed very low basal levels of DAPK without induction. Addition of 5μg/ml tetracycline into the culture medium for 48 hours resulted in induction of DAPK expression to high levels (Figure 3.13 b). Therefore, the effect of DAPK on the microtubule associating proteome could be determined by differential analysis of microtubules prepared from non-induced and induced samples. After 3 cycles of polymerisation, proteins were separated by SDS-PAGE and visualised using colloidal blue staining (Figure 3.13 a) to visualise any large changes in the amount of protein mioties after DAPK expression. Over 50 distinct bands were observed, however no differentially expressed moieties were observed using this method. The presence of MAP1B, DAPK tubulin and actin was verified by western blot analysis of the preparation (Figure 3.13 b).

Purified microtubule samples prepared from induced cells were labeled with Cy5 (red) and the reference preparation with Cy3 (green) and isoelectrically focused

overnight between pH 4 and pH 8. After focusing samples were separated on an 8% gel resulting in a duel stained 2D gel profile (Figure 3.13 c). Pattern recognition software determined that the intensity of 41 spots was 3-fold decreased as compared to the reference, and that 238 spots were increased above this threshold (Figure 3.13 d). Thus demonstrating that exogenous DAPK induces a wide variety of changes to the microtubule associated proteome.

3.3 Discussion

3.3.1 Use of the Phage Peptide Combinatorial Library to Identify Novel Protein Interactions

One of the difficulties of cancer research in humans is that investigation of non-conserved biochemical pathways cannot rely on classic genetic screens such as those employed in model organisms. An additional difficulty is that signalling pathways that often evolve quickly are not always conserved and so extrapolation from lower organisms may not be feasible. Therefore methods in cancer research to identify novel protein signalling interactions have generally included antibody based immunoprecipitation methods such as TAP-tagging, two-hybrid methods and peptide aptamers. These techniques have advantages and disadvantages ranging from *in-vivo* relevance to incomplete representation of a library. There is a growing realisation that signalling interactions are often regulated by linear interaction motifs often as small as 4 amino acids. Such small peptide motifs may act as scaffolds to anchor a protein to a target or to allosterically alter function or they may be acceptor motifs for posttranslational modification. As such, proteomic methods geared towards identifying bioreactive linear binding motifs will assist in expanding the known "interactome" of a target protein.

Peptide display technologies may be prone to giving false positives owing in part to the fact that the displayed peptide might interact with contaminants that are inevitably present with proteins purified using most methods. The purity of the GST-DAPKcore preparation was assessed using SDS-PAGE in conjunction with

coomassie blue staining (Figure 3.1 a). This method is sensitive enough to detect contaminants in the preparation at concentrations above the 10nm range. Even though it was not possible to determine the extent of contamination with proteins below this concentration, the purity was considered sufficient. This assumption was verified post-isolation of the phage peptides by using an ELISA based method to evaluate the specificity of binding (Figure 3.6 b). The GST-DAPKcore preparation was compared to a GST-only control prepared from *E.coli*. Here, binding of phage peptide to GST-DAPKcore was 3 fold higher than to GST alone. This suggested that the non-specific element of phage peptide binding was much smaller than specific binding. This non-specific binding to GST alone was likely due to the biotinilated peptide used in the ELISA assay being at a concentration many orders of magnitude higher than the phage peptide would be in the combinatorial library.

The phage peptide combinatorial library was presented to bait protein isolated on the solid phase. As a consequence of this, a method was required that would allow DAPKcore to be captured in an active and conformationaly stable state. Enzyme that was precipitated on ELISA wells using glutathione was able to efficiently bind p53. Also, presentation of docking site peptides that reflect the calcium-calmodulin family binding site within the MDM2 ubiquitination signal of p53, resulted in increased association between DAPK and p53. This indicated that the DAPKcore was alostericaly modified by these peptides. Also, isolated kinase released a proportion of bound p53 when ATP cofactor was added. These observations, taken together demonstrated that glutathione captured kinase is able to interact with target protein in 3 distinct ways; through binding, via docking site mediated allosteric interaction and by phosporylation which requires precise substrate recognition. Therefore DAPKcore

captured in the solid phase was a good target protein for phage display because any binding peptides should reflect those that bind in an *in-vivo* situation.

Three rounds of biopaning were conducted. It was hoped that this would strike a balance between obtaining an unmanageable number of peptides usually obtained after just 2 rounds and isolating too few peptides after more than 3 rounds. If only 2 rounds of biopanning are conducted then there is a risk that false positives will be obtained as a result of none-specific binding of weaker interactors. After 3 rounds the number of false positives is significantly reduced as strongly interacting peptides are enriched at the expense of weaker non-specific interactions that are diluted. The disadvantage of using three rounds is that the number of different peptides obtained is decreased as the stronger binders become more prevalent. It was determined by previous work that in order to conserve resources the optimum number of phage plaques to be processed for sequencing is just 6 after 3 rounds of panning to identify the prevailing interacting peptides. After elution with ATP for example, sequencing of 6 phage plaques revealed that they displayed 2 groups of 2 identical peptides (Figure 3.4 a: peptides 1 and 2, peptides 3 and 4), confirming that the optimum number of plaques had been sequenced.

The sequenced phage displayed peptides were inputted into a BLAST search program optimised to find short nearly exact hits from the entire known human proteome. Hits that consisted of 5 or more identical amino acids were determined to be statistically significant. This is because the chances that 5 amino acids would appear at specific places at random in a 12mer peptide are much greater than the expected number of genes in the human proteome. As such, isolated peptide with 5

or more amino acids in common with known protein was considered for further analysis. Also, a search was undertaken to try and identify any motifs arising from more than one peptide. However, only one such motif was found by grouping together 2 distinct peptides (Figure 3.4 a: peptides 5 an6 6). This motif was then inputted into the e-motif database to search for homologous motifs within the human proteome. However, this revealed no significant hits. In addition to this, in total 6 individual binding peptides were isolated that had no significant homology to any known protein in the data base, 3 eluted using ATP and 3 with low pH. Given that these peptides were isolated after 3 rounds of panning along side other peptides with high sequence homology to known proteins it remains unlikely that these are genuinely unrelated to any naturally occurring peptide. The fact that no homologous hits were found could be due to a number of reasons: Firstly, linear interaction motifs can often consist of as little as 4 amino acids in succession but these would be flagged as insignificant during the search process. Secondly homologous proteins are found by the pattern recognition algorithms employed by the BLAST search program. These algorithms can not easily find all patterns such as those with more than one gap between groups of homologous residues, and as such the search process will miss these. Lastly, the isolated peptides may be homologous to known proteins with respect to amino acid chemistry rather than simply because of sequence homology. For example, using the search method employed, it was not possible to highlight residues with a similar charge or with similar functional groups. Therefore a more sophisticated bioinformatics method is required for future studies that can address these issues.

3.3.2 The Nature of the MAP1B to DAPK Protein-Protein Binding

In mouse and rat, the MAP1B gene is transcribed into 3 different transcripts that vary at their N-termini (Kutschera et al., 1998). The first transcript contains exons 1 through to 7, whereas the second and the third transcripts contain either exon 3A or exon 3U fused 5' to exon 3. The fusion of exon 3U with 3 results in removal of the start codon, so that transcription is started further down stream in exon 4. This rodent transcript with exon 3U corresponds to human MAP1B transcript variant 2 whose translation is also started further down stream at the corresponding start codon. In both the human and rat, this leads to expression of 2 distinct isoforms of MAP1B, variant 2 having an N-terminal truncation that has an otherwise identical amino acid sequence. The isolated phage peptide with significant homology to MAP1B maps to the N terminus of transcript variant 1 and so is not present on transcript variant 2. Therefore, fragments of both variants were cloned from human fetal brain RNA providing a convenient system to study the 2 MAP1B variants, one with (V1) and one without (V2) the putative binding motif. In addition to the V1 and V2 fragments, the N-terminal 126 amino acids were separately cloned to make a mini protein containing the proposed DAPK interaction site. Full length MAP1B was obtained from a commercial source owing to the difficulty in cloning such a large transcript. Unfortunately full length transcript variant 2 could not be obtained.

Once cloned, the constructs were sub-cloned into expression vectors for protein expression to study interaction with DAPK. Initially expressed MAP1B was introduced to DAPK isolated in an ELISA well in the solid phase. All constructs that contained the N-terminal phage peptide mapped site could efficiently bind to DAPK, whereas V2 could not (Figure 3.9 a). N126 and V1 were able to bind with higher

affinity than the full length protein indicating that regulatory elements may be present C-terminal to the proposed binding site. This was reproduced by co-transfection of both proteins followed by immunoprecipitation, where only V1 was able to pull down DAPK (Figure 3.9 b). This indicates that the N-terminal region containing the putative interacting motif is the primary binding site for DAPK on MAP1B. However, it is still possible that there is another interaction site further down stream that is not covered by V2. Mouse anti-DAPK antibody (BD Biosciences - See figure 2.1) was used for the reverse IP in these experiments to attempt to pull down co-transfected MAP1B variants. However, IP using this antibody was not successful on a number of occasions. The epitope of this monoclonal antibody maps to somewhere within the ankyrin repeat domain, a domain thought to be critical for protein-protein interactions. Therefore, it is proposed that this reverse IP was not successful because of anti-DAPK antibody epitope masking. Subsequent experiments revealed however, that transfection of HA-tagged wild-type DAPK used in conjunction with anti-HA pull down can be used to purify exogenous DAPK-containing multi-protein complexes from cells (Figure 3.9 c). Given more time the V1/V2 co-ip would be repeated using this relatively new method of HA-tag pull down.

A body of literature deals with DAPK and its association with microfilaments. As a consequence of this it was predicted that immunoprecipitation of DAPK would pull down actin. Given the fact that the HA-pull down was so efficient it is surprising that all actin in the lysate was left in the unbound fraction and so not co-precipitated with DAPK (Figure 3.9 c). This was the case in all the IP experiments, where no evidence of actin co-IP with DAPK was detected. Again, there could be numerous reasons for

this; owing to the limitations associated with co-IP methods, such as epitope masking or sub-optimal salt concentrations in the buffer. DAPK association with actin is critical for it activity in cells (Bialik et al., 2004) and so it is unlikely that DAPK does not interact with actin in the cell lines tested. It is proposed that a likely reason for the lack of actin co-IP was because the microfilaments remained intact and insoluble during the lysis procedure. Any DAPK bound to microfilaments would then be spun down into the pellet during lysis clearance. A simple method that could be used to test this hypothesis would involve the use of microfilament disrupting drugs such as latrunculin A during lysis. Then, any DAPK associated with actin would be dissolved and available for co-immunoprecipitaion. This experiment could also answer questions pertaining to the nature of MAP1B interaction with DAPK. One such question is do MAP1B and DAPK form complexes on microfilaments? In this case, MAP1B and DAPK would both be liberated by latrunculin A and could co-IP with actin.

Extremely weak DAPK and MAP1B-containing co-IPs were obtained from A549 cells where both proteins are endogenously expressed (Figure 3.10 a). This could again be due to methodological reasons, but could equally represent the real situation in these cells. The assumption that only a small proportion of MAP1B interacts with DAPK in A549 cells was tested using a chromatograpic method. Here, a small proportion of MAP1B co-eluted with DAPK in fractions from an ion exchange column. Multi-protein complexes in these co-eluting fractions, were then subsequently fractionated according to size using a gel filtration column. A large proportion of MAP1B and DAPK then co-eluted in a heavy molecular weight fraction, providing corroborating evidence that a small proportion of endogenous

MAP1B and DAPK are present in complexes A549 cells. These complexes, of around 600kDA are 160 kDa heavier than a dimer of DAPK (160kDa) and MAP1B heavy chain (280kDa) would be. It is therefore probable that other protein moieties would be associated in this putative multi-protein complex.

It should be mentioned that there are problems associated with this tandem chromatography approach: Firstly, ion exchange chromatography, unlike size exclusion, can disrupt multi-protein complexes by virtue of the ionic strength of the elution, therefore more DAPK and MAP1B may in fact bind than the co-elution profile might suggest. Secondly, this approach does not provide any proof of direct interaction, and only suggests such an association when taken into account with other evidence. For example, MAP1B and DAPK could co-elute after ion- exchange and size exclusion by chance. In other words, they could be in separate complexes roughly of the same charge and weight. It should be said however that the chances of this happening randomly are diminished as two tandem purifications were performed. Lastly, this method required a lot of starting material, so that there would be just enough protein to analyse by western blot after the final step. As a consequence, there was not enough protein to set up a co-IP using co-eluting fractions. This was unfortunate because such an experiment would be good evidence of an interaction. As a result, any future work would benefit greatly from such an experiment if it was successful, but more starting material is required.

In summary, the immunoprecipitation methods employed in this thesis are a good starting point, and could be optimised further to gather information about DAPK and MAP1B interactions in cells. Some IPs did not work in the reverse direction,

probably due to epitope masking and this could be resolved using newer antibodies or epitope tags. Also, the use of microfilament disrupting may help to dissolve any residual DAPK and bound proteins that would otherwise remain insoluble and unavailable for analysis. Also, the weak endogenous interaction in A549 cells in conjunction with chromatography is suggestive that the two endogenous proteins interact but is not a complete proof. Therefore further experimentation is required to determine the extent of endogenous MAP1B and DAPK interaction in other cancer cell lines and also in primary cell lines.

It may be that the MAP1B with DAPK interaction is occluded in cancer cells to provide a survival advantage to these cells. A possible mechanism for this would be via differential expression of the DAPK binding site (as in transcript variant 1) by alteranative splicing. This would provide a switch that could regulate any functional consequence of MAP1B interaction with DAPK. This idea is supported by the fact that only slower migrating bands of MAP1B co-eluted with DAPK and that this band could be transcript variant 1. There may therefore need to be a stimulus to induce interaction between the two. For example, this may be in the form of a cell death or survival signal or cell migration. It has been extensively reported that ectopic expression of DAPK is sufficient to induce programmed cell death accompanied by associated morphological changes (Bialik and Kimchi, 2006). This suggests that an increase in DAPK levels by transfection is sufficient to induce DAPK-related effects and as a result, signaling events down-stream of DAPK are activated. This could explain why transfected DAPK interacted with MAP1B whereas endogenous protein did not. If this is the case, screening of cells treated with various stimuli would reveal a stress that induces MAP1B interaction with DAPK.

A binding interaction between DAPK and MAP1B raises the question; does DAPK interact with the microtubule network in cells? Co-immunoprecipitation methods were unable to address this because tubulin is approximately the same size as IgG heavy chain and so can not be observed by western blot in samples containing immunoglobulin. Further experimentation involving conjugation of antibody to the beeds could be employed to address this. However, a tubulin cycling assay was employed to measure DAPK association with polymerised tubulin *in-vitro.* Transfected HA-DAPK was able to strongly interact with tubulin prepared from the panel of cancer cell lines; A549, HCT116 and A375 cells, after 1 cycle of polymerisation. This correlated with MAP1B-tubulin association in A549 and A375 cells. It is interesting that in HCT116 cells transfected MAP1B did not interact with tubulin when co-transfected with DAPK. This could indicate that in this cell line transfected DAPK inhibits MAP1B binding to tubulin. It is proposed that this is an artefact. During the first cycle of polymerisation a large proportion of DAPK is left in the supernatant. Therefore co-transfected MAP1B would be held in the supernatant by excess DAPK whereas endogenous MAP1B in the other cell lines is not.

After 3 polymerisation cycles the majority of endogenous MAP1B and transfected DAPK is bound to microtubules (Figure 3.12 b). It is very striking that DAPK interacts with polymerised tubulin so strongly and this proves that DAPK can interact with microtubules *in-vitro*. This is at odds with a previously published research paper suggesting that DAPK interacts with microfilaments alone and does not interact with microtubules (Levy-Strumpf and Kimchi, 1998). In this paper the authors assay the amount of liberated DAPK under different lysis conditions. After

addition of the microfilament disrupting agent latrunculin A they show that there is an increased amount of DAPK in the lysate, showing that DAPK is liberated by dissociation of the actin cytoskeleton. However after addition of the microtubule disrupting drug nocodazol they observe no effect on the amount of DAPK in the lysate which they interpret as suggesting that DAPK was not bound to microtubules. However this interpretation does not take into account the fact that microtubules spontaneously depolymerise at low temperature during the lysis. Therefore the validity of these results is questionable. In any case the polymerisation cycling assay employed in this thesis does not determine if DAPK can associate with microtubules in cells *in-vitro*. Therefore further experimentation is required to confirm or refute this.

A final observation relating to the interaction of DAPK with the microtubule network was that actin did not co-bind in the *in-vitro* cycling assay. Given that DAPK can interact with actin, it was feasible that actin could be co-precipitated with DAPK. It seems likely however that DAPK can only interact with either actin or, as in this case, with tubulin.

3.3.3 Proteomic Analysis of Microtubule Associated Proteins

DIGE proteomic analysis of microtubule preparations with and without DAPK expression resulted in 2D gel differential profiles with approximately 300 differentially regulated spots (Figure 3.13). This was in contrast to profiles seen after 1D gel analysis visualised by colloidal blue staining, where no differences could be seen (Figure 3.13 a). However, DAPK was clearly abundant in the induced preparation (Figure 3.13 b) suggesting that 1D electrophoresis was not sensitive

enough to resolve this. Also, most of the differentially regulated spots were along horizontal sections of the 2D gel (Figure 3.13 d). This suggests that the majority of changes induced by DAPK were as a result of post-translational modification, affecting the isoelectric point of protein moieties rather than their migration through the gel.

Approximately 200 above 3-fold differentially regulated spots were flagged by the automated analysis (Figure 3.13 d). Some of these would be false positives/negatives due to background and some would be the same spot flagged multiple times due to the nature of the employed pattern recognition software. However, there were clearly many differential spots that are unlikely to be false. These were mainly up-regulated along horizontal sections of the profile in the induced sample, suggesting that DAPK induced post-translational modification of microtubule associated proteins. These could be directly modified by DAPK catalytic activity or could be modified by other enzymes activated by DAPK.

These experiments demonstrated the utility of this approach to determine differential post-translational modifications of the microtubule proteome induced by DAPK. Therefore, this experiment should be repeated, followed with mass spectrometrical analysis of the differential spots. This powerful technique would then uncover the identity of differentially regulated protein moieties, providing invaluable information about DAPK action in relation to microtubules.

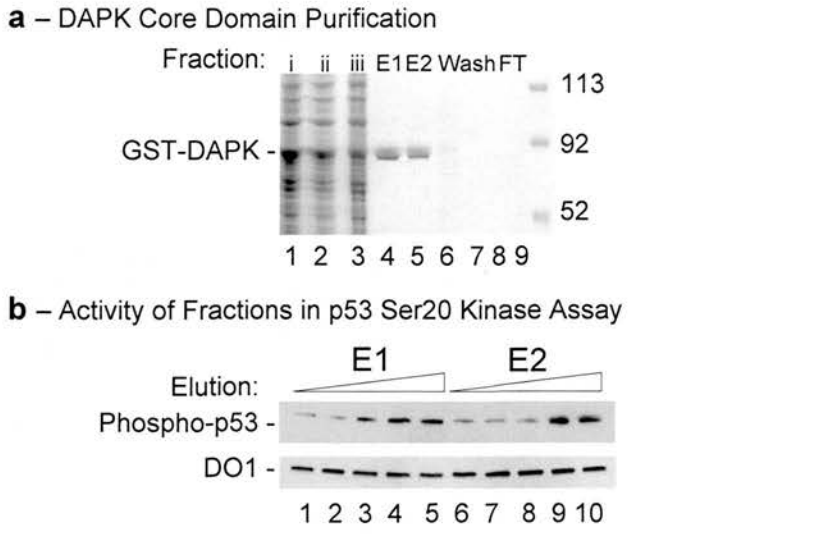

FIGURE 3.1 Purification of Active DAPK-1 Kinase Domain. **(a)** Sf9 cells were infected with baculovirus encoding GST-tagged DAPK core kinase domain (GST-DAPK) The indicated fractions were separated by SDS-PAGE and stained with Coomassie blue. Induced (lanes 1-2) and non-induced (lane 3) lysates were applied to a Glutathione column for affinity purification. Protein is depicted in the flow through (lane 9), in the wash (lanes 6-8), and in the Glutathione eluates from induced cultures (lanes 4 and 5). **(b)** GST-DAPK eluates E1 and E2 (lanes 1-5 and lanes 6-10 are increasing amounts of eluates E1 and E2, respectively) were titrated in a non-radioactiv kinase assay using p53 as a substrate and evaluated using phospho-specific antibodies to the Ser20 phosphoaccepter that is in the p53 activation domain (Craig et al., 2007) and to total p53 using DO-12 MAb. **(c)** The specific activity of DAPK purified using different methods in a p53 kinase assay was tested. Kinase reactions were assembled in buffer containing p53 and the indicated kinase (lane 1 = no kinase, lane 2 = HIS-tagged DAPK-1 from E. coli, lane 3 = GST-tagged DAPK from E. coli and lane 4 = GST-tagged DAPK fom Sf9 insect cells. Lane 5 depicts HIS-tagged CHK2 from Sf9 cells as a comparison. Again, the reaction products were analysed for p53 phosphorylation using phospho-specific antibodies to phospho-Ser20 and to total p53 using DO-12 MAb.

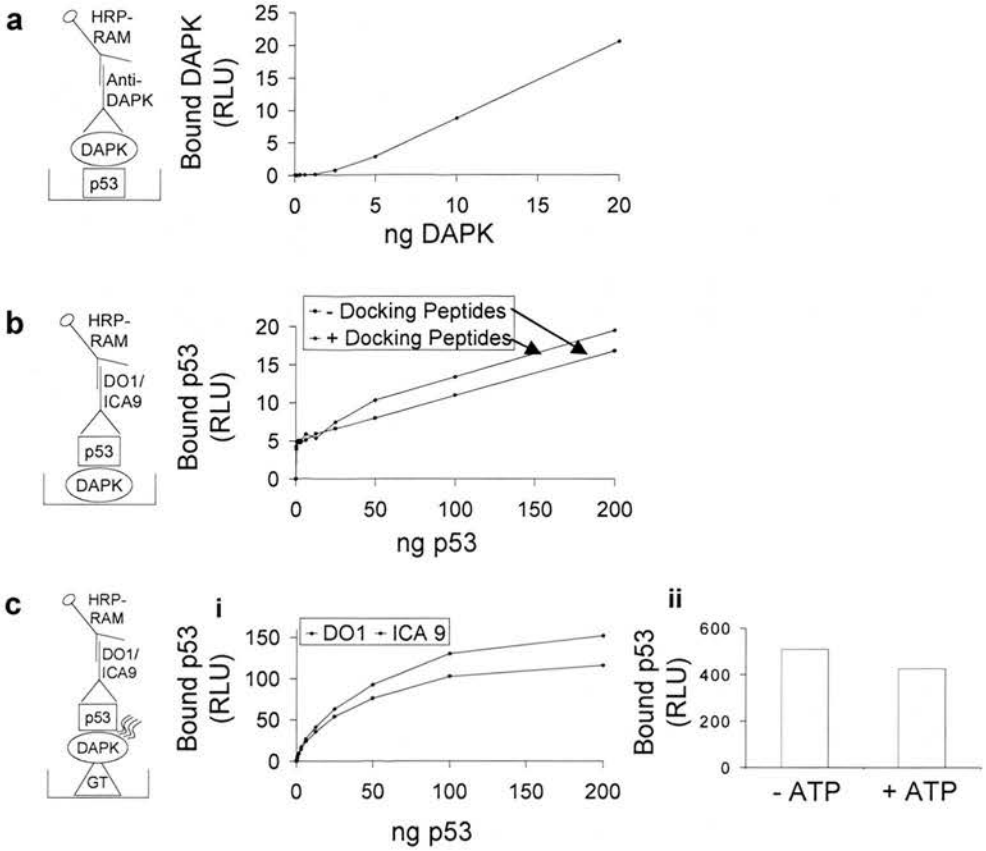

FIGURE 3.2 Integrity of DAPK Kinase Domain in the Solid Phase. The conformational integrity of GST-DAPKcore was evaluated using a two-site ELISA assay binding to p53. The protein-protein complexes were detected with anti-GST IgG or anti-p53 IgG (DO-1 or ICA-9), as indicated, and detected using peroxidase labelled anti-mouse or anti-rabbit IgG followed by ECL quantitation using a Fluoroskan plate reader. The diagrams to the left of each figure reflect the order of protein complex formation from protein in the solid phase through to the HRP-20 antibody detection system. The binding activity in the ordinate (relative light units) is plotted as a function of increasing amounts of protein. **(a)** DAPK titration and evaluation of binding to p53 in the solid phase. **(b)** p53 titration and evaluation of binding to DAPK in the solid phase without and with *BOX-V* docking-site peptides that map to the calcium-calmodulin kinase interaction site in the core domain of p53 (Craig et al., 2007). **(c) i** p53 titration and evaluation of binding to GST-DAPK in the solid phase. **ii** 100 ng of p53 was incubated in kinase buffer and ATP with GST-DAPKcore in the solid phase for 30 minuets.

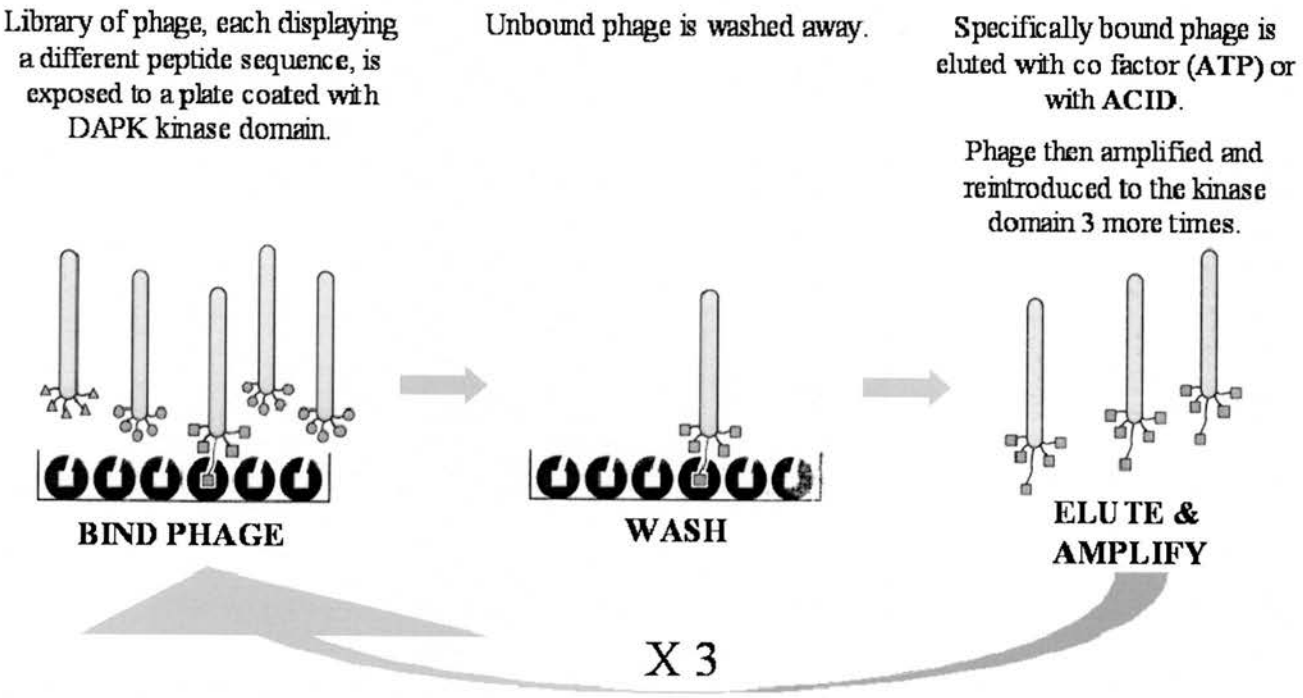

FIGURE 3.3 The Phage Peptide Display Biopanning Process. Active GST-DAPKcore fractions (As in FIGURE 3.1) were adsorbed onto ELISA wells and presented to a combinatorial 12-mer peptide-phage library. Interacing phage were eluted with ATP-containing buffer or with acid. Eluted phage were propagated in *E. coli*, amplified, and concentrated for the subsequent round of screening.

a – ATP Elution

Phage ATP 1,2	TLPSPLALLTVH	
Sp1	SQ**PSPLALL**AAT	Sp1-4 family of transcription factors
Sp2	SQ**PSPLALL**AAT	
Sp3	**T**Q**PSPLALL**AAT	
Sp4	SQ**PSPLALL**AAT	
Phage ATP 3,4	SPPSNLIPPTLR	No significant homology found
Phage ATP 5	ATWSHHLSSAGL	
Phage ATP 6	QTRPHHLRSATQ	
Φ-5	A**T**WS**HHL**S**SA**GL	
Φ-6	Q**T**RP**HHL**R**SA**TQ	
Motif	**T**XX**HLL**X**SA**	

b – Acid Elution

Phage Acid 1	LPF**EEHLRR**PV**G**	
MAP1b	IVT**EEHLRR**AI**G**	
Phage Acid 2	SNL**P**QS**WPPHQ**W	
PML	TYH**P**PA**WPPHQ**P	
Phage Acid 3	Q**GAWHP**S**R**TH**F**L	
RPL3	I**GAWHP**A**R**VA**F**S	
Phage Acid 4	TQPPIPPSRTLH	No significant homology found
Phage Acid 5	TFGLWQPGVQST	
Phage Acid 6	WHWSWFSHFPSA	

FIGURE 3.4 Peptide Sequences Isolated After Three Rounds of Panning. Peptides were eluted from DAPK with **(a)** ATP or **(b)** acid. After 3 rounds of panning, phage displaying DNA was sequenced and the corresponding amino acid deduced. Isolated peptides are summarised as indicated.

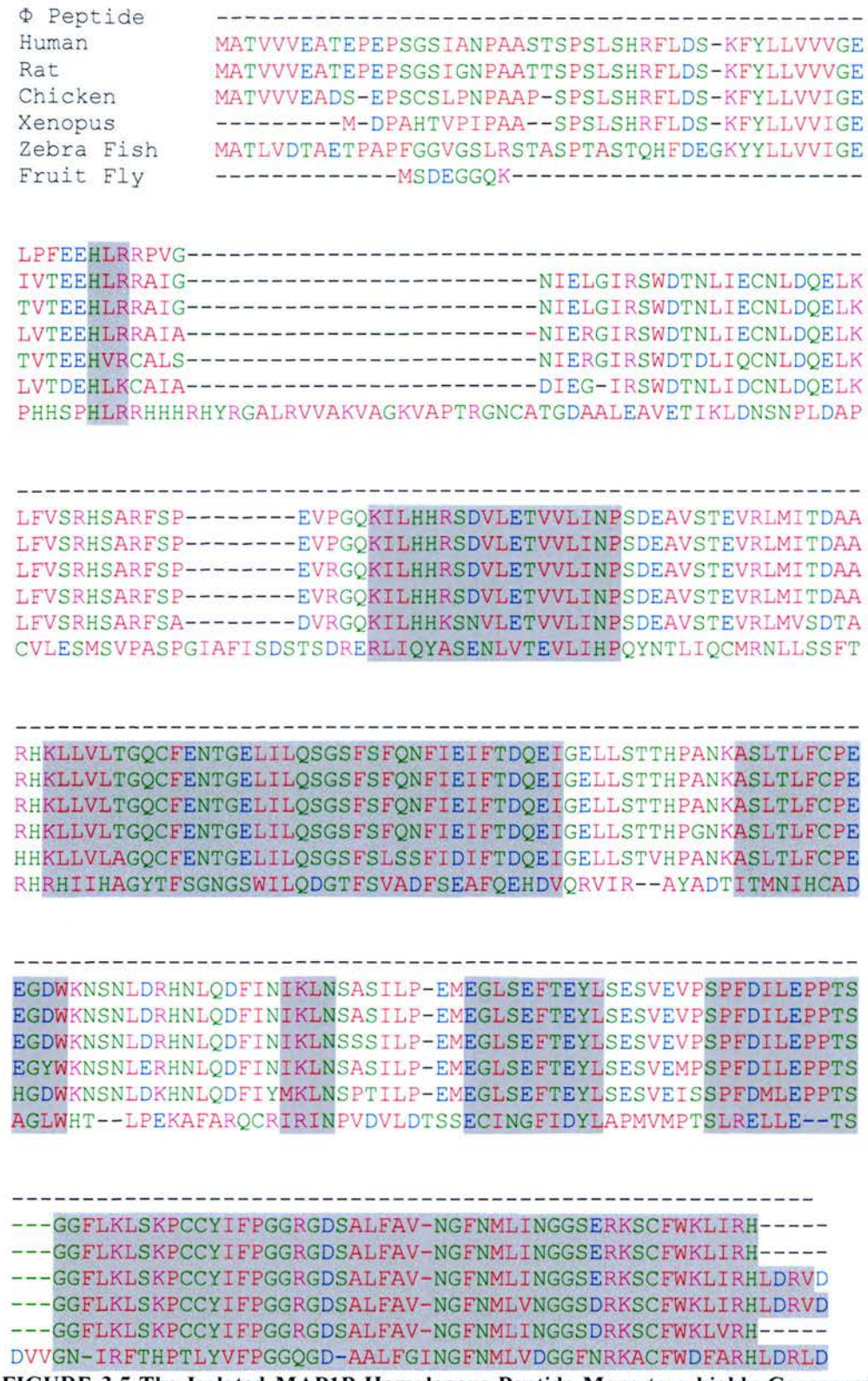

FIGURE 3.5 The Isolated MAP1B-Homologous Peptide Maps to a highly Conserved Motif on the N-terminus of MAP1B. Human MAP1B amino acid sequence data was retrieved from genbank and used to find paralogues from rodent, avian, amphibian, fish and insect species using blast searching of the homologene data base. Clustalw was used to compile multiple alignments using the obtained sequences. Residues with similar chemistry were coloured blue (negative charge), pink (positive charge), red (non-polar) and blue (polar). Shaded areas are highly conserved from invertebrates.

a – Assay Optimisation

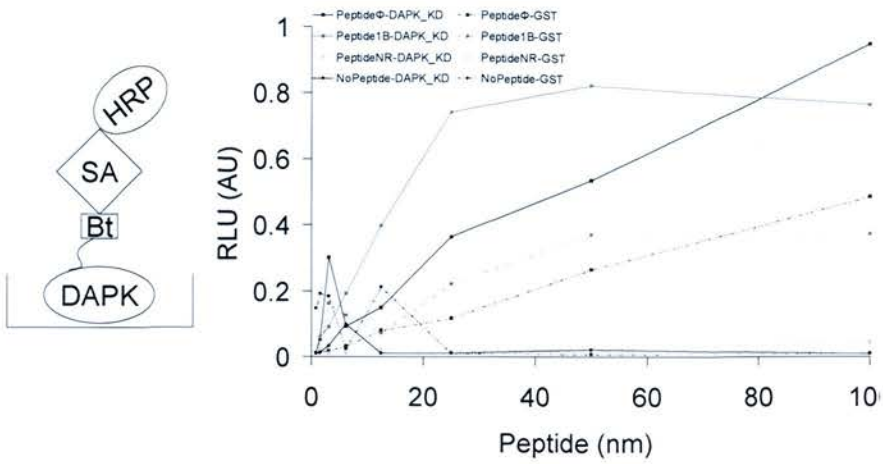

b – Quantification of Peptide Binding

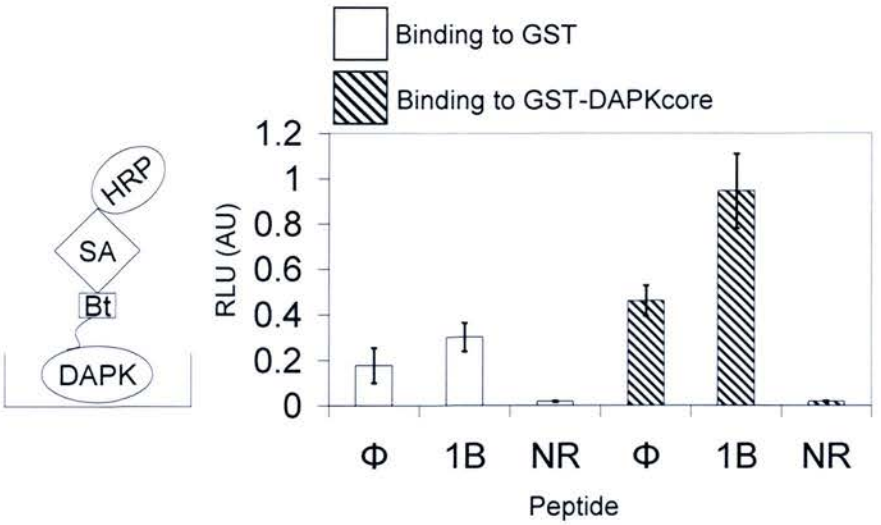

FIGURE 3.6 Specific Binding of the Φ-peptide and Mapped MAP1B Peptide to GST-DAPKcore. Microtitre wells were coated with anti-GST IgG followed by incubation with GST only or with GST-tagged DAPKcore as indicated. Synthetic peptide (Φ) with homology to MAP1B (Φ - LPFEEHLRRPVG), the corresponding homologous peptide derived from MAP1B (1B - IVTEEHLRRAIG), or control peptide (NR) were added into to the wells. Peptide complexes were quantified using streptavidin peroxidase. The data are plotted as peptide-binding activity (RLU) as a function of target protein in the solid phase. The diagram to the left of figures reflect the order of protein complex formation between DAPK in the solid phase and peptide through to the HRP-20 antibody detection system. **(a)** Titration of dissolved peptide onto GST-DAPKcore in the solid phase. **(b)** Addition of 50ng peptide to GST-DAPKcore in the solid phase, error bars show standard deviation.

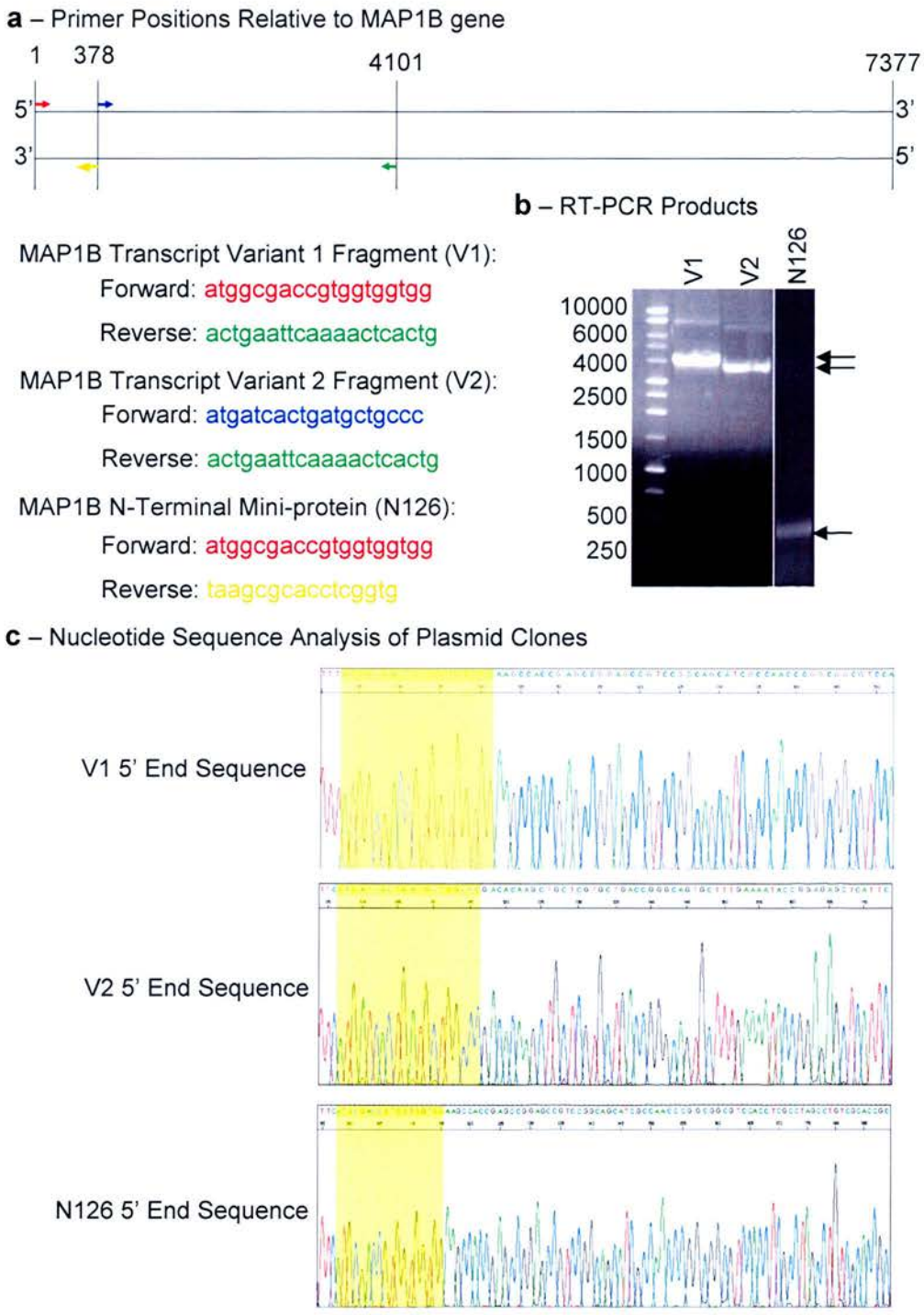

FIGURE 3.7 Cloning of MAP1B Fragments from Human Brain Total-RNA. (a) Primers were designed for cloning fragments of MAP1B transcript variant 1 (V1) and transcript variant 2 (V2) using 5' primers at positions 1 (red arrow) and 327 (blue arrow) respectively and 3' primers at position 4101 (with respect to the full length MAP1B cDNA sequence). The N-terminal mini-protein; N126 was cloned using reverse primers designed at position 378. **(b)** RT-PCR products were resolved on a 1% agarose gel before gel purification and subsequent cloning into gateway pDONR221 plasmid. **(c)** Sequences from the 5' positions of each clone in pDONR221 vector are shown.

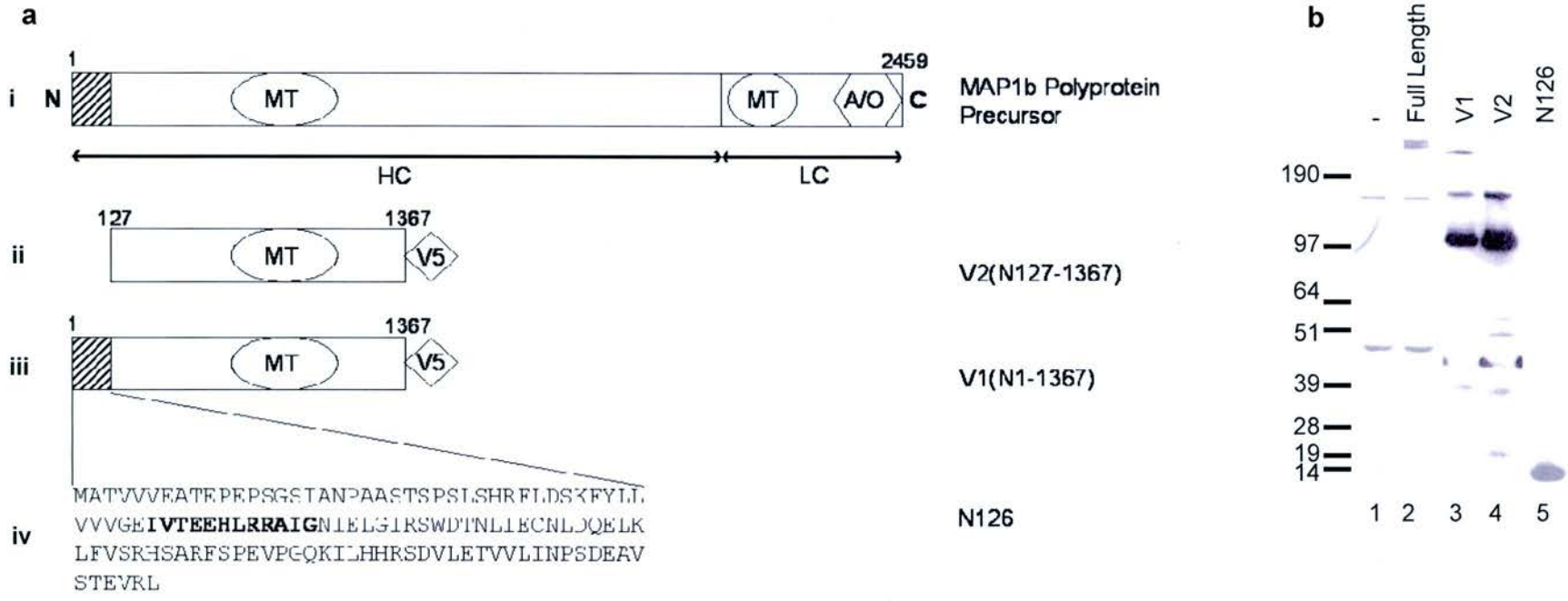

FIGURE 3.8 Schematic of Cloned MAP1B Constructs Relative to the Full Length MAP1B Protein. **(a)** A Schematic of fragments of **ii,** splice variant V2 (containing the N-terminal DAPK1 binding peptide) and **iii,** variant V2 (lacking the N-terminal binding peptide) are drawn bellow **i,** the full length protein. The sequence of the mini-protein containing the N-terminal 126 amino acid is shown (**iv**), where the bold region highlights the location of the DAPK binding peptide. HC = MAP1B heavy chain, LC = MAP1B light chain (or LC1), MT =. Mictotubule binding domain, A = actin binding O = oligomerisation domain. V5 = C-terminal V5 epitope tag. Hatched area is the N-terminal 126 amino acids **(b)** Expression vector containing the full length MAP1B protein was obtained from a commercial source and is expressed as a doublet in HCT116 cells (Lane 2). V1 and V2 (Lanes 3 and 4) expression pattern and N126 (lane 5) are shown.

a – Transfected MAP1B Binding to DAPK on Solid Phase

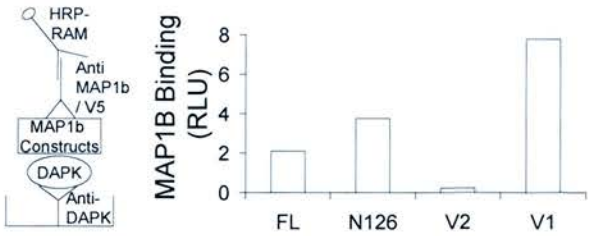

b – Exogenous MAP1B and DAPK Association in HCT116 Cells

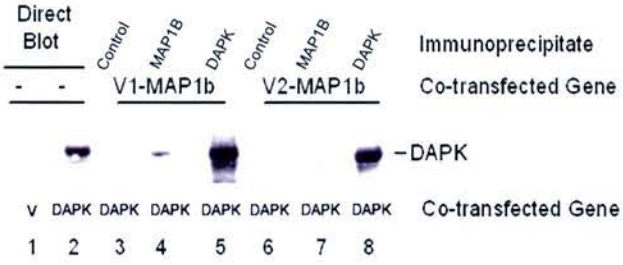

c – Endogenous MAP1B Pull-down by HA-DAPK Transfection

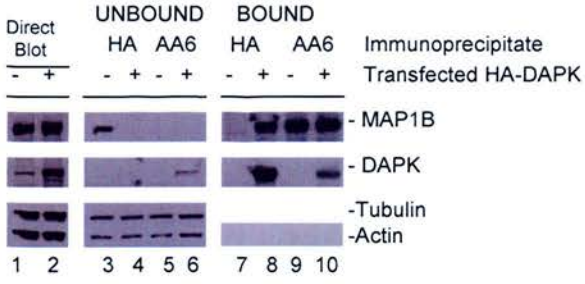

FIGURE 3.9 Interaction of Tranfected DAPK with MAP1B Protein in Cells. (a) Expression Vectors (1 µg of each) native DAPK and MAP1B variants were co-transfected into HCT116 cells. After 24 h, cultures were lysed and processed for two-site ELISA. The binding of MAP1B variants to DAPK was quantified using the appropriate anti-V5 or AA6 anti-MAP1B IgG and secondary antibody linked to peroxidase followed. Peroxidase activity was detected by ECL. **(b)** Vectors encoding V5-tagged MAP1B (V1 [lanes 3-5] or V2 [lanes 6-8]) and native DAPK (1 µg of each) were co-transfected into HCT116 cells and after lysis, the amount of DAPK bound in the anti-V5 immune complex was quantified by immunoblotting with anti-DAPK IgG. **(c)** A375 cells were transfected with either HA-DAPK or vector control for 24 hours, harvested in NP-40 lysis buffer and the resultant lysate cleared for co-immunoprecipitation. Complexes were precipitated using anti-HA or AA6 (anti-MAP1B) antibodies. MAP1B and HA-DAPK protein in the input lysate (lanes 1 and 2) and resulting unbound (3 to 6) and bound immunoprecipitate (7 to 10) fractions were detected by immunoblot. The extent of tubulin co-precipitation could not be determined in lanes 7-10 because the heavy chain from the IgG used in immunoprecipitation co-migrated with tubulin and masked the signal.

a Using N126 as a Substrate for GST-DAPKcore

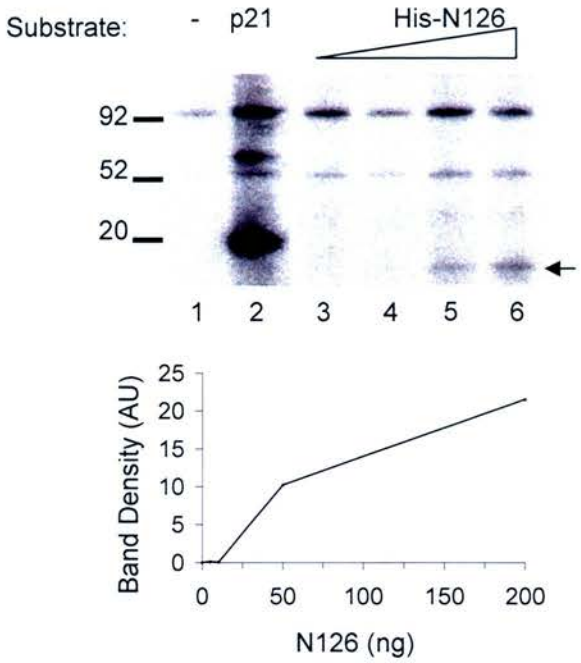

b Candidate Phosphoaccepter Site on N126

1-matvvveatepepsgsianpaastspslshrfldskfyllvvvgeivtee - 50
51-hlrraignielgirswdtnliecnldqelklfvsrhsarfspevpgqkil - 100
101-hhrsdvletvvlinpsdeavstevrl

FIGURE 3.10 The N126 MAP1B Mini-protein is Phosphorylated by GST-DAPKcore *in-vitro*. His tagged N126 mini-protein was over expressed in E.coli before gentle lysis and purification of soluble peptide using nickle beads. Purified protein was then added to a radioactive kinase assay before separation using a 4-12% gradien novex SDS-PAGE gel. **(a)** Autoradiograph of His-N126 titrated into kinase assay buffer containing 32P-labelled ATP and DAPK (lanes 3-6). No substrate (lane 1) and p21 substrate (lane 2) controls are shown. Graph below shows band density of phosporylated His-N126 as a function of the amount of protein in the reaction. (b) The sequence of N126 is shown with the candidate phosphoaccepter site (bold) and upstream positively charged residues highlighted in red.

a – Immunopecipitation of Endogenous MAP1B and DAPK from A549 Cells.

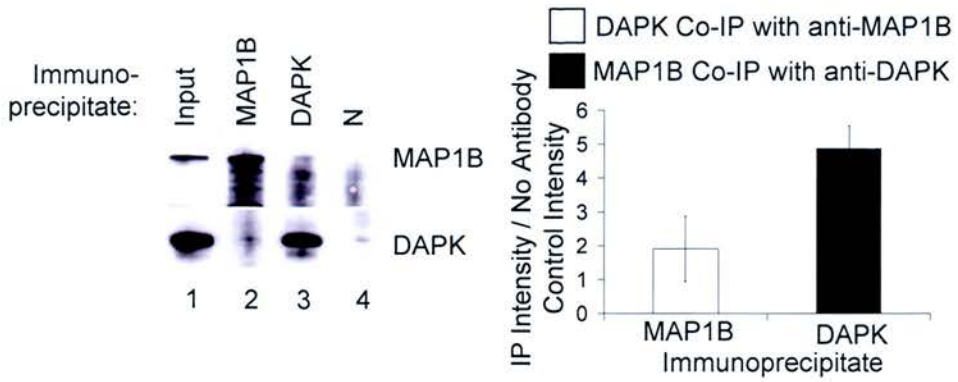

b – Ion Exchange Chromatography of Crude A549 Cell Lysate

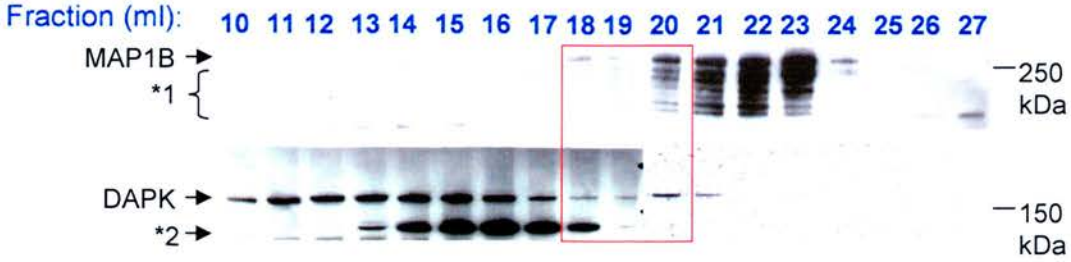

c – Gel Filtration of Chromatography of Pooled Factions 18-21

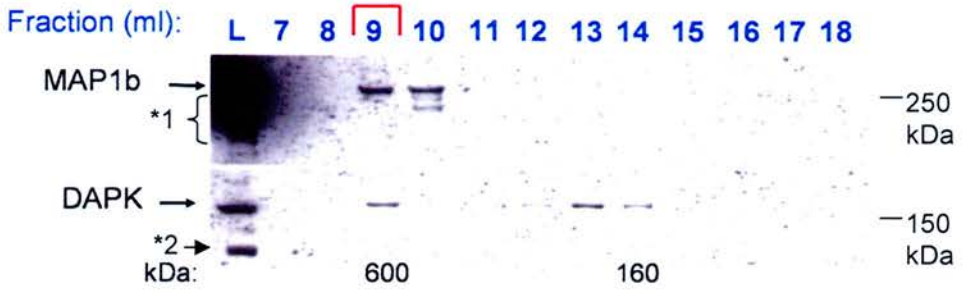

FIGURE 3.11 Isolation of High Molecular Weight Multi-Protein Complexes From A549 Cells. A549 cells that contain large amounts of endogenous MAP1B and DAPK were used as a source for study of endogenous protein. **(a)** Cells were lysed in native lysis buffer and MAP1B was precipitated using Mab AA6 beads and DAPK precipitated using anti-DAPK Mab beads. Input protein levels and no-antibody control precipitate is shown. The mean ratio between co-precipitated protein and the corresponding no-antibody control precipitation is plotted as a function of precipitating antibody. Error bars show standard deviation of the means from 3 separate precipitations. **(b)** A549 cells were lysed and protein applied to an ion exchange column followed by elution with an increasing salt gradient. Fractions were immunoblotted for DAPK and MAP1B (as indicated). **(c)** Fractions containing co-eluting pools of DAPK and MAP1B were applied to a Superose-6 gel filtration column and the elution of DAPK and MAP1B was analysed by immunoblotting as indicated. The elution of two molecular weight markers at 600 and 160 kDa are highlighted. *1 = degradation products. *2 = none-specific band.

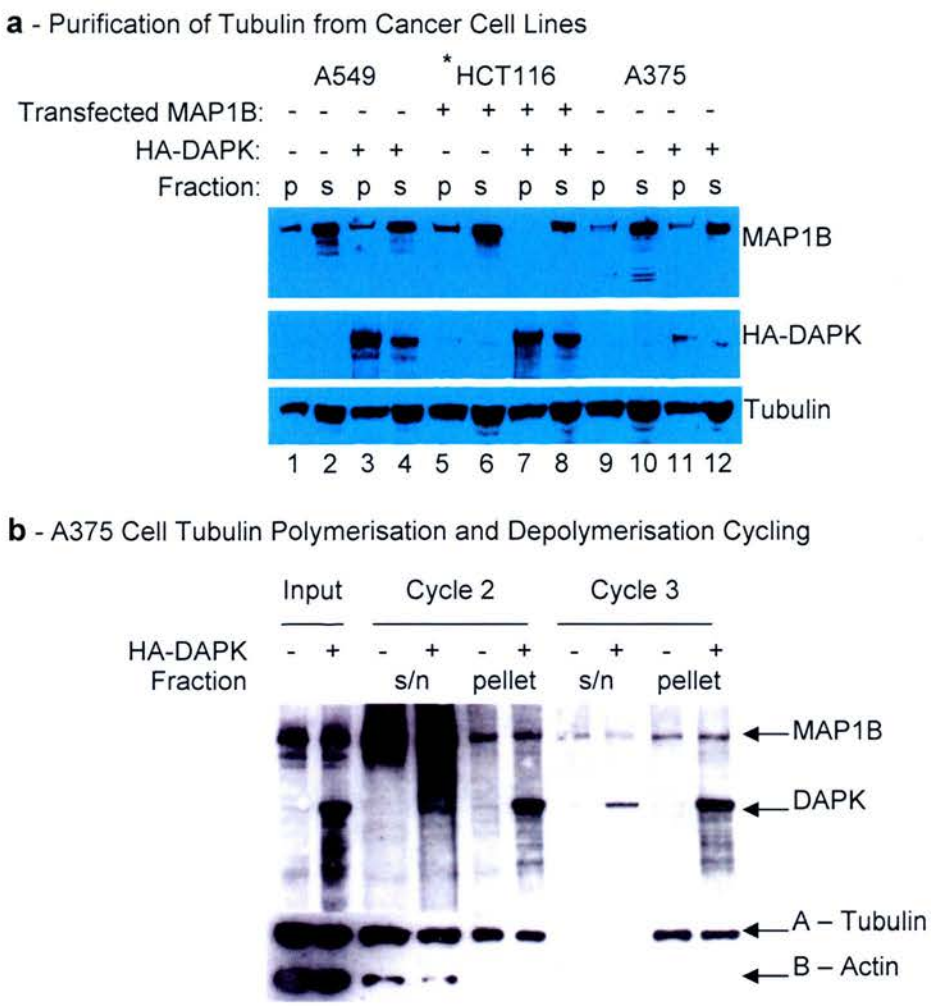

FIGURE 3.12 DAPK and MAP1B Co-precipitate with Microtubules During Temperature Dependent Microtubule Polymerisation/Depolymerisation Cycling. The indicated panel of cancer cell lines were transfected for 24 hours with vector control or HA-DAPK. MAP1B was co-transfeced into all HCT116 cultures because this cell line does not express large amounts of endogenous MAP1B. Cell cultures were then harvested and lysed in microtubule polymerisation buffer supplemented with 0.1% triton and then span 3 times for 15 minuets to create thoroughly clear lysate. Lysates were then incubated at 37C for 40 minuets with 1mM GTP to allow formation of microtubules. After polymerisation, samples were span at 13000g for 20 minuets at 25C to pellet the microtubules. Microtubules were then re-suspended in gel loading buffer and the protein separated using 4-12% gradient SDS-PAGE. (P) = microtubule pellet and (S) = supernatant. **(b)** A375 cells were transfected with HA-DAPK for 24 h before lysis and tubulin polymerisation and depolymerisation cycling. After 3 cycles, the resulting pellets and supernatants (S/N) were probed for MAP1B, HA-DAPK, tubulin and actin, as indicated.

FIGURE 3.13 a

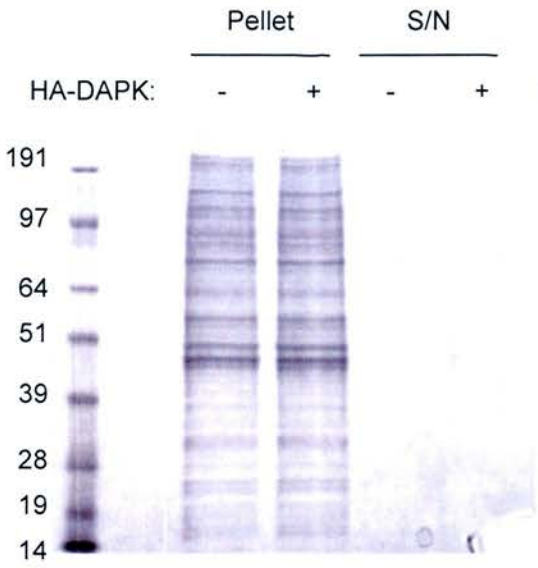

b

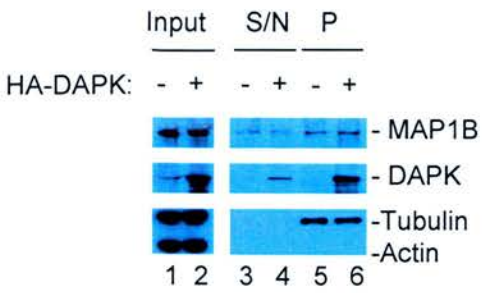

c

DAPK Induced Cells (Cy5 Labelled)

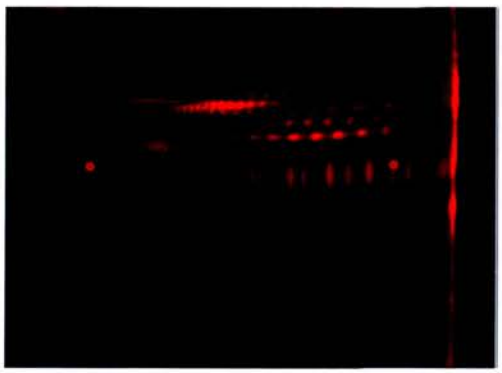

Non-Induced Reference Sample (Cy3 Labelled)

Merge

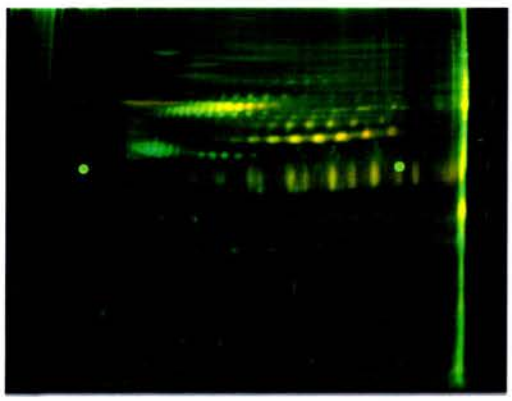

FIGURE 3.13 d

Cy5 – DAPK Induced

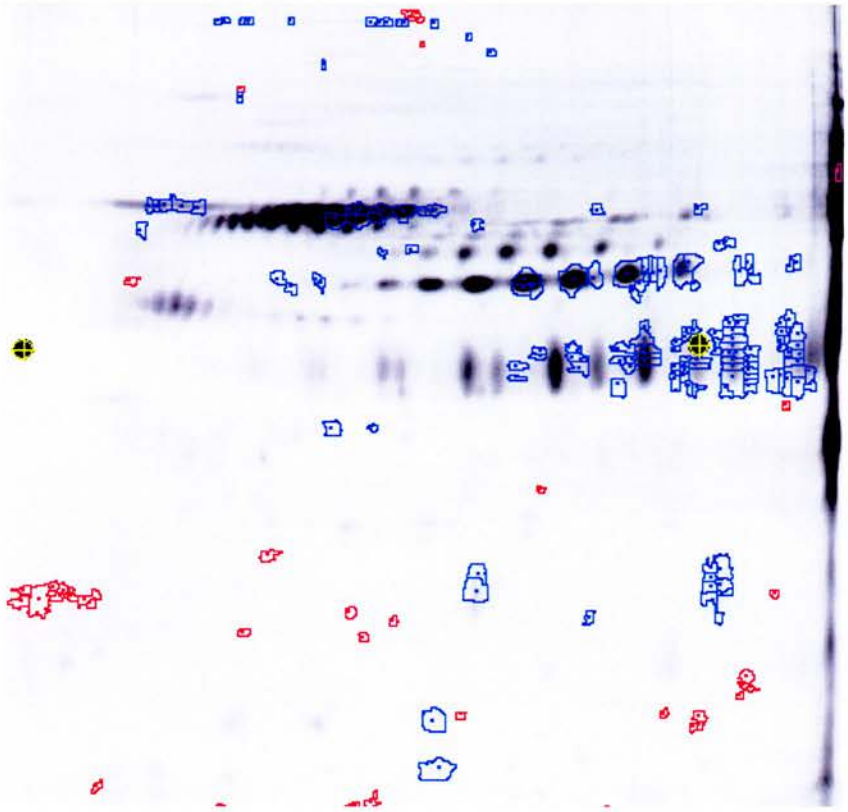

Cy3 – Non-Induced

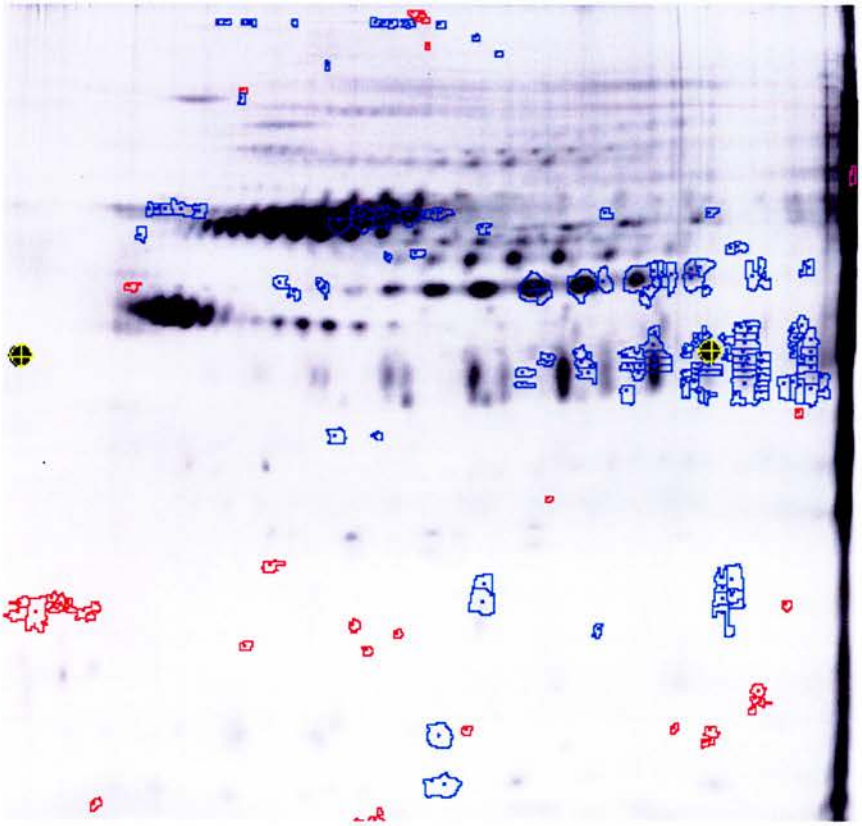

FIGURE 3.13 Use of Fluorescence 2-D Difference Gel Electrophoresis (DIGE) to Determine DAPK-Induced Changes to the Microtubule Associated Proteome

A stable tetracycline-inducible DAPK cell line was created using A375 cells that contain high levels of endogenous MAP1B. Cultures were treated with 5μg/ml tetracycline (+) to induce DAPK or treated with vehicle control (-) providing a reference sample, for 48 hours. $1*10^{\wedge 8}$ Cells were then harvested with microtubule polymerisation buffer, sonicated 10X for 10 seconds and then ground using a dounce tissue grinder before allowing microtubules to depolymerise on ice for 30 minuets. Lysates were then cleared 3 times at 13000g for 30 minuets before addition of 1mM GTP for 30 minuets at 37C to allow microtubules to form. After polymerisation, microtubules were separated by centrifugation at 13000g for 1 hour before depolymerisation on ice for a further 40 minuets. Microtubules were then polymerised and depolymerised a total of 3 times to prepare pure microtubules and specifically interacting proteins. Proteins in the pellet and supernatant prepared from Induced and non-induced samples were separated by SDS- PAGE and examined by colloidal blue staining (**a**). MAP1B, DAPK, Tubulin and Actin levels were assessed by immunoblot (**b**). (**c**) For DIGE analysis 50μg induced sample was labelled with Cy5 (red channel) and 50μg of reference (non-induced) sample with Cy3 (green channel). (**d**) Differential spots were noted (with respect to Cy3 labelled gel) above the 3-fold threshold level: Decreased (red outline) 41 spots (6%) Increased (blue outline) 238 spots (3.1%).

Chapter 4

4.1 Introduction

A novel interaction between DAPK and MAP1B has been discovered by employing a phage peptide display based interaction screen. Using *in-vitro* and cell based assays, this interaction has been determined to occur primarily via an interface located at the amino-terminus of MAP1B transcript variant 1. Interaction with MAP1B transcript variant 2 therefore is reduced suggesting that alternate splicing of MAP1B could be a mechanism for regulation of this interaction. In addition to this, the N-terminal 126 amino acids of MAP1B can be phosphorylated by purified DAPK kinase domain *in-vitro*, making the N-terminus of MAP1B a putative substrate for DAPK.

The interrelation between MAP1B, which is a microtubule associating protein, and DAPK, primarily thought of as an actin associating protein, suggests that DAPK may interact with a wider range of cytoskeletal elements than was previously thought. This is of particular interest because DAPK and MAP1B co-purify with microtubules from cells. Further investigation is warranted to study the relevance of the interaction between DAPK and MAP1B for signal transduction events during cell fate decisions and tumour suppression.

4.1.1 Discovery and Structure of MAP1B

MAP1B was discovered in the mid nineteen eighties as one of three microtubule associating high molecular weight proteins (Noble et al., 1989; Riederer et al., 1986). At the time, independent studies showed that MAP1B is expressed in embryonic brain as a major component of the neuronal cytoskeleton. It is known to be the earliest expressed embryonic MAP present in axons, somata and dendrites, where it is particularly abundant in developing axons. In the brain, MAP1B is at its most abundant at birth and its expression decreases with progression of post natal development of the nervous system. Therefore, MAP1B was quickly defined as a developmentally regulated protein and subsequent *in-vitro* and *in-vivo* models have proven this (Tucker, 1990; Tucker et al., 1988; Tucker et al., 1989; Tucker and Matus, 1987; Tucker and Matus, 1988; Viereck et al., 1989; Vouyiouklis and Brophy, 1993) (see section 4.1.2).

MAP1B is a very large protein that migrates with an apparent molecular weight of 320 kDa. However, its calculated molecular weight is smaller than this at 255 kDa, composed of 2462 amino acids. The microtubule binding domain of MAP1B consists of KKEE or KKEVI motif repeats and a further twelve imperfect repeat motifs of 15 amino acids in length. MAP1B not only binds microtubules but also to microfilaments via two actin-binding sites; binding site 1, at the N-terminus ending at position 517 and binding site 2, toward the C-terminus at positions 2336 – 2549 within the light chain region (Figure 3.5). The C-terminus of the heavy chain contains a hydrophilic region (amino acids 1866-2071) consisting of 12 imperfect repeat motifs of YSYETXEXTTXXPXX). Both the heavy chains and light chains can dimerise or oligomerise. The oligomerisation domain on LC1 is at its N terminus

near to the actin binding domain, whist the oligomerisation domain of MAP1B-HC is unknown (for review see (Riederer, 2007).

The full length human MAP1B gene is transcribed into mRNA of approximately 11 kb in length from a locus on the long arm of chromosome 15 (Lien et al., 1991). Human MAP1B shares 90% sequence homology to rat and mouse genes that have been studied as models for human MAP1B. Analysis of the MAP1B gene revealed two independent TATA boxes within the promoter (Liu and Fischer, 1996). These can independently direct expression when fused to reporter, and are infact part of two separate promoters that can direct temporal and tissue specific expression depending on the given situation (Liu and Fischer, 1996). This is controlled by the homeoprotein transcription factors engrailed and HNF3beta/Foxa2 that overlap (Foucher et al., 2003). This is a highly conserved mechanism where Foxa2 binding inhibits expression that would be otherwise driven by the positive regulator engrailed. In addition to alternative splicing at the 5' end (see above for details) transcripts of MAP1B are regulated by alternate splicing in the 3' UTR. This is thought to control cell specific expression of MAP1B where different splice patterns are seen in neuronal, kidney and skeletal muscle tissues (Liu and Fischer, 1996).

As explained previously, the MAP1B gene is expressed as a poly-precursor protein post translationaly cleaved at a position near amino acid 2100 (Figure 3.4). This yields a heavy chain (MAP1B HC) and a light chain (LC1) that can subsequently interact with each other. Both MAP1B and the closely related MAP1A and are cleaved in this manner yielding two regulatory heavy chains (MAP1B-HC and MAP1A-HC) and two light chains (LC1 (of MAP1B) and LC2 (of MAP1A)) that

can form a dimer involving any one heavy chain and light chain. The combination of chains in the complex is governed by poly-agglutination that controls the relative abundance and composition of MAPs in complex with microtubules. Cessation of neuronal development and cellular differentiation is associated with a switch between MAP1B chains to MAP1A chains. There are also separate homologous proteins that can interact in this manner. This includes LC3 which is an autophagy associated protein (Kabeya et al., 2000)and RASSF1A, a candidate tumour suppressor closely related to MAP1B-HC (Dallol et al., 2004; Liu et al., 2005a; Liu et al., 2005b).

Reading research published over recent years it is clear that MAP1B is involved in a variety of cell functions. In fact the name microtubule associated protein may now be misleading because MAP1B has been found to interact with multiple proteins involving many cellular compartments. Although a proportion of MAP1B is located on microtubules there is also a large soluble fraction in the cytosol. By turnover studies it was determined that there are multiple forms of MAP1B with multiple half lives. In in 10 day old rat brain there are two soluble forms with half-lives of 5.8 days and 4.8 days whilst the insoluble form has a half life of.18.5 days (Safaei and Fischer, 1990).

4.1.2 MAP1B, A Differentiation-Associated Protein

MAP1B is expressed as homologues in many species through vertebrate animals to invertebrates such as flies (Figure 3.4). Fascinatingly, the trypanosome parasite responsible for African sleeping sickness: *Trypanosoma brucei*, expresses a 110 kDa protein with 60% homology to MAP1B, and this is thought to be associated with

molecular mimicry during parasite-host interaction (Baron et al., 2007). In continuously growing fish such as the tench, MAP1B is expressed in the nervous system throughout the organisms life span correlating with its development, suggesting that MAP1B is closely related to developmental differentiation in these fish (Tomasiewicz and Wood, 1999).

Studies of MAP1B knock out mice have shown that MAP1B protein is required for co-ordination of cytoskeletal components during neuronal differentiation. The fact that MAP1B mutants survive indicates that MAP1B is not essential for development. Rather, study of null embryos has revealed that MAP1B knock out leads to delayed neuronal development and abnormal morphology of individual cells. These cells, cultured from knock out mice tissues, are deficient in morphologies characteristic of differentiation including axon formation and neurite out growth and this correlates with cytoskeletal defects such as reduced microtubule bundling in these cells (Bouquet et al., 2004).

Not only is MAP1B present in developing tissues it is also expressed in primary cultures and various cell lines. In cell culture, neuronal cells that resemble committed CNS precursor cells (NT2/D1 cells) express MAP1B along with other markers of neuronal cell fate. Knock down of MAP1B with antisence mRNA inhibits neural growth factor (NGF)-induced PC12 cell differentiation, whereas subsequent antisense removal leads to recovery of differentiation of these cells (Brugg and Matus, 1988).

4.1.3 Post-Translational Modification of MAP1B

MAP1B is expressed as poly-precursor protein that is cleaved into heavy and light chains. These can subsequently interact with each other and with closely related map proteins to form a dimer involving any one heavy chain and light chain. The combination of chains in the complex is governed by post translational poly-agglutination regulating the abundance and composition of MAPs on microtubules.

MAP1B phosphorylation plays a crucial role in modulation of its function. Over the years multiple kinases have been found to phosphorylate many separate sites on MAP1B. Two programs of MAP1B phosphorylation are often defined in research papers referred to as mode I and mode II phosphorylation. Mode I phosphorylation is primarily catalysed by proline-directed kinases (PDK's) and is associated with early development, whereas mode II phosphorylation is sustained into adulthood. These different modes have been studied in tissues, primary culture and in cell lines.

The list of characterised MAP1B kinases include mode II kinase; CK2, and kinases responsible for mode I phosphorylation including; cyclin dependent kinases such as cdc2, glycogen synthase kinase 3 (GSK3) or cdk5 and Jun N-terminal Kinase (JNK) (For review see (Riederer, 2007)). The main documented roles for these kinases include phosphorylation of MAP1B within or near to the heavy chain microtubule binding domain. It is not surprising therefore that modification by these kinases results in differential regulation of MAP1B association with tubulin. For example, JNK1 and cdk5 activity is for the most part believed to induce microtubule stability via modification of MAP1B, whereas modification by GSK3β is considered to induce dynamically unstable microtubules. However the exact role for these kinases

via association with MAP1B is often controversial, with different reports sometimes offering opposing evidence (see sections 4.1.5 and 4.1.6).

4.1.4 GSK3β Signalling to MAP1B

Maintaining a fraction of dynamically unstable microtubules in neuronal cells is important for axon growth and path finding. Phillip Gordon-Weak's group have demonstrated that GSK3β plays a central role in the control of neuronal microtubule dynamics acting as a molecular switch to regulate microtubule stability during axonogenesis (Goold and Gordon-Weeks, 2001; Goold and Gordon-Weeks, 2003; Goold and Gordon-Weeks, 2005; Goold et al., 1999). Known phosphoaccepter sites for GSK3β on MAP1B include ser1260 and thr1265 in growing axons. Expression of GSK3β induces PC12 cell differentiation and modulates microtubule stability via phosphorylation of MAP1B at these sites. Chemical inhibition of GSK3β on the other hand, inhibits the induction of morphological changes indicative of MAP1B loss in neurons including; reduction in axon elongation and alteration of microtubule and F-actin distribution. This shows that signalling through GSK3β modifies MAP1B function during differentiation. During NGF induced PC12 cell differentiation, the mitogen activated protein kinase (MAPK) pathway is upstream of GSK3β in signalling to MAP1B. This is induced by NGF that docks with the tropomyosin-related tyrosine kinase (TrkA) receptor. Engagement of factor with receptor leads to activation of GSK3β that is then able phosphorylate MAP1B. TrkA can trigger a number of signaling pathways, including the MAPK pathway and the phosphatidylinositol-3 kinase (PI3K) pathway. Using pharmacological inhibitors in PC12 cells sympathetic neurons in culture and in vitro kinase and activation assays

Gordon Weaks' lab determined that the MAPK pathway, and not the PI3K pathway, links NGF signaling to GSK3β activation. As a consequence, NGF increases differentiation and neurite growth rates by coupling the MAPK pathway to the activation of GSK3β and thereby phosphorylation of MAP1B (Goold and Gordon-Weeks, 2005).

4.1.5 MAP1B and the Role of JNK in Neuronal Survival and Degeneration

Whereas GSK3β activity is associated with dynamic instability of microtubules, JNK on the other hand is believed to phosphorylate MAP1B leading to induction of stable microtubules. Hoshino's group in 2003 observed that pharmacological inhibition of JNK *in-utero* lead to irregular neuron morphology and increased stable microtubules and this correlated with decreased phosphorylation of MAP1B (Kawauchi et al., 2003). The authors concluded that this raised the possibility of involvement of JNK in controlling tubulin dynamics in migrating neurons by MAP1B phosphorylation (Kawauchi et al., 2003). They also published evidence in 2005 showing that a JNK inhibitor suppressed mode I phosphorylation of MAP1B in primary and slice cultures providing corroborating evidence that mode I phosphorylation of MAP1B is facilitated by JNK leading to increased microtubule stability. (Kawauchi et al., 2005). Also, an independent study was published in 2005 using Jnk1(-/-) knock out mice that exhibited a progressive loss of MTs within axons and dendrites correlating with MAP1B hypophosphorylation in the Jnk1(-/-) brains. Here, the authors suggest this resulted in compromised ability of MAP1B to bind MTs and promote their assembly. These studies together suggest that JNK1 is required for maintaining cytoskeletal stability in neuronal cells and negatively regulates MAP1B activity and

MT assembly (Chang et al., 2003). There is no evidence however showing that JNK can directly phosphorylate MAP1B and only a correlation exists between JNK activity, microtubule stability and MAP1B phosphorylation. This raises the possibility that other kinases could be responsible for this effect.

The JNK genes are responsible for coding a wide variety of peptides. The JNK family consists of three genes (JNK1, JNK2, JNK3) coding for many splice variants, of which 10 have (Gupta et al., 1996)been characterised. In addition to this, isoform and substrate specific functions add a further layer of complexity. JNK activity is classically associated with phosphorylation and activation of c-Jun transcription factor, but the role of JNK is much wider than that. Other substrates are known such as activating transcription factor 2 (ATF2), Elk-1 and p53 in the nucleus, and 14-3-3, Smac and Bcl-2 in (Moretti et al., 2007)cytoplasmic compartments. Therefore the JNK pathway has many multifaceted functions through multiple pathways.

Classically, activity of the JNKs (or stress associated protien kinases - SAPKs) were considered an anti-proliferation or degenerative signal having initially been characterised in response to stresses such as (Newbern et al., 2007) cytokines and osmotic stress. It is interesting therefore that JNK has been implicated in signalling to MAPs in brain, where it is believed to confer neuronal stability and has a neuro-protective effect. The JNKs are activated by various stimuli during neural development as well as being activated during neuronal death following a stress. Yet to date, no differences have been defined between JNK activity in differentiating neurons and its activity in dying ones, and this strongly suggests the JNK pathway maybe involved in the regulation of both circumstances.

Neurons require target-derived trophic support for survival. The term 'trophic support' is a general term used to encompass a range of factors that impact neuronal survival (e.g., growth factors, structural/metabolic precursors and even blood supply etc.). In motoneuron cell culture for example, skeletal muscle extract is often used as a supplement containing a range of trophic factors. In motoneurons deprived of trophic support, pharmacological inhibition of JNK attenuates death associated events such as caspase activation, and nuclear condensation. Suggesting that JNK activity promotes programmed cell death in these circumstances. However, inhibition of JNK in healthy motoneurons supplied with trophic support results in increased degenerative associated events such as lowered mitochondrial membrane, and attenuation of neurite outgrowth with associated reduction in phosphorylation of MAP1B. These findings highlight the dualistic nature of JNK activity in both survival and degeneration of neuronal tissues (Newbern et al., 2007) During development, neural cells must compete with each other for limited trophic support (Levi-Montalcini, 1987). This presumably leads to temporal and pathway specific differences in the regulation of cell death or survival and so leads to selective vulnerability of specific cell populations. In other words, the activity of JNK could regulate survival or growth depending upon the given situation during development.

4.1.6 MAP1B Modification by Cyclin Dependent Kinase 5 (cdk5)

The role for cdk5 in regulation of MAP1B and its resulting impact on microtubule dynamics is also unclear. Initial studies found that a Cdk5 inhibitor did not suppress mode I phosphorylation of MAP1B in primary and slice cultures. Primary culture studies showed an involvement of Cdk5 in regulating microtubule dynamics

however, but this did not effect MAP1B phosphorylation status. On the other hand, an increase in phosphorylated MAP1B was observed in COS7 cells when Cdk5 was co-transfected with p25 which is a co-factor specifically produced in pathogenic brains. The authors concluded from this evidence that mode I phosphorylation of MAP1B is not facilitated by Cdk5 in the normal developing cerebral cortex, only by Cdk5/p25 in diseased state brain tissue (Kawauchi et al., 2005).

In an apparent contradiction to this, two separate studies provide evidence that Cdk5 induces Mode I phosphorylation of MAP1B in developing cerebral cortex. During differentiation of neurons their axons elongate and perform steering reactions to coordinate connections with neighboring cells. Mode I phosphorylated MAP1B is present in stable regions and not in unstable regions of turning axons, whereas the total pool of MAP1B is expressed throughout in the entire growth cone of extending axons. The first report demonstrated that inhibition Cdk5 results in reduction of mode 1 phosphorylated MAP1B in steering axons. This was supported by inhibition of Cdk5 by antibodies or the inhibitor Roscovitine that resulted in growth cone collapse and axon retraction preventing axon outgrowth. Here the authors conclude that the presence of Cdk5-phosphorylated MAP1B in stabilised growth cone areas can be attributed to the local activation of Cdk5 and that this highlights a role for cdk5 in steering and path finding of growth cones (Hahn et al., 2005) . A mechanism for this was reported in an independent study where Reelin, a factor crucial for regulating neuronal migration and path finding in the developing brain, induced mode I MAP1B phosphorylation, both *in-vivo* and *in-vitro*, through cdk5 activation. Therefore a proposed function for cdk5 is integration of Reelin signalling through

induction of post-translational modifications on MAP1B in the growth cone of extending axons (Gonzalez-Billault et al., 2005).

A possible explanation for the apparent contradictions between studies involving cdk5 action and MAP1B could be that signals activated in a "diseased state" brain are also activated in the developing brain. This would be a similar situation to JNK that is also active in differentiating and injured neurons. This implies that pathological brain is similar to developing brain in this respect and that signals during both processes converge through MAP1B. For example, during development of the central nervous system, most developing cells are surplus to requirement and are removed by programmed cell death. There has to be therefore a balance between survival of neurons that have made correct connections with neighbouring cells and the death of neurons that are not required. Differentiating cells, like regenerating neurons in injured brain will display differentiation associated morphologies such as axon migration and path finding. As described above, these morphologies are controlled by signalling through JNK and cdk5 pathways impinging on MAP1B, therefore it can be assumed that MAP1B could play a central role in the control of life or death decisions, much like DAPK plays a central role in this process also.

4.1.7 Convergence of DAPK and MAP1B Expression Patterns, Biochemistry and Function

The rat pleochromocytoma 12 (PC12) cell line is an experimentally tractable model used to study neuronal differentiation in cell culture. MAP1B protein expression is induced by treatment of PC12 cells with NGF, commensurate with differentiation of these cells and axon out growth. This is in addition to activation of ERK/MAPK

pathway leading to mode I phosphorylation of MAP1B by GSK3β and is commensurate with cytoskeletal rearrangements and neurite out growth. Also, DAPK catalytic activity and protein levels increase after nerve growth factor (NGF)-induced differentiation of rat PC12 cells (Schumacher et al., 2002a). This suggests that DAPK and MAP1B may both be co-regulated during neuronal differentiation. The following discussion highlights functional and biochemical overlap between the DAPK and MAP1B pathways.

4.1.7.1 DAPK *and MAP1B in Neural Plasticity*

The brain with its axon and dendrite circuitry is not "hard-wired". Rather, neural networks are deemed plastic because they are modifiable by experience, where the brain has a significant ability to adapt not only during early development, but also in adulthood. Even during development, precise axonal connections are formed in the brain based on the actual experience of a given organism, and the adult brain retains a capacity for adaptation in response to continued interaction with its environment. This experience-dependent plasticity is not only the basis for learning and memory it is also crucial for the brain to recover from damage and disease states. A lack of neuronal plasticity during later adulthood is responsible for age-related brain degeneration and cognitive decline.

Using Northern blot analysis and *in-situ* hybridisation, DAPK mRNA levels were observed to be highest in the brain and lung during development (Yamamoto et al., 1999). DAPK mRNA expression starts at around embryonic day 13 in the brain and then throughout embryonic development. Specifically, DAPK is expressed at the highest levels in proliferative regions within cerebral cortex, hippocampus, and cerebella Purkinje cells. Thereafter, DAPK mRNA levels gradually decline

postnataly with the exception of hippocampus where expression remains high. This observation suggests that not only may DAPK play a role in neurogenesis but also in neural plasticity in adult brain hippocampus. Like DAPK, MAP1B is developmentally regulated and present at high concentrations in developing neuronal tissues. After development, both proteins are depleted, where MAP1B chains are replaced with MAP1A chains. There are however, exceptions to this rule, and it is recognised that DAPK and MAP1B are both expressed in areas of adult brain associated with neuroplasticity. In adult brain, MAP1B is also found in selected areas where there is active neural outgrowth, including the olfactory bulb and regions of the brain associated with neuronal plasticity such as the hippocampus and the dendrites of Purkinje cells in the cerebellum.

In adult brain DAPK is highly expressed in hippocampal neurons and is implicated in spatial learning and memory. DAPK-mutant mice have been bread by deleting 74 amino acids from the DAPK core kinase domain, creating a kinase dead mouse (Chevalier, 2006). These mice were used to study the effect of DAPK kinase mutation on the regulation of spatial memory using Morris water maze tests. This test involves recording the ability of mice to locate a hidden escape platform in a pool of water. Both mutant and wild-type mice were able to learn the water maze however mutant mice had an increased ability to memorise the platform position compared to wild-type mice. This was observed in the original test where the platform was present in one location and also in a reversal test, where the DAPK mutant mice quickly learned the location of the platform located at a different position. Therefore DAPK kinase-dead mutant mice exhibit superior spatial learning

in addition to a more precise memory than wild-type littermate's (Yukawa et al., 2006).

It is highly likely therefore that both MAP1B and DAPK, being expressed in areas associated in neuroplasticity in adult brain, such as the hippocampus, are both involved in regulating neuronal path finding, survival and plasticity-associated cell fate decisions in these tissues.

4.1.7.2 DAPK *and MAP1B in Recovery from Brain Injury*

During recovery from central nervous system (CNS) and peripheral nervous system (PNS) injury MAP1B is expressed in regenerating neurons. After injuries such as ischemia after stroke or after chemically induced seizure, both DAPK and MAP1B expression is sharply increased. This elevation in expression of both proteins correlates with differentiation-associated morphologies such as axon regeneration and path finding and cytoskeletal rearrangements (Popa-Wagner et al., 1999a; Popa-Wagner et al., 1999b; Schmoll et al., 2001; Schumacher et al., 2002b).

The function and biochemistry of DAPK in brain injury has been studied by two independent groups; Henshall's group and Wattersons's group. Initially Watterson's group, using a rat model of neonatal cerebral hypoxia-ischemia (HI) quantified an increase in DAPK activity in hippocampus homogenates from injured right hemisphere compared to the uninjured left hemisphere, 7 days after injury (Schumacher et al., 2002b). This preliminary observation raised the possibility that DAPK activity was associated with recovery from HI, during neuronal repair and differentiation. These studies were backed up by corroborating evidence from Henshall's group using a model of focally induce siezure in rats that causes neuronal

injury within the hippocampus. DAPK was found to be constitutively expressed in uninjured hippocampus by western blot analysis. However, immunohistochemistry study showed that seizures triggered an increase in the counts of DAPK expressing cells specifically in affected areas. This was accompanied by changes in DAPK interaction with death associated factors as determined by binding studies. Interestingly, DAPK co-immunoprecipitation with actin was increased immediately after injury and then was reduced after only 4 hours of recovery. After injury DAPK also co-precipitated with antibodies directed to tumour necrosis factor receptor 1 (TNF1) and the Fas-associated death domain protein, commensurate with caspase-8 proteolysis, suggesting that the TNF pathway is involved in activating DAPK in this model. In contrast to this, within surviving fields of the hippocampus, DAPK interacted with the chaperone protein 14-3-3 known to be involved in molecular sequestration of cell death promoters. This is interesting because it provides a mechanism by where DAPK can be activated or repressed depending on the context within specific fields of the brain. The importance of DAPK in response to seizure in human brain was examined in further study (Henshall et al., 2004). DAPK expression and localisation in hippocampal resections from patients with intractable temporal lobe epilepsy was compared to autopsy controls. Here, expression of DAPK was significantly increased in epilepsy brain compared to control brain commensurate with increased FADD co-immunoprecipitation. This suggests that DAPK is activated by the TNF pathway in both human and rat in response to siezure.

It is worth noting that the research papers from Henshall's group present data that contradicts the prevailing view of DAPK as a promoter of cell death only (Cohen and Kimchi, 2001). For example they demonstrate a high constitutive and post-seizure

expression of DAPK within both surviving and in vulnerable hippocampal regions. In addition to this they show that although seizure increases the number DAPK expressing cells, these out number TUNEL positive cells within the cortex, which is also largely resistant to cell death using their model. These data suggest that DAPK may have alternative roles within these resistant tissues. This also brings to mind studies showing anti-apoptotic effects of DAPK from non-neuronal tissues, where mouse DAPK inhibited TNF-induced cell death, also in contradiction to the DAPK dogma (Jin et al., 2001; Jin et al., 2002; Jin et al., 2006). The studies in human brain showed that levels of both DAPK and DAPK interacting protein 1 (DIP-1) were increased in the cytoplasm and endoplasmic reticulum fractions in epilepsy brains (Henshall et al., 2004). This correlated with increased DAPK binding to DIP-1 as determined by immunprecipitation. Again, this could be in contradiction to the prevailing view because DIP-1 is a ubiquitin E3 ligase and so likely to be a positive regulator of DAPK sequestration and degradation. Therefore according to dogma, increased DIP-1 binding might suggest reduced DAPK activity. Even more strikingly, the authors observed increased auto-phosphorylation of DAPK at the phosphoaccepter serine 308. And although the authors mistake this for an activating modification, phosphorylation at this site is actually considered an auto-inhibitory modification, reducing DAPK activity. Again though, other studies directly contradict this (see section 1.8 for a detailed review of these studies). Further investigation is therefore needed to clarify what role DAPK performs in non-dying cells such as in normal brain. In other words, how does DAPK contribute to the cell fate decision making process in different situations during development and during recovery from injury in the brain? Also, is the situation in the brain replicated in non-

neuronal tissues and in diseases such as cancer where there is very good evidence that DAPK is a tumour suppressor (see section 1.3)?

Old age is associated with an enhanced susceptibility to stroke and poor recovery from brain injury. One potential mechanism for this is by alteration of the activity of brain plasticity-promoting factors. Behaviorally, aged rats are more severely impaired by stroke than are young rats, and they also show diminished functional recovery. After induced stroke in rats, infarct volume and the severity of the initial damage is not increased by age, rather there are differences in the cytological and biochemical response to the stroke. In older rats, stroke is associated with increased neuronal degeneration, premature accumulation of BrdU-positive cells and accelerated apoptosis. Expression of MAP1B and other plasticity-associated proteins are delayed in the aged rats and there is also an increase in the amount of the neurotoxic C-terminal fragment of the β-amyloid precursor protein (βAPP) (Popa-Wagner et al., 2007). Therefore, although aged brain is able to respond to injury, the timing of the cellular and biochemical response is dissregulated. Therefore, it is proposed that this model would provide a convenient system to elucidate the exact role of MAP1B and also DAPK in regeneration by comparison of the biochemistry of stroke in aging brain to young brain.

4.1.7.3 MAP1B and DAPK *Responses to Neuronal Guidance Cues*

The human central nervous system contains around 10^{12} neurons and around 10^{15} synaptic contacts between them. Therefore there is an extremely precise pattern of connections in the human brain established during embryonic and early postnatal development. Once postmitotic neurons have migrated from proliferative sites their axons must select the correct targets, usually some distance away and this is directed

by the action of chemotropic molecules. It is interesting that chemotropic molecules are not only involved in guidance of axons, but they also influence cell fate decision making. This is perhaps not surprising given that there is a high level of programmed cell death during normal neural development a process often referred to as neural Darwinism (Edelman, 1993). During this process during early development neurons and their synapses are overproduced and subsequently lost as cells compete for brain space. This is analogous to the process of synaptic pruning in adult brain where axons will only persist if they have become members of functional neuronal networks (Toulouse et al., 1986).

4.1.7.4 MAP1B and DAPK *Response to Netrin Signalling*

Netrins are secreted chemotrophic proteins important for contact-mediated stimulation of axonal guidance and growth. There are 4 members of the netrin family (netrin 1-4) in vertebrates. Netrins 1 and 2 engage with the cell surface receptors; deleted in colon cancer (DCC), neogenin and the Unc5H 1-4 family. Binding to DCC or neogenin results in attraction of the axon toward the molecular source, whereas interaction with the Unc5H family results in repulsion (for review see (de Castro Soubriet, 2001)). Engagement with both types of netrin receptors exerts a survival-promoting (trophic) effect on neurons.

The signalling cascades governing neuronal migration link extracellular signals to cytoskeletal components. For example, as mentioned in section 4.1.7.3, MAP1B is required for Reelin signalling in neuronal migration and axonal guidance via the GSK3β and cdk5 pathways, resulting in changes in the dynamic instability of microtubules and cross-talk between microtubules and actin filaments. A separate study has demonstrated that Netrin-1 also regulates mode I MAP1B phosphorylation

of MAP1B both *in-vitro* and *in-vivo*. This activity also depends on GSK3 and cdk5 kinases. Here, MAP1B deficient neurons had reduced chemoattractive response to Netrin 1 in vitro and MAP1B mutant mice had abnormalities indicative of netrin 1-deficient signaling. This implicated MAP1B as a downstream effector in the Netrin-1 guidance pathway (Del Rio et al., 2004).

Cell surface receptors are often thought of as inactive until bound by ligand, however, it has been recently discovered that some receptors are active in absence of ligand. A class of these receptors are called dependence receptors that induce death signals when the ligand is absent from the cell. As a result, expression of these receptors leads to dependence on ligand for cell survival. As well as being a system to allow correct patterning of neuronal development, this provides a mechanism allowing inhibition of tumor growth, by programmed cell death induction in miss placed cells that would usually only grow in settings of ligand unavailability (For review see (Bernet and Mehlen, 2007). The netrin 1 receptors (Unc5H1-4) have recently been described as dependence factors, and so are able to trigger cell death in the absence of netrin 1.

The netrin-binding dependence factor: UNC5H2, is a death domain containing protein that interacts with DAPK by a homeotypic binding interaction via their two death domains. Death induced by expression of UNC5H2 in the absence of netrin was attenuated by the ablation of DAPK protein in cells derived from knockout mice, indicating that interaction between the two proteins effects UNC5H2 death promotion (Bialik and Kimchi, 2006; Gozuacik and Kimchi, 2006). However, Netrin- 1 binding to UNC5H2 had no effect on its binding to DAPK but removal of

ligand led to dephosphorylation of DAPK at Ser308 which the authors say is indicative of DAPK activation. It is very interesting that netrin 1 is implicated in both regulation of neuronal cell guidance and in tumourigenesis, because this provides a possible biochemical link between MAP1B function and DAPK death signaling.

4.1.7.5 Semophorin 3A and Induction of Programmed Cell Death in Neurons

The Semophorins are a separate large family of chemotactic molecules comprising approximately 30 members. Semophorins are either secreted or expressed as transmembrane proteins with a common "sema" domain which confers the binding specificity of each (reviewed (de Castro, 2003; de Castro and Bribian, 2005)). Class 3 semaphorins bind selectively to the neuropilin receptors neurophillin 1 and 2 where they cause chemorepulsion of growing axons often accompanied by collapse of the effected neuron leading to programmed cell death during early development. Experimentally, neuronal apoptosis is induced by exposure to semaphorin 3A (Sema3A) that can be blocked by antibodies against neuropilins. These molecules are also secreted by early apoptotic neurons suggesting that, before their death, these neurons may produce destructive axon guidance molecules affecting neighboring cells and thus transferring a bystander effect across specific neuronal populations (Shirvan et al., 1999).

An internalised form of Sema3A is associated with degeneration of neurons in hippocampus during Alzheimer's disease (AD). During this process an internalised form of Sema3A is accumulated in dying neurons correlating with the appearance of phosphorylated MAP1B. This suggests that Sema3A signaling may be coupled to alteration of cytoskeletal dynamics during neurodegeneration in AD. In addition to this, a multi-protein complex was isolated from human AD hippocampus consisting

of MAP1B, Sema3A, collapsin-response mediator protein 2 (CRMP-2) and Plexins A1 and A2 (Good et al., 2004). Therefore sema3A is implicated in programmed cell death during not only early development, but also during brain damage as a result of AD. Also, this is an example of MAP1B involvement in degeneration of neuronal tissues.

4.1.8 A Role for the DAPK and MAP1B Interaction in Cell Fate Decision Making?

The detailed review of the literature detailed in the above discussion suggests that there is considerable overlap between the known roles of DAPK and MAP1B in neuronal development. Both proteins are highly expressed throughout early developing brain, and then reduced in adult brain, indicating that they both have roles important to neural development. During NGF-induced differentiation of PC12 cells, both MAP1B and DAPK expression is induced, preceding differentiation in these cells. Both proteins are expressed in areas of adult brain associated with neuroplasticity, and are expressed during recovery from injuries arising form seizure and stroke. Finally, both DAPK and MAP1B are central in signalling by netrins, which act as guidance factors and as survival factors.

Although the majority of research involving MAP1B has been focused on its role during axon growth, there is a growing body of evidence showing that it has many more functions. Regulation of cytoskeletal dynamics is a major effecter of MAP1B activity, but this is not the only way it can affect cytological response. The fact that there is a large soluble cytosolic fraction of MAP1B only goes to highlight this. A brief search of the published literature shows that MAP1B is often thought of in 2

complimentary ways; 1) That is it a marker of neuronal development and recapitulation of development during regeneration, perhaps as a positive regulator of survival, 2) That is it is a marker of neuronal plasticity, facilitating axon growth and path finding in these cells. However, a more detailed study of the published evidence presented above leads to the hypothesis; 3) That MAP1B is a marker of neuronal injury, involved in life or death decision-making in regenerating tissues. This hypothesised role for MAP1B is not incompatible with points 1 and 2, on the contrary, it is highly likely that they should compliment each other as a consequence of the neural growth and regeneration process.

MAP1B knockout mice survive into adulthood, but have defected brains, not only due to abnormal axon morphology but also due to delayed neural development and altered brain size. This indicates that MAP1B knock-out causes miss-regulation of neural development above the level of axonal growth, possibly due to altered cell fate decision making. In a cell culture based situation, MAP1B knockout by anti-sense mRNA in PC12 cells causes inhibition of NGF-induced differentiation on the whole, not simply inhibition of axon generation. Subsequent removal of anti-sense mRNA then results in differentiation. This suggests that cell fate is regulated by MAP1B and not simply just axon growth and path finding. MAP1B phosphorylation state can be regulated by the JNKs/SAPKs, kinases classically involved in signalling anti-proliferation or degeneration. However, in the brain JNK is active during diverse situations such as differentiation, regeneration and degeneration, not involving the activities of cJun. This suggests that other down-stream factors, possibly including MAP1B, are critical for regulation of cell fate after JNK signalling. The cell guidance factors, netrin and semophorin are both known to influence neuronal

survival, and both have been shown to influence MAP1B phosphorylation state. This is perhaps the most compelling evidence that MAP1B could be integral in cell fate decision making in plastic fields of the brain.

Recent reports have highlighted a role for MAP1B in the control of programmed cell death in neurons. β-amyloid (Aβ) accumulates in the brain after injury and is also associated with various pathologies such as AD and Down's syndrome. β-amyloid causes programmed cell death and degeneration in neuroal tissues . An important report shows that MAP1B V1 expression is induced in cultured cortical neurons by active β-amyloid fragments. Over-expression of MAP1B-V1 in these cells causes programmed cell death whereas MAP1B-V2 does not. This is evidence that the N-terminal 126 amino acids of MAP1B is a programmed cell death-effecting signal. In addition to this, a recent report published in Nature provides evidence that the Giant axonal neuropathy (GAN) gene, gigaxonin induces degradation of MAP1B light chain (LC1), and that this induces programmed cell death in cultured neurons. Over expression of MAP1B lead to programmed cell death in wild-type neurons whereas reduction of MAP1B expression in GAN-null neurons enhanced survival. This is corroborative evidence showing that MAP1B can act as an effecter of programmed cell death and implicates MAP1B in neurodegenerative disease.

Both MAP1B and DAPK are cytoskeletal-associated proteins previously explicated to influence cytoskeletal dynamics. Data is presented in this study suggesting that DAPK interacts with MAP1B via an N-terminal interaction site. Also, *in-vitro* study shows that DAPK can bind to polymerised microtubules. Both MAP1B and DAPK have been previously shown to interact with actin and microfilaments, however it

was not possible to reproduce this using the microtubule polymerisation assay or the co-IP experiments presented in this thesis chapter. Further experimentation is required to study interaction between DAPK, MAP1B and both the microtubule and microfilament cytoskeletal elements. This may shed light on the role of MAP1B interaction with DAPK.

Although only a small proportion of endogenous MAP1B and DAPK proteins from A549 cells co-bound, HA-DAPK transfection into MAP1B-expressing A375 cells was sufficient to induce interaction between the two. DAPK transfection has been shown in numerous studies to be sufficient to induce DAPK-related signalling and subsequent cell death. Therefore it is assumed that MAP1B binding to DAPK was induced by over expression of DAPK. To prove that this is not a transfection artefact, a non-synthetic signal needs to be found that will induce interaction of endogenous DAPK with MAP1B. This can only be achieved after further DAPK transfection studies have been directed in order to determine the down-stream effects of this interaction.

A mechanism that could explain the different roles of MAP1B, could be by differential post-translational modification. For example, there are two broad modes of MAP1B phosphorylation; Mode I and Mode II that show different intracellular localisation. Also, it has been reported that under different circumstances, MAP1B phosphorylation may lead to microtubule stability or dynamic-instability. This apparent contradiction could come about by phosphorylation by different enzymes on different phosphoaccepters leading to an allosteric change in MAP1B or a change in down stream MAP1B binding, or both. More detailed studies of MAP1B

interacting proteins are required in order to understand their role in cell fate decision making processes.

Is MAP1B a positive or negative regulator of DAPK activity in cancer cells? This is the vital question that needs to be answered with regards to MAP1B influence on DAPK action. Therefore initial experiments should be designed to address this. This would address 2 further fundamental questions; 1) is there a functional interaction between MAP1B and DAPK in cells and 2) Does this interaction impinge on tumour suppression?

4.2 Results

4.2.1 MAP1B Protein is Expressed in a Wide Variety of Cancer Cell Lines.

Previous research has shown that MAP1B and DAPK are both implicated in brain developmental processes and during response to disease states in the brain including after injury and following seizures. Although, it is well known that DAPK is expressed in a range of normal tissues, the extent of MAP1B expression in tissues other than brain has not been determined. An exception to this is in the male reproductive organs, where MAP1B has been shown to be expressed in efferent ductules and epididymis (DB et al., 2006), although the role of MAP1B in these tissues is not well defined. A vast body of research has been published over resent years showing conclusively that DAPK expression is attenuated by epigenetic silencing in many cancer types. However, as is the case with many tumour suppressor proteins, DAPK expression can also be elevated in cancers (Stevens et al., 2007) and in cancer cell lines, where presumably the tumour suppressor pathway has been inactivated further downstream or where other co-factors have been modified during cancer progression. Here paradoxically, expression of tumour suppressor protein is elevated, indicative of a response to aberrant growth. Under non-disease conditions this effect might be sufficient to induce growth inhibition, but during disease progression this response has been inactivated.

The extent of MAP1B expression in cancer cell lines was initially examined by bioinformatics using the Cancer Genome Anatomy Project data base. MAP1B is

expressed in many cancer cell lines, especially those derived from lung, CNS and renal cancers (Figure 4.1 a). DAPK is also expressed in many of the NCI60 cell lines, especially in renal cancer and melanoma. Also, DAPK is highly expressed in some lung cancer lines like A549s. Although DAPK is down regulated in CNS carcinoma lines, MAP1B is strikingly expressed to very high levels in all the CNS lines. Unfortunately, only the top 10 positively or negatively correlating genes could be retrieved using this method. Therefore it was not possible to obtain a statistical analysis of any possible correlation between DAPK and MAP1B expression levels.

The protein level of MAP1B in available cell lines was determined by western blot using the highly specific mouse monoclonal antibody clone AA6, that recognises all forms of MAP1B (Figure 4.2). MAP1B was expressed at high levels in A549, A375, PC12 and HEK293 cells, comparable to the level of expression in embryonic rat brain. It is interesting that multiple bands were observed, generating a different banding pattern in each cell line. There could be many reasons for this including alternative splicing, incomplete cleavage into heavy chain and light chain and various types of post-translational modification. In any case, this data suggests that MAP1B is expressed as many different isoforms in different cell lines.

4.2.2 Development of a Cell Growth Assay to Characterise the DAPK and MAP1B Interaction

A variety of assays have been developed to measure the activity of DAPK with respect to multiple specific pathways including apoptosis, autophagy and membrane blebbing assays. Therefore, an assay was developed to directly determine the activity of DAPK independent of the mode of action. The effect of DAPK on cell growth in a

clonogenic assay was measured, since this measures cell survival under long-term conditions and often gives distinct results, and hence different information from more acute assays. Short term over expression of DAPK gene relies on transient transfection where treatment can be achieved for a maximum of 24 to 48 hours. Stable transfection using antibody resistance (such as genetacin or blastocidin) as a selection marker on the other hand, allows for over expression of gene for as long as is required.

When DAPK was stably transfected into HCT116 cells (that have an active p53 pathway), a reduction in cell growth was observed relative to the cell growth achieved using a vector control transfection (Figure 4.3, a i). This effect was more pronounced at lower plating densities, whereas at higher densities DAPK induced cell growth inhibition is saturated.

Various links between the DAPK pathway and the p53 pathway have been observed in previous studies. For example, DAPK can phosphorylate p53 Ser20, an important phosphoaccepter site involved in the regulation of p53 transactivation activity. Also, over expression of DAPK activates an ARF dependent p53 induced checkpoint to protect cells from oncogenic transformation (see section 1.4.4). Therefore, the sensitivity of the clonogenic assay and its ability to quantify changes in DAPK induced growth inhibition was determined by measuring the effect of p53 status.

As expected, HCT116 p53-null cells did not respond to DAPK over expression in the same way. There was in fact an increase in cell survival in the p53-null cells relative to cell growth allowed by vector control transfection (Figure 4.3, a ii). This effect is illustrated (Figure 4.3, a iii). Again, this was more pronounced at lower plating

densities. These data indicate that DAPK mediated suppression of cell growth can be p53-dependent and illustrate the utility of this cell growth assay in measuring DAPK activity in cells.

The cell growth assay was used to determine whether co-transfected MAP1B antagonises or stimulates DAPK function as a growth suppressor. When DAPK or MAP1B variants were stably over expressed in cells a decrease in cell growth was observed (Figure 4.3 b). This growth inhibitory effect of MAP1B was significantly reduced at higher plating densities. By contrast, a striking reduction in colony formation was observed when DAPK and MAP1B transcript variant 1 were co-expressed. This effect was most pronounced at higher plating densities, where the co-operation between MAP1B variant 1 and DAPK was synergistic. DAPK did not synergise with MAP1B variant 2 with respect to cell growth as measured by this assay. However it was not possible to rule out cooperation with endogenous DAPK in this cell line, which expresses significant amounts of the kinase. These data suggest that that MAP1B can co-operate with DAPK to reduce cell growth at high cell densities when the activity of either gene alone is limited. This co-operation requires MAP1B N-terminal 126 amino acids only present on transcript variant 1.

4.2.3 Characterisation of the MAP1B and DAPK Interaction Using an Optimised Cell Growth Assay

The N-terminus of transcript variant 1 has been show to be a binding interface between MAP1B and the DAPK kinase domain. When transcript variant 1 is over expressed with DAPK, cell growth is reduced at high plating densities. This optimal plating density was used in subsequent cell growth assays designed to further

characterise the MAP1B and DAPK interaction. As shown previously, MAP1B variants V1 and V2 have a negligible effect on colony survival at this plating density. V1, which is able to bind with DAPK kinase domain was able to synergise with DAPK and reduce cell survival (Figure 4.4, a). whereas, the form of MAP1B unable to bind tightly to DAPK, V2, was not able to co-suppress with DAPK. Interestingly, the N-terminus (N126) was able to mimic V1 and formed a synthetic lethal interaction with DAPK. These data correlate the binding assay data, where the N-terminus of MAP1B is able to bind to DAPK, with a genetic cooperation as determined using a cell growth suppressor assay.

The contribution of DAPK protein domains to cell growth inhibition was then tested using the developed clonogenic assay. To this end DAPK kinase domain and the Death Domain of DAPK were stably transfected into cells with control vector or with full length MAP1B. The DAPK core domain did not cooperate with full-length MAP1B and in fact inhibited the growth suppression induced by MAP1B alone (Figure 4.4 b). This indicated that the transfected kinase domain can possibly act in a dominant negative manner by competing with the endogenous full length DAPK protein. The isolated Death Domain, though unable by itself to induce significant inhibition of cell growth, was able to cooperate with full-length MAP1B to suppress cell growth in a synthetic lethal interaction. These experiments indicate that in addition to binding with the DAPK kinase domain, MAP1B co-operation with DAPK involves a death domain interaction and that the death domain can form a synthetic lethal interaction with MAP1B. It is unknown whether this death domain interaction involves the recruitment of an additional unknown co-factor, or whether

the synthetic lethal effect is as a consequence of direct interaction between MAP1B and the DAPK death domain.

Next, a panel of DAPK mutants including the kinase dead version (K42A) and a form of DAPK with the negatively regulating calmodulin domain deleted were evaluated to determine if DAPK kinase activity was required for optimal cooperation with MAP1B using. These genes were transfected into A375 cells that express large amounts of endogenous MAP1B and only a small amount of DAPK. MAP1B expression can be efficiently reduced in this cell line by siRNA transfection 24 hours prior to treatment with gene of interest (Figure 4.4 c ii). Using this system of stable transfection into A375 cells with or without a reduction in endogenous MAP1B, it was possible to evaluate the effect of exogenous DAPK kinase activity without interference from endogenous kinase. Over expression of both wild type DAPK and calmodulin deleted DAPK reduced cell growth, and this was reduced in cells with attenuated MAP1B expression (Figure 4.4 c i). Ablation of DAPK kinase activity by mutation of K42 to A42 completely eliminated DAPK induced cell growth suppression with or without endogenous MAP1B. These data are strong evidence suggesting that MAP1B co-operates with DAPK to reduce cell growth and that this requires functional DAPK kinase activity.

The cell growth assay was used to measure the inhibition of growth of coherent cells in culture due to transfected gene activity. However, this assay does not provide information relating to the method of cell growth inhibition. There are many mechanisms that could reduce cell growth as a result of trans-gene activity, including apoptosis, autpphagic cell death, cell cycle regulation or cell senescence amongst

many. When DAPK was transfected into HCT116 cells for 24 hours there was an increase in the number of non-viable cells as determined by counting trypan blue positive cells (Figure 4.4 d). This effect was reduced by K42A mutation, suggesting that death was dependent on an active kinase domain, however deletion of the CaM regulatory region had no significant effect. DAPK-induced loss of cell viability was enhanced by co-transfection of full length MAP1B (Figure 4.4 d – shaded bars), demonstrating that MAP1B can synergise with DAPK to induce cell death in this cell line. This is not only evidence that DAPK-induced death is enhanced by MAP1B expression, but it also suggests that cell death is a mechanism that could account for MAP1B enhanced growth-suppression (Previous assay: Figure 4,4 a).

4.2.4 The Effect of MAP1B and DAPK Over Expression on the p53 Pathway

Using the cell growth assays, it was determined that transcript variant 1 of MAP1B can co-operate with DAPK to reduce colony growth at high plating densities. This co-operation required active DAPK kinase activity and transfected DAPK kinase domain blocked growth suppression in a dominant negative manner. DAPK activity has been implicated by previous studies in interaction with and activation of the p53 pathway. This is supported by the cell growth assay optimisation data (Figure 4.3 a) where DAPK activity is suppressed by p53 inactivation using the isogenic HCT116 cell lines. It is widely accepted that DAPK has p53 dependent and independent functions and so the p53 status of cell lines is therefore an important factor to consider when studying DAPK activity (see section 4.3.3.2).

It was demonstrated that DAPK activity in the cell growth assay was dependent on wild type p53, and so experiments were conducted in order to determine if DAPK

interaction with MAP1B could influence and act through the p53 pathway. 3 tumour cell lines which express wild type p53 were examined for DAPK and MAP1B expression (Figure 4.5 a). DAPK and MAP1B were expressed at highest levels in A549 cells, whilst DAPK is lower in A375 cells. Interestingly, in the isogenic HCT116 cell line panel, DAPK expression is minimal in the p21-null cell line, whilst MAP1B is lower in the p53 null and p21 null cells. DAPK3/ZIPK and DAPK2 protein expression was also assayed. Expression of both proteins is unchanged across the HCT116 panel, indicating that the effect of p53 status in these cell lines was specific to DAPK1 alone and not a general effect on DAPK family members.

p53 activity results in the transactivation of target genes with regulatory and functional roles within the p53 pathway. Therefore, a principle method to determine the status of the p53 pathway is to assay for target gene expression. For example, when HCT116 parent cells are transfected with GST-DAPK1 or GST-DAPK3, induction of p21 target protein is both p53-dependent and is DAPK1 specific (Figure 4.5 b i). Whereas, expression of the negative regulator MDM2 is not enhanced suggesting that DAPK can indeed activate the p53 pathway.

When DAPK and MAP1B were transfected alone into HCT116 cells there was an increase in the amount of p21 protein, modified Bax, and marginal increases in Ser20-phosphorylated p53 protein, suggesting that MAP1B alone can activate the p53 pathway independently. As a control, X-ray exposure can induce significant amounts of p21, Ser20-phosphorylation of p53, and Bax-adduct formation. However, co-transfection of both MAP1B and DAPK only marginally stimulated Ser20 phosphorylation and Bax and p21 protein induction above the levels stimulated by

either gene alone. Therefore a trend was observed indicating that MAP1B and DAPK can activate the p53 pathway, yet this assay was not sensitive enough to provide significant information about the interaction of DAPK with MAP1B.

Using the p21 expression assay it was not feasible to determine if DAPK and MAP1B could act independently or in cooperation to activate p53. Therefore the cell growth assay was set up in conjunction with the 3 HCT116 isogenic cell lines so that the influence of p53 and its down stream target p21 could be assessed. In this situation the effect of p53 and p21 inactivation on cell growth inhibition could be quantified (Figure 4.5 c). To this end cells were co-transfected with DAPK and MAP1B V1, known to interact with DAPK or with V2 that would act as a negative control. As observed previously, p53 knock out reduced the ability of DAPK alone to inhibit cell growth (Figure 4.5 c i) whereas transfection of V1 or V2 alone was insufficient to reduce cell survival in either cell line as compared to growth allowed by the empty vector control. Co-over expression of DAPK with V2 did not reduce growth significantly as compared to the situation with DAPK alone in either cell line. Co-transfection of DAPK with V1 resulted in a striking reduction in survival in not only the p53 wild type, but also in the p53 functional null cell line as well. This situation was repeated using the p21 null line where DAPK and V1 co-operate to reduce cell growth in both cell lines. These data clearly show that the synergy between DAPK and MAP1B does not require an intact p53 pathway, both at the level of functional p53 protein and at the level of the p53 transactivation target, p21. Nevertheless, cell growth co-repression was attenuated in the p53 null background (Figure 4.5 c i; data highlighted by asterisk) indicating that the p53 pathway can enhance the synergistic growth suppression.

4.2.5 Induction of Apoptosis by MAP1B and DAPK

Apoptotic programmed cell death is activated in damaged or senescent cells, allowing them to be removed from otherwise healthy tissues. Removal of apoptotic cells by phagocytosis is carried out by white blood cells such as macrophages or dendritic cells. Phagocytic cells recognise apoptotic cells that present negatively charged phosphatidylserine on their cell surface. In non-apoptotic cells, phosphatidylserine is detained on the inner surface of the cell membrane. Then, during the early stages of apoptosis, phosphatidylserine is transported to the outer cell surface to be detected by phagocytes. Annexin V specifically binds to phosphatidylserine on the cell surface of apoptotic cells. This property can be utilised to detect apoptotic cells using fluorophore-conjugated annexin 5.

The annexin V assay was employed to assess the extent of apoptotic cell death during MAP1B and DAPK co-transfection. Given that this assay is optimised to detect early stage apoptotic cells, it was necessary to set up a time course study to gauge the optimal treatment time. HCT116 cells were co-transfected with a 2-way titration of MAP1B and DAPK expression plasmid DNA for 12, 24 and 48 hours (Figure 4.6 a). Then, the extent of apoptosis was quantified using FACS analysis. As the phosphatidylserine is flipped from the inner to outer surface of the membrane, cells are stained with fluorescent Annexin V. This can be visualised by plotting Annexin V fluorescence on the ordinate axis. In addition, cells were stained with propidium iodide (PI), which is a non-membrane permeable nuclear stain. So as a consequence, only cells with perturbed membranes will be positive for PI staining. The extent of PI staining can be visualised by plotting on the abscissa. Therefore, Annexin V staining and PI staining can be monitored on a single scatter plot. This

scatter plot is then divided onto 4 quadrants; Lower Left (LL), Lower Right (LR), Upper Right (UR) and Upper Left (UL) each containing a separate population of cells with a distinct combination of staining. LL cells are negative for both and so are designated non-apoptotic. LR cells are the cell populations of interest because they are annexin V positive, and so early-apoptotic. The upper quadrants contain populations of cells only positive for PI (UL) and populations of cells positive for both stains. This indicates that the cell membrane is compromised, perhaps as a consequence of later stage apoptosis. Still, data from the upper quadrants can not be considered informative because these populations will be contaminated by non-viable cells that have not necessarily undergone an apoptotic program, such as necrotic cells. Transfection of 0.5μg of plasmid DNA of either MAP1B or DAPK was sufficient to induce detectable apoptosis after 24 hours (Figure 4.6 a). Prior to this, after only 12 hours transfection, no apoptosis was detected. After 48 hours, no above-background annexin V staining was detected. Thus 24 hours post-transfection was determined to be an optimal time point to study early apoptosis using this assay. At this time point, 0.5μg of DAPK DNA alone was able to induce 17.5% annexin V positive cells, and 0.5μg of MAP1B 16.5% annexin V positive cells. Titration of more DNA did not significantly enhance the response. In addition, co-transfection of any combination of amounts of DAPK and MAP1B DNA did not lead to an increase in early stage apoptosis. This would suggest that 0.5μg of expression plasmid was able to saturate this assay. In other words, 18% annexin V staining is approximately the maximum allowed using this system of transfected cells. As a result, the effect of 200ng of MAP1B and DAPK was assayed after 24 hours transfection (Figure 4.6 b). A transfection of 200ng apoptosis inducing tumour necrosis factor receptor

expression vector was included as a positive control. Over expression of DAPK alone resulted in 8.72% of cells in the LR quadrant and expression of MAP1B 8.60%. Co-expression from both vectors resulted in 9.99% of cells in the LR quadrant. These data indicate that MAP1B and DAPK ectopic expression can induce apoptosis in this cell line. However, co-expression of both exogenous proteins did not enhance the apoptotic response. Therefore, the synergistic interaction between the 2 proteins, uncovered using the growth suppression assay can not be as a result of early apoptotic induction induced immediately after vector transfection.

The annexin V apoptosis assay can only be reliably used to assess the extent of early stage apoptosis within cell populations. Measurement of later stages of apoptosis relies on other methods to observe events such as chromatin condensation or DNA fragmentation. The terminal transferase dUTP nick end labeling (TUNEL) assay, utilises an antibody based method to detect nicks in DNA which are identified by terminal transferase. This enzyme catalyses the addition of dUTPs that are then secondarily labelled with a fluorescent marker. This assay is optimised to specifically detect DNA lesions formed during the later stages of apoptosis and so provides a 'second opinion' to the annexin V assay. MAP1B and DAPK were transfected into HCT116 cells on coverslips using vector DNA amounts equivalent to those used in the optimised annexin V assay (Figure 4.6 b). Both vectors could independently induce apoptosis where specifically, MAP1B transfection alone was able to induce TUNEL positive staining approximately 3 fold higher than DAPK alone. Co-transfection of MAP1B with DAPK in this assay did not result in any increase in TUNEL staining as compared to MAP1B alone. Taken together, results from the annexin V and TUNEL assays indicated that synergy in the co-growth suppression

assay can not be explained by way of an apoptosis mechanism. Although transfection of MAP1B and DAPK alone can clearly induce apoptosis, no co-operation between the two was observed. Therefore this evidence supports the idea that apoptosis induced immediately after MAP1B and DAPK transfection would not impact on the long term growth suppression observed in the synergistic growth suppression assay. In other words, these data suggest that apoptosis is not a mechanism that would explain the positive cooperation between the two proteins in the clonogenic assay.

4.2.6 The Impact of DAPK and MAP1B on the Cell Cycle

Tumour suppressor pathways often have a cell cycle regulatory element. After p53 activation by DNA damage for example, cell cycle arrest at G1 is activated if the severity of damage does not warrant programmed cell death. Arrest of the cell cycle is often transient, allowing progression after damage repair, but can be permanent if damage is too great. In this way, cell cycle arrest may act as a survival mechanism in addition to a being a system that halts aberrant cell growth.

Although ectopically expressed MAP1B and DAPK can independently induce an apoptotic response, there is no evidence showing that both proteins can act in concert to enhance this response. It is unlikely therefore that the observed synergistic growth suppression works though an apoptotic cell death pathway. To attempt to discern the mechanism of DAPK and MAP1B induced cell growth repression, both genes were over expressed in HCT116 cells. Any perturbation in cell cycle parameters was then assayed by measuring cell nuclei size using FACS analysis. Cell cycle profiles were determined for vector control, MAP1B or DAPK transfected and MAP1B with DAPK co-transfected samples (Figure 4.8 i). DAPK transfection alone stimulated a

reproducible 12% increase in the G1 population accompanied by a reciprocal decrease in the G2 population (Figure 4.8 ii). MAP1B alone stimulated a slight but significant increase in the G1 population also at the expense of the G2 population. However MAP1B co-transfection with and DAPK did not enhance cell cycle distribution as compared to DAPK transfection alone. Again, no evidence of co-operation between DAPK and MAP1B was observed using this assay, therefore DAPK and MAP1B synergistic co-growth suppression is likely to not be linked to cell cycle changes induced in the short term after transfection.

4.2.7 The Autophagic Cell Death Program is Induced by DAPK and MAP1B

In addition to the documented role of DAPK during type I (apoptotic) cell death, published data also implicates DAPK in type II (autophagic) cell death where overexpression of DAPK in HEK293 cells leads to caspase independent cell death in conjunction with formation of autophagic vesicles (Inbal et al., 2002). Autophagic vesicles can be distinguished from regular lysosomes at the molecular level because they are decorated with Light Chain 3 (LC3) (Tanida et al., 2005). Interestingly, LC3 is a member of the MAP1 family of microtubule proteins and is homologous to the light chains; LC1 and LC2, of MAP1A and MAP1B respectively. A report has recently been published showing that LC3 interacts with high affinity to MAP1B (Halpain and Dehmelt, 2006), where phosphorylated MAP1B associates with autophagosomes.

The effect of MAP1B and DAPK co-expression on autophagy in HEK293 cells that stably express the autophagy marker GFP-LC3 was assessed (Kochl et al., 2006). During Autophagy, this marker decorates autophagosomes so that they can be

identified and quantified as GFP-LC3 foci which fluoresce much brighter than the diffuse GFP-LC3 background. By this method, the autophagic index is calculated as (GFP-LC3 Foci per Field) / (Total Cells per Field). HA-DAPK induces GFP-LC3 foci formation 32 hours after transfection (Figure 4.9 a). Before 32 hours, no foci were observed, and after 48 hours transfection the number of foci induced was depleted by around a half. Thus there was a very tight time window of loci induction. Subsequent GFP-LC3 loci assays were performed at this time point. This result provides further evidence that DAPK is involved in the autophagy pathway, supporting the previous work reported from other laboratories.

HEK293 cells express large amounts of MAP1B can that can be substantially reduced by MAP1B siRNA (Figure 4.9 bi). This provides a convenient system where by the effect of endogenous MAP1B protein levels on HA-DAPK-induced foci formation can be monitored. Cells were treated with MAP1B siRNA or siRNA control for 32 hours before transfection with HA-DAPK. As expected, HA-DAPK efficiently induced LC3 foci formation (Figure 4.9 b i), reproducing the results from the optimisation experiment (Figure 4.9 a). MAP1B siRNA reduced the number of GFP-LC3 foci formed by approximately a half. The effect of MAP1B on the number of LC3 foci formed, is illustrated (Figure 4.9 b ii). The fact that MAP1B depletion can attenuate DAPK induced autophagosome formation provides strong evidence to suggest that MAP1B is involved in DAPK induced Autophagy.

During autophagy, soluble LC3 (LC3-I) is cleaved and lipidated to form LC3-II and this cleavage event can be monitored using western blot analysis. HEK293 GFP-LC3 cells were co-transfected with MAP1B and DAPK and the extent of GFP-LC3

modification was quantified. As a positive control, separate cultures were starved using balanced salt solution for 2 hours to efficiently induce autophagy (Figure 4.10 a). MAP1B and DAPK could both independently stimulate LC3 modification as compared to the vector only transfection control. A higher level of LC3 modification was observed when the genes were co-transfected. This provides further evidence to substantiate the claim that DAPK is a positive regulator of Autophagy. Also the fact that MAP1B transfection alone can induce LC3 modification further implicates MAP1B in the autophagic process. The ratio of lipidated GFP-LC3-II to soluble GFP-LC3-I was quantified using densitometic analysis of respective bands on the western blot. Densitometry revealed that although there was an increase in GFP-LC3 modification when both proteins were co expressed, this increase was only additive when compared to DAPK or MAP1B expression alone. As a consequence, it was desirable to provide further evidence to establish if MAP1B and DAPK act through the same pathway, or independently to induce LC3 modification. The contribution of MAP1B to DAPK induced LC3-II production was assessed further by depleting endogenous MAP1B protein using siRNA. Reduction of MAP1B levels resulted in the ablation of LC3-II formation otherwise induced by transfected HA-DAPK (Figure 4.10 b). The DAPK kinase death mutant K42A was unable to induce modification of LC3 providing a solid negative control for this transfection assay. Induction of LC3 modification therefore was dependent on DAPK kinase activity and not just an artefact of protein over-expression.

GFP-LC3 foci formation and LC3 modification are established biomarkers often used to specifically quantify the extent of autophagy in cell culture. Therefore, taken together, these data establish a positive role for MAP1B in DAPK-induced

autophagy. This correlates with the extent of DAPK-induced cell death in these cultures that is both MAP1B and DAPK-kinase activity dependent. In addition, these data correlate with the growth suppression data, where co-transfection of DAPK with MAP1B resulted in synergy to reduce cell growth.

4.2.8 MAP1B Enhances DAPK Induced Cell Membrane Blebbing

Cell membrane blebbing is characteristic of DAPK action in cells, and is a robust marker of DAPK-induced cell death. Therefore, a membrane blebbing assay was set up to quantify changes in transfected DAPK activity. Ectopic over-expression of DAPK protein in HCT116 cells was able to efficiently induce membrane blebbing relative to that induced by control vector transfection. In this cell line approximately 40% of DAPK positive cells have cell membrane blebbing morphology after 24 hours treatment (Figure 4.11 a). Over expression of MAP1B alone lead to only a slight stimulation of membrane blebbing. Co-transfected MAP1B synergised with transfected DAPK to stimulate membrane blebbing in over 80% of co-transfected cells. These data provide molecular evidence that a functional cooperation exists between MAP1B and DAPK to induce the morphologic changes that are characteristic of DAPK action in cells.

In order to determine the effect of DAPK kinase activity in this assay, a panel of HA-DAPK kinase activity mutant expression vectors were assessed for their membrane blebbing inducing activity in A375 cells (Figure 4.11 b i). Kinase activated ΔCAM had enhanced activity as a greater proportion of cells had membrane blebbing morphology, whereas the kinase activity attenuated mutant K42A had a reduced ability to cause membrane blebbing activity. This is a reproduction of previous work

showing that the membrane blebbing function of DAPK is kinase activity dependent. When endogenous levels of MAP1B were depleted by siRNA, the ability of wild type (WT) and kinase activated (ΔCAM) to induce membrane blebbing was reduced. This was in contrast to the situation after K42A transfection, where MAP1B depletion had no significant effect on the proportion of cells with membrane blebbing morphology. This indicates that, not only is the K42A mutant's membrane blebbing activity reduced, but this mutant is also unable to functionally interact with MAP1B in this assay. To further substantiate this claim, the MAP1B mutants V1 and V2 were inputted into this assay using co-transfection with DAPK into HCT116 cells. As was the case after over-expression in A375 cells, MAP1B enhancement of DAPK induced membrane blebbing was dependent on kinase activity where the activity of K42A was independent of MAP1B (Figure 4.11 b ii). Co-transfection of DAPK with the MAP1B mutant lacking the N-terminal DAPK binding site (MAP1B-V2) resulted in reduced membrane blebbing activity, relative to full-length MAP1B and MAP1B-V1 which have the N-terminal binding site.

These data generated by the blebbing assays strongly correlate with the data generated by the growth suppression assay (Figure 4.4), where MAP1B synergy with DAPK is dependent on DAPK kinase activity and also on the MAP1B N-terminal 126 amino acids. Synergy in the growth suppression assay was not dependent on functional p53. This was determined in the HCT116 p53 null line because MAP1B transcript variant 1 co-operated with DAPK regardless of p53 status. This situation was repeated using the blebbing assay where MAP1B and DAPK co-operation was also independent of p53 status (Figure 4.11 c). This further strengthens the correlation between observations using the growth suppression and blebbing assays.

4.2.9 Inhibition of DAPK and MAP1B Synergy by the Autophagy Inhibitor 3-MA

The results from the above studies show that there is a striking correlation between the effect of DAPK and MAP1B co-operation on growth suppression, autophagy and cell membrane blebbing. These data were strengthened by controls, where co-operation in each case relied on active DAPK kinase and the presence of the N-terminal binding site on MAP1B. Nevertheless, it was still necessary to establish if the observed correlation, between the induction of autophagy, the stimulation of membrane blebbing and inhibition of cell growth was in fact due to a causal relationship stimulated by cooperation between MAP1B and DAPK.

Cell membrane blebbing is a well defined marker for the activity of ectopic DAPK in transfected cells. For that reason this marker has been employed in numerous previously published studies. The studies above show that using this marker, assays can be accurately and rapidly conducted owing to the fact that transient transfection of DAPK is sufficient to stimulate a reproducible end point. In addition to this, the specificity of this assay can easily be controlled for. For example, empty vector transfection alone will give a read out for background blebbing and the functional null mutants; DAPK K42A or MAP1B-V2, can be used as specificity controls. Given that membrane blebbing is an end-point that can be utilised in the short term, and that this end point strongly correlates with the longer term growth suppression from multiple studies, further analysis was conducted using the membrane blebbing assay.

The methylated nucleotide 3-methyladenine (3-MA) is a well characterised pharmacological inhibitor of autophagy (Seglen and Gordon, 1982). Therefore, it was predicted that if there was a causal relationship between autophagy and

membrane blebbing, then DAPK-induced blebbing would be decreased by 3-MA. To test this, 3-MA was added to HA-DAPK transfected cells to determine the extent of HA-DAPK-induced membrane blebbing that was due to autophagy. A375 cells were transfected with DAPK for 18 hours and treated with a concentration range of 3-MA for 6 hours before fixing and staining to visualise HA-DAPK transfected cells. 3-MA was able to reduce membrane blebbing at low concentrations (2-5μM) and completely blocked blebbing at higher concentrations (10μM) (Figure 4.12 a). Given that 3-MA is an inhibitor of autophagy, this dose-dependent reduction in blebbing indicates that there is a causal relationship between DAPK-induced autophagy and DAPK-induced membrane blebbing. What's more, this positions the influence of 3-MA up-stream of blebbing and indicates that, under these conditions HA-DAPK-induced blebbing is dependent on an active autophagy program.

To determine if blebbing induced by cooperation between DAPK and MAP1B was due to autophagy, A375 cells were co-transfected for 18 hours and treated with 10μM of the autophagy inhibitor 3-MA before fixing and staining for co-transfected cells. 3-MA treatment completely blocked membrane blebbing in co-transfected cells (Figure 4.12 b) providing further evidence that MAP1B cooperates with DAPK to induce autophagy in these cells corroborating with evidence from the GFP-LC3 foci assay (Figure 4.10). Also, these data indicate that there is a causal relationship between DAPK:MAP1B co-induced blebbing and autophagy. Additionally, these data place cooperation-induced autophagy up stream of membrane blebbing.

A recent study suggests that 3-MA can also inhibit the PI3k pathway (Ito et al., 2007). Therefore, a second autophagy inhibitor was used to rule out the possibility

of non-specific action through the PI3k pathway. The anti-malarial drug chloroquine modulates autophagocytic protein degradation in the lysosome system, thereby inducing the formation of rimmed vacuoles consisting of autophagosomes fused to autolysosomes (Suzuki et al., 2002). The exact effect this has depends on the cell type and model being observed (Xu et al., 2007; Zaidi et al., 2001), but chloroquine is generally considered to be an inhibitor of autophagy. It was therefore predicted that this drug would reduce DAPK and MAP1B induced autophagy and so co-transfected cells were treated, fixed and stained before scoring for cell membrane blebbing. Autophagy is a caspase-independent cell death program and so a pan-caspase inhibitor treatment was included as a negative control. As expected, 3-MA blocked membrane blebbing induced by co-transfection (Figure 4.12 c). Chloroquine also reduced the percentage of blebbing co-transfected cells although it was not as efficacious as 3-MA in these conditions. This reproduced the observation that autophagy inhibitors block blebbing, providing corroborative evidence. The pan-caspase inhibitor did not have any effect on blebbing, also evidence that DAPK and MAP1B induced blebbing is as a result of caspase-independent autophagy and not apoptosis.

From the above studies it was concluded that transfected DAPK and MAP1B synergise to induce membrane blebbing in cells and this is dependent on an active autophagic program (Figure 4.12). Given that membrane blebbing is a marker of DAPK-induced programmed cell death, this suggests that DAPK and MAP1B synergise to induce programmed cell death to reduce cultured cancer cell growth (Figure 4.4), and this is independent of apoptosis (Figure 4.6, 2.7 and 2.12 c) or cell cycle regulation (Figure 4.8).

Further study is proposed to strengthen the evidence suggesting that DAPK:MAP1B cooperation-induced membrane blebbing depends on an active autophagic program. Specific inhibitors of PI3k such as wortmanin or LY29Y002 could be used as controls to determine if PI3k activity is required for blebbing. Also, siRNA to autophagy genes such as ATG5 or beclin should also inhibit blebbing. This approach, using siRNAs to specificly knock-down autophagy genes could also be used to uncover the biocehemical elements required for DAPK:MAP1B induced blebbing.

4.2.10 Transfected HA-DAPK Co-localises with Cortical Actin During Membrane Blebbing

Immunofluorescence studies were designed to attempt to further understand the mechanism of DAPK and MAP1B induced membrane blebbing. Immunoflourescense imaging methodology was chosen to supplement the biochemical studies (Figurea 1.9 and 1.11) where actin did not co-immunoprecipitate with MAP1B and DAPK in HA-DAPK transfected A375 cells. This was suprising given the known role of DAPK as a microfillament associating protein, and given that MAP1B has actin binding domains on its heavy and light chains. It was speculated that this could be due to limitations of the co-IP, in which microfilaments would not be dissolved during the gentle lysis conditions. Also, the *in-vitro* microtubule polymerisation cycling studies (Figure 4.12) determined that DAPK binds to microtubules and this discovery is at odds with previously published research that emphasises DAPK interaction with actin and microfilaments. It was hoped that this discrepancy could be addressed using imaging studies after obtaining corroborating evidence.

Initially, it was necessary to image HA-DAPK transfected cells to define DAPK transfection-induced morphological changes. A375 cells were transfected with HA-DAPK or GFP control for 24 hours before fixing and staining to visualise the transfected cell population. A phalliodin counter-stain was employed to visualise F-actin fibers. The fibroblast-like morphology of A375 cells was unchanged by GFP transfection (Figure 4.13 a), where GFP is diffuse throughout the cell and the F-actin distribution is unchanged. However, HA-DAPK transfected cells could be split into 3 distinct subpopulations each with a different class of morphological change defined as subpopulations 1, 2 and 3 (Figure 4.13 b, c and d). Subpopulation 1 consisted of large, spread-out and healthy looking cells with very little or no change in morphology as compared to surrounding non-transfected cells (Figure 4.13 b). Cells grouped into subpopulation 2 had gross changes in cell morphology including cytoplasmic shrinkage, large bulbous processes and small membrane blebs (Figure 4.13 c). Cells grouped into sub population 3 were much smaller and had multiple large cell membrane blebs (Figure 4.13 d). Also, it was observed that cells grouped into sub-population 2 had HA-DAPK co-localised with cortical F-actin fibers.

Three subpopulations of cells were observed after 24 hours of HA-DAPK transfection, each with a different extent of cell membrane blebbing, with no blebs in subpopulation 1, a few small blebs in subpopulation 2 and a larger number of large blebs in subpopulation 3. This superficial observation indicates that there is a sequence of events starting in subpopulation 1 and ending in subpopulation 3. This assumption was tested using a time course of transfected cultures by counting the number of cells at each time point. The percentage of cells in subpopulation 3 increases over time whist the percentage in subpopulation 1 decreases (Figure 4.13

e). The proportion of cells in subpopulation 2 increases from 12 to 24 hours and then decreases from 24 to 48 hours. Thus, it can be assumed that subpopulation 1 precedes subpopulation 2 precedes subpopulation 3 with regards to time.

To attempt to discover which protein domain of HA-DAPK is responsible for inducing these morphological changes, a series of C-terminal deletion mutants were transfected into A375 cells and the percentage of transfected cells in each population was determined. Removal of the C-terminal death domain form HA-DAPK resulted in a significant increase in the proportion of cells in subpopulation 1 accompanied by a decrease in populations 2 and 3 (Figure 4.13 f). This was enhanced by additional removal of the death domain to cytoskeleton-binding domain linker region. Interestingly, subsequent removal of the cytoskeleton-binding domain yielded an active construct consisting of amino acids 1-641 which includes the N-terminal kinase domain and the ankyrin repeat domain. Additional removal of the ankyrin repeats yielded a less active construct, reduced in ability to induce morphological changes. These data suggest that the death domain is critical for DAPK-induced morphological changes. Also, the fact that the 1-641 construct is synthetically active, suggests that there is a negative regulatory element within the cytoskeletal binding domain and that the ankyrin repeat domain is a positive effectors of morphological change. The effect of kinase activity on induction of morphological changes was assessed using the constitutively active ΔCaM and the kinase attenuated K42A mutants. The ΔCaM mutant was superactive with respect to morphology change, as the percentage of cells in subpopulation 1 was decreased accompanied by an increase in the proportion of subpopulation 2 and 3 cells (Figure 4.13 g). The K42A mutant's ability to induce morphological change was attenuated as the number of cells

retained in subpopulation 1 was increased. Together, these data suggest that DAPK-induced morphological changes are dependent on kinase activity and death domain signaling that is negatively regulated by elements within the cytoskeletal binding domain and positively regulated by the ankyrin repeat domain.

4.2.10.1 Transfected DAPK *Co-localises with Cortical F-actin in Cells Grouped in Subpopulation 2.*

Analysis of the images obtained during morphological assessment lead to the observation that HA-DAPK co-localised with cortical F-actin fibers in cells grouped into subpopulation 2 (Figure 4.13 c). However, this has not been reported previously in any published research involving detailed cell imaging of the effects of transfected DAPK (Bialik et al., 2004). Therefore this effect staining was examined in detail from numerous independent cultures (and 2.14 a), where HA-DAPK staining at the cell membrane was observed in each. In order to determine the position of the nucleus in these cells, cultures wares counterstained with TOPRO nuclear stain. Here, HA-DAPK clearly stains the cell periphery, near to the plasma membrane. These experiments demonstrated that the observed cortical stain was not due to an "edge-effect" where the nucleus compresses the cell contents to the edge of the cell.

4.2.11 Endogenous MAP1B Co-localises with Transfected HA-DAPK at Cortical F-actin in Cells Grouped in Subpopulation 2.

Having defined the immunofluorescent staining patterns of transfected HA-DAPK, it was then desirable to observe the location of endogenous MAP1B in the 3 defined subpopulations. A375 cells were transfected with HA-DAPK for 24 hours before triple staining for HA, MAP1B (using Mab AA6) and F-actin using phalliodin counter-stain. The MAP1B staining in cells grouped in subpopulation 1 was

unchanged as compared to the surrounding non-transfected cells (Figure 4.15 a). However, MAP1B staining in subpopulation 2 cells was concentrated at the cell periphery, co-localising with cortical F-actin and HA-DAPK (Figure 4.15 b). MAP1B staining in subpopulation 3 was concentrated in the blebs, co-staining with HA-DAPK (Figure 4.15 c). This superficial observation suggested that MAP1B was concentrated with HA-DAPK at cortical F-actin near to the cell membrane. Therefore, the fluorescent intensity of MAP1B in the cytoplasm was compared to the fluorescent intensity of MAP1B in the cortical region in order to quantify this observation. In each cell in subpopulation 2, the ratio of the average intensity of MAP1B in the cortical region to the average intensity of MAP1B in the cytoplasm was increased as compared to the average fluorescence ratio in surrounding non-transfected cells (Figure 4.12 b and d). These data provide a quantitative analysis of the initial superficial observation and show that endogenous MAP1B is co-located with HA-DAPK at cortical F-actin during in cell subpopulation 2. This suggests that MAP1B and DAPK interact with F-actin during the initial stages of HA-DAPK transfection-induced membrane blebbing.

In order to determine the protein domain of DAPK that is responsible for induction of MAP1B-F-actin co-localisation, a series of DAPK C-terminal deletion constructs were transfected into A375 cells. The average cortical to cytoplasmic MAP1B staining ratio was compared to average ratios generated from transfected cell populations. Data are averages of 10 cells from 3 independent experiments. Transfection of wild-type HA-DAPK (WT) resulted in an average ratio of 2, where the average MAP1B staining intensity in the cortex was twice as intense as the average staining in the cytoplasm (Figure 4.15 e). The average ratio was decreased

upon removal of death domain but remained significantly higher than in non-transfected controls (p=0.001). Additional removal of the linker region resulted in a ratio that was less than 1 and not significantly higher than in non-transfected controls. Subsequent removal of the cytoskeletal domain resulted in an average ratio that was significantly higher than the non-transfected control cells (p=0.01). Additional removal of the ankyrin repeat domain reduced the ratio to less than 1 and not significantly higher than in non-transfected controls. Co-transfection of HA-DAPK with GFP control had no effect on the intensity ratio of cortical to cytoplasmic GFP. The effect of kinase activity on the MAP1B staining ratio was determined using the ΔCaM and K42A mutant panel. Deletion of the calmodulin regulatory domain (CaM) resulted in an increase in the average cortical to cytoplasmic MAP1B ratio, and mutation of K42 to alanine significantly decreased the ratio (Figure 4.15 f). The ratio of cortical to cytoplsmic HA-DAPK was also quantified using the same method to allow quantification of DAPK staining at cortical F-actin. Here, the average intensity of wild type HA-DAPK (FL) was 3 times higher than in the cytoplasm. This ratio was slightly enhanced by deletion of the calmodulin domain and significantly reduced by mutation of K42 to alanine. This confirmed that DAPK was also co-located with cortical F-actin in these cells.

Considered together, these data suggest that; A) MAP1B co-locates with cortical F-actin during HA-DAPK-induced cell morphology changes, B) That this involves DAPK death domain signaling, is enhanced by the ankyrin repeats and is negatively regulated by elements within the cytoskeletal-binding domain, and finally C) That this is dependent on DAPK kinase activity.

4.2.12 Transient Localisation of Co-transfected MAP1B and HA-DAPK with Microfilaments and Microtubules

Microtubule polymerisation and depolymerisation cycling revealed that transfected HA-DAPK efficiently binds to purified microtubules prepared *in-vitro*. This was an entirely novel discovery and could be controversial given previous work describing DAPK as an actin associating protein, in addition to previous studies showing that nocodazol treatment does not increase DAPK levels in cell lysates (Cohen and Kimchi, 2001). However, this study did not take temperature dependent depolymerisation of tubulin into account and so its validity is questionable.

It was not possible to use co-IP studies to determine the amount of tubulin that co-immunoprecipitates with DAPK because of interference with the heavy chain of immunoglobulin. Therefore, immunofluorescent studies were undertaken to determine if DAPK can co-localise with microtubules in cells. HA-DAPK was co-transfected with full length native MAP1B in A375 cells for 10, 18 and 32 hours before fixing and staining for MAP1B, HA, A-tubulin, and F-actin using phalliodin counter-stain. During fixation of cells, the cytoplasm was partially extracted using 0.01% Triton X100 in microtubule stabilising buffer, a technique often used to visualise the microtubule cytoskeleton in cells (Tanaka et al., 1992). As expected, after 10 hours treatment the majority of co-transfected cells had morphology which could be grouped into subpopulation 1. In these cells, HA-DAPK and MAP1B clearly co-localised with microtubules, especially at the microtubule organising center (MTOC) (Figure 4.16 a). After 18 hours, the majority of co-transfected cells could be grouped into subpopulation 2 or 3, with gross morphological changes and blebs (Figure 4.16 b). Co-localisation with tubulin was less pronounced in stage 2

cells than in stage 1 cells, rather the transfected proteins strikingly decorated F-actin fibers. This was accompanied by a reduction in microtubule staining intensity, and the MTOC was less defined. After 48 hours all co-transfected cells had shrunk and had extensive membrane blebs. In these cells, the Triton X100 fixation method revealed that both MAP1B and DAPK decorate cortical F-actin filaments around the surface of the blebs. These data show that DAPK and MAP1B transiently interact with microtubules in cells grouped into subpopulation 1 and then with F-actin in cells grouped into subpopulations 2 and 3. In addition to this, microtubule staining intensity was reduced in subpopulation 2 cells suggesting that co-transfection of the 2 proteins induced general collapse of the microtubule cytoskeleton after 18 hours.

4.3 Discussion

4.3.1 Functional Transfection Assays Reveal a Genetic Interaction between DAPK and MAP1B

There is a growing body of evidence showing that DAPK is a tumour suppressor kinase, silenced by promoter methylation in many cancer types (Raval et al., 2007). During the course of these studies various wide ranging biochemical and genetic mechanisms of DAPK action in cancer have been suggested including autophagy and apoptosis in response to diverse signaling events. These signals include cytokines such as TNFα, TGFβ and ceramide, physical events such as cell-matrix detachment and genetic transformation stimulated by aberrant oncogene activation (see section 1.4). As a result, DAPK is increasingly thought of as a key programmed cell death signaling protein, having a major effect on cell fate decision making.

Given the wide ranging role of DAPK in programmed cell death, it is likely that this protein should interact with and influence many signaling pathways in cancer. The underlying biochemical events are just beginning to be understood, with recent papers documenting interactions with the ERK MAPK pathway, the JNK/SAPK pathway and in signaling to ribosomal S6-kinase (Anjum et al., 2005; Raval et al., 2007; Schumacher et al., 2006; Stevens et al., 2007). And the consequence of DAPK activity has been advanced in recent papers providing evidence of DAPK interaction with actin/myosin microfilaments, suggesting a role for DAPK in effecting cytoskeletal dynamics. The studies presented in this thesis add to these findings, showing that DAPK can effect type II programmed cell death, through interaction

with MAP1B. It is proposed that this interaction induces cytoskeletal alterations involving both microtubules and microfilaments, causing cell membrane blebbing and leading to eventual suppression of cell growth. In chapter 3, evidence was presented demonstrating that the kinase domain of DAPK binds to MAP1B via an interface towards the N-terminus of transcript variant 1. This novel biochemical interaction was studied using the functional studies presented in chapter 4 in order to determine its consequence on cancer cell biology.

4.3.2 The Use of Rudimentary Cell Growth Assays to Quantify the Activity of Death-Inducing Trans-genes

A cell growth assay was developed to measure the effect of MAP1B on DAPK-induced tumour suppression. This assay proved invaluable, allowing it to be rapidly established that MAP1B is a positive regulator of DAPK-induced growth suppression. This observation was of particular use because it clarified some of the conflicting reports showing that DAPK and MAP1B can both be effectors of growth inhibition or even growth stimulation under different circumstances (see section 4.1.8) . Comparing this assay to subsequent assays performed during the course of these studies, an array of consistent data is presented detailing observations showing that both MAP1B and DAPK are negative regulators of cell growth.

The sensitivity of the cell growth assay proved more than adequate to resolve the difference in activities between mutant genes in different genetic backgrounds. For example, it was able to determine that, whilst knock out of p53 blocked DAPK-induced growth inhibition (Figure 4.3a), this had very little effect on co-operation of MAP1B with DAPK (Figure 4.5c i). Also, this assay was sensitive enough to discern

differences in DAPK catalytic activity as a result of K42A mutation or removal of the calmodulin domain (Figure 4.4 c), showing that DAPK-kinase activity was necessary for co-growth suppression.

Expression plasmids were expressed in cell lines for 24-48 hours before re-plating and antibody selection of transfected cells. Thereafter cultures were left to develop for a further 7 days, during which time cells were expressing the desired gene at high levels. This resulted in a situation where the short term effects of over expression were combined with the enduring effects, allowing measurement of cell growth-inhibition in the long term. This was the advantage of the assay as well as its biggest disadvantage, because subsequent assays relied on transient transfection to determine the mechanism of cell growth suppression and were therefore limited to short term observations. As a result, it was not possible to be 100% certain that effects observed after transient transfection based assays reflected the situation in the clonogenic assay. In other words, transfection assays might have been unable to account for the result of long term stable expression. For example, even though MAP1B and DAPK induced apoptosis independently, no co-operation was observed between the two (Figure 4.6 and 2.7), but it was not feasible to rule out the possibility that co-operation might occur over longer time periods. The same applies to cell cycle regulation, where again either protein alone stimulated accumulation of cells in G1, yet co-expression of both proteins did not enhance this effect (Figure 4.8). This might be of particular relevance because cell cycle effects are cumulative and so often inhibit cell growth measured over longer time periods. Using these assays it was therefore not feasible to rule out the possibility that apoptosis or cell cycle

regulation could contribute to MAP1B and DAPK co-growth repression in the longer term.

Although the cell growth assay proved useful for determining the effects of transgene expression on long-term cell growth, it could not provide information relating to the underlying mechanisms of cell growth modification. There are many mechanisms that could explain the reason for growth repression induced by over expression of a given protein, some relying on programmed cell death, or some relying on inhibition of cell division including cell cycle regulation or events leading to cell senescence. In any case, short-term expression of DAPK and MAP1B resulted in cooperative induction of cell death as determined by trypan blue exclusion assay (Figure 4.4 d). As such it seems highly likely that MAP1B and DAPK co-growth repression observed over the long term would be as a result of a cell death-inducing mechanism.

Clonogenic assays are based on the fact that under normal conditions, non-cancerous cells should not survive without trophic support from neighboring cells. The reason for this is two-fold as cell growth is dependent on direct cell-cell contact and on diffusible factors such as mitogens. These are required to inform the cell that it is in a position to survive or to divide depending on the given situation. This is a mechanism to prevent aberrant cell growth and migration, thereby preventing cancerous growth. However, the situation is partially reversed in actively dividing cells grown in culture, such cancer cell lines that are able to grow under abnormal conditions. These cell lines will expend when separated after trypsinisation and re-plating, providing that they are seeded above a critical concentration of cells per unit volume of media. Below this concentration, a fraction of plated cells will die due to

lack of trophic support. It is this property of cancer cell lines that is exploited by clonogenic cell growth assays, as stable expression of transgene will then alter the ability of cells to expand after seeding.

The ability of DAPK and MAP1B to reduce cell growth was highly dependent on seeding density. For example, when only 2500 (approx.) cells were plated, V1 or V2 alone were sufficient to reduce cell growth (Figure 4.3 b). Yet, as more cells were added, the ability of V1 or V2 to reduce cell growth was diminished to almost vector control levels. However, transfection of V1 with DAPK resulted in a very high level of synergistic growth inhibition at all seeding densities, low to high. This was in contrast to V2 transfection with DAPK, where at high densities the growth inhibitory effect was simply additive. As a consequence, this higher seeding density was used for all subsequent growth assays. This density dependent effect could offer a clue as to the *in-vivo* relevance of DAPK interaction with MAP1B. It can be speculated that a critical concentration of diffusible factor is required to activate the interaction. This could be a cell-cell communication molecule, or could simply be as a consequence of higher levels of dead cells in the plating media killed by the selection antibiotic. No transfection method is 100% efficient and so non-transfected cells are present upon re-plating that will die due to the absence of antibody resistance marker. These dying cells will then release cell contents and death markers into the surrounding media, thereby stimulating a bystander effect where DAPK and MAP1B co-transfected cells die. This line of thought would imply that DAPK and MAP1B are involved signal transduction from death inducers such as inflammatory cytokines and tumour necrosis factors.

The *in-vivo* relevance of DAPK and MAP1B-induced co-growth repression has not been studied. Therefore, it is not possible to know if the results obtained using transfected cancer cells would be replicated in a whole organism situation. This issue could be addressed using a system of multiple knock-out cell xenotransplantation into immuno-compromised mice. Many reports have shown that highly metastatic cancer variants have hyper-methylated DAPK promoters and this is often in contrast to low metastatic counterparts (see section 1.3). Restoration of DAPK to normal levels in high-metastatic Lewis carcinoma cells suppresses their ability to metastases after injection into nude mice (Inbal et al., 1997). It would be interesting to determine if MAP1B expression would enhance the anti-metestatic ability of these clones to understand to role of MAP1B in inhibition of cancer progression.

4.3.3 The p53 Pathway in DAPK- and MAP1B-Induced Programmed Cell Death

Multiple studies have shown that over-expression of DAPK is sufficient in initiating cell death programs. It is a generally held view that simple over-expression of one death-promoting gene alone is usually not adequate to induce cell death, because other negatively regulating elements come into play. This is clearly not the case with DAPK, where ectopic expression of this kinase has been extensively used to trigger programmed cell death in many circumstances (Gozuacik and Kimchi, 2006). In this study it is demonstrated that overexpressed DAPK induces autophagy that is attenuated by siRNA knock-down of MAP1B (Figures 2.9 and 2.10). Pharmacological inhibition of autophagy by 3-MA not only blocks DAPK-induced cell membrane blebbing, but also blocks synergistic membrane blebbing co-induced by MAP1B with DAPK. Given that membrane blebbing is a robust hallmark of

DAPK overexpression-induced PCD, these results suggest that MAP1B co-operates with DAPK to induce Type II autophagic PCD.

The majority of studies have dealt with DAPK overexpression-induced type I PCD, where the kinase can induce apoptosis in cells both expressing and not expressing functional wild-type p53. For example, exogenous expression of DAPK in p53 negative Hep3B hepatoma cells causes caspase-dependent apoptosis characterised by nuclear fragmentation. Interestingly, treatment of Hep3B cells with TGF-β induces DAPK expression and apoptosis which can be attenuated by endogenous DAPK inactivation (Jang et al., 2002). This suggests that expression of DAPK to physiological levels is sufficient to induce apoptosis in p53 negative cells. However, knock-out of p53 from primary mouse and rat embryonic fibroblasts is sufficient to block apoptosis induced by exogenous DAPK (Raveh et al., 2001). As such, there are clearly p53-dependent and -independent pathways stimulated by DAPK that can induce apoptosis depending on tissue type and cellular context. A clue as to the specificity of p53 action in DAPK-induced programmed cell comes from a resent study where synthesised overlapping fragments of p21 were been used as peptide ligands for characterisation in phosphorylation assays and for manipulation of DAPK interactions. Strikingly, three distinct p21-derived peptides bound to the DAPKcore kinase domain and stimulated DAPK activity specifically toward p53 and not toward the well characterised *in-vivo* substrate MLC or to p21 itself (Fraser and Hupp, 2007). These data provide an incite into the multi-faceted nature of DAPK, suggesting that DAPK integration with the p53 pathway is distinct from DAPK modification of cytoskeletal dynamics.

4.3.3.1 The p53 Pathway in DAPK and MAP1B Induced Cell Cycle Perturbation

p53 activation in response to cellular stress can result in a number of physiological end points, ranging from cell death to cell cycle arrest. The cell fate decision of whether to die or to repair as a result of stress is thought to depend on the severity of the damage. If damage is not to great, then a major down stream effect of p53 activation is cell cycle arrest, allowing cells to enter a quiescent state. Transfection of DAPK, or to a lesser extent MAP1B, resulted in a significant accumulation of cells in the G1 phase of the cell cycle in HCT116 p53 wild type cells after 24 hours (Figure 4.8 i), and this was accompanied by a reciprocal reduction in G2 cells. This suggests that either protein transfected alone is capable of initiating a G1 arrest program in these cells. However, co-transfection of both proteins together did not enhance this effect indicating that they act through separate pathways to activate cell cycle arrest. Even though MAP1B did not co-operate with DAPK in this assay, it is still entirely novel and very interesting that DAPK alone can initiate G1 arrest. Given that DAPK interacts with and modifies p53 and p21, both key effectors of G1 arrest, it seems highly likely that these interactions will play a part. Therefore it is easy to envisage a series of experiments designed to study and characterise DAPK-induced G1 arrest in conjunction with p53 and p21 knock-down. This seems especially compelling given that p21 or p53 knock-out can both strikingly reduce DAPK-induced cell growth inhibition in the isogenic HCT116 lines (Figure 4.5 c).

4.3.3.2 The p53 pathway in DAPK and MAP1B Induced Growth Supression

Whilst the p53 pathway is strongly implicated in DAPK-induced apoptosis, there is no evidence suggesting that this pathway is involved in regulating DAPK-induced autophagic cell death. For example, DAPK siRNA knockdown studies have

demonstrated that DAPK is necessary for autophagic cell death, induced either by IFN-γ in HeLa cells or by steroid withdrawal and amino acid starvation of 293T and MCF-7 cells (Inbal et al., 2002; Shani et al., 2004). Whilst MCF7 cells are p53 wild type, both HeLa and 293T cells express viral SV40 T-antigen, and as such are p53 dysfunctional. Therefore, autophagic cell death does not require an intact p53 pathway and can be induced in both wild type and functional-null backgrounds.

The above highlights the importance of defining the role of p53 in DAPK-induced cell death programs. DAPK transfection induced accumulation of p21 protein (Figure 4.5 b i and ii). Given that DAPK expression can activate p53, it seems likely that this is as a result of enhanced p53 transactivation and subsequent increased p21 mRNA expression. This is accompanied by an increase in Ser20 phosphorylation, also evidence that p53 is activated by DAPK expression in this system. Transfection of DAPK also lead to increased bax expression, accompanied by increased bax modification. Bax protein levels are regulated by ubiqitination as part of regulation of late stage apoptosis. The pattern of modification of bax seen after DAPK transfection could therefore be due to ubiquitination, negatively regulating the levels of late-stage apoptosis seen in these cells (see below).

Using the cell growth assay, it was determined that p53 played a positive role in DAPK transfection-induced growth repression in HCT116 cells (Figure 4.3 a). Here, knock-out of p53 in this cell line resulted in increased cell growth as compared to the wild type control. However, when MAP1B was co-transfected, synergistic interaction was observed regardless of p53 status (Figure 4.5 c). It should be noted however that p53 functional knock-out did slightly but significantly reduce the total

co-growth repression. This could indicate that presence of p53 protein enhances co-operation but is not necessary for co-operation in this cell situation. This could be explained by the fact that the p53 null HCT116 cell-line is in reality a functional null, created by deletion of exon 1. This does not result in complete loss of expression but rather results in expression of truncated protein missing the N-terminal transactivation domain, ΔN-p53. This protein is expressed as an isoform by alternative initiation of translation at codon 40. As a result, interaction with p53 out-with the transaction domain is still possible and this may result in partial activity. It is feasible that MAP1B co-operation with DAPK may signal in-part through elements on ΔN-p53. In any case, although it is clear that p53 plays an important role in DAPK signaling during cell death initiated in multiple cell types and in many situations, it has not been possible to coherently ascertain the role of p53 in MAP1B co-operation with DAPK. Therefore it is proposed that the growth assay should be repeated in a panel of p53 wild-type and true null lines in order to verify the extent of p53 dependence.

4.3.4 DAPK and MAP1B induced Type I and Type II Cell Death

Apoptotic cells undergo ordered DNA fragmentation that can be observed as a distinct ladder after agarose gel electrophoresis or as a sub-G1 peak during cell cycle analysis using FACS. This effect is specific to apoptotic cell death. Necrotic cells undergo random fragmentation of DNA that presents as a smear and will not establish a sub-G1 peak. Autophagic cells undergo nuclear condensation but this is not accompanied by ordered fragmentation, rather DNA is randomly degraded and as such does not accumulate as a sub-G1 peak. Transfection of 200ng of either DAPK

or MAP1B alone stimulated a transient presentation of phosphatidylserine (PS) on the outer membrane of approximately 10% of cells (Figure 4.6 b). This effect was seen after 24 hours only, where after 48 hours, no above-background external phosphatidylserine was observed (Figure 4.6 a). After 32 hours of transfection, apoptotic DNA fragmentation was also slightly increased (Figure 4.7), as determined by TUNEL staining. This indicated that there was a small increase in late stage apoptosis in the transfected culture. Even though the measured percentage of DAPK or MAP1B transfected cells with positive staining was 5 and 15 fold higher (respectively) than that of vector control transfected cells, the actual number of cells was very small. Only 0.5% of cells were TUNEL positive after DAPK transfection and 1.4% after MAP1B transfection. This is in comparison to the relatively high number of phosphatidylserine (PS) positive cells at 8.72 and 8.6% respectively after 24 hours. These data, where PS presentation was transient and not accompanied by DNA fragmentation, suggest that PS presentation is uncoupled from ordered DNA fragmentation in DAPK and MAP1B transfected cells. This is backed by data obtained by FACS cell cycle analysis where there was no observed increase the percentage of cells with sub-G1 DNA (Figure 4.8) after ectopic expression of either protein. Therefore, even though transfection of DAPK with MAP1B lead to synergistic long-term co-growth repression, this could not have been due to short term apoptosis involving ordered DNA fragmentation.

4.3.4.1 MAP1B, DAPK and Phosphatidylserine Externalisation

It was interesting that PS presentation was uncoupled from ordered DNA fragmentation. The purpose of PS externalisation is to encourage engulfment of the effected cell by phagocytes. Phagocytosis of apoptotic and necrotic cells has been

extensively studied, where in both cases clearance of dying cells leads to recycling of nutrients and reduction of inflammation. Very recent data has been published detailing how cells dying through autophagy are removed from developing tissues (Qu et al., 2007)and from a second study using cultured MCF-7 cells (Petrovski et al., 2007). Autophagic cell death is involved during PCD in development spanning from early developmental processes such as cavitation through to later events such as synaptic pruning (Luo and O'Leary, 2005). Data is presented in the first study using mammalian embryoid bodies (EBs) derived from the autophagy gene - atg5 knock-out cells. Interestingly, these atg5 knock-out EBs failed to cavitate, due to impaired clearance of cell corpses, rather than impairment of PCD *per se*. Dying cells in the knock-our EBs failed to express externalised PS, and so were not recognised by phagocytes for clearance. Also, atg5 knockouts contained low levels of cellular ATP, and treatment with metabolic substrate could restore PS externalisation and engulfment. From this data the authers conclude that autophagy contributes to cell clearance during PCD by a mechanism that involves the generation of energy dependent PS externalisation (Qu et al., 2007). MCF-7 cells are often used as a model to study autophagy because they undergo autophagic cell death upon treatment with multiple stimuli. In the second paper, tamoxifen treated autophagic MCF7 cells were engulfed by human macrophages and by bystander MCF7 cells. This effect required an intact PS pathway and could be blocked by addition of the autophagy inhibitor, 3-methyladenine (Petrovski et al., 2007). Thus these two recent papers provide compelling evidence that the autophagic program is required for clearance of dying cells, and that this involves externalisation of PS. This supports the theory that there is a complex interplay between autphagy and apoptosis where

here, nutrient deprivation-dependent autophagy stimulates PS-externalisation during apoptosis. Either MAP1B or DAPK alone are able to promote LC3 modification (Figure 4.10 a), suggesting that either protein alone is sufficient to initiate autophagic pathways. This could explain why MAP1B and DAPK transfected cells present PS as determined by the annexinV assay and yet apoptosis rates are low as determined by TUNEL and sub-G1 DNA quantitation using FACS. (Figure 4.6 vs. 2.7 and 2.8). Nevertheless, DAPK co-transfection with MAP1B did not enhance PS presentation, suggesting that this is a distinct pathway from LC3 modification (Figure 4.10 b) and autophagosome sequestration (Figure 4.9 b) which involves a synergistic interaction. These data support the prevalent model is that DAPK can be linked to various biochemical pathways depending on the cellular setting, and that these culminate in different forms of cell death. They also support the theory that there is a complex interplay between type I and type II PCD (see the end of section 1.8).

4.3.4.2 MAP1B is a positive Regulator of DAPK-Induced Type II Cell Death

Autophagosomes were observed in DAPK transfected cell populations as determined by the GFP-LC3 foci assay (Figure 4.9). In addition to this, DAPK transfection stimulated LC3 modification that was dependent on kinase activity (Figure 4.10). These data correlate with DAPK-induced cell growth inhibition and cell viability loss, which was also dependent on an active kinase domain (Figure 4.4). This evidence corroborates with that of published data showing that DAPK can induce autophagic cell death dependent on DAPK catalyitic activity (Inbal et al., 2002). MAP1B siRNA significantly reduced GFP-LC3 foci formation (Figure 4.9 b) and LC3 modification (Figure 4.10 b), showing that MAP1B is a positive regulator of DAPK induced autophagy. MAP1B has a positive role in regulating DAPK-induced

cell membrane blebbing, where co-transfection is synergistic and MAP1B knock-down attenuates blebbing (Figure 4.11). Because these effects can be blocked by the autophagy inhibitors (Figure 4.12c), and because blebbing is a robust marker of DAPK-induced cell death, these data strongly suggest that MAP1B is a positive regulator of DAPK-induced type I autophagic cell death.

4.3.4.3 MAP1B as a Regulator of Autophagy

It is possible that MAP1B alone was weakly able to induce autophagy. MAP1B transfection alone lead to LC3 modification (Figure 4.10 a), and to a slight induction of cell membrane blebbing as compared to transfection controls (Figure 4.11 b). However, it was not possible to rule out the possibility this was due to interaction with low levels of endogenous DAPK. Recent papers have considered the possibility that MAP1B could have a negative effect on neuronal cell growth (see section 4.1.8). Stable over-expression of mouse Mtap1B-LC1 (the mouse MAP1B LC1 homologue) in NIH 3T3 cells lead to reduction of cell proliferation, evident after 5 days post-plating (Lerch-Gaggl et al., 2007). This suggests that MAP1B-LC1 alone was sufficient to reduced cell growth after a time similar to that in these studies (Figure 4.3 b). Gigaxonin expression leads to degradation of MAP1B-LC1 in cortical neurons (Allen et al., 2005). Degradation of LC1 by gigaxonin leads to enhanced survival of neurons, and gigaxonin null neurons accumulate LC1. Accumulation of LC1 results in reduction in neuron survival evident after 7 days when compared to wild-type cultured neurons. In addition to this, over expression of full length MAP1B in neurons leads to cell death characteristic of gigaxonin null neurons, and siRNA of MAP1B leads to enhanced survival. These data provide additional evidence from an independent study clearly showing that MAP1B can be a negative regulator of cell

survival. In Y Uchida's paper (Uchida, 2003), data is presented indicating that over expression of MAP1B fragments containing the N-terminal 126 amino acids results in cell death accompanied by neurite out-growth. This suggests that extension of neurites correlates with sensitivity to death, in accordance to the hypothesis presented in section 4.1.8 based on the well known tenet that progression of neuronal development must be accompanied by significant loss of superfluous cells. It is interesting that additional data is presented in this paper showing that MAP1B V1 (containing the N-126 amino acid domain) sensitises neurons to cell death after serum withdrawal. Uchida concluded that MAP1B over expression resulted in neurons dying through via type 1 death, however there is little evidence to support this as dying cells were scored by nuclear staining. It would not easily be able to distinguish apoptotic cells from autophagic cells using this method and so it is possible that these neurons were dying via a type II cell death program. Further evidence to support this comes from published data showing that serum withdrawal is able to stimulate autophagic cell death in multiple cell lines (Inbal et al., 2002; Shani et al., 2004), and from data presented in this thesis indicating that that MAP1B over expression is able stimulate autophagy (Figure 4.10 a and 2.11 b). Also, nuclear staining of MAP1B transfected cells revealed that nuclei were condensed (Figure 4.14 b) and so could easily be mistaken for apoptotic cells using this method. It is still unknown if MAP1B alone is able to stimulate cell death in the absence of endogenous DAPK. MAP1B over expression was able to reduce cell proliferation in HCT116 cells plated at low density (Figure 4.3b), and reduce survival or cause cell death in cultured developing neurons in multiple studies (Allen et al., 2005; Lerch-Gaggl et al., 2007; Uchida, 2003). HCT116 cells and developing neurons both

contain significant amounts of endogenous DAPK, which might contribute to MAP1B activity in each case.

4.3.4.4 Type I and Type II Cell Death and the p53 Pathway

As detailed above, DAPK-induced autophagic cell death is independent on p53 as determined in previous studies (Inbal et al., 2002; Shani et al., 2004)using both p53 wild-type and p53 null cell lines. However, in most cases ablation of p53 activity reduces DAPK ability to induce apoptosis (Gozuacik and Kimchi, 2006; Raveh et al., 2001). It is not surprising therefore that MAP1B co-operation with DAPK was also largely independent on p53 (Figure 4.5 c) if this interaction proceeds through an autophagic program (Figure 4.9, 2.10 and 2.12) and not through an apoptotic program (Figure 4.6, 2.7 and 2.8). Co-operation between MAP1B and DAPK in the blebbing assay was also independent of p53 (Figure 4.11c), rather this interaction could be blocked by pharmacological autophagy inhibition (Figure 4.12 b, c, d). These corroborative data developed from multiple assays provide compelling evidence that MAP1B interacts with DAPK to induce a p53-independent autophagic Type II cell death program.

4.3.5 Plasma Cell-Membrane Blebbing as a Marker of Programmed Cell Death

The first paper demonstrating that DAPK was involved in autophagic cell death was published in April 2002 by Adi Kimchi's group (Inbal et al., 2002). Prior to this, DAPK and its two other family members; DRP-1 (DAPK2) and Dlk/ZIPK (DAPK3), had been characterised as apoptosis-inducing proteins and positive effectors of cell membrane blebbing (Shohat et al., 2002). In 2001 a paper was published by Prehn's group detailing studies demonstrating ZIPK's involvement in cell death programs.

ZIPK-induced apoptosis was blocked by over expression of the apoptosis inhibitor Bcl-Xl and by the pan caspase inhibitor zVAD-fmk (Murata-Hori et al., 2001). They publish data showing that neither treatment blocked membrane blebbing induced by ZIPK, and so concluded that protection by Bcl-Xl or caspase inhibition was down stream of blebbing. However, if resent published data is taken into account, showing that all three DAPK family members can induce blebbing independent of apoptosis (Inbal et al., 2002; Shani et al., 2004), it now seems likely that the Bcl-XI and caspase pathways are in fact uncoupled from plasma membrane blebbing induced by DAPK family members. MAP1B synergistic cooperation with DAPK could not be blocked by caspase inhibitors and did not induce DNA fragmentation (Figure 4.12 c), and so this strongly suggests that membrane blebbing induced by the DAPK:MAP1B cooperation is independent of type I cell death.

4.3.5.1 Membrane Blebbng and Actin/Myosin Contraction

F-actin is necessary for membrane blebbing, where the concentration of cortical F-actin at the base of blebs correlates with bleb size (Cunningham, 1995; Laster and Mackenzie, 1996; Rajashree et al., 2005). Through interaction with F-actin, the myosin family of motor proteins provide the contraction force necessary to form blebs. Non muscle myosin (myosin II) is essential for basic cellular processes such as cytokinesis, stress fiber forces, secretion of vesicles and maintenance of the cortical actin layer. Myosin II contractile activity is stimulated by phosphorylation of myosin regulatory light chain (MLC) at serine 19 by myosin regulatory light chain kinase (MLCK) (Kohama et al., 1996; Gallagher et al., 1997). This then promotes interaction of the myosin head with actin allowing the myosin ATPase to produce sliding force. Phosphorylation of MLC by MLCK is positively regulated by the small

G protein, Rho which stimulates Rho kinase (ROCK), which phosphorylates and inactivates MLC phosphatase (Sebbagh et al., 2001). In addition to this, both ROCK and MLCK can phosphorylate MLC ser19, increasing myosin contractile activity (Amano et al., 1996).

Current dogma dictates that cell membrane blebbing is a hallmark of extranuclear apoptosis, induced during the early stages of type I cell death (Mills et al., 1998). During apoptotic blebbing, myosin light chain (MLC) is phosphorylated by myosin light chain kinase (MLCK) mediated by the small GTPase Rho (Mills et al., 1998). ROCK1 stimulated by Rho is cleaved by caspase-3 thereby removing its carboxy-terminal inhibitory domain. This results in constitutive ROCK kinase activity and subsequent increase in phosphorylation of MLC. This phosphorylation then leads to membrane blebbing that can be abrogated by inhibition of caspases (Sebbagh et al., 2005; Sebbagh et al., 2001).

ROCK1 mediated activation of MLC is an example of a mechanism of caspase dependent apoptotic membrane blebbing (Coleman et al., 2001). However, membrane blebbing has been shown to be caspase independent in many cases (reviews: (Borner and Monney, 1999; Borner et al., 1999)), suggesting that it can proceed without cleaved ROCK. The kinase domain of DAPK shares a high degree of sequence homology with ROCK (Deiss et al., 1995; Feinstein et al., 1995a; Feinstein et al., 1995b)and is able to phosphorylate MLC at ser 19 *in-vitro* and in cells (Kuo et al., 2003). MLC phosphorylation by DAPK then induces actin-myosin contraction independent of ROCK and Rho. This shows that DAPK acts as an additional effecter of membrane blebbing, acting independently of caspase cleaved

ROCK. Therefore, it is proposed that the cell has multiple MLC kinases, able to induce blebbing through multiple pathways.

4.3.5.2 Membrane Blebbing and Type II Cell Death

It is widely accepted that apoptosis can proceed independently of caspases. In this case, cell death is still characterised by the supposed hallmarks of apoptosis including cell membrane blebbing and ordered fragmentation of DNA whilst the organelles remain largely intact (review (Borner and Monney, 1999; Borner et al., 1999). The DAPK family of proteins are unique in being the only known proteins to induce membrane blebbing independently of ordered fragmentation of DNA. Transfected DAPK1, 2 or 3 induce caspase independent cell death in cells that have condensed but non-fragmented nuclei, and no loss of mitochondrial membrane potential (Inbal et al., 2002; Shani et al., 2004).These cells have multiple autophagic vesicles and so are categorised as autophagic, yet in addition to this they have extensive cell membrane blebbing. This would explain why MAP1B co-operated with DAPK to induce autophagic vesicles and membrane blebbing (figures 2.6, 2.7 and 2.8) independently of caspases (Figure 4.12), yet did not co-operate to induce apoptosis (Figures 2.9 2.10 and 2.11). Considered together, these results suggest that MAP1B cooperates with DAPK to induce membrane blebbing in non-apoptotic cells, which instead have hallmarks of autophagic cell death including autophagosomes.

4.3.6 A Role for MAP1B and DAPK in the Control of Matastasis?

4.3.6.1 Membrane Blebbing and Migration

Although plasma cell membrane blebbing has been used as a marker for cell death programs, the exact physiological significance of blebbing is unclear. Blebbing has

been observed during cytokenesis, during cellular locomotion, during differentiation and during apoptosis where it is thought to be involved in antigen recognition (see (Verhoef et al., 2004) for discussion). It is possible that blebbing might be an epiphenomenon simply resulting from activation of cortical actin contraction, or equally it might have a positive function in these processes. A recent paper clearly shows that blebbing triggers assembly of F-actin that integrates into the cortex as blebs form. The authers suggest that this might function as a pathway for new cortex generation when cells need to expand their surface area, such as during cytokinesis or during cell movement (Charras et al., 2006).

There is mounting evidence showing that plasma membrane blebbing correlates with increased levels of cell migration. For example; 1) The transmembrane 4 L6 family member 5 (TM4SF5) interacts with and activates integrin A2, preventing migration in cancer cells. Ablation of this interaction with anti-A2 antibodies induces migration of cells accompanied by membrane blebbing. (Lee et al., 2006). 2) Stimulation of small cell lung cancer cells with hepatocyte growth factor (HGF) leads to increased migration of cellular clusters. This correlates with increased formation of filopodia and induction of membrane blebbing (Maulik et al., 2002). However, these studies do not determine if membrane blebbing is required for migration, and simply show a correlation. On the other hand, transfection of dominant-active Rho-kinase leads to increased MLC phosphorylation and myosin contraction. This also correlates with membrane blebbing, and inhibition of cell polarisation (Gutjahr et al., 2005). Cell polarisation is essential for coordination of cell migration, and so this study suggests that membrane blebbing is as a consequence of negatively regulated migration. To address this apparent contradiction, the authers show that basel levels of Rho-kinase

activity is required to maintain polarity and migration. Only when Rho-kinase activity is increased above a certain level do cells go crazy and bleb. These studies strongly suggest that migration is tied to membrane blebbing and that blebbing is the physiological consequence of highly active myosin contraction. Therefore, regulation of myosin contraction to above basal levels can negatively regulate migration.

4.3.6.2 Cell Migration and Metastasis

Metastasis is believed to involve active migration of cancer cells, and not simply due to random detachment and re-attachment of cells. During metastasis, migration and invasion is highly coordinated and depends on re-organisation of the cytoskeleton resulting in altered cell-cell and extracellular matrix (ECM) adhesion properties (Guo et al., 2006) (Carragher and Frame, 2004). Cancer cells migrate singly or as collective groups along collagen fibres involving assembly of cell protrusions, and ECM-degrading focal adhesions arbitrate intravasation (Condeelis et al., 2005). Comparison of gene expression profiles between primary and metastatic lines and between chemotaxing and stationary cells has revealed that multiple cytoskeletal components and regulatory proteins are up-regulated during this process (Condeelis et al., 2005).

MAP1B is involved in the regulation of cytoskeletal dynamics during extension of axons and dendrites and neuronal cell migration. Phosphorylation of MAP1B by multiple kinases alters its interaction with the cytoskeleton leading to dynamicity or stability depending on the pattern of modification (see section 4.1.3). Migrating axons are then guided by signals to MAP1B including chemorepulsive or attractive factors such as semophorins or netrins. As such, MAP1B plays a central role in the regulation of neuronal cell migration and axon movements. It would seem likely

therefore that MAP1B could play a role in regulation of cell movement in non-neuronal tissues or in cancer. This might seem possible in light of studies showing that MAP1B is extensively expressed in cancer cell lines (Figure 4.1, 2.2), that are highly metastatic.

4.3.6.3 DAPK and Anoikis in the Regulation of Metastasis

In an *in-vivo* cell-injection metastasis model, expression level of DAPK is inversely correlated with the metastatic activity, and reintroduction of DAPK into highly metastatic tumors suppresses their ability to form metastases in mice (Inbal et al., 1997). Most normal cells require cell-cell contact or contact with the ECM for survival and inadequate or aberrant ECM interaction can cause programmed cell death. This phenomenon is termed anoikis (Frisch and Ruoslahti, 1997; Frisch and Screaton, 2001) and provides a mechanism for maintenance of the organisation of tissues. Resistance to anoikis results in anchorage independence, which is a hallmark of malignant tumor cells. Anchorage independence then leads to miss-regulated adhesion and migration as the disconnected cells are permitted to survive, thus promoting metastasis.

ECM adhesion is mediated by integrins present on the cell surface. Integrins can be activated by intracellular signals, called inside-out signals that converge on the cytoplasmic domain of integrins and induce a high affinity state. DAPK over-expression was found to inhibit cell adhesion through inactivation of integrins. This occurred in numerous cell lines positive for p53 (such as 3T3 cells) and in cells with inactivated p53 (such as 293T cells). Also, inhibition of cell adhesion by DAPK was independent of apoptosis as determined by caspase cleavage assays and by nuclear fragmentation assays and was not affected by pretreatment of cells with the broad-

spectrum caspase inhibitors. However, transfected cells displayed the expected DAPK-induced morphology changes such as blebbing (Wang et al., 2002). Detached cells then died from both p53 positive and negative lines, suggesting that they entered a p53 independent type II cell death program. This study provides evidence that DAPK induces caspase-independent membrane blebbing and that this induces cell detachment resulting in anoikis.

4.3.6.4 Anoikis in Type II Cell Death?

Anoikis, is often thought to proceed through type I cell death programs after aberrant cell detachment. However, there is evidence to suggest that type II cell death is able to activate anoikis. Treatment of MCF-7 cells with tamoxifen induces autophagy. When plated on a non-adhesive substratum these cells die by anoikis after induction autophagy as revealed by monodansylcadaverine staining, LC3 expression and scoring of autophagosomes by electron microscopy. This effect could be blocked by inhibition of autophagy by 3-MA, but this did not stop cells dying when plated on adhesive substrate (Petrovski et al., 2007). Thus, aniokis can be activated by autophagic programs when cells are not provided with support from the substratum.

4.3.6.5 DAPK and Cdc42

DAPK can also inhibit cell migration by suppressing the integrin-Cdc42 cell polarity pathway that is essential for directional persistence and directed migration. This action of DAPK blocks migration and invasion of tumour cells (Kuo et al., 2006). Interestingly, DAPK inhibition of migration is documented to take place in tumour lines that are resistant to DAPK-induced apoptosis. This could be as a consequence of DAPK's multiple functions, initiating apoptosis where possible or activating an

anti-migratory program in resistant tissue. This anti-migratory program might involve cell death programs other than apoptosis, such as autophagy.

4.4 Is Aberrant Cell Migration Regulated by Autophagic Cell Death?

As discussed above, cell migration involves dynamic reorganisation of cytoskeletal networks. Cells migrate by protrusions in the forward end and retraction in the rear end. It is extremely interesting that both MAP1B and DAPK can induce cell protrusions and alterations in cell migration by regulation of components of the cytoskeleton. HA-DAPK-transfected cells grouped into subpopulation 2 often had large extended processes in addition to blebs (Figure 4.13c), where DAPK co-located with cortical F-actin (Figure 4.14). Also, transfected and endogenous MAP1B co-located with HA-DAPK at cortical actin (Figure 4.15 d, 2.16 b). This suggested that MAP1B played a positive role in this process, especially as knock-out of MAP1B reduced the number of cells and as MAP1B co-transfection increased this number (Figure 4.11). Therefore it seems very possible that cooperation of MAP1B with DAPK might be involved in regulation of cell movement in these cells.

It is proposed that further study should be geared to address the relationship between MAP1B and DAPK with regards to cell migration and metastasis. The molecular and cell biological aspects could be studied using cell imaging of extensions produced in subpopulation 2 cells, to find out if MAP1B is required for this process. But perhaps more importantly, the physiological implication of this process could be investigated in animal tumour models. For example, it would be desirable to determine if MAP1B is required for DAPK's inhibition of metastasis, and to what role does MAP1B play in carcinoma cell migration. What's more, the fact that this is coupled to MAP1B

and DAPK co-stimulated autophagy, suggests that the availability of growth factors and nutrients could play an integral role in this process.

Chemical inhibition of autophagy in MAP1B and DAPK co-transfected cells not only blocked plasma membrane blebbing but also blocked HA-DAPK association with cortical actin and inhibited that formation of large cell extensions (Figure 4.12d). In light of the discussion above, this suggests that there is a complex interplay between autophagy, blebbing and cell migration, and that this process can be stimulated by cooperation between MAP1B and DAPK. It has been previously documented that DAPK is a novel effecter of caspase-independent non-apoptotic membrane blebbing (Inbal et al., 2002; Shani et al., 2004). However, it is entirely novel that the membrane blebbing function of DAPK can be blocked by pharmacological inhibition of autophagy (Figure 4.12). Interestingly, this suggests that the autophagic function of DAPK is up stream of blebbing. Induction of autophagy by steroid withdrawal or by removal of amino acids can be attenuated by disruption of DAPK activity by dominant negative mutant transfection or by siRNA to DAPK (Inbal et al., 2002). This correlates with reduction in DAPK-induced membrane blebbing and as such this suggests that starvation can induce DAPK-dependent blebbing in addition to DAPK-dependent autophagy. It remains to be seen if MAP1B interaction with DAPK can be stimulated by steroid withdrawal or amino acids starvation, and this is an area of research that must be addressed. It seems likely that amino acid withdrawal would be a positive regulator of DAPK and MAP1B co-induced blebbing and autophagy.

Migration of cancer cells can be initiated as a result of lack of nutrient availability. This is thought to initiate matastasis as well as angiogenesis in order to provide the developing tumour with increased nutrition. Therefore, if nutrient deprivation induces autophagy and migration, it seems this could be regulated by blebbing and cell death by an anoikis mechanism. Miss regulation of this process could then provide a survival advantage to cells, as they would become anchorage independent. It is proposed that DAPK signaling to MAP1B would be required for sensing aberrant cell detachment as a result of autophagy during nutrient deprivation. However, this interaction was stimulated by over expression of DAPK, which is known to be sufficient to initiate DAPK-dependent processes.

4.5 Cytoskeletal Aspects of the Interaction between DAPK and MAP1B

To attempt to uncover the underlying biochemical mechanism of cooperation between DAPK and MAP1B, cell imaging studies were performed to visualise the cytoskeletons of HA-DAPK transfected A375 cells. These cells contain high levels of endogenous MAP1B, thus creating a system able to track changes in cytoskeletal distribution of MAP1B resulting from transfected DAPK activity.

4.5.1 DAPK and MAP1B Interaction with the Contractile Cortex?

Underneath the cell membrane is a meshwork of cytoskeletal proteins able to initiate directional forces called the contractile cortex. Cell membrane blebbing is initiated by detachment of a small area of membrane from the contractile cortex. These are is then inflated, forming a spherical protrusion 1–10 μm in diameter filled with cytosol (Cunningham, 1995). After expansion, the contractile cortex then reassembles under the bleb membrane, and the bleb can then be retracted. If retraction proceeds, the

bleb cortex then reintegrates into the cell cortex. Bleb inflation is thought to be driven by intracellular pressures generated by myosin II contraction within the actin cortex because drugs that relax the cortex by inhibiting actin or myosin II also inhibit blebbing (Charras et al., 2006).

During HA-DAPK induced morphological changes, polymerised F-actin remains visible in all 3 subpopulations, and is strongly stained. This is especially true for cortical actin that stains brighter as blebbing progresses (Figure 4.13). During this process DAPK and MAP1B co-localise with cortical actin (Figure 4.14 a, Figure 4.15), where the mean staining intensities in the cortex are 2 and 3 fold higher than in the cytoplasm respectively (Figure 4.15 f – Bars labeled FL). This is in comparison to in the non-transfected situation where MAP1B mean staining intensity in the cortex is 70% of that in the cytoplasm (Figure 4.15 f – Bars labeled N/T). This effect, where MAP1B is relocated to the cortex does not involve migration of all cytoplasmic proteins because when GFP is co-transfected it does not change location (Figure 4.15 f). Therefore this effect is either specific to MAP1B or involves a sub-set of the cytoplasmic proteome. The above data strongly suggest that DAPK activates translocation of MAP1B to cortical actin during membrane blebbing. This could only be the case if there was a temporal relationship between cells in each subpopulation, and that the mix of subpopulations comes about due to differences in cell cycle distribution when the cells are transfected. Common sense would suggest that this would be the case, but evidence to support this comes from the fact that the proportion of subpopulation 1 cells decreases with time, subpopulation 3 cells increases and subpopulation 2 cells increases before retreating after 24 hours (Figure 4.13 e). A detailed search through the published literature reveals that this concept

has been addressed before. Dlk/ZIPK (DAPK3) transfection has been shown to induce blebbing in D-283 cells in the 3 distinct stages identical to the ones detailed here, and the authors are quick to conclude that the first precedes the second precedes the third (Shani et al., 2004). Also, DAPK1 and DAPK2 have both been shown to induce distinct morphological stages, some cells having no blebs, a with few small blebs, and others with extensive larger blebs, again identical to the situation presented here (Inbal et al., 2002; Shani et al., 2004). Therefore there is little room for doubt that there is a temporal relationship between the subpopulations of cells induced by HA-DAPK transfection. As a result it can be safely concluded that DAPK induces translocation of MAP1B to cortical F-actin during membrane blebbing.

Considered as a whole, the data detailed in the above summary suggest that DAPK and MAP1B interaction with cortical F-actin progressively increases as blebbing progresses. Thus, the proteome of the contractile cortex is changed by the activity of DAPK transfection. This effect, where the constituent proteins of the cortex changes during blebbing has been documented in a recent study. This paper describes the complex situation where the cytoskeletal proteins of the contractile cortex and constituent actin filaments are rearranged during formation, extension and retraction of blebs (Charras et al., 2006). This involves sequential recruitment of myosin kinases and structural scaffolds, that can be altered by specific elements depending upon the situation. Thus, bleb formation and function is controlled by local changes in the proteome of the contractile cortex (see Figure 4.17, taken from this paper). The fact that MAP1B and DAPK are recruited to the cortex during blebbing strongly suggests that they should play an integral part in this process during autophagic

membrane blebbing. Further detailed study is required to understand the role of MAP1B interaction with DAPK with regards to the contractile cortex.

4.5.2 A Role for DAPK in Regualtion of Microtubule Dynamics?

Surprisingly, DAPK was able to interact strongly with microtubules purified from transfected A375 cells (Figure 4.12). This interaction resulted in a change to the proteome of purified microtubules (Figure 4.13), showing that transfected DAPK is a novel modifier of the microtubule cytoskeleton purified from cells. As a result, cell imaging studies were conducted using transfected A375 cells fixed by partial cytoplasmic extraction. This allowed visualisation of the cytoskeleton and associated proteins by fluorescent imaging. Transfected MAP1B and DAPK clearly co-localise with microtubules after 10 hours co-transfection into A375 cells (Figure 4.16 a). These also seem to partially co-localise with F-actin at what is likely to be the microtubule organising center (MTOC). After 18 hours co-transfection MAP1B co-localises with DAPK predominantly at cortical F-actin fibres (Figure 4. 16 b), reproducing the results obtained using single transfection of DAPK (Figure 4.15). What's more, the MTOC in these cells (after 18 hours) is degraded, and is not stained by tubulin or F-actin, MAP1B or DAPK. This proceeds extensive membrane blebbing observed at the later time point (Figure 4.16 c) where is it difficult to discern the specific pattern of staining due to cell shrinkage. However, it looks as though DAPK, MAP1B and F-actin strongly stain the outer rim of blebs (Figure 4.16 c – Example 3).

The action of the contractile cortical actin in cell membrane relies on the status of the microtubule cytosleleton. Microtubule disassembly by disrupting drugs is known to stimulate blebbing by inducing phosphorylation of MLC leading to actomyosin

contraction (Kolodney and Elson, 1995). Therefore, it is extremely encouraging that DAPK transfection stimulated the disruption of microtubules during induction of membrane blebbing. This suggests that MAP1B with DAPK can induce blebbing and that this involves changes in the dynamics of and proteome of mictrotubules as well as changes in the dynamics and proteome of contractile cortical actin.

The above studies using cell imaging show that there is a complex interplay between the microtubule and microfilament cytoskeletons during membrane blebbing, and highlight a role for DAPK and MAP1B in this process. The action of DAPK induced blebbing is synergistically enhanced by MAP1B, and given that DAPK can bind directly to MAP1B, and that this induces microtubule disrupction, this suggests that there is a novel pathway involving the two proteins, to induced cell membrane blebbing via interaction with microtubules..

4.5.3 Microtubules in Autophagy

2 recent papers have been published showing that microtubules play an important role in autophagy because they support production and transport of microtubules (Fass et al., 2007; Kochl et al., 2006). In both cases, treatment of cells with microtubule disrupting drugs that depolymerise tubulin resulted in reduction in the number of mature autophagosomes. This might suggest that DAPK induced depolymerisation of microtubules would also inhibit the production of autophagosomes and thereby inhibit autophagic cell death. However, this superficial contradiction can be easily explained. Firstly, initial treatment with the disrupting drug lead to an initial transient 2-fold increase in autophagosomes (Kochl et al., 2006) before total disruption of microtubules was observed. Secondly, the drugs used, vinblastine and nocodazole induced non-reversible disruption of microtubules

by inhibiting polymerisation of tubulin dymers. Thirdly, disruption by drugs did not affect the life span or function of autophagosomes that had already been formed (Fass et al., 2006) and; Lastly, DAPK and MAP1B transiently interact with intact microtubules before depolymerisation, suggesting that there would be a time window in which microtubules would be intact. Therefore, taken together these results can be interpreted as that the formation of autophagosomes requires microtubules in a dynamic state that; Firstly would lead to a transient production of autophagosomes immediately after disrupting drug treatment, before; Secondly, the disrupting drugs artificially reduced tubulin into a dimeric state thereby inhibiting dynamics. This would thirdly, not effect the life span of autophagosomes already produced. So lastly, DAPK and MAP1B -induced loss of microtubule polymerisation suggests an increase in dynamic microtubules that would in fact stimulate autophagosome production. Therefore, it is proposed that DAPK interacts with MAP1B to induce dynamic microtubules to stimulate the formation of autophagosomes.

The above proposal seems especially likely because MAP1B is known to play a major role in regulation of microtubule dynamics and because autophagosomes are produced near to the microtubule organising center, as noted by one of the papers discussed above (Fass et al., 2006). This is an area of co-localisation between MAP1B, DAPK, tubulin and F-actin observed here (Figure 4.16 a), suggesting that DAPK and MAP1B could play a part in this process. Also, in a recent paper, MAP1B was demonstrated to interact with high affinity to the autophagosome marker and LC1 related LC3 (Wang et al., 2006) inhibiting autphagosome production. Therefore the authors conclude that MAP1B binding to LC3 is inhibitory to autophagy. It is therefore possible that release of MAP1B from LC3 could be

refractory to this inhibition. As such, one could speculate that interaction with and modification of MAP1B by other factors might stimulate autophagosome production by liberating the otherwise tightly bound LC3. Of course, DAPK is a prime candidate for this because it binds to MAP1B during induction of autophagy and this involves transient co-localisation at the MTOC, the site of autophagosome production.

a - MAP1B RNA Expression in the NCI60 Cancer Cell Lines as Determined by Microarray Analysis

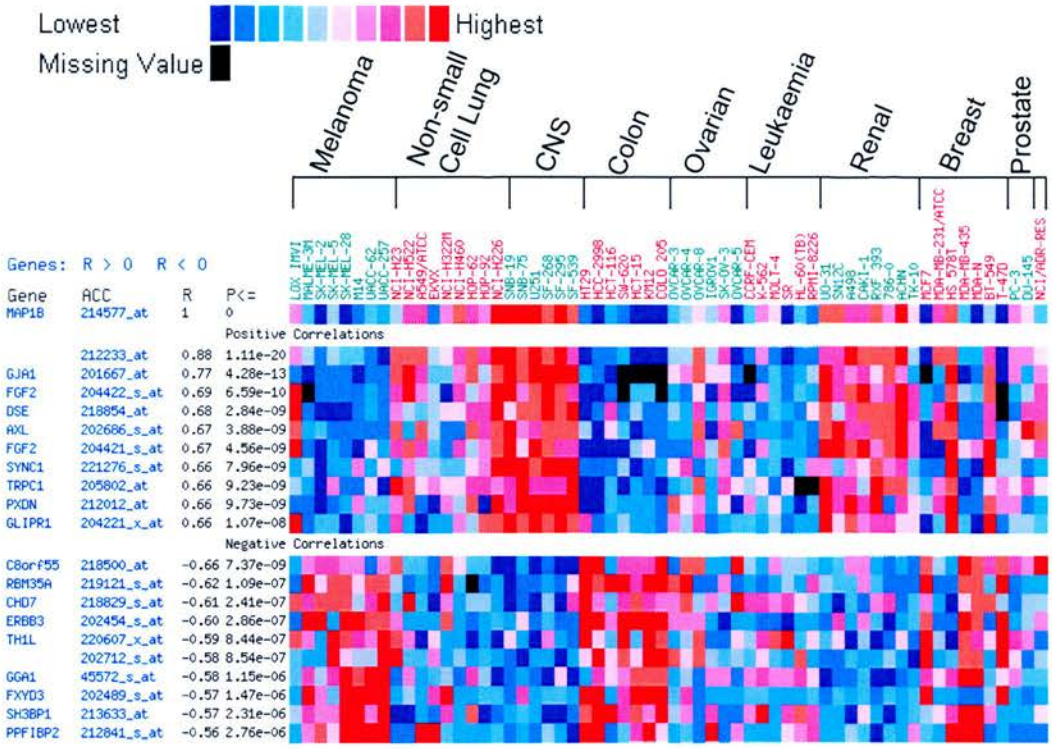

b - DAPK RNA Expression in the NCI60 Cancer Cell Lines as Determined by Microarray Analysis

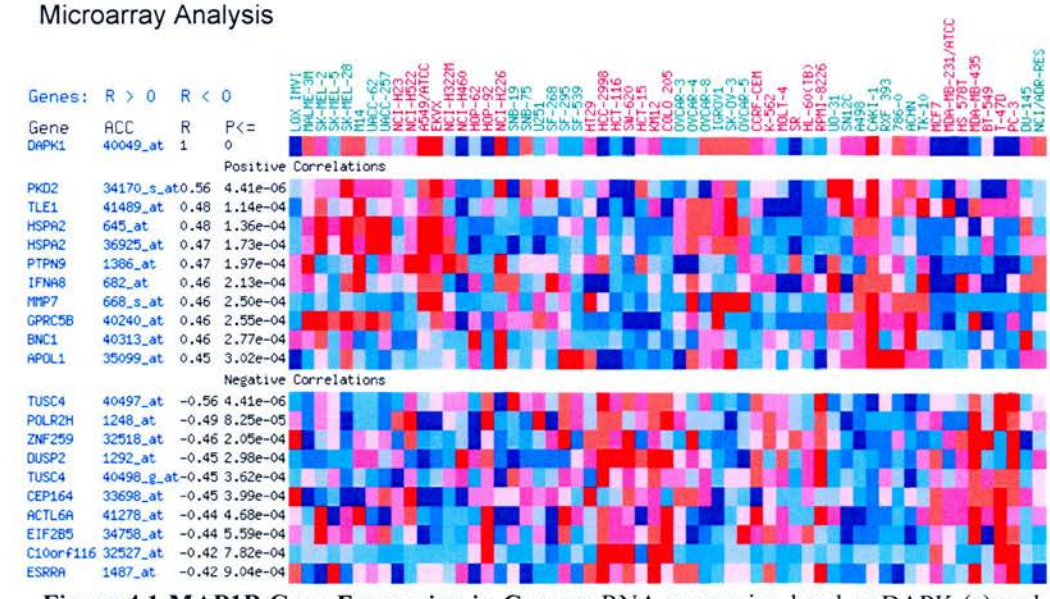

Figure 4.1 MAP1B Gene Expression in Cancer. RNA expression level or DAPK (a) and MAP1B (b) as determined by microarray analysis of the NCI60 cell lines. High expression is represented as red colour through to low expression as blue. Genes with similar expression patterns are listed as positive correlations, and genes with opposing patterns as negative correlations. Data were obtained from the Cancer Genome Anatomy Project (http://cgap.nci.nih.gov/).

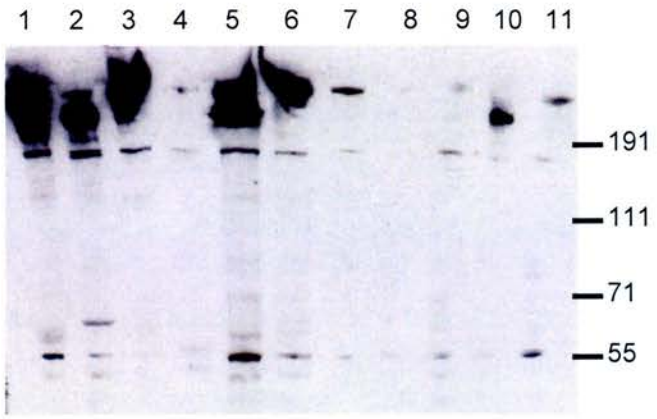

1	Rat Embryonic Whole-Brain Lysate (S3 Fraction)
2	A549 – Human Lung Carcinoma
3	A375 – Human Malignant Melanoma
4	HCT116 – Human Colon Carcinoma
5	PC12 – Rat Pheochromocytoma
6	HEK293 – Human Embryonic Kidney
7	LNCaP – Human Prostate Carcinoma
8	MCF7 – Human Breast Epithelial Adenocarcinoma
9	H1299 – Human Non-Small Cell Lung Cancer
10	Human Normal Foreskin Fibroblast
11	SKNAS – Human Neuroblastoma

Figure 4.2 MAP1B Protein is Expressed in Cell Lines. Cells lines were grown to 80% confluency, scraped and lysed with denaturing RIPA lysis buffer. Proteins from 30µg of each sample were separated by SDS-PAGE in 4-12% gradient gels before transfer onto a nitrocellulose membrane. Mouse monoclonal anti-MAP1B antibody AA6, a highly specific antibody that recognises all forms of MAP1B was used to probe the membrane.

a Development of a Cell Growth Assay to Measure DAPK Activity

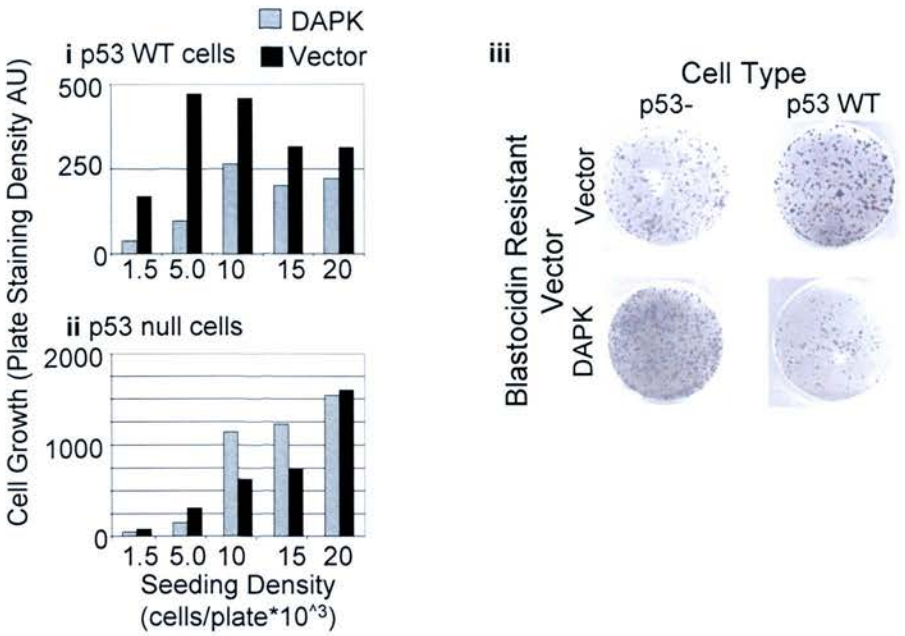

b Cell growth assay optimisation using MAP1B and DAPK co-transfection

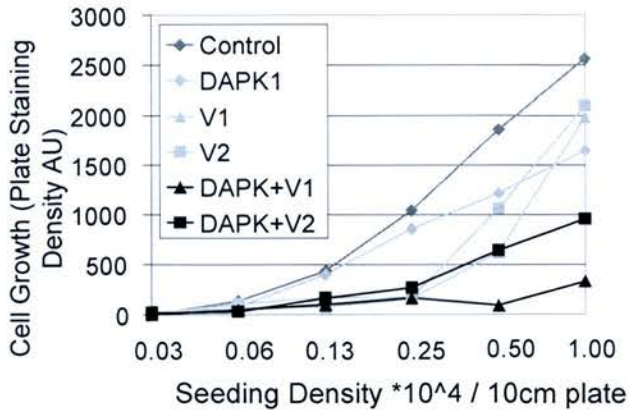

Figure 4.3 Development of a Cell Growth Assay to Quantify DAPK and MAP1B Function. **(a)** HCT116 Cells **(i)** or the p53-null derivative **(ii)** were co-transfected with vector control or DAPK expression plasmids conferring resistance to blastocidin as indicated. 48 hours later, cells were trypsinised and plated at differing densities in media containing blastocidin. Cell growth was visualised by dye staining, photographed and quantified using densitometry. Graphs show plate staining as a function of seeding density after DAPK or empty vector expression plasmid transfection. **(iii)** Representative photographs showing the extent of cell growth 1 week after plating 10000 cells. **(b)** HCT116 cells were co-transfected with the indicated blastocidin resistance marker vectors for 48 hours. Cells were then trypsinised and plated at differing densities in media containing blastocidin. Cell growth was visualized by dye staining and quantified using densitometry. Plotted data is cell growth as a function of cell density after MAP1B-V1 or MAP1B-V2 and DAPK or empty vector co-transfection.

Figure 4.4 a Domains of MAP1B that Cooperate with DAPK

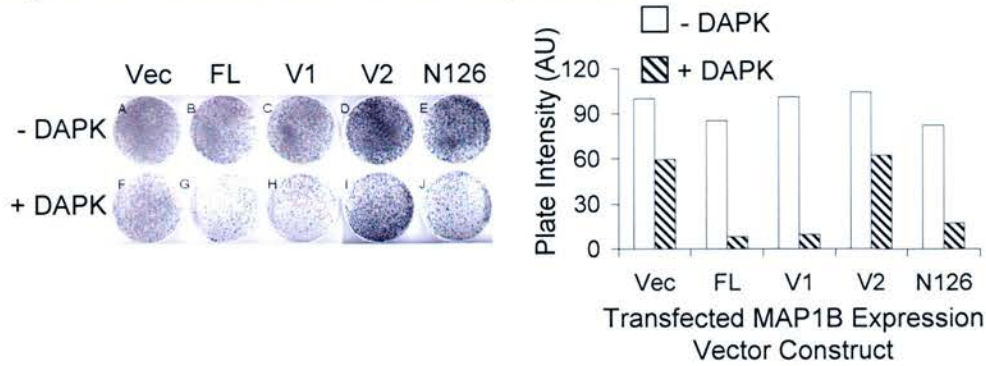

b Domains of DAPK that Cooperate with MAP1B

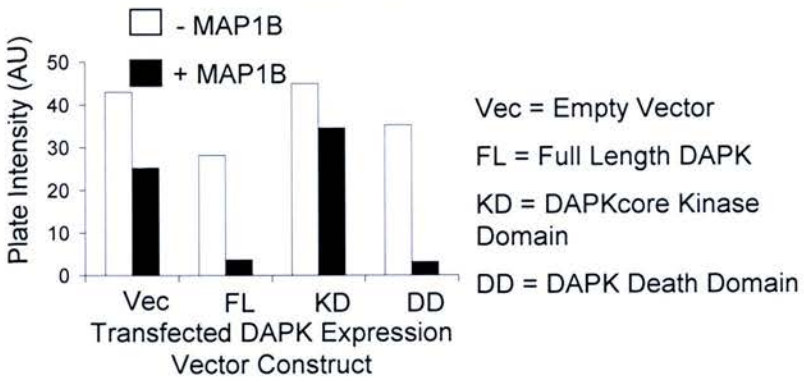

c Effect of DAPK Kinase Activity on Cell Growth Co-repression

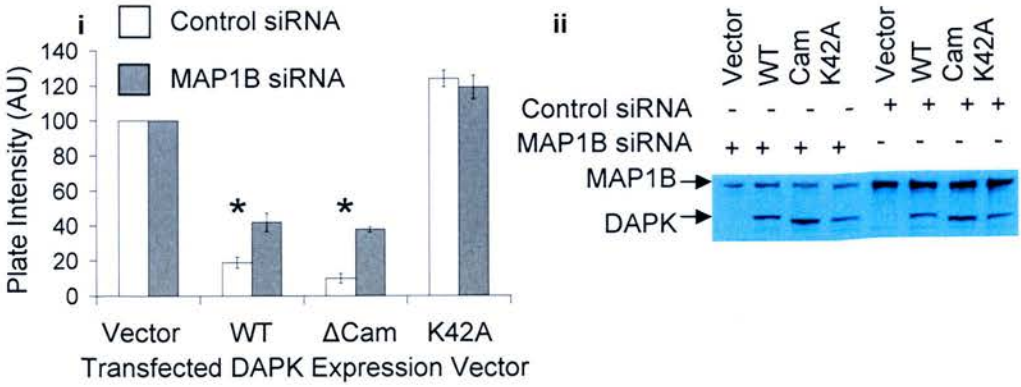

d Effect of Transfected DAPK Kinase Activity on Cell Viability

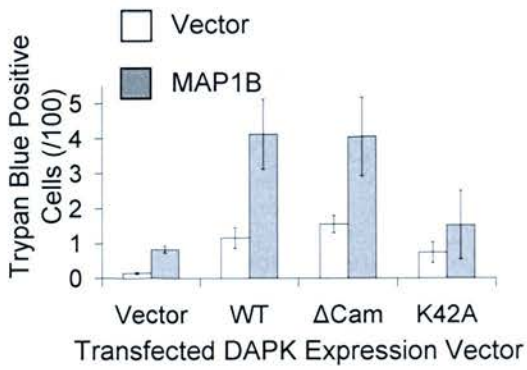

Figure 4.4 Characterisation of the DAPK:MAP1B Interaction Using the Optimised Cell Growth Assay. Cells were co-transfected with expression vectors conferring antibody resistance markers. 48 hours later after trypsinisation, 10000 cells were plated in media containing the selective antibiotic. Cell growth was visualized by Giemsa dye staining and quantified using densitometry. Plotted data are relative plate densities as a function of co-transfected expression vectors. **(a)** The indicated MAP1B constructs (full length MAP1B (FL), V1, V2, or N126) and/or DAPK were co-transfected in HCT116 cells before selection of transfected cells using blastocidin. Photograph shows extent of cell growth after 1 week. **(b)** DAPK constructs and/or full length MAP1B were co transfected in HCT116 cells before selecting co-transfected cells using blastocidin. **(c)** A375 cells were transfected with MAP1B siRNA for 48 hours before a further transfection with the indicated expression vectors for 24 hours. **i** Cells were then trypsinised and 10000 cells plated in media containing geneticin. Graph shows mean extent of cell growth as a function of co-transfected expression plasmids (Vec = Empty Vector, WT = wild type, ΔCam =Calmodulin domain deleted, K42A = Kinase dead). Error bars are standard deviation. * = significant difference as determined by students t-test. **ii** Western blot showing effect of MAP1B siRNA in this experiment. **(d)** 24 hours after transfection, adherent cells were by suspended by trypsin digestion and pooled with floating cells from the growth medium. Suspended cultures were then stained with trypan blue to visualise non-viable cells. Graph shows mean non viable cells as a function of transfected HA-DAPK expression vectors (error bars show standard deviation of data from 3 counts).

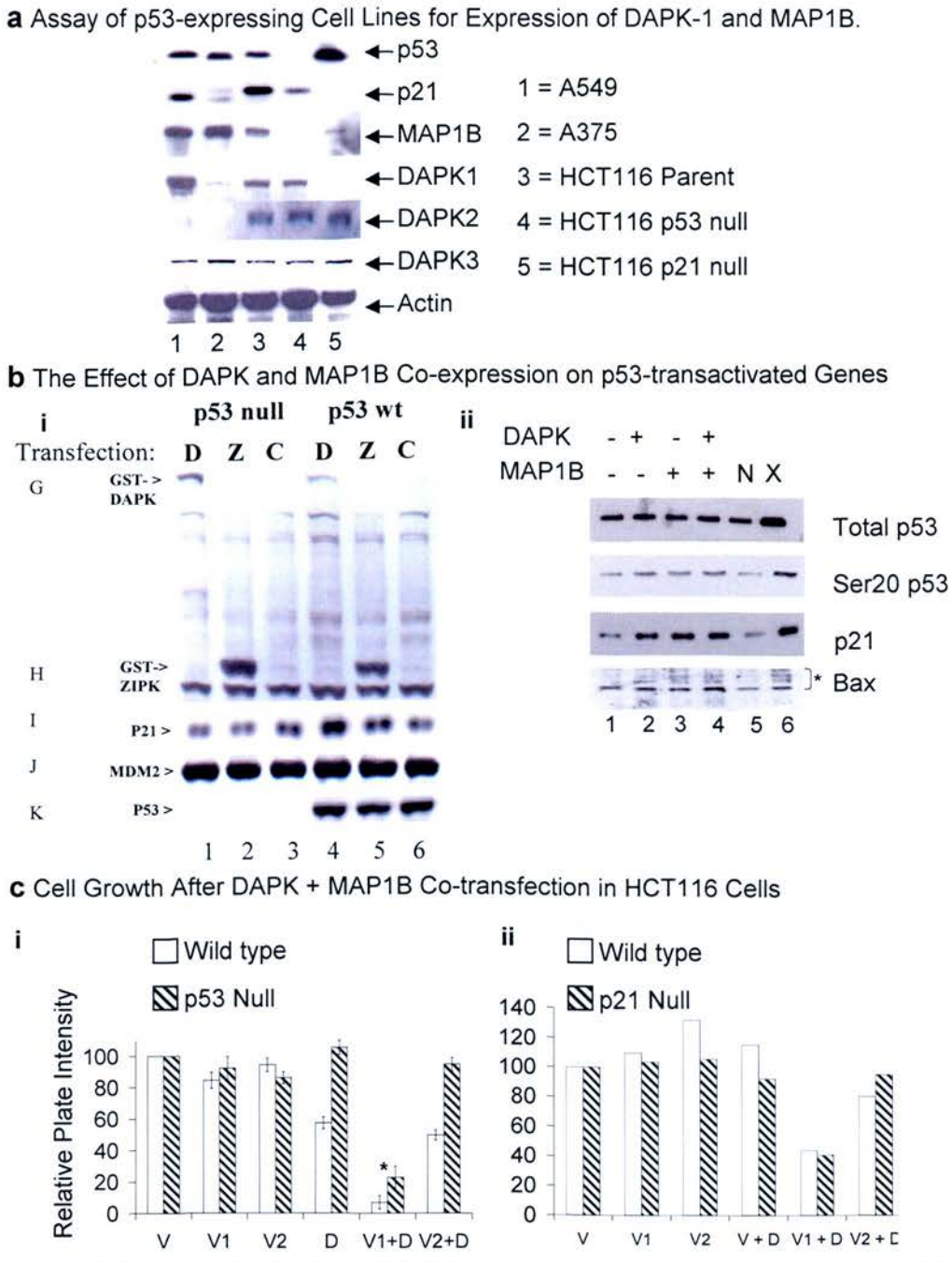

Figure 4.5 Effects of DAPK and MAP1B Co-expression on the p53 Pathway. (a) Cell lines that express wild type p53 were grown to 80% confluency, lysed and assayed for protein expression using antibodies to p53, p21, MAP1B, DAPK1, DAPK2, and DAPK3 as indicated. **(b) i** HCT116 parent type (lanes 4-6) and p53 null (lanes 1-3) cells were transfected with GST-DAPK1 (lanes 1 and 4), GST-DAPK3 (lanes 2 and 5) or GST (lanes 3 and 6). Lysates were assayed for expression of GST tag, p53 and the p53-transactivated proteins p21 and MDM2. **ii** HCT116 parent type cells were co-transfected with vector (lane 1), DAPK1 (lane 2), MAP1B (lane 3), DAPK1 + MAP1B (lane 4), left untreated (lane 5) or treated with X-rays (8 Gy, lane 6) and harvested for immunoblotting to detect: p53 protein; Ser20-phospho-p53 protein; p21 protein, or Bax adducts (as indicated). **(c)** Cells were co-transfected with blastocidin-resistant vector, vector control (V), MAP1B variants (V1 or V2), DAPK1 (D), as indicated) and 48 hours later, were trypsinized and plated in media containing blastocidin. Cell growth was visualized by dye staining and quantified using densitometry. Cell growth of HCT parent cells was compared to p53 null **(i)** or p21 null **(ii)** derivatives.

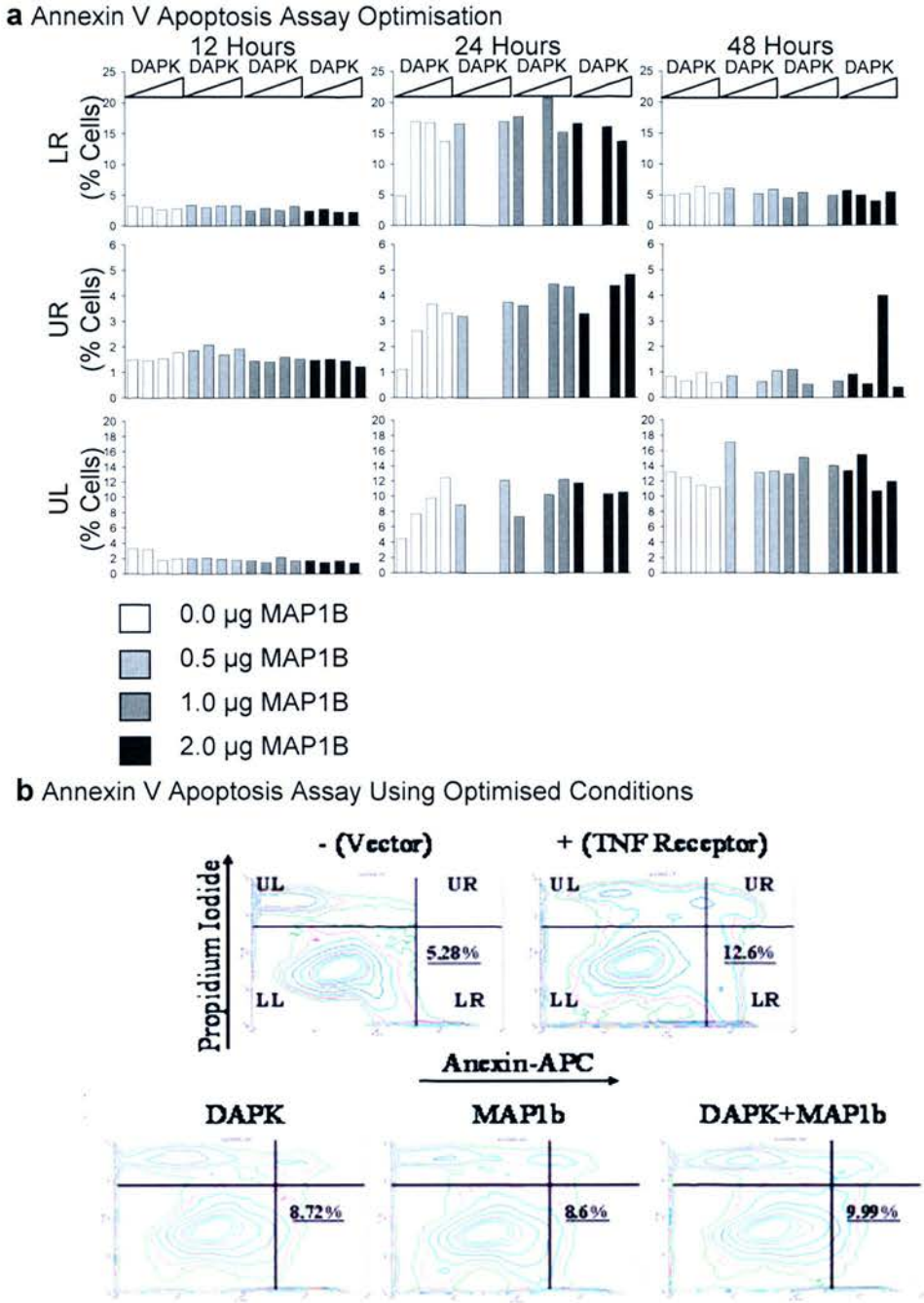

Figure 4.6 Optimisation of an Annexin V Apoptosis Assay Using Fluorescent Activated Cell Sorting (FACS) Analysis. (a) HCT116 cells were co-transfected with MAP1B and DAPK titrations of 0, 0.5, 1.0 and 2.0µg of expression plasmid DNA for the indicated times. After transfection, cells were suspended, washed and co-stained for external cell membrane phosphatidylserine using APC-conjugated AnnexinV. The membrane integrity of cells was determined by co-staining with propidium iodide. Using FACS, cells were assayed for APC fluorescence on the ordinate and for propidium iodide flourescence on the abscissa. Cells were separated into four populations: 1 negative staining viable non-apoptotic cells (lower left quadrant LL), 2 annexinV positive apoptotic cells (lower right quadrent LR), 3 annexinV + propidium iodide positive late apoptotic cells (upper right quadrant UR) and 4 propidium iodide positive non-viable cells (upper left quadrant UL). Blank spaces are missing data points. **(b)** HCT116 cells were co-transfected with 200ng of the indicated expression plasmids for 24 hours and assayed for early apoptotic cells (LR quadrants). A tumour necrosis factor receptor (TNFR) expression plasmid was used as a positive control.

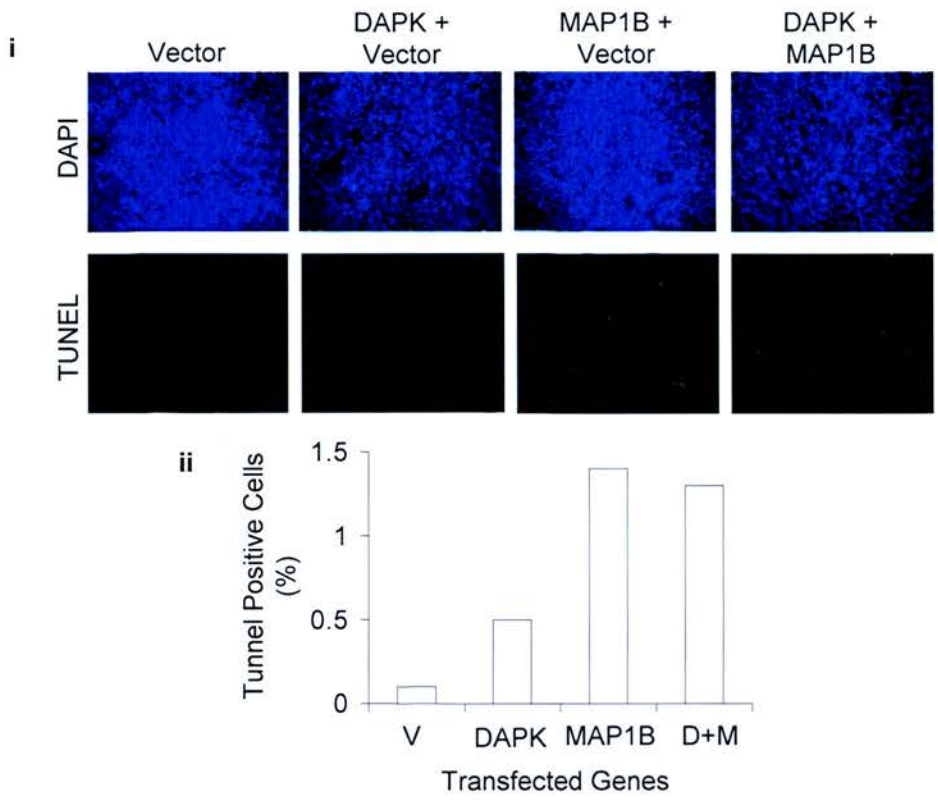

Figure 4.7 Quantitation of Late Stage Apoptosis Induced by DAPK and MAP1B Co-Expression Using the TUNEL assay. HCT116 cells were grown on cover slips and co-transfected with 300ng of the indicated expression plasmids for 32 hours before fixing and staining. **i** Green fluorescent TUNEL staining was observed by fluorescent microscopy using the 10X objective and quantified by image analysis. The total cell population was visualised using DAPI nuclear counterstaining. **ii** % cells positive for TUNEL staining.

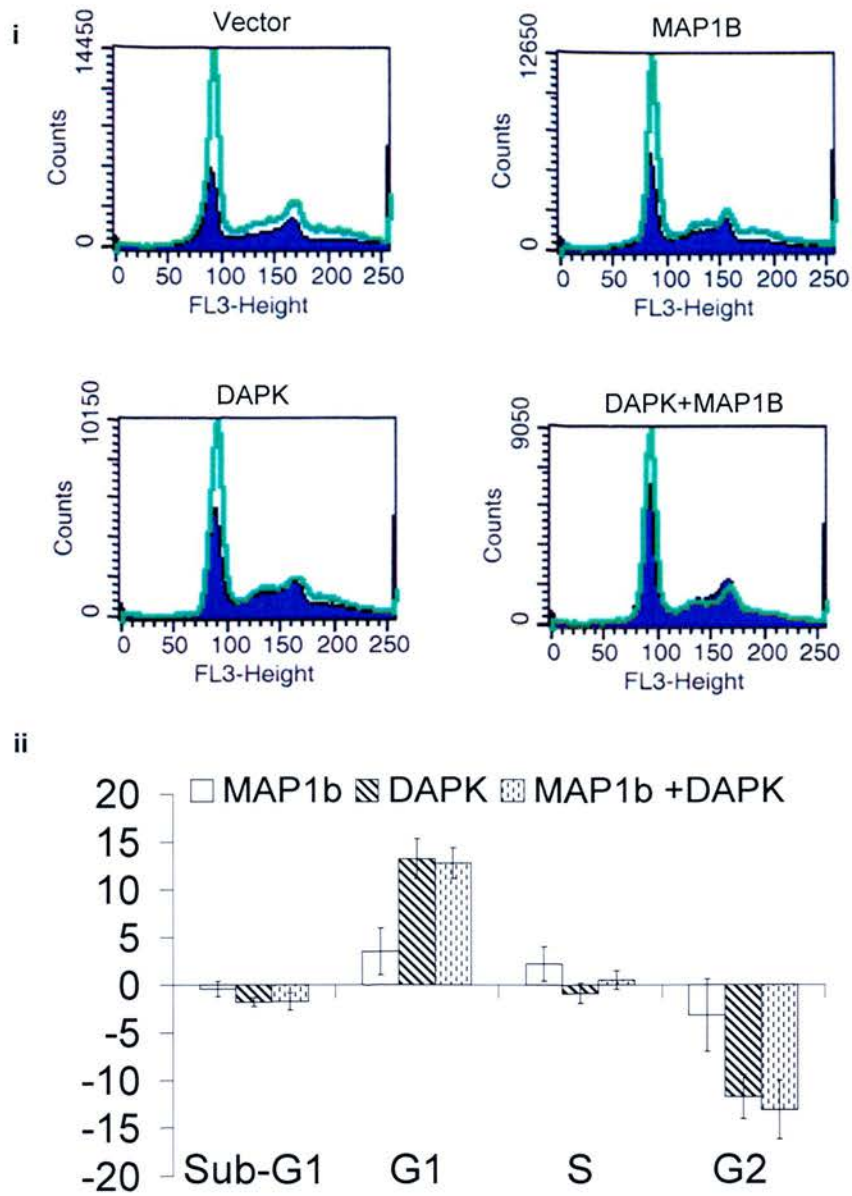

Figure 4.8 The Effect of DAPK and MAP1B Co-transfection on Cell Cycle Distribution as Determined by FACS Analysis. HCT116 cells were co-transfected with 500ng of the indicated expression plasmids and GFP marker for 24 hours before fixing with 70% ethanol overnight. Cell nuclei were stained with propidium iodide. Transfected cells were gated by GFP marker fluorescence before sorting according to size as determined by propidium iodide fluorescence. **i** Representative cell cycle profiles of GFP positive cells (shaded blue). Green line is profile of total cells (not to scale). **ii** Mean percentage change in cell cycle parameters as compared to vector control. Data are means of 4 independent experiments (error bars show standard deviation).

Figure 4.9 a Optimisation of the LC3 Foci Assay

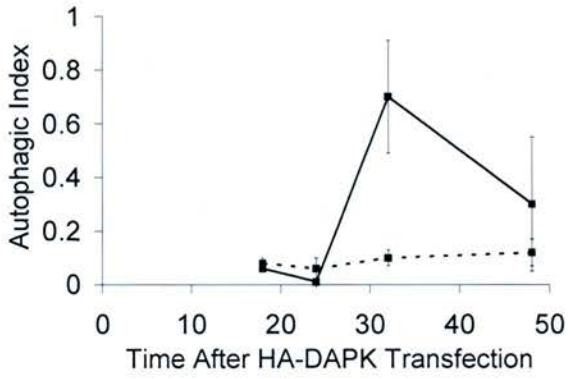

b The Effect MAP1B Knockdown on DAPK-Induced LC3 Foci Formation

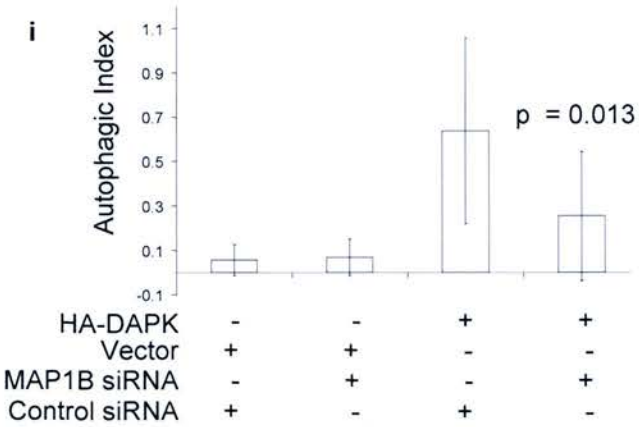

Figure 4.9 b ii

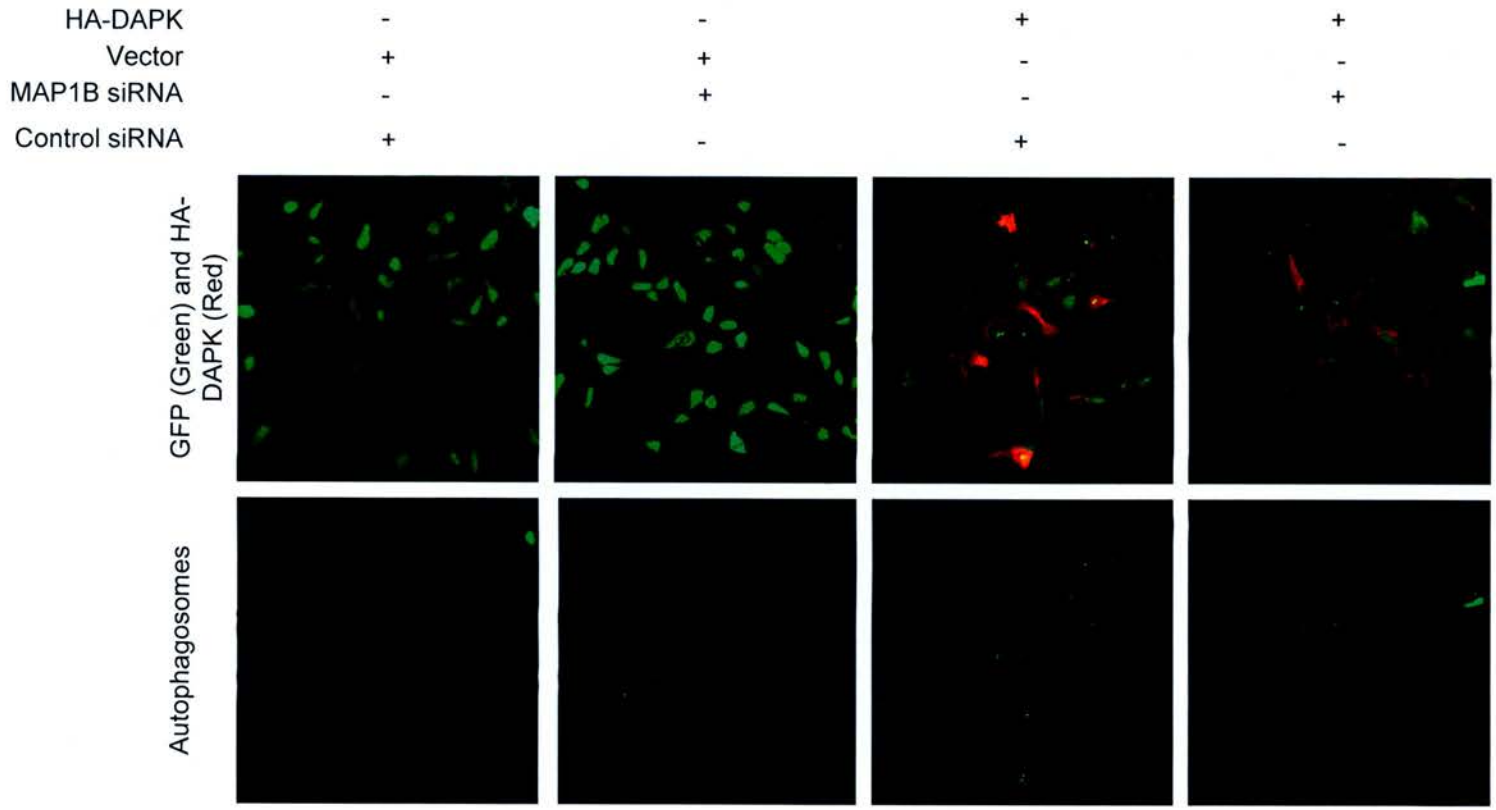

Figure 4.9 Attenuation of DAPK-Induced GFP-LC3 Foci Formation by MAP1B Depletion. HEK293 cells that that stably express the GFP-LC3 autophagy biomarker (35) were transfected with the indicated expression vectors. Cultures were fixed and stained for transfected gene in the red channel before examination by confocal microscopy using a X63 objective. GFP-LC3 decorated autophagosomes were visualised by elevating the fluorescent threshold in the green channel thereby producing saturated foci. The autophagic index was calculated as the mean LC3-foci per field / total number of cells per field. **(a)** Cultures were transfected with HA-DAPK for the indicated times before fixing, staining and GFP-foci counting. Data points are mean autophagic index calculated from 10 random fields. Error bars show standard deviation. **(b)** Cells were treated with MAP1B siRNA or control siRNA for 32 hours before HA-DAPK transfection for a further 32 hours. **i** Cells were immunostained for HA-DAPK (red) and GFP-LC3 (green). Bars show mean autophagic index from 10 random fields (error bars show standard deviation). Students T-test was used to calculate the significance of the difference between DAPK transfected cultures with and without MAP1B knock down ($p = 0.013$). **ii** Example fields showing GFP fluorescence and HA-DAPK staining (red). The GFP-LC3 foci from each field are shown in the bottom panels.

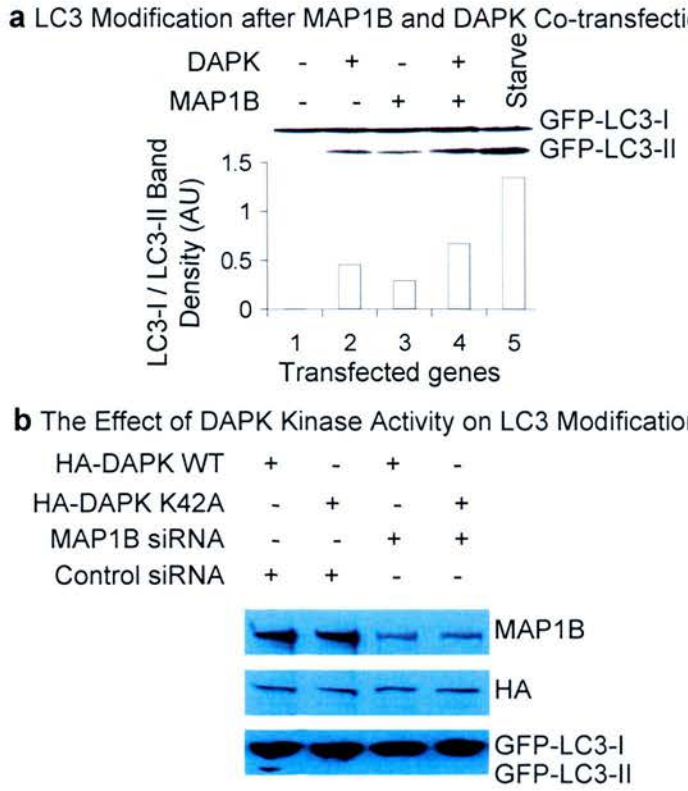

Figure 4.10 The Effect of MAP1B and DAPK on Autophagy as Determined by LC3 Cleavage. LC3 is post translationally cleaved and lipidated during formation of autophagic vesicles. LC3 cleavage is therefore a biomarker for the extent of autophagy within cells. **(a)** HEK293 cells stably expressing the GFP-LC3 marker were co-transfected with the indicated expression vectors. 32 hours later cells were harvested, lysed and assayed for LC3 protein modification using GFP antibody. The ratio of LC3 modification from GFP-LC3-I to GFP-LC3-II is plotted as a function of co-transfected genes. **(b)** The effect of DAPK kinase activity on GFP-LC3 modification was determined using kinase-activated (ΔCam) and -inactivated (K42A) constructs in A375 cells with or without endogenous MAP1B. Cells were treated with MAP1B siRNA for 32 hours before co-transfection with the indicated plasmids for a further 32 hours and assayed for GFP-LC3 modification using anti-GFP antibody.

a MAP1B and DAPK Cooperate to Induce Membrane Blebbing.

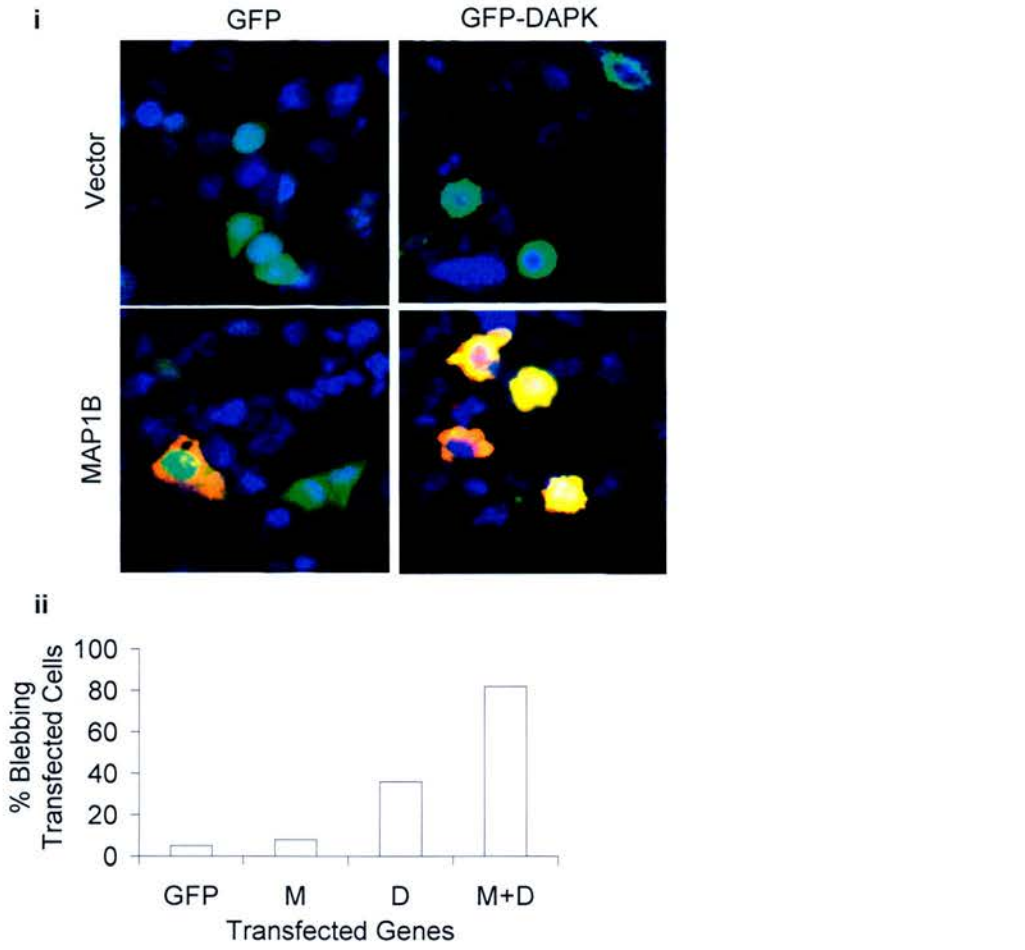

b Effect of Kinase Activity on DAPK and MAP1B Induced Membrane Blebbing

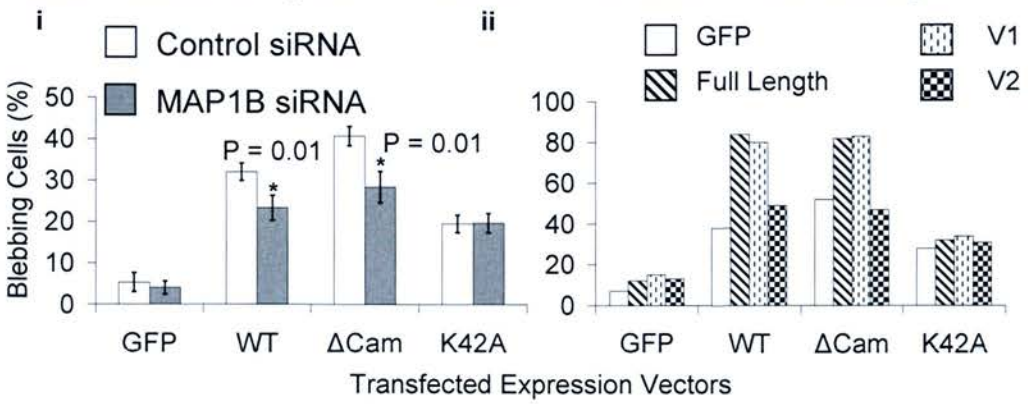

c Effect of p53 Status on DAPK and MAP1B Induced Membrane Blebbing

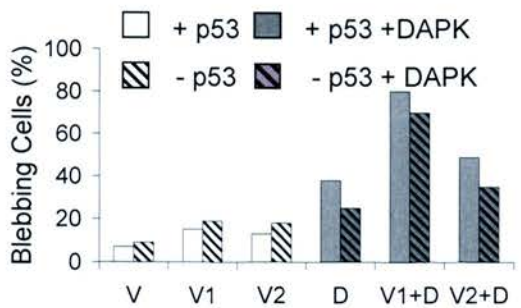

Figure 4.11 DAPK Mediated Cell Membrane Blebbing is Stimulated by MAP1B. (a) i HCT116 Cells were co-transfected with GFP vector and empty vector, GFP and MAP1B, GFP-DAPK and empty vector or GFP-DAPK and MAP1B as indicated on the four images. Transfected cells were visualised by flourescent microscopy and evaluated for membrane blebbing using a X100 objective as described previously (16). **ii** 200 co-transfected cells were scored for blebbing morphology along transverse sections of cover slips. Graph shows the mean percentage blebbing cells from 3 representative experiments (error bars show standard error). **(b)** Transfected cell populations were assessed for membrane blebbing morphology (as in a i). **i** A375 Cells were treated with MAP1B siRNA or siRNA control for 48 hours before transfection with the indicated HA-tagged DAPK genes (WT = wild type, ΔCam =Calmodulin domain deleted, K42A = Kinase dead). Transfected cells were stained using anti-HA antibody. Data are mean % blebbing cells from 3 independent cover slips. Error bars show standard deviation. * = p as determined by students T-test. **ii** HCT116 Cells were co-transfected with full-length native MAP1B, V5-tagged V1 or V2 constructs or GFP and HA-tagged full-length, ΔCAM or K42A DAPK constructs. Co-transfected cells were screened using the appropriate antibody stains. **(c)** HCT116 parent or p53 null cells were co-transfected with empty vector (V), V1 or V2 and empty vector or wild type DAPK (D) as indicated on the ordinate. Cultures were fixed and stained with anti V5 and anti DAPK antibody to visualise transfected cells. 200 co-transfected cells were scored for membrane blebbing morphology along transverse sections of cover slips. Bars are mean percentage blebbing cells.

Figure 4.12 a Effect 3-Methyladenine on HA-DAPK-Induced Membrane Blebbing

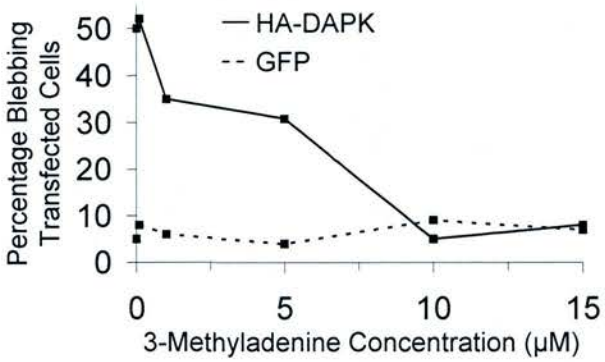

b Effect 3-Methyladenine on HA-DAPK and MAP1B Induced Membrane Blebbing

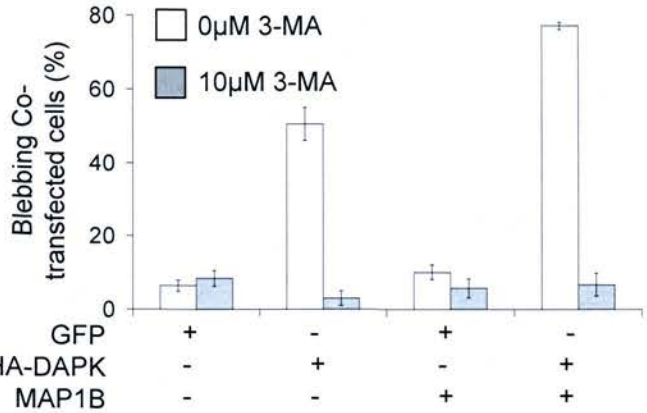

c Inhibition of Membrane Blebbing by Autophagy Inhibitors

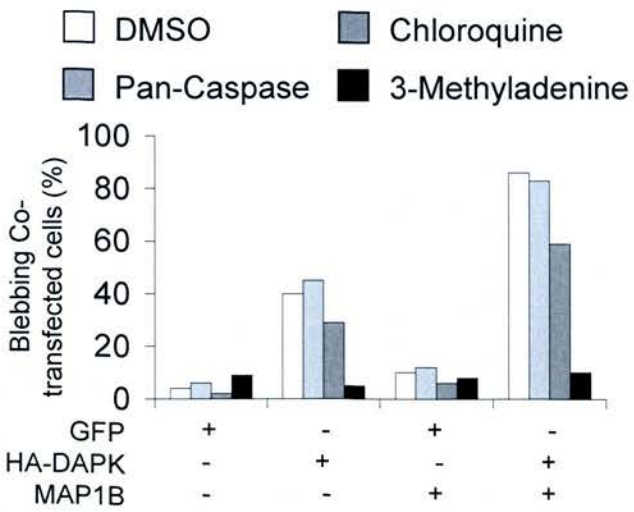

Figure 4.12 d 3-MA treated DAPK and MAP1B co-transfected cells

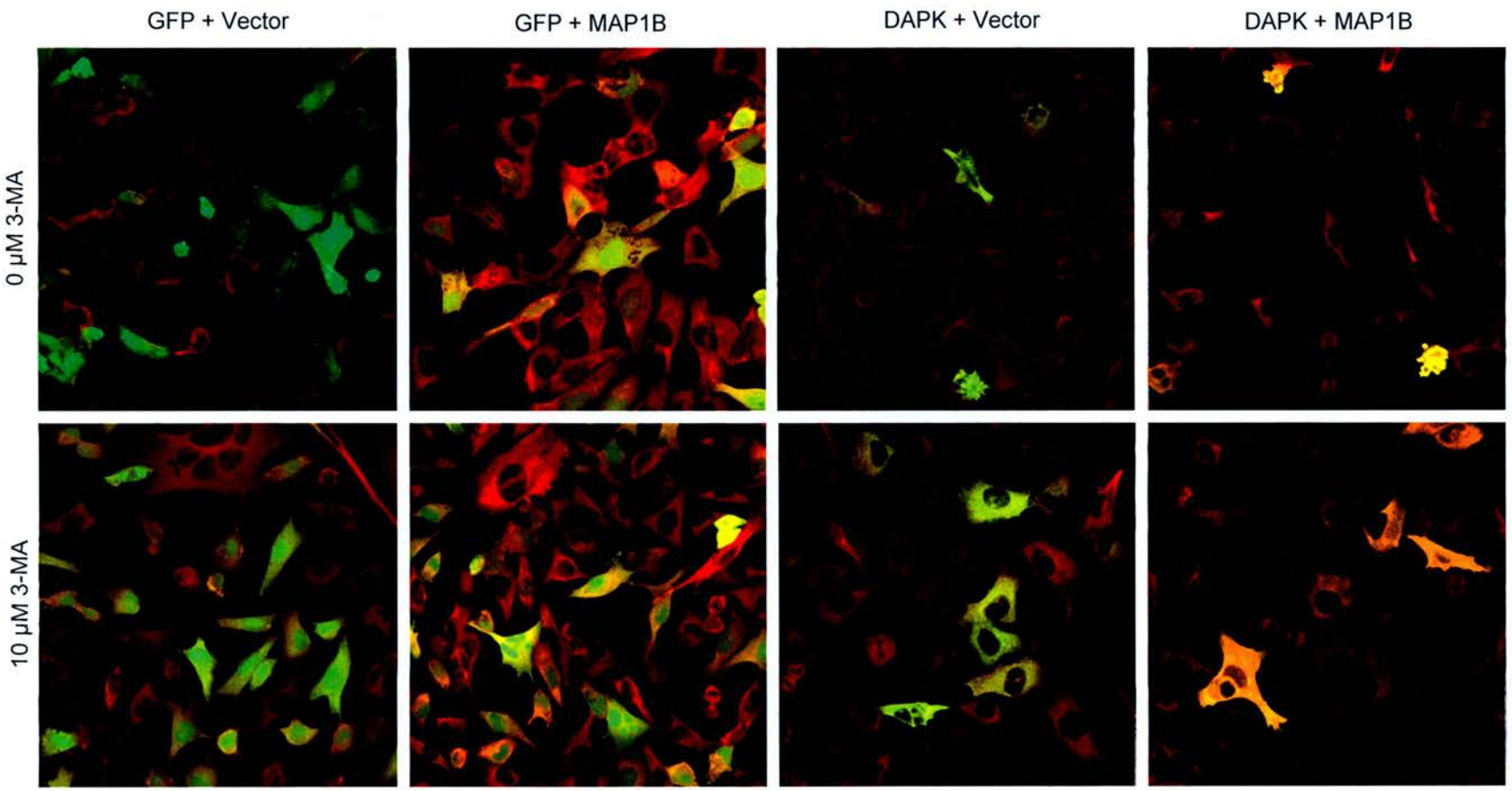

Figure 4.12 HA-DAPK and MAP1B Stimulated Membrane Blebbing is Blocked By Pharmacological Inhibition of Autophagy. (a) A375 cells were transfected with HA-DAPK for 18 hours before treatment with the indicated concentrations of the autophagy inhibitor 3-Methyladenine (3-MA). Cells were fixed and stained with anti-HA rat monoclonal antibody 2A10 and Alexa488 anti-mouse secondary antibody. Transfected cells were assessed for membrane blebbing by fluorescent microscopy using a X100 objective. 200 transfected cells were counted per data point. **(b)** Cultures were co-transfected with the indicated expression vectors for 18 hours before treatment with 10μM 3-MA for 6 hours. Cells were fixed and stained with anti-MAP1B MAb (AA6) and rat monoclonal anti-HA. Co-transfected cells were assessed for membrane blebbing as above. Data are the mean percentage transfected cells from 3 independent experiments. Error bars show standard deviation. **(c)** Cells were transfected with the indicated expression vectors before treatment with either 10 μM 3-MA, 20 μM chloroquine or 10 μM pan-caspase inhibitor as indicated for 6 hours. The percentage of membrane blebbing cells was calculated as above. **(d)** MAP1B and HA-DAPK was stained with antibody as above for imaging using a confocal microscope. Images are random fields from each treatment.

Figure 4.13 a GFP Transfected A375 Cell Morphology

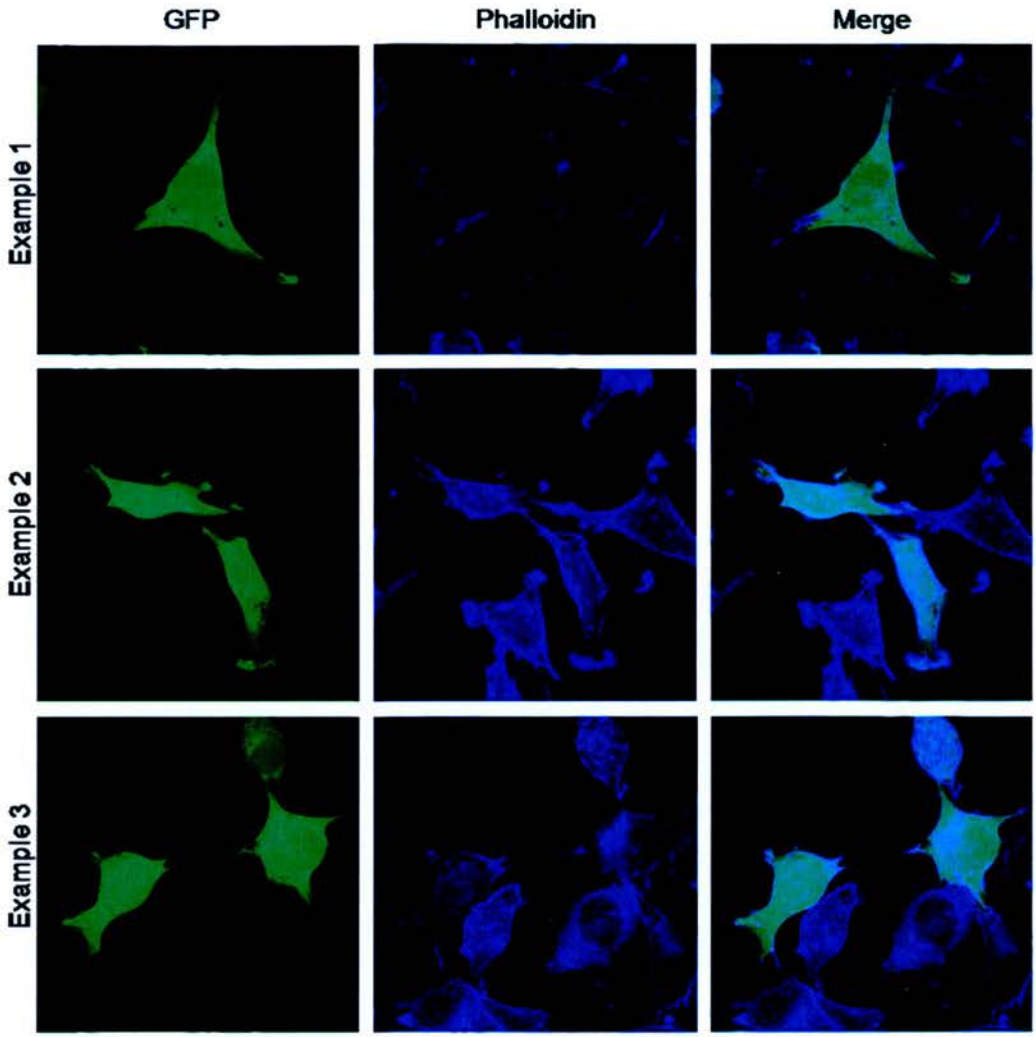

Figure 4.13 b HA-DAPK Transfected A375 Cells: Subpopulation 1

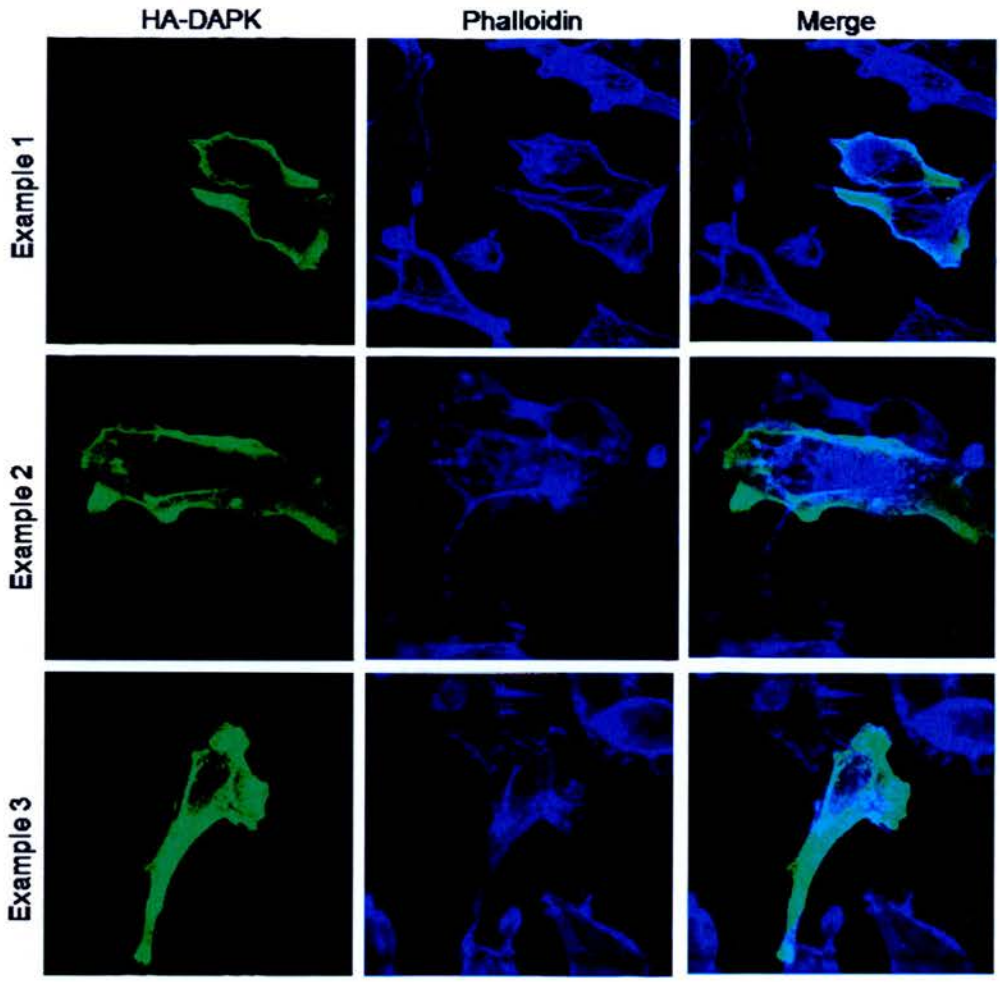

Figure 4.13 C HA-DAPK Transfected A375 Cells: Subpopulation 2

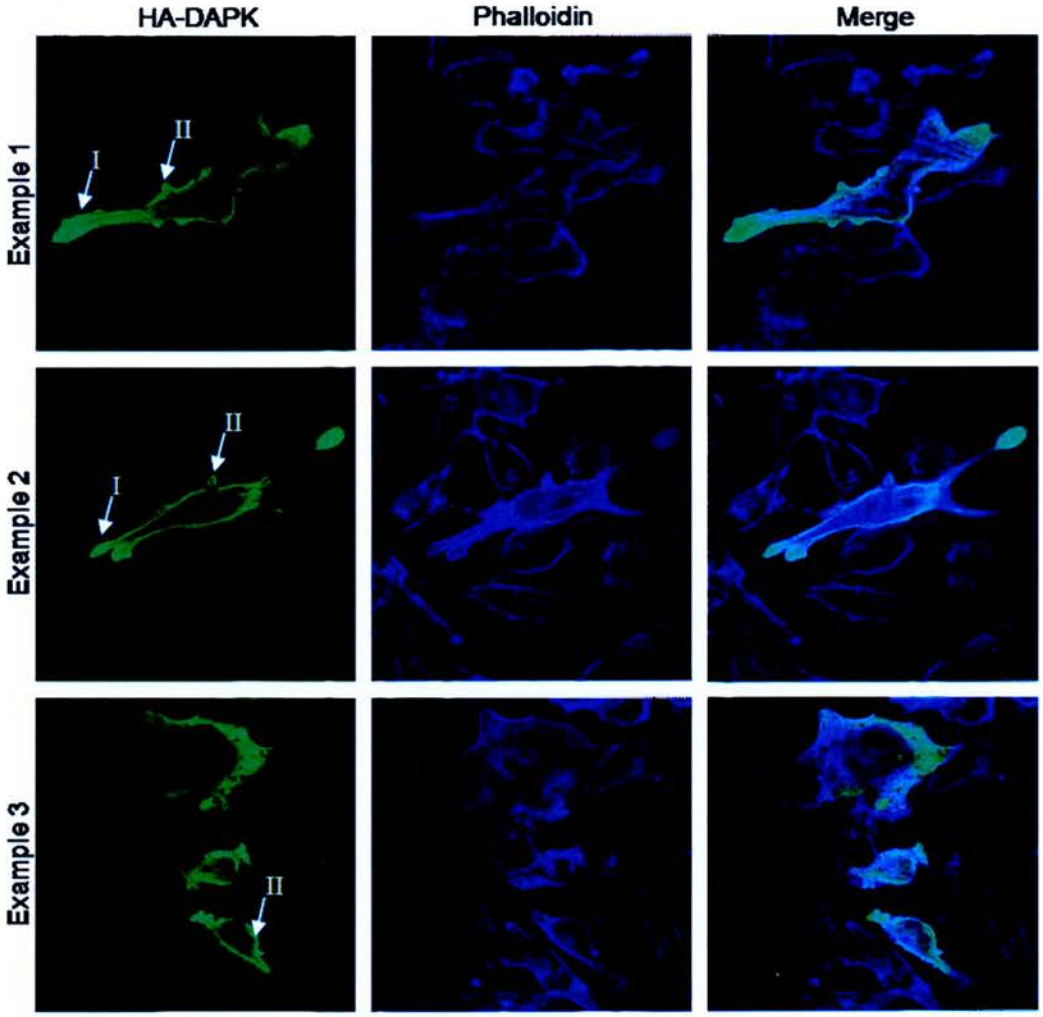

Figure 4.13 d HA-DAPK Transfected A375 Cells: Subpopulation 3

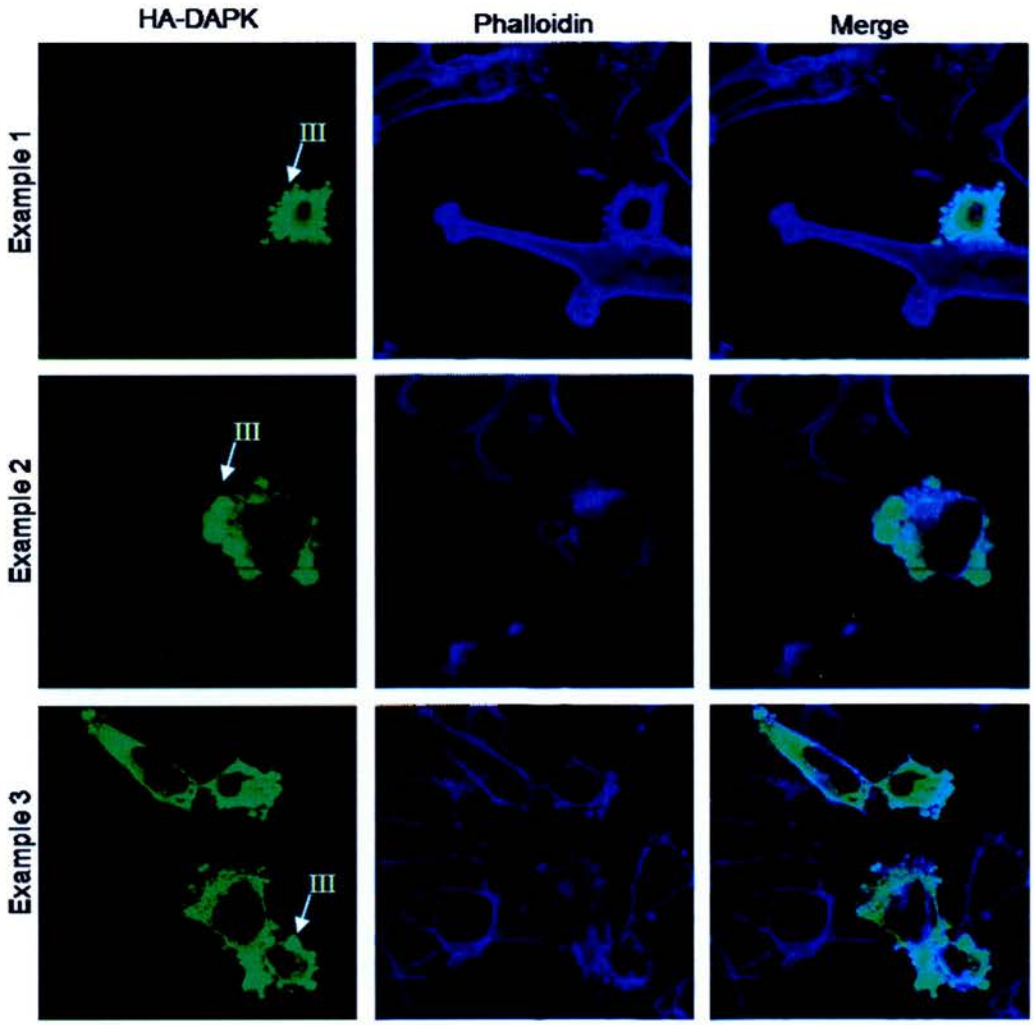

Figure 4.13 e – Time Course of Induced Morphological Changes

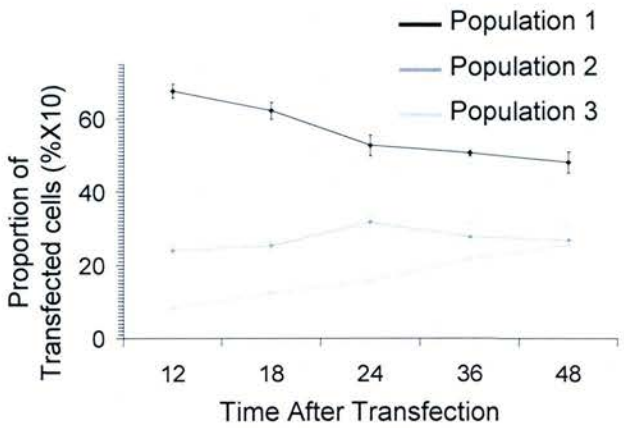

f – HA-DAPK Domains: Morphology Distribution After 24 Hours

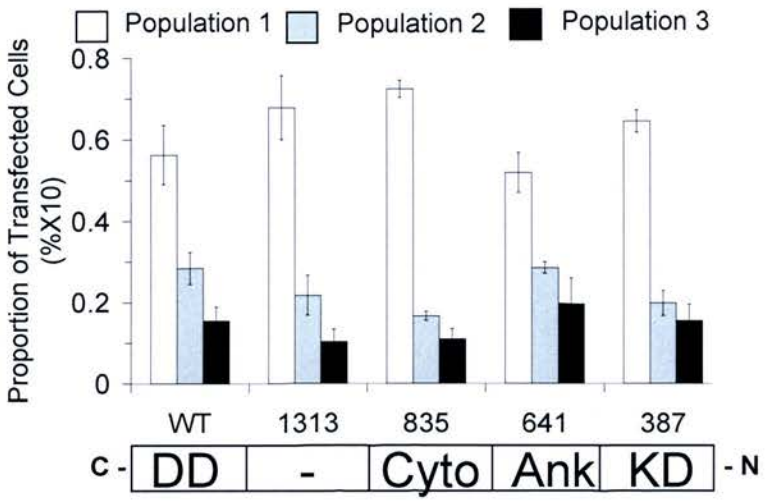

g – HA-DAPK Kinase Mutants: Morphology Distribution After 24 Hours

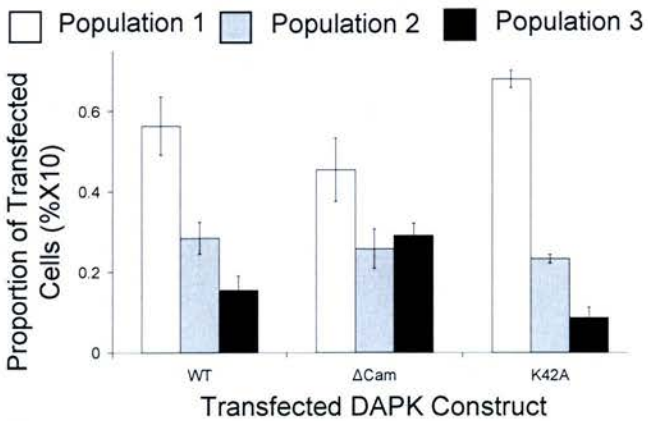

Figure 4.13 HA-DAPK Transfection-Induced Morphological Changes are Grouped into 3 Categories. A375 cells were transfected with GFP or HA-DAPK for 24 hours before fixing and stained with anti-HA rat monoclonal antibody 2A10 and Alexa488 anti-rat secondary antibody. F-actin was visualised using phalliodin counter-stain. Fluorescent micrographs were taken using a confocal microscope using a X100 objective. **(a)** GFP transfected cells had normal fibroblast-like morphology. **(b)** HA-DAPK transfected cells with no change in morphology were grouped into subpopulation 1. **(c)** Cells with, large extended processes **(I)** and/or small membrane blebs **(II)** were grouped into subpopulation 2. **(d)** Cells grouped into sub population 3 had multiple large membrane blebs **(III)**. **(e)** The mean percentage of cells in each subpopulation was determined from at least 3 independent transfected cultures fixed at the indicated times. Error bars show standard deviation. **(f)** The mean percentage of cells in each subpopulation was calculated from cultures transfected with HA-tagged wild type (WT), death domain deleted (amino acids 1-1313), linker region deleted (amino acids 1-835), cytoskeletal-binding domain deleted (amino acids 1-641) or kinase domain only (amino acids 1.387). **(g)** Mean percentage of cells in each subpopulation was calculated from cultures transfected with HA-tagged kinase wild type (WT), kinase activated (Cam), or Kinase inactivated (K42A) constructs.

Figure 4.14 a – Transfected HA-DAPK Association with Cortical Actin in Transfected Cell Subpopulation 2

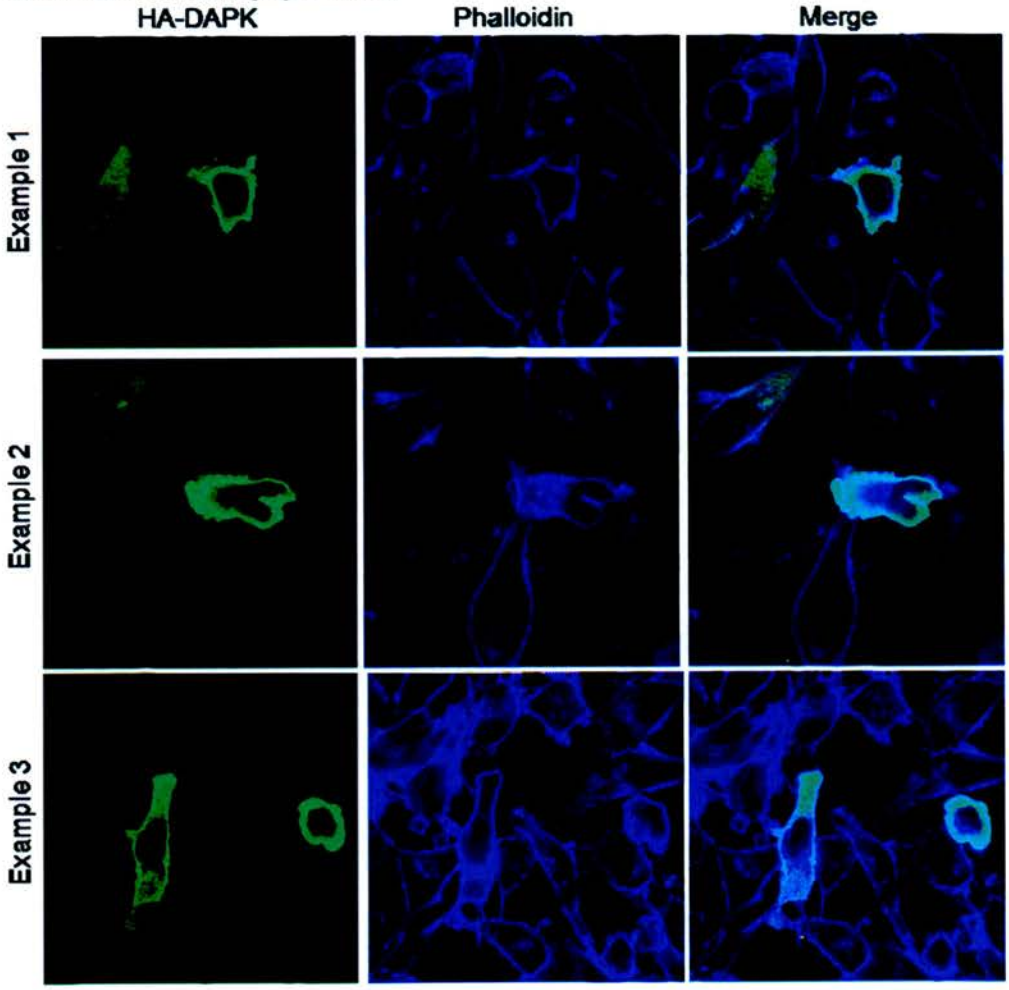

Figure 4.14 b – HA-DAPK Association with Cortical Actin in Cell Transfected Ell Subpopulation 2 – Nuclear stain

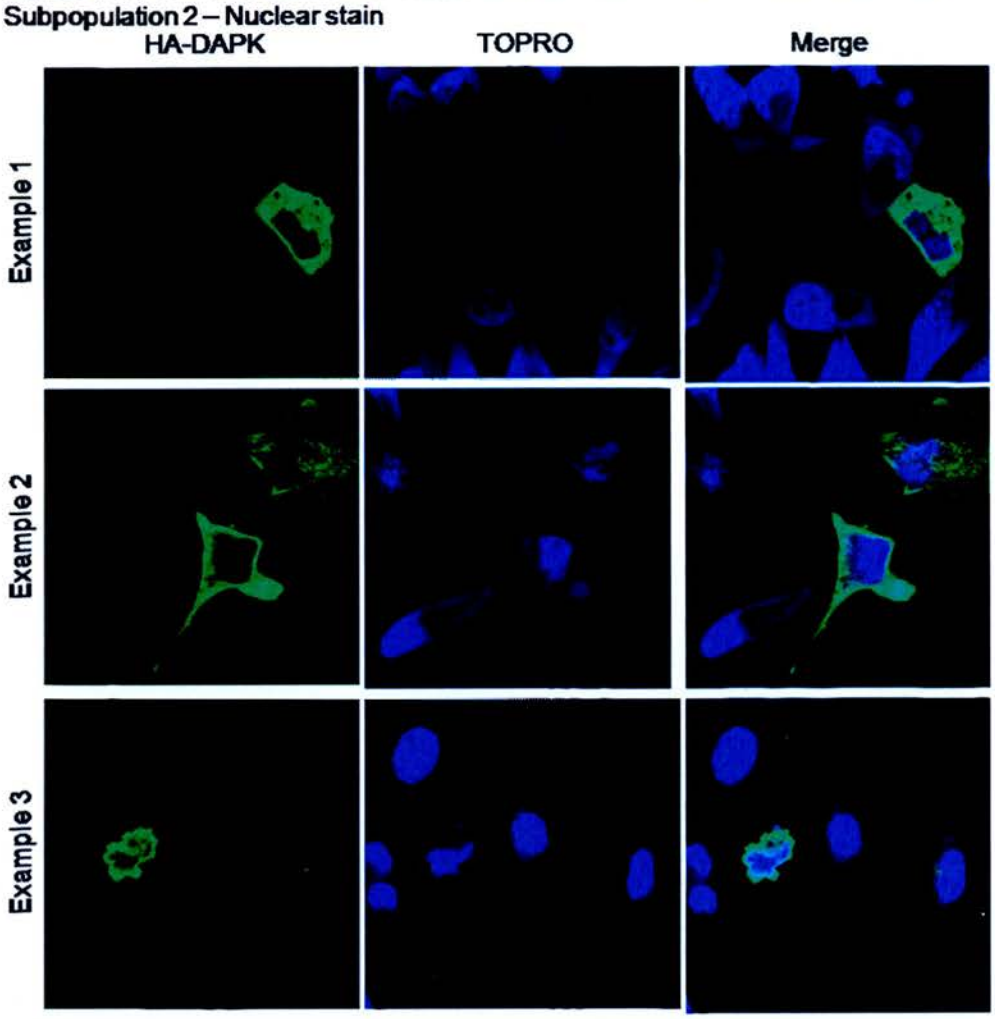

Figure 4.14 Transfected HA-DAPK Decorates Cortical F-actin Fibres. A375 cells were transfected with HA-DAPK for 24 hours before fixing and staining. Fluorescent micrographs were taken using a confocal microscope using a X100 objective. **(a)** Cortical F-actin was visualised using phalliodin counter-stain. 3 representative fields with subpopulation 2 cells are shown. **(b)** Cell nuclei were visualised using TOPRO nuclear stain. 3 representative fields with subpopulation 2 cells are shown.

Figure 4.15 a Endogenous MAP1B Location In HA-DAPK Transfected A375 Cells: Transfected Cell Subpopulation 2

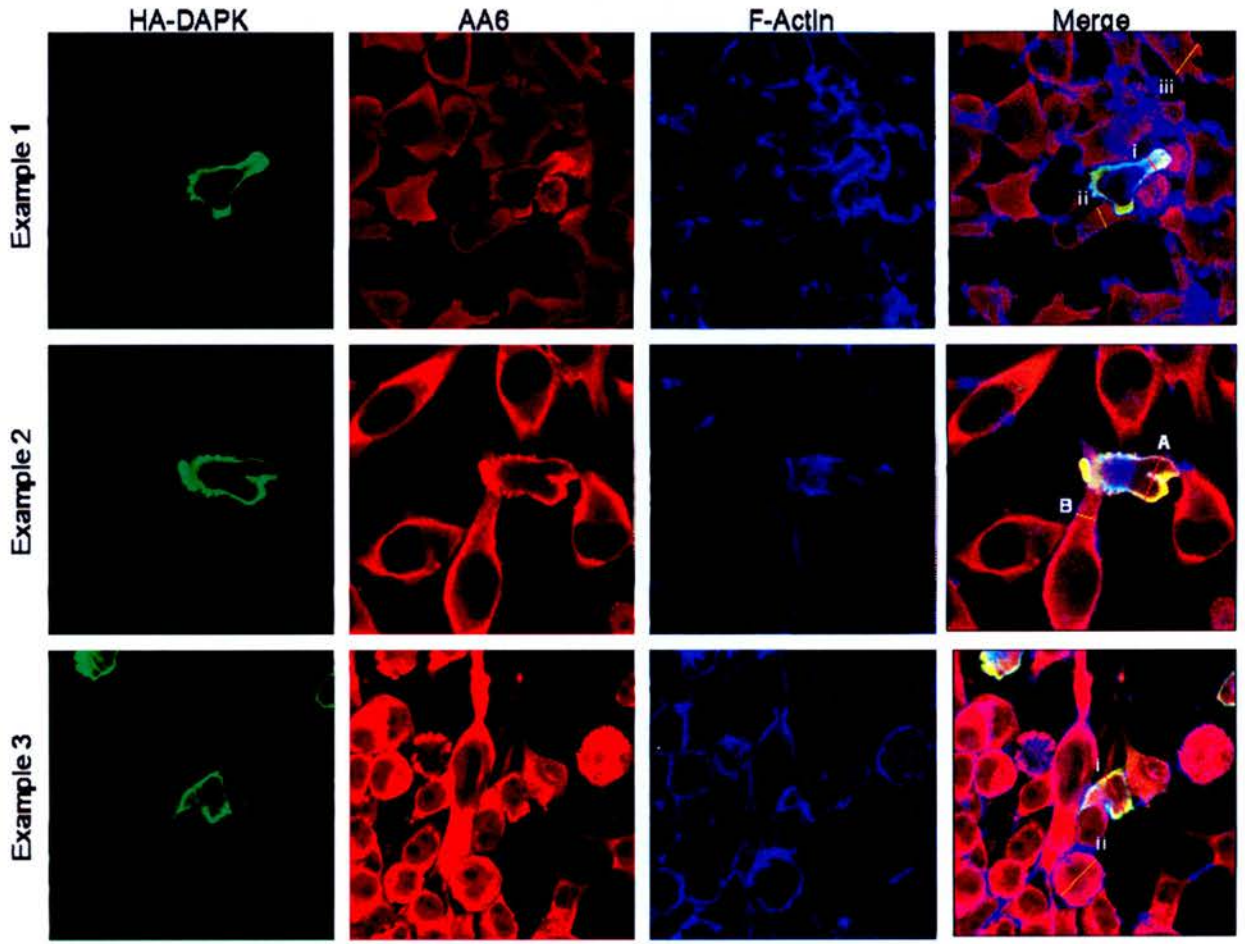

Figure 4.15 b – Fluorescence Intensity of Endogenous MAP1B and Transfected HA-DAPK Relative to Cortical F-actin in Subpopulation 2

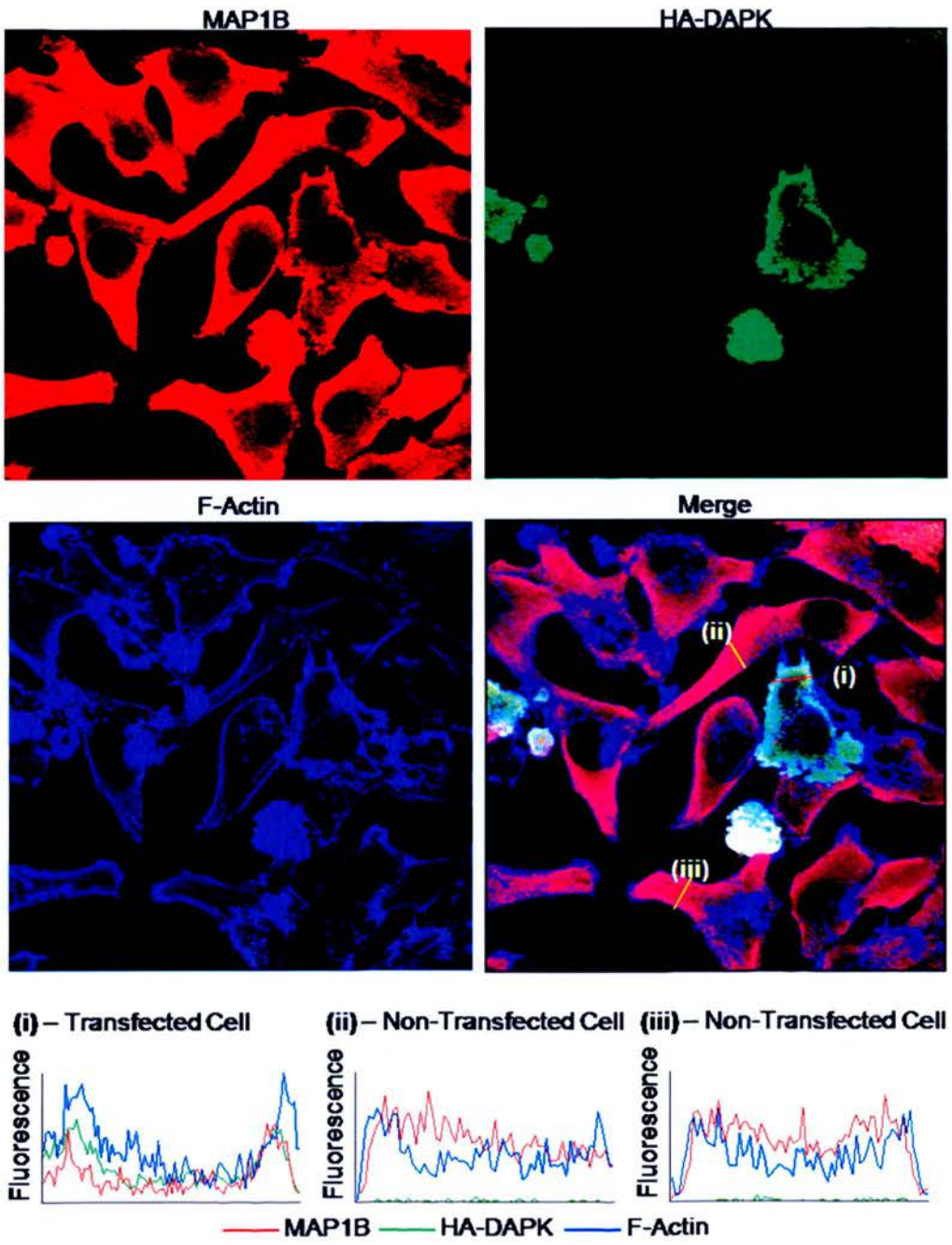

c – Quantification of Endogenous MAP1B Staining Intensity at Cortical F-actin in Cell Subpopulation 2

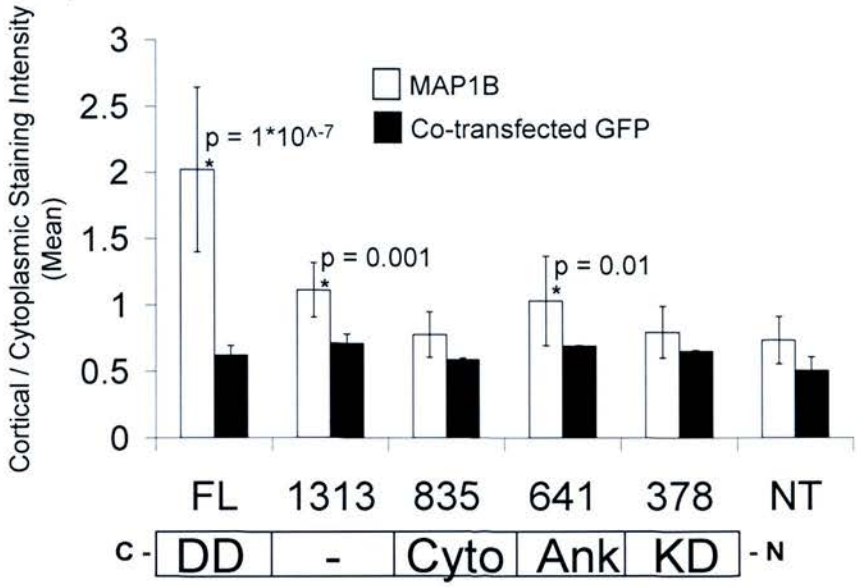

d – Quantification of Endogenous MAP1B and transfected HA-DAPK Staining Intensities at Cortical F-actin in Cell Subpopulation 2

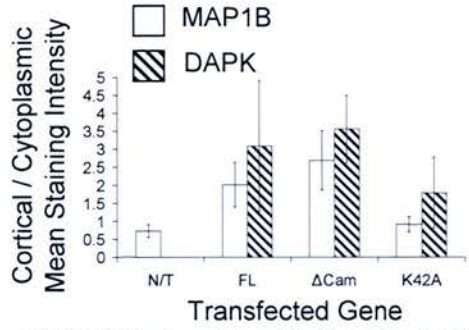

Figure 4.15 Endogenous MAP1B Co-locates with Transfected HA-DAPK at Cortical F-actin Fibres in Cells Grouped in Subpopulation 2. A375 cells were transfected with HA-DAPK for 24 hours before fixing and staining for HA, endogenous MAP1B (using MAb AA6) and F-actin using phalloidin. Cells were grouped into subpopulations as in Figure 4.13). Representative fields are shown with cells from subpopulation 1. Fluorescent micrographs were taken using a confocal microscope using a X100 objective. **(a)** Example of cells categorised in subpopulation 2. **(b)** Fluorescence histogram plots were used to quantify the staining intensity of HA, MAP1B and F-actin along transverse sections of transfected **(i)** and neighbouring non-transfected **(ii and iii)** cells. Figure shows a representative field with cell grouped into subpopulation 2. **(c)** Cultures were transfected with HA-tagged full length DAPK (FL), death domain deleted (amino acids 1-1313), linker region deleted (amino acids 1-835), cytoskeletal-binding domain deleted (amino acids 1-641), kinase domain only (amino acids 1.387) or vector control (NT). Separate control cultures were co-transfected with GFP before fixing and staining for HA-tag in the red channel. The average fluorescence intensity of MAP1B or GFP co-located with cortical F-actin was compared to the average fluorescence intensity of MAP1B or GFP in the cytoplasm to derive an average staining intensity ratio. Data are the average ratio from 3 experiments of 10 subpopulation 2 cells each. Error bars show standard deviation. The significance of the increase in ratio from vector only -transfected cells was calculated using students T-test (*). **(d)** The effect of DAPK kinase activity on cortical F-actin localisation was determined using DAPK kinase mutant constructs as indicated. Data are mean MAP1B or DAPK cortical to cytoplasmic ratios. Error bars show standard deviation.

Figure 4.16 a Co-Transfection of MAP1B and HA-DAPK A375 Cells: 10 Hours Post Transfection

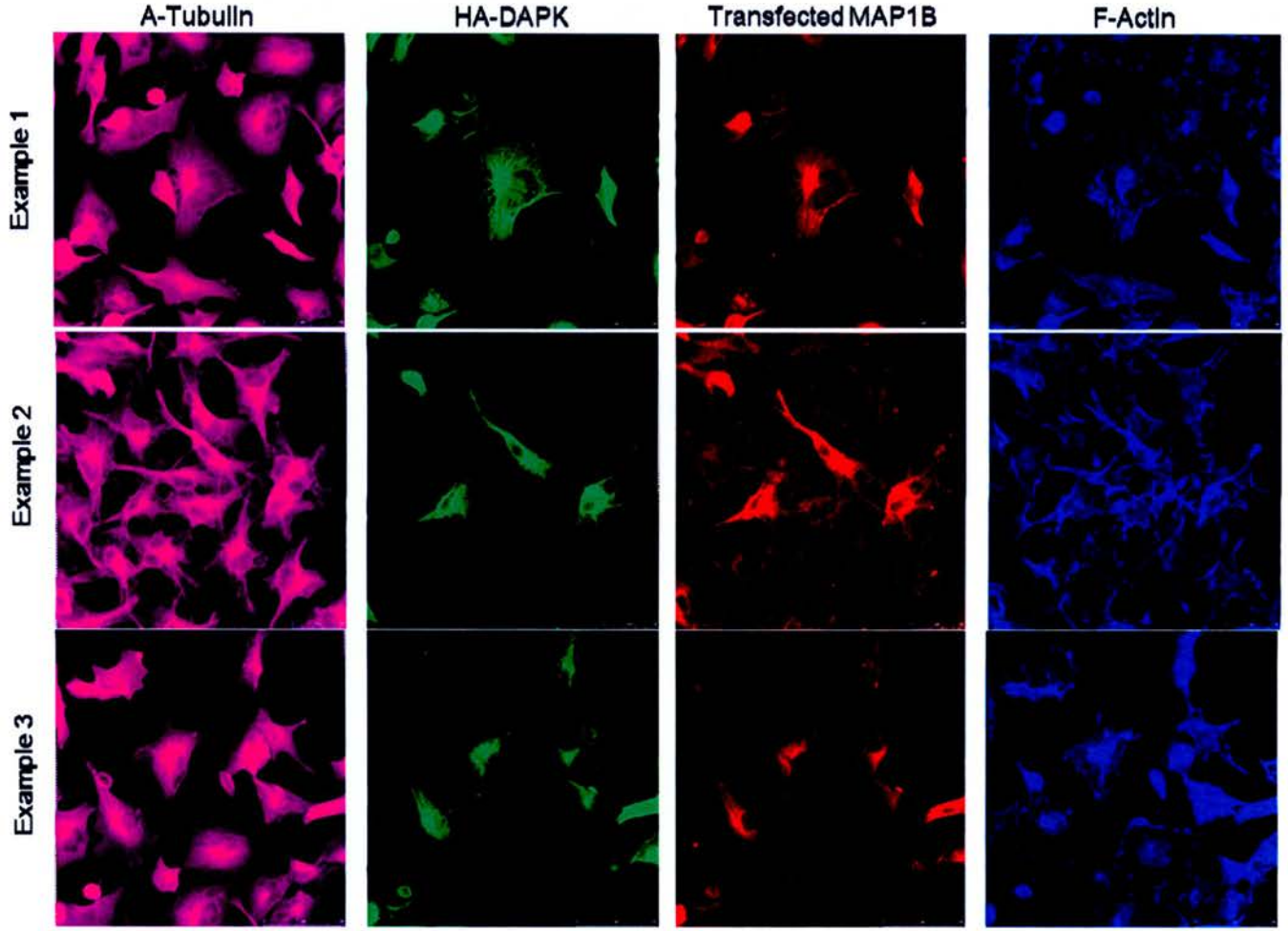

Figure 4.16 b Co-Transfection of MAP1B and HA-DAPK A375 Cells: 18 Hours Post Transfection

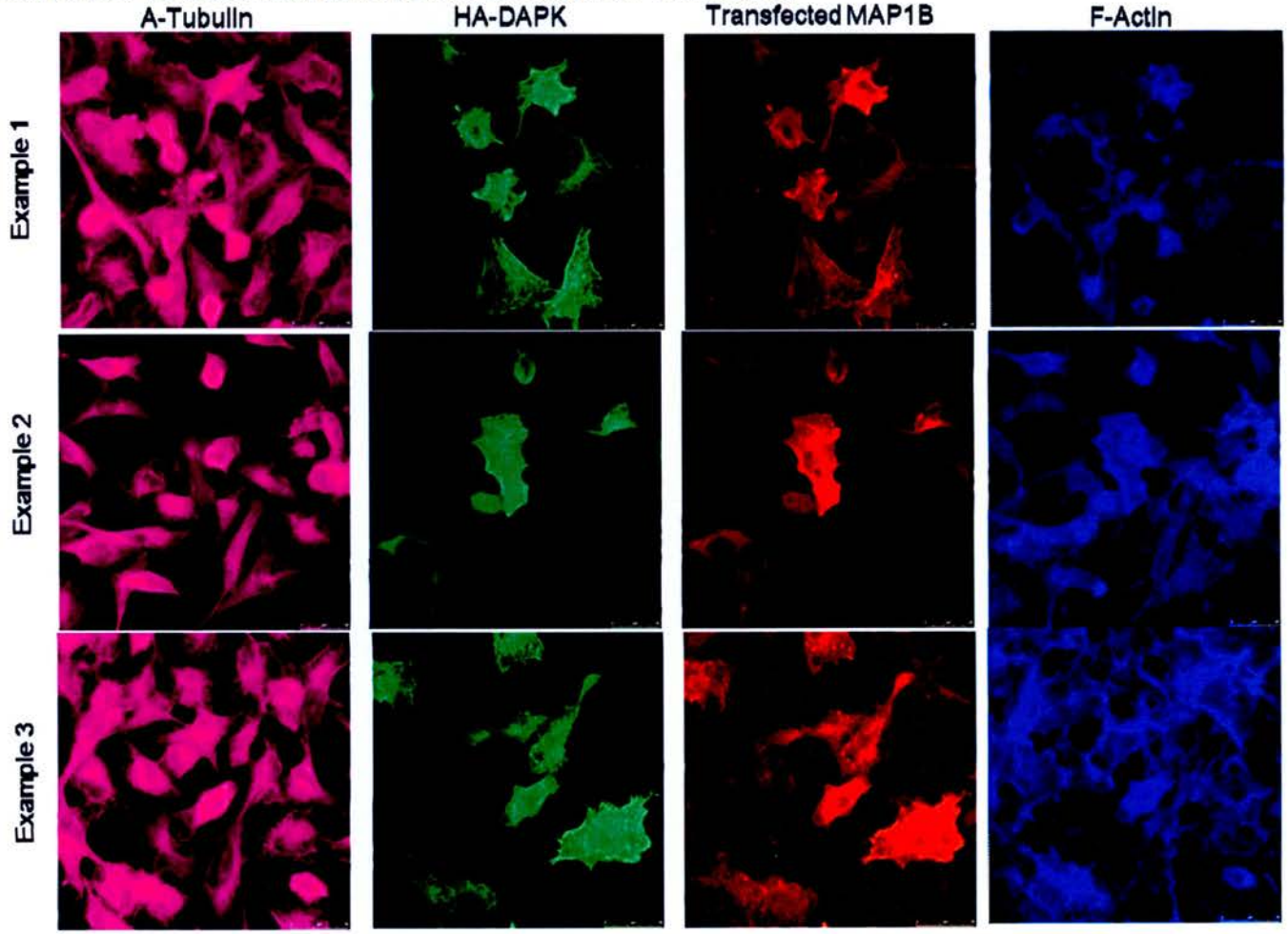

Figure 4.16 C Co-Transfection of MAP1B and HA-DAPK A375 Cells: 32 Hours Post Transfection

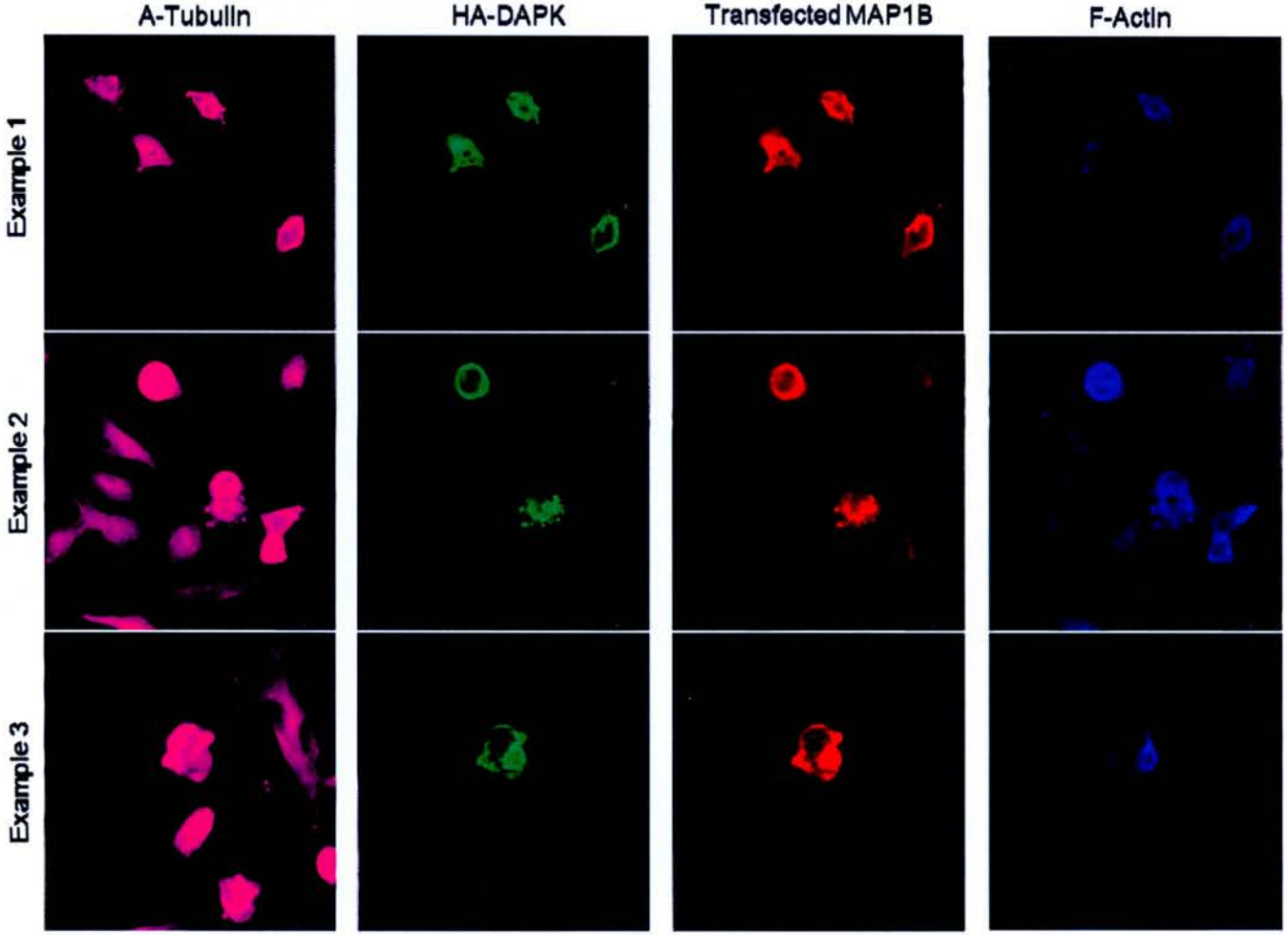

Figure 4.16 Co-Transfected MAP1B and DAPK Transiently Co-locate with Microtubules After 10 Hours. A375 cells were co-transfected with HA-DAPK and MAP1B for 10 hours **(a)**, 18 hours **(b)** and 32 hours **(c)** before fixing by partial cytosol extraction with 3% formaldehyde in PHEM buffer supplemented with 0.01% triton for 15. Cytoskeletons were then stained with rat anti-HA, mouse anti-MAP1B (AA6) and rabbit anti-tubulin antibodies followed by the appropriate highly cross-adsorbed alexa dye conjugated secondary antibodies. F-actin fibres were visualised using phalloidin counter-stain.

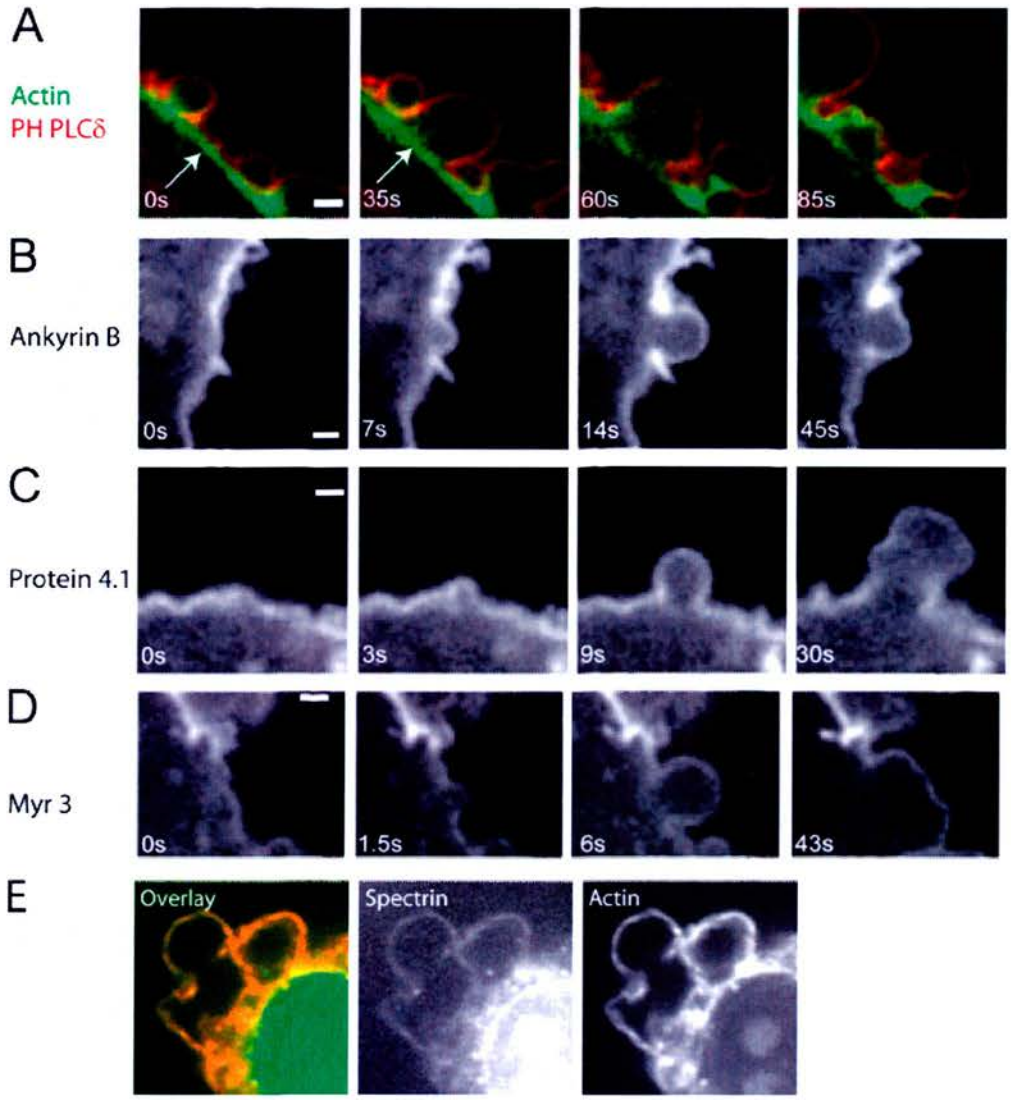

Figure 4.17 Dynamic Regulation of the Contractile Cortex Proteome During Plasma Membrane Blebbing. All images were acquired using confocal microscopy. Timing relative to the first image is indicated in white text. (A) Localization of the membrane marker (the PH domain of PLCδ, red) and actin (green) during bleb expansion and retraction. The actin cortex is intact during bleb expansion (arrows) and is disassembled at later time points. (B–D) Ankyrin B (B), protein 4.1 (C), and myosin I (myr3, D) localize to the cell membrane throughout the life of a bleb. (E) Spectrin (green) colocalizes with actin (red) in retracting blebs. Bars, 1 μm.

Figure is from: GT. Charras, CK Hu, M Coughlin and TJ Mitchison1 JCB (2007)

Chapter 5

Conclusion and Future Perspectives

DAPK is a tumour suppressor that plays a wide ranging role in the regulation of cell death. In order to understand the mechanisms of DAPK induced cell death more fully it was necessary to discover new interaction partners for DAPK protein. This objective has been accomplished, and three novel interactions are now proposed. Firstly: a novel interaction with MAP1B transcript variant 1, as uncovered by the phage display screen, secondly a novel interaction with the microtubule network, as suggested by in-vitro microtubule cycling and 2D gel analysis and substantiated by immunofluorescent co-localisation, and thirdly a novel interaction with the contractile cortex is proposed based on immunofluorescent studies. The physiological relevance of these interactions has been studied and a role for each during DAPK-induced cell growth inhibition is proposed (Figure 5.1).

The novel interaction with MAP1B occurs primarily via a short linear interaction motif (Figure 3.9 a and b) that is conserved through vertebrate species from drosophila (Figure 3.5). This is surprising given the rate of evolution of most interaction motifs that are less constrained throughout evolution. It is possible that this motif is present on other proteins and could direct interactions between them. Therefore it is proposed that further study should be undertaken to determine the frequency of this motif in the proteome using bioinformatics. In conjunction with further binding studies, this may then lead to discovery of other novel DAPK interactors.

Interaction with MAP1B was initiated by transfection of DAPK (Figure 3.9 c), whereas evidence suggests that a very small proportion of the two proteins interact in non-transfected cells (Figure 3.11 a), although high molecular weight complexes can be purified that contain both (figure 3.11 c). Therefore it is proposed that further study needs to be conducted to determine if a physiologically relevant stimulus can initiate complex formation, possibly starting with autophagy-inducing stimuli such as amino acid starvation.

The discovered DAPK association with microtubules provides a valuable insight into DAPK effects in cells. This interaction appears to be transient and correlates with disruption of microtubules (Figure 4.16) and with post-translational modification of the microtubule associated proteome (Figure 3.13). As such, it likely that DAPK effects microtubule dynamics either directly or though activation of MAP1B activity. Also, DAPK and MAP1B transiently co-locate at the microtubule organising center (MTOC) (Figure 4.16), the site of autophagosome production. This correlates with stimulation of autophagosome production (Figure 4.9 and 4.10) and it is proposed that this might require dynamic microtubules (see section 4.5.3). Therefore an interesting line of investigation would be to determine if DAPK effects the rate of microtubule formation using the in-vitro polymerization assay, and whether this influences the rate of autophagosome production. Thus determining one way or another, whether DAPK effects microtubule dynamics to increase autophagosome production. This is an attractive possibility because MAP1B interacts strongly with LC3 (see section 4.5.3). And so further investigation is also warranted to determine if DAPK effects this interaction and how this impacts on autophagosome production and autophagic cell death.

MAP1B and DAPK co-locate to the contractile cortex after DAPK transfection (Figure 4.15). Given that cell membrane blebbing is highly regulated and involves transient changes in the cytoskeletal-associated proteome (Figure 4.17), this indicates that MAP1B and DAPK play a direct role in the mechanics of membrane blebbing. This, in addition to DAPK sharing a high degree of homology with the MLCK kinase domain, a known bleb-inducer, suggests that DAPK catalytic activity towards MLC could be positively regulated by MAP1B. Therefore examination of the phosphorylation status of MLC at Ser19 would help to reveal the mechanism of action of DAPK and MAP1B co-induced blebbing (see section 4.3.5.1).

Finally, the wider physiological relevance of DAPK and MAP1B co-induced autophagic cell death needs to be investigated. It is proposed that migration of cancer cells can be regulated by local availability of nutrients in the cells microenvironment (see section 4.4). It is proposed that this may regulate rates of metastasis (see section 4.3.6), and also of angiogenesis when tumours require access to metabolic substrates. Therefore because firstly, DAPK and MAP1B have known roles in the regulation of cell migration (see sections 4.1.7 and 4.3.6) and secondly that both proteins influence cell survival, it is proposed that they operate in synergy to regulate the rate of possible nutrient-dependent migration by initiating autophagic cell death in response to tumour growth and/or during development when cells are surplus to requirement.

Also, following from this, it could be speculated that nutrient availability may be a key regulator of developmental processes in addition to apoptosis. Type II cell death being a more ancient form of programmed cell death may crudely regulate development and be highly dependent on nutrient availability or levels of tropic

support. Apoptosis on the other hand, having evolved more recently is activated by a much wider range of stimuli, and would exert a more controllable regulation on development. Ultimateley, development and proliferation would be a regulated by a mixture of the both.

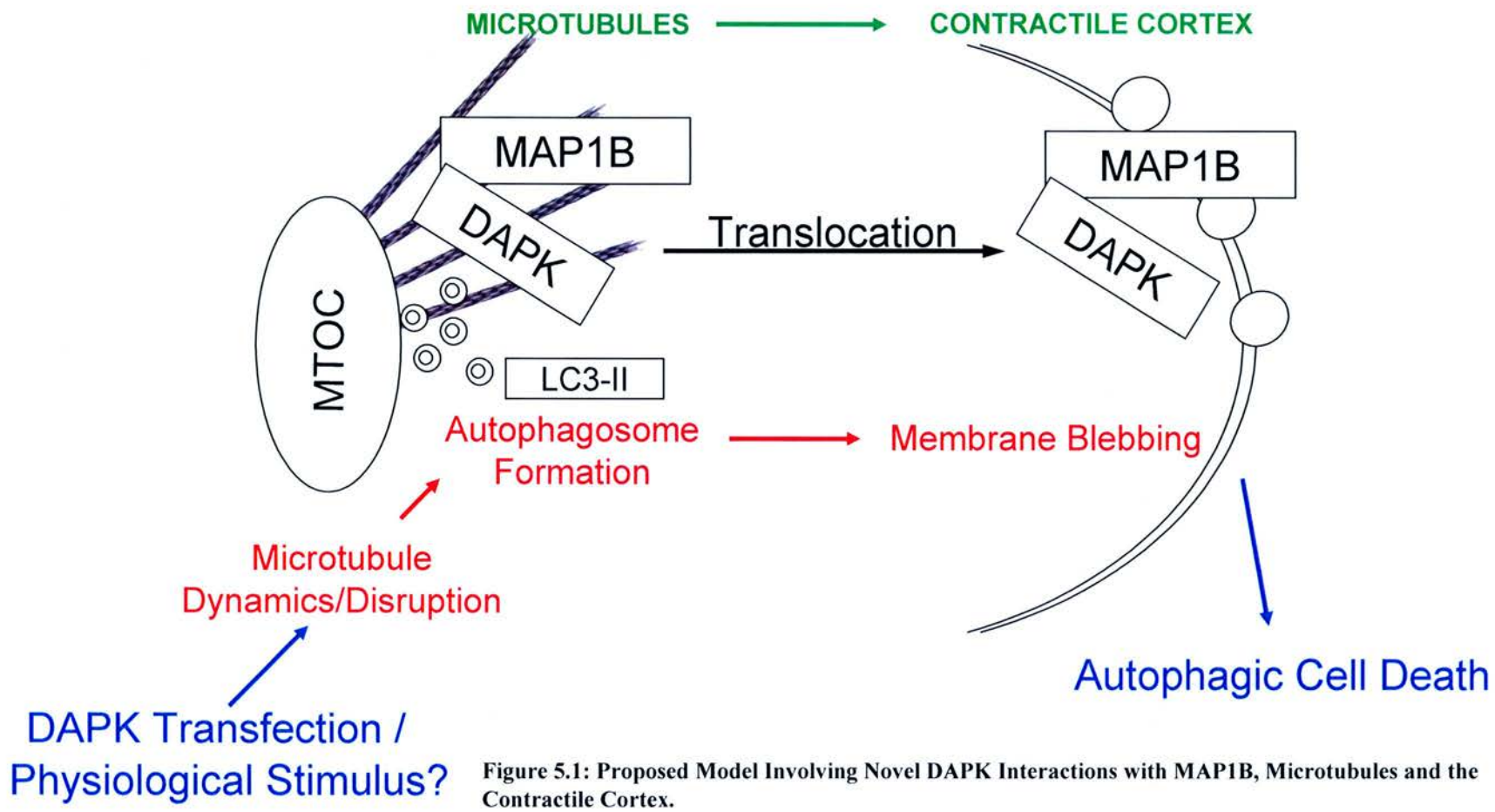

Figure 5.1: Proposed Model Involving Novel DAPK Interactions with MAP1B, Microtubules and the Contractile Cortex.

Acknowledgments

Dr Lindsay Burch (University of Edinburgh, Cell Signalling Unit), performed the phage display screen.

The ion exchange experiments including cell culture, lysis and preparation were performed by Dr Jenny Fraser (University of Edinburgh, Cell Signalling Unit).

Gel filtration experiments were jointly performed by Dr T. Hupp (University of Edinburgh, Cell Signalling Unit) and myself.

DIGE analysis was conduced by Dr R. Burchmore (Functional Genomics Department, Glasgow University).

Cell cycle analysis experiments were jointly performed by Dr Kay Samuel (University of Edinburgh, John Hughes-Bennett Laboritories) and myself.

The TUNEL assays were performed by Dr C. Stevens University of Edinburgh, Cell Signalling Unit).

References

Allen, E., Ding, J., Wang, W., Pramanik, S., Chou, J., Yau, V., and Yang, Y. (2005). Gigaxonin-controlled degradation of MAP1B light chain is critical to neuronal survival. Nature *438*, 224-228.

Amano, M., Ito, M., Kimura, K., Fukata, Y., Chihara, K., Nakano, T., Matsuura, Y., and Kaibuchi, K. (1996). Phosphorylation and activation of myosin by Rho-associated kinase (Rho-kinase). J Biol Chem *271*, 20246-20249.

Anglade, P., Vyas, S., Javoy-Agid, F., Herrero, M. T., Michel, P. P., Marquez, J., Mouatt-Prigent, A., Ruberg, M., Hirsch, E. C., and Agid, Y. (1997). Apoptosis and autophagy in nigral neurons of patients with Parkinson's disease. Histol Histopathol *12*, 25-31.

Anjum, R., Roux, P. P., Ballif, B. A., Gygi, S. P., and Blenis, J. (2005). The tumor suppressor DAP kinase is a target of RSK-mediated survival signaling. Curr Biol *15*, 1762-1767.

Avantaggiati, M. L., Ogryzko, V., Gardner, K., Giordano, A., Levine, A. S., and Kelly, K. (1997). Recruitment of p300/CBP in p53-dependent signal pathways. Cell *89*, 1175-1184.

Baker, S. J., and Reddy, E. P. (1998). Modulation of life and death by the TNF receptor superfamily. Oncogene *17*, 3261-3270.

Barlev, N. A., Liu, L., Chehab, N. H., Mansfield, K., Harris, K. G., Halazonetis, T. D., and Berger, S. L. (2001). Acetylation of p53 activates transcription through recruitment of coactivators/histone acetyltransferases. Mol Cell *8*, 1243-1254.

Baron, D. M., Kabututu, Z. P., and Hill, K. L. (2007). Stuck in reverse: loss of LC1 in Trypanosoma brucei disrupts outer dynein arms and leads to reverse flagellar beat and backward movement. J Cell Sci *120*, 1513-1520.

Bateman, A., Birney, E., Cerruti, L., Durbin, R., Etwiller, L., Eddy, S. R., Griffiths-Jones, S., Howe, K. L., Marshall, M., and Sonnhammer, E. L. (2002). The Pfam protein families database. Nucleic Acids Res *30*, 276-280.

Baud, V., and Karin, M. (2001). Signal transduction by tumor necrosis factor and its relatives. Trends Cell Biol *11*, 372-377.

Bernet, A., and Mehlen, P. (2007). Dependence receptors: when apoptosis controls tumor progression. Bull Cancer *94*, E12-17.

Bialik, S., Bresnick, A. R., and Kimchi, A. (2004). DAP-kinase-mediated morphological changes are localization dependent and involve myosin-II phosphorylation. Cell Death Differ *11*, 631-644.

Bialik, S., and Kimchi, A. (2006). The death-associated protein kinases: structure, function, and beyond. Annu Rev Biochem *75*, 189-210.

Bogarad, L. D., and Deem, M. W. (1999). A hierarchical approach to protein molecular evolution. Proc Natl Acad Sci U S A *96*, 2591-2595.

Borner, C., and Monney, L. (1999). Apoptosis without caspases: an inefficient molecular guillotine? Cell Death Differ *6*, 497-507.

Borner, C., Monney, L., Olivier, R., Rosse, T., Hacki, J., and Conus, S. (1999). Life and death in a medieval atmosphere. Cell Death Differ *6*, 201-206.

Bouquet, C., Soares, S., von Boxberg, Y., Ravaille-Veron, M., Propst, F., and Nothias, F. (2004). Microtubule-associated protein 1B controls directionality of growth cone migration and axonal branching in regeneration of adult dorsal root ganglia neurons. J Neurosci *24*, 7204-7213.

Brakensiek, K., Langer, F., Kreipe, H., and Lehmann, U. (2004). Low level of DAP-kinase DNA methylation in myelodysplastic syndrome. Blood *104*, 1586-1587; author reply 1587-1588.

Brugg, B., and Matus, A. (1988). PC12 cells express juvenile microtubule-associated proteins during nerve growth factor-induced neurite outgrowth. J Cell Biol *107*, 643-650.

Burch, L., Shimizu, H., Smith, A., Patterson, C., and Hupp, T. R. (2004a). Expansion of protein interaction maps by phage peptide display using MDM2 as a prototypical conformationally flexible target protein. J Mol Biol *337*, 129-145.

Burch, L. R., Scott, M., Pohler, E., Meek, D., and Hupp, T. (2004b). Phage-peptide display identifies the interferon-responsive, death-activated protein kinase family as a novel modifier of MDM2 and p21WAF1. J Mol Biol *337*, 115-128.

Bursch, W. (2004). Multiple cell death programs: Charon's lifts to Hades. FEMS Yeast Res *5*, 101-110.

Carragher, N. O., and Frame, M. C. (2004). Focal adhesion and actin dynamics: a place where kinases and proteases meet to promote invasion. Trends Cell Biol *14*, 241-249.

Cataldo, A. M., Hamilton, D. J., and Nixon, R. A. (1994). Lysosomal abnormalities in degenerating neurons link neuronal compromise to senile plaque development in Alzheimer disease. Brain Res *640*, 68-80.

Chang, L., Jones, Y., Ellisman, M. H., Goldstein, L. S., and Karin, M. (2003). JNK1 is required for maintenance of neuronal microtubules and controls phosphorylation of microtubule-associated proteins. Dev Cell *4*, 521-533.

Charras, G. T., Hu, C. K., Coughlin, M., and Mitchison, T. J. (2006). Reassembly of contractile actin cortex in cell blebs. J Cell Biol *175*, 477-490.

Chen, C. H., Wang, W. J., Kuo, J. C., Tsai, H. C., Lin, J. R., Chang, Z. F., and Chen, R. H. (2005). Bidirectional signals transduced by DAPK-ERK interaction promote the apoptotic effect of DAPK. Embo J *24*, 294-304.

Chevalier, R. L. (2006). Pathogenesis of renal injury in obstructive uropathy. Curr Opin Pediatr *18*, 153-160.

Clarke, P. G. (1990). Developmental cell death: morphological diversity and multiple mechanisms. Anat Embryol (Berl) *181*, 195-213.

Cohen, O., Feinstein, E., and Kimchi, A. (1997). DAP-kinase is a Ca2+/calmodulin-dependent, cytoskeletal-associated protein kinase, with cell death-inducing functions that depend on its catalytic activity. Embo J *16*, 998-1008.

Cohen, O., Inbal, B., Kissil, J. L., Raveh, T., Berissi, H., Spivak-Kroizaman, T., Feinstein, E., and Kimchi, A. (1999). DAP-kinase participates in TNF-alpha- and Fas-induced apoptosis and its function requires the death domain. J Cell Biol *146*, 141-148.

Cohen, O., and Kimchi, A. (2001). DAP-kinase: from functional gene cloning to establishment of its role in apoptosis and cancer. Cell Death Differ *8*, 6-15.

Coleman, M. L., Sahai, E. A., Yeo, M., Bosch, M., Dewar, A., and Olson, M. F. (2001). Membrane blebbing during apoptosis results from caspase-mediated activation of ROCK I. Nat Cell Biol *3*, 339-345.

Condeelis, J., Singer, R. H., and Segall, J. E. (2005). The great escape: when cancer cells hijack the genes for chemotaxis and motility. Annu Rev Cell Dev Biol *21*, 695-718.

Craig, A., Scott, M., Burch, L., Smith, G., Ball, K., and Hupp, T. (2003). Allosteric effects mediate CHK2 phosphorylation of the p53 transactivation domain. EMBO Rep *4*, 787-792.

Craig, A. L., Blaydes, J. P., Burch, L. R., Thompson, A. M., and Hupp, T. R. (1999a). Dephosphorylation of p53 at Ser20 after cellular exposure to low levels of non-ionizing radiation. Oncogene *18*, 6305-6312.

Craig, A. L., Burch, L., Vojtesek, B., Mikutowska, J., Thompson, A., and Hupp, T. R. (1999b). Novel phosphorylation sites of human tumour suppressor protein p53 at Ser20 and Thr18 that disrupt the binding of mdm2 (mouse double minute 2) protein are modified in human cancers. Biochem J *342 (Pt 1)*, 133-141.

Craig, A. L., Chrystal, J. A., Fraser, J. A., Sphyris, N., Lin, Y., Harrison, B. J., Scott, M. T., Dornreiter, I., and Hupp, T. R. (2007). The MDM2 ubiquitination signal in the DNA-binding domain of p53 forms a docking site for calcium calmodulin kinase superfamily members. Mol Cell Biol *27*, 3542-3555.

Cunningham, C. C. (1995). Actin polymerization and intracellular solvent flow in cell surface blebbing. J Cell Biol *129*, 1589-1599.

Dallol, A., Agathanggelou, A., Fenton, S. L., Ahmed-Choudhury, J., Hesson, L., Vos, M. D., Clark, G. J., Downward, J., Maher, E. R., and Latif, F. (2004). RASSF1A interacts with microtubule-associated proteins and modulates microtubule dynamics. Cancer Res *64*, 4112-4116.

Dawson, R., Muller, L., Dehner, A., Klein, C., Kessler, H., and Buchner, J. (2003). The N-terminal domain of p53 is natively unfolded. J Mol Biol *332*, 1131-1141.

DB, C. Q., da Silva, A. M., Gutierrez-Ospina, G., Porto, C. S., Grossman, G., Petrusz, P., and Avellar, M. C. (2006). Cells positive for microtubule-associated protein 1B (MAP 1B) are present along rat and human efferent ductules and epididymis. Cell Tissue Res *325*, 125-133.

de Castro, F. (2003). Chemotropic molecules: guides for axonal pathfinding and cell migration during CNS development. News Physiol Sci *18*, 130-136.

de Castro, F., and Bribian, A. (2005). The molecular orchestra of the migration of oligodendrocyte precursors during development. Brain Res Brain Res Rev *49*, 227-241.

de Castro Soubriet, F. (2001). [Chemotropic molecules as a mechanism for the orientation of axon growth and nerve migration during the development of the nervous system of mammals]. Rev Neurol *33*, 54-68.

Deiss, L. P., Feinstein, E., Berissi, H., Cohen, O., and Kimchi, A. (1995). Identification of a novel serine/threonine kinase and a novel 15-kD protein as potential mediators of the gamma interferon-induced cell death. Genes Dev *9*, 15-30.

Del Rio, J. A., Gonzalez-Billault, C., Urena, J. M., Jimenez, E. M., Barallobre, M. J., Pascual, M., Pujadas, L., Simo, S., La Torre, A., Wandosell, F., *et al.* (2004). MAP1B is required for Netrin 1 signaling in neuronal migration and axonal guidance. Curr Biol *14*, 840-850.

Dornan, D., Eckert, M., Wallace, M., Shimizu, H., Ramsay, E., Hupp, T. R., and Ball, K. L. (2004). Interferon regulatory factor 1 binding to p300 stimulates DNA-dependent acetylation of p53. Mol Cell Biol *24*, 10083-10098.

Dornan, D., and Hupp, T. R. (2001). Inhibition of p53-dependent transcription by BOX-I phospho-peptide mimetics that bind to p300. EMBO Rep *2*, 139-144.

Dornan, D., Shimizu, H., Burch, L., Smith, A. J., and Hupp, T. R. (2003a). The proline repeat domain of p53 binds directly to the transcriptional coactivator p300 and allosterically controls DNA-dependent acetylation of p53. Mol Cell Biol *23*, 8846-8861.

Dornan, D., Shimizu, H., Perkins, N. D., and Hupp, T. R. (2003b). DNA-dependent acetylation of p53 by the transcription coactivator p300. J Biol Chem *278*, 13431-13441.

Dyson, H. J., and Wright, P. E. (2005). Intrinsically unstructured proteins and their functions. Nat Rev Mol Cell Biol *6*, 197-208.

Edelman, G. M. (1993). Neural Darwinism: selection and reentrant signaling in higher brain function. Neuron *10*, 115-125.

Espinosa, J. M., and Emerson, B. M. (2001). Transcriptional regulation by p53 through intrinsic DNA/chromatin binding and site-directed cofactor recruitment. Mol Cell *8*, 57-69.

Fass, E., Amar, N., and Elazar, Z. (2007). Identification of essential residues for the C-terminal cleavage of the mammalian LC3: a lesson from yeast Atg8. Autophagy *3*, 48-50.

Fass, E., Shvets, E., Degani, I., Hirschberg, K., and Elazar, Z. (2006). Microtubules support production of starvation-induced autophagosomes but not their targeting and fusion with lysosomes. J Biol Chem *281*, 36303-36316.

Feinstein, E., Druck, T., Kastury, K., Berissi, H., Goodart, S. A., Overhauser, J., Kimchi, A., and Huebner, K. (1995a). Assignment of DAP1 and DAPK--genes that positively mediate programmed cell death triggered by IFN-gamma--to chromosome regions 5p12.2 and 9q34.1, respectively. Genomics *29*, 305-307.

Feinstein, E., Kimchi, A., Wallach, D., Boldin, M., and Varfolomeev, E. (1995b). The death domain: a module shared by proteins with diverse cellular functions. Trends Biochem Sci *20*, 342-344.

Foucher, I., Montesinos, M. L., Volovitch, M., Prochiantz, A., and Trembleau, A. (2003). Joint regulation of the MAP1B promoter by HNF3beta/Foxa2 and Engrailed is the result of a highly conserved mechanism for direct interaction of homeoproteins and Fox transcription factors. Development *130*, 1867-1876.

Fraser, J. A., and Hupp, T. R. (2007). Chemical genetics approach to identify peptide ligands that selectively stimulate DAPK-1 kinase activity. Biochemistry *46*, 2655-2673.

Frisch, S. M., and Ruoslahti, E. (1997). Integrins and anoikis. Curr Opin Cell Biol *9*, 701-706.

Frisch, S. M., and Screaton, R. A. (2001). Anoikis mechanisms. Curr Opin Cell Biol *13*, 555-562.

Gonzalez-Billault, C., Del Rio, J. A., Urena, J. M., Jimenez-Mateos, E. M., Barallobre, M. J., Pascual, M., Pujadas, L., Simo, S., Torre, A. L., Gavin, R., *et al.* (2005). A role of MAP1B in Reelin-dependent neuronal migration. Cereb Cortex *15*, 1134-1145.

Gonzalez-Gomez, P., Bello, M. J., Alonso, M. E., Lomas, J., Arjona, D., Aminoso, C., De Campos, J. M., Isla, A., Gutierrez, M., and Rey, J. A. (2003). Frequent death-

associated protein-kinase promoter hypermethylation in brain metastases of solid tumors. Oncol Rep *10*, 1031-1033.

Good, P. F., Alapat, D., Hsu, A., Chu, C., Perl, D., Wen, X., Burstein, D. E., and Kohtz, D. S. (2004). A role for semaphorin 3A signaling in the degeneration of hippocampal neurons during Alzheimer's disease. J Neurochem *91*, 716-736.

Goold, R. G., and Gordon-Weeks, P. R. (2001). Microtubule-associated protein 1B phosphorylation by glycogen synthase kinase 3beta is induced during PC12 cell differentiation. J Cell Sci *114*, 4273-4284.

Goold, R. G., and Gordon-Weeks, P. R. (2003). NGF activates the phosphorylation of MAP1B by GSK3beta through the TrkA receptor and not the p75(NTR) receptor. J Neurochem *87*, 935-946.

Goold, R. G., and Gordon-Weeks, P. R. (2005). The MAP kinase pathway is upstream of the activation of GSK3beta that enables it to phosphorylate MAP1B and contributes to the stimulation of axon growth. Mol Cell Neurosci *28*, 524-534.

Goold, R. G., Owen, R., and Gordon-Weeks, P. R. (1999). Glycogen synthase kinase 3beta phosphorylation of microtubule-associated protein 1B regulates the stability of microtubules in growth cones. J Cell Sci *112 (Pt 19)*, 3373-3384.

Gozuacik, D., and Kimchi, A. (2004). Autophagy as a cell death and tumor suppressor mechanism. Oncogene *23*, 2891-2906.

Gozuacik, D., and Kimchi, A. (2006). DAPk protein family and cancer. Autophagy *2*, 74-79.

Guo, W., Pylayeva, Y., Pepe, A., Yoshioka, T., Muller, W. J., Inghirami, G., and Giancotti, F. G. (2006). Beta 4 integrin amplifies ErbB2 signaling to promote mammary tumorigenesis. Cell *126*, 489-502.

Gupta, S., Barrett, T., Whitmarsh, A. J., Cavanagh, J., Sluss, H. K., Derijard, B., and Davis, R. J. (1996). Selective interaction of JNK protein kinase isoforms with transcription factors. Embo J *15*, 2760-2770.

Gutjahr, M. C., Rossy, J., and Niggli, V. (2005). Role of Rho, Rac, and Rho-kinase in phosphorylation of myosin light chain, development of polarity, and spontaneous migration of Walker 256 carcinosarcoma cells. Exp Cell Res *308*, 422-438.

Hahn, C. M., Kleinholz, H., Koester, M. P., Grieser, S., Thelen, K., and Pollerberg, G. E. (2005). Role of cyclin-dependent kinase 5 and its activator P35 in local axon and growth cone stabilization. Neuroscience *134*, 449-465.

Halpain, S., and Dehmelt, L. (2006). The MAP1 family of microtubule-associated proteins. Genome Biol *7*, 224.

Henshall, D. C., Araki, T., Schindler, C. K., Shinoda, S., Lan, J. Q., and Simon, R. P. (2003). Expression of death-associated protein kinase and recruitment to the tumor

necrosis factor signaling pathway following brief seizures. J Neurochem *86*, 1260-1270.

Henshall, D. C., Schindler, C. K., So, N. K., Lan, J. Q., Meller, R., and Simon, R. P. (2004). Death-associated protein kinase expression in human temporal lobe epilepsy. Ann Neurol *55*, 485-494.

Hoogervorst, E. M., de Vries, A., Beems, R. B., van Oostrom, C. T., Wester, P. W., Vos, J. G., Bruins, W., Roodbergen, M., Cassee, F. R., Vijg, J., *et al.* (2003). Combined oral benzo[a]pyrene and inhalatory ozone exposure have no effect on lung tumor development in DNA repair-deficient Xpa mice. Carcinogenesis *24*, 613-619.

Inbal, B., Bialik, S., Sabanay, I., Shani, G., and Kimchi, A. (2002). DAP kinase and DRP-1 mediate membrane blebbing and the formation of autophagic vesicles during programmed cell death. J Cell Biol *157*, 455-468.

Inbal, B., Cohen, O., Polak-Charcon, S., Kopolovic, J., Vadai, E., Eisenbach, L., and Kimchi, A. (1997). DAP kinase links the control of apoptosis to metastasis. Nature *390*, 180-184.

Ito, S., Koshikawa, N., Mochizuki, S., and Takenaga, K. (2007). 3-Methyladenine suppresses cell migration and invasion of HT1080 fibrosarcoma cells through inhibiting phosphoinositide 3-kinases independently of autophagy inhibition. Int J Oncol *31*, 261-268.

Jang, C. W., Chen, C. H., Chen, C. C., Chen, J. Y., Su, Y. H., and Chen, R. H. (2002). TGF-beta induces apoptosis through Smad-mediated expression of DAP-kinase. Nat Cell Biol *4*, 51-58.

Jin, Y., Blue, E. K., Dixon, S., Hou, L., Wysolmerski, R. B., and Gallagher, P. J. (2001). Identification of a new form of death-associated protein kinase that promotes cell survival. J Biol Chem *276*, 39667-39678.

Jin, Y., Blue, E. K., Dixon, S., Shao, Z., and Gallagher, P. J. (2002). A death-associated protein kinase (DAPK)-interacting protein, DIP-1, is an E3 ubiquitin ligase that promotes tumor necrosis factor-induced apoptosis and regulates the cellular levels of DAPK. J Biol Chem *277*, 46980-46986.

Jin, Y., Blue, E. K., and Gallagher, P. J. (2006). Control of death-associated protein kinase (DAPK) activity by phosphorylation and proteasomal degradation. J Biol Chem *281*, 39033-39040.

Jin, Y., and Gallagher, P. J. (2003). Antisense depletion of death-associated protein kinase promotes apoptosis. J Biol Chem *278*, 51587-51593.

Kabeya, Y., Mizushima, N., Ueno, T., Yamamoto, A., Kirisako, T., Noda, T., Kominami, E., Ohsumi, Y., and Yoshimori, T. (2000). LC3, a mammalian homologue of yeast Apg8p, is localized in autophagosome membranes after processing. Embo J *19*, 5720-5728.

Katzenellenbogen, R. A., Baylin, S. B., and Herman, J. G. (1999). Hypermethylation of the DAP-kinase CpG island is a common alteration in B-cell malignancies. Blood *93*, 4347-4353.

Kawai, T., Akira, S., and Reed, J. C. (2003). ZIP kinase triggers apoptosis from nuclear PML oncogenic domains. Mol Cell Biol *23*, 6174-6186.

Kawai, T., Matsumoto, M., Takeda, K., Sanjo, H., and Akira, S. (1998). ZIP kinase, a novel serine/threonine kinase which mediates apoptosis. Mol Cell Biol *18*, 1642-1651.

Kawai, T., Sanjo, H., and Akira, S. (1999). Duet is a novel serine/threonine kinase with Dbl-Homology (DH) and Pleckstrin-Homology (PH) domains. Gene *227*, 249-255.

Kawauchi, T., Chihama, K., Nabeshima, Y., and Hoshino, M. (2003). The in vivo roles of STEF/Tiam1, Rac1 and JNK in cortical neuronal migration. Embo J *22*, 4190-4201.

Kawauchi, T., Chihama, K., Nishimura, Y. V., Nabeshima, Y., and Hoshino, M. (2005). MAP1B phosphorylation is differentially regulated by Cdk5/p35, Cdk5/p25, and JNK. Biochem Biophys Res Commun *331*, 50-55.

Kerr, J. F., Wyllie, A. H., and Currie, A. R. (1972). Apoptosis: a basic biological phenomenon with wide-ranging implications in tissue kinetics. Br J Cancer *26*, 239-257.

Kochl, R., Hu, X. W., Chan, E. Y., and Tooze, S. A. (2006). Microtubules facilitate autophagosome formation and fusion of autophagosomes with endosomes. Traffic *7*, 129-145.

Kolodney, M. S., and Elson, E. L. (1995). Contraction due to microtubule disruption is associated with increased phosphorylation of myosin regulatory light chain. Proc Natl Acad Sci U S A *92*, 10252-10256.

Kuo, J. C., Lin, J. R., Staddon, J. M., Hosoya, H., and Chen, R. H. (2003). Uncoordinated regulation of stress fibers and focal adhesions by DAP kinase. J Cell Sci *116*, 4777-4790.

Kuo, J. C., Wang, W. J., Yao, C. C., Wu, P. R., and Chen, R. H. (2006). The tumor suppressor DAPK inhibits cell motility by blocking the integrin-mediated polarity pathway. J Cell Biol *172*, 619-631.

Kutschera, W., Zauner, W., Wiche, G., and Propst, F. (1998). The mouse and rat MAP1B genes: genomic organization and alternative transcription. Genomics *49*, 430-436.

Lander, E. S., Linton, L. M., Birren, B., Nusbaum, C., Zody, M. C., Baldwin, J., Devon, K., Dewar, K., Doyle, M., FitzHugh, W., *et al.* (2001). Initial sequencing and analysis of the human genome. Nature *409*, 860-921.

Laster, S. M., and Mackenzie, J. M., Jr. (1996). Bleb formation and F-actin distribution during mitosis and tumor necrosis factor-induced apoptosis. Microsc Res Tech *34*, 272-280.

Lee, S. Y., Kim, Y. T., Lee, M. S., Kim, Y. B., Chung, E., Kim, S., and Lee, J. W. (2006). Focal adhesion and actin organization by a cross-talk of TM4SF5 with integrin alpha2 are regulated by serum treatment. Exp Cell Res *312*, 2983-2999.

Lerch-Gaggl, A. F., Sun, K., and Duncan, S. A. (2007). Light chain 1 of microtubule-associated protein 1B can negatively regulate the action of Pes1. J Biol Chem *282*, 11308-11316.

Levi-Montalcini, R. (1987). The nerve growth factor thirty-five years later. In Vitro Cell Dev Biol *23*, 227-238.

Levy-Strumpf, N., and Kimchi, A. (1998). Death associated proteins (DAPs): from gene identification to the analysis of their apoptotic and tumor suppressive functions. Oncogene *17*, 3331-3340.

Lien, L. L., Boyce, F. M., Kleyn, P., Brzustowicz, L. M., Menninger, J., Ward, D. C., Gilliam, T. C., and Kunkel, L. M. (1991). Mapping of human microtubule-associated protein 1B in proximity to the spinal muscular atrophy locus at 5q13. Proc Natl Acad Sci U S A *88*, 7873-7876.

Lin, Y., Stevens, C., and Hupp, T. (2007). Identification of a dominant negative functional domain on DAPK-1 that degrades DAPK-1 protein and stimulates TNFR-1-mediated apoptosis. J Biol Chem *282*, 16792-16802.

Liu, D., and Fischer, I. (1996). Two alternative promoters direct neuron-specific expression of the rat microtubule-associated protein 1B gene. J Neurosci *16*, 5026-5036.

Liu, F. (2003). Receptor-regulated Smads in TGF-beta signaling. Front Biosci *8*, s1280-1303.

Liu, L., Vo, A., Liu, G., and McKeehan, W. L. (2005a). Distinct structural domains within C19ORF5 support association with stabilized microtubules and mitochondrial aggregation and genome destruction. Cancer Res *65*, 4191-4201.

Liu, L., Vo, A., Liu, G., and McKeehan, W. L. (2005b). Putative tumor suppressor RASSF1 interactive protein and cell death inducer C19ORF5 is a DNA binding protein. Biochem Biophys Res Commun *332*, 670-676.

Llambi, F., Lourenco, F. C., Gozuacik, D., Guix, C., Pays, L., Del Rio, G., Kimchi, A., and Mehlen, P. (2005). The dependence receptor UNC5H2 mediates apoptosis through DAP-kinase. Embo J *24*, 1192-1201.

Luo, L., and O'Leary, D. D. (2005). Axon retraction and degeneration in development and disease. Annu Rev Neurosci *28*, 127-156.

MacPherson, D., Kim, J., Kim, T., Rhee, B. K., Van Oostrom, C. T., DiTullio, R. A., Venere, M., Halazonetis, T. D., Bronson, R., De Vries, A., *et al.* (2004). Defective apoptosis and B-cell lymphomas in mice with p53 point mutation at Ser 23. Embo J *23*, 3689-3699.

Martoriati, A., Doumont, G., Alcalay, M., Bellefroid, E., Pelicci, P. G., and Marine, J. C. (2005). dapk1, encoding an activator of a p19ARF-p53-mediated apoptotic checkpoint, is a transcription target of p53. Oncogene *24*, 1461-1466.

Maulik, G., Kijima, T., Ma, P. C., Ghosh, S. K., Lin, J., Shapiro, G. I., Schaefer, E., Tibaldi, E., Johnson, B. E., and Salgia, R. (2002). Modulation of the c-Met/hepatocyte growth factor pathway in small cell lung cancer. Clin Cancer Res *8*, 620-627.

McEntyre, J. R., and Gibson, T. J. (2004). Patterns and clusters within the PSM column in TiBS, 1992-2004. Trends Biochem Sci *29*, 627-633.

Mills, J. C., Stone, N. L., Erhardt, J., and Pittman, R. N. (1998). Apoptotic membrane blebbing is regulated by myosin light chain phosphorylation. J Cell Biol *140*, 627-636.

Mills, K. R., Reginato, M., Debnath, J., Queenan, B., and Brugge, J. S. (2004). Tumor necrosis factor-related apoptosis-inducing ligand (TRAIL) is required for induction of autophagy during lumen formation in vitro. Proc Natl Acad Sci U S A *101*, 3438-3443.

Moretti, L., Cha, Y. I., Niermann, K. J., and Lu, B. (2007). Switch between apoptosis and autophagy: radiation-induced endoplasmic reticulum stress? Cell Cycle *6*, 793-798.

Murata-Hori, M., Fukuta, Y., Ueda, K., Iwasaki, T., and Hosoya, H. (2001). HeLa ZIP kinase induces diphosphorylation of myosin II regulatory light chain and reorganization of actin filaments in nonmuscle cells. Oncogene *20*, 8175-8183.

Nakatsuka, S., Takakuwa, T., and Aozasa, K. (2001). [Hypermethylation of DAP-kinase gene CpG Island in malignant lymphoma with B-cell phenotype]. Rinsho Byori *49*, 1242-1247.

Nakatsuka, S., Takakuwa, T., Tomita, Y., Miwa, H., Matsuzuka, F., and Aozasa, K. (2000). Role of hypermethylation of DAP-kinase CpG island in the development of thyroid lymphoma. Lab Invest *80*, 1651-1655.

Neduva, V., and Russell, R. B. (2005). Linear motifs: evolutionary interaction switches. FEBS Lett *579*, 3342-3345.

Newbern, J., Taylor, A., Robinson, M., Lively, M. O., and Milligan, C. E. (2007). c-Jun N-terminal kinase signaling regulates events associated with both health and degeneration in motoneurons. Neuroscience *147*, 680-692.

Noble, M., Lewis, S. A., and Cowan, N. J. (1989). The microtubule binding domain of microtubule-associated protein MAP1B contains a repeated sequence motif unrelated to that of MAP2 and tau. J Cell Biol *109*, 3367-3376.

Paglin, S., Hollister, T., Delohery, T., Hackett, N., McMahill, M., Sphicas, E., Domingo, D., and Yahalom, J. (2001). A novel response of cancer cells to radiation involves autophagy and formation of acidic vesicles. Cancer Res *61*, 439-444.

Pelled, D., Raveh, T., Riebeling, C., Fridkin, M., Berissi, H., Futerman, A. H., and Kimchi, A. (2002). Death-associated protein (DAP) kinase plays a central role in ceramide-induced apoptosis in cultured hippocampal neurons. J Biol Chem *277*, 1957-1961.

Petrovski, G., Zahuczky, G., Katona, K., Vereb, G., Martinet, W., Nemes, Z., Bursch, W., and Fesus, L. (2007). Clearance of dying autophagic cells of different origin by professional and non-professional phagocytes. Cell Death Differ *14*, 1117-1128.

Popa-Wagner, A., Carmichael, S. T., Kokaia, Z., Kessler, C., and Walker, L. C. (2007). The response of the aged brain to stroke: too much, too soon? Curr Neurovasc Res *4*, 216-227.

Popa-Wagner, A., Fischer, B., Platt, D., Neubig, R., Schmoll, H., and Kessler, C. (1999a). Anomalous expression of microtubule-associated protein 1B in the hippocampus and cortex of aged rats treated with pentylenetetrazole. Neuroscience *94*, 395-403.

Popa-Wagner, A., Schroder, E., Schmoll, H., Walker, L. C., and Kessler, C. (1999b). Upregulation of MAP1B and MAP2 in the rat brain after middle cerebral artery occlusion: effect of age. J Cereb Blood Flow Metab *19*, 425-434.

Puntervoll, P., Linding, R., Gemund, C., Chabanis-Davidson, S., Mattingsdal, M., Cameron, S., Martin, D. M., Ausiello, G., Brannetti, B., Costantini, A., *et al.* (2003). ELM server: A new resource for investigating short functional sites in modular eukaryotic proteins. Nucleic Acids Res *31*, 3625-3630.

Qu, X., Zou, Z., Sun, Q., Luby-Phelps, K., Cheng, P., Hogan, R. N., Gilpin, C., and Levine, B. (2007). Autophagy gene-dependent clearance of apoptotic cells during embryonic development. Cell *128*, 931-946.

Rajashree, R., Blunt, B. C., and Hofmann, P. A. (2005). Modulation of myosin phosphatase targeting subunit and protein phosphatase 1 in the heart. Am J Physiol Heart Circ Physiol *289*, H1736-1743.

Raval, A., Tanner, S. M., Byrd, J. C., Angerman, E. B., Perko, J. D., Chen, S. S., Hackanson, B., Grever, M. R., Lucas, D. M., Matkovic, J. J., *et al.* (2007). Downregulation of death-associated protein kinase 1 (DAPK1) in chronic lymphocytic leukemia. Cell *129*, 879-890.

Raveh, T., Berissi, H., Eisenstein, M., Spivak, T., and Kimchi, A. (2000). A functional genetic screen identifies regions at the C-terminal tail and death-domain of death-associated protein kinase that are critical for its proapoptotic activity. Proc Natl Acad Sci U S A *97*, 1572-1577.

Raveh, T., Droguett, G., Horwitz, M. S., DePinho, R. A., and Kimchi, A. (2001). DAP kinase activates a p19ARF/p53-mediated apoptotic checkpoint to suppress oncogenic transformation. Nat Cell Biol *3*, 1-7.

Reed, J. C., Doctor, K. S., and Godzik, A. (2004). The domains of apoptosis: a genomics perspective. Sci STKE *2004*, re9.

Riechmann, L., and Winter, G. (2000). Novel folded protein domains generated by combinatorial shuffling of polypeptide segments. Proc Natl Acad Sci U S A *97*, 10068-10073.

Riederer, B., Cohen, R., and Matus, A. (1986). MAP5: a novel brain microtubule-associated protein under strong developmental regulation. J Neurocytol *15*, 763-775.

Riederer, B. M. (2007). Microtubule-associated protein 1B, a growth-associated and phosphorylated scaffold protein. Brain Res Bull *71*, 541-558.

Safaei, R., and Fischer, I. (1990). Turnover of cytoskeletal proteins in vivo. Brain Res *533*, 83-90.

Sanjo, H., Kawai, T., and Akira, S. (1998). DRAKs, novel serine/threonine kinases related to death-associated protein kinase that trigger apoptosis. J Biol Chem *273*, 29066-29071.

Schmoll, H., Badan, I., Fischer, B., and Wagner, A. P. (2001). Dynamics of gene expression for immediate early- and late genes after seizure activity in aged rats. Arch Gerontol Geriatr *32*, 199-218.

Schneider-Stock, R., Roessner, A., and Ullrich, O. (2005). DAP-kinase--protector or enemy in apoptotic cell death. Int J Biochem Cell Biol *37*, 1763-1767.

Schon, O., Friedler, A., Bycroft, M., Freund, S. M., and Fersht, A. R. (2002). Molecular mechanism of the interaction between MDM2 and p53. J Mol Biol *323*, 491-501.

Schumacher, A. M., Velentza, A. V., and Watterson, D. M. (2002a). Death-associated protein kinase as a potential therapeutic target. Expert Opin Ther Targets *6*, 497-506.

Schumacher, A. M., Velentza, A. V., Watterson, D. M., and Dresios, J. (2006). Death-associated protein kinase phosphorylates mammalian ribosomal protein S6 and reduces protein synthesis. Biochemistry *45*, 13614-13621.

Schumacher, A. M., Velentza, A. V., Watterson, D. M., and Wainwright, M. S. (2002b). DAPK catalytic activity in the hippocampus increases during the recovery

phase in an animal model of brain hypoxic-ischemic injury. Biochim Biophys Acta *1600*, 128-137.

Sebbagh, M., Hamelin, J., Bertoglio, J., Solary, E., and Breard, J. (2005). Direct cleavage of ROCK II by granzyme B induces target cell membrane blebbing in a caspase-independent manner. J Exp Med *201*, 465-471.

Sebbagh, M., Renvoize, C., Hamelin, J., Riche, N., Bertoglio, J., and Breard, J. (2001). Caspase-3-mediated cleavage of ROCK I induces MLC phosphorylation and apoptotic membrane blebbing. Nat Cell Biol *3*, 346-352.

Seglen, P. O., and Gordon, P. B. (1982). 3-Methyladenine: specific inhibitor of autophagic/lysosomal protein degradation in isolated rat hepatocytes. Proc Natl Acad Sci U S A *79*, 1889-1892.

Shani, G., Henis-Korenblit, S., Jona, G., Gileadi, O., Eisenstein, M., Ziv, T., Admon, A., and Kimchi, A. (2001). Autophosphorylation restrains the apoptotic activity of DRP-1 kinase by controlling dimerization and calmodulin binding. Embo J *20*, 1099-1113.

Shani, G., Marash, L., Gozuacik, D., Bialik, S., Teitelbaum, L., Shohat, G., and Kimchi, A. (2004). Death-associated protein kinase phosphorylates ZIP kinase, forming a unique kinase hierarchy to activate its cell death functions. Mol Cell Biol *24*, 8611-8626.

Sherr, C. J., and Weber, J. D. (2000). The ARF/p53 pathway. Curr Opin Genet Dev *10*, 94-99.

Shieh, S. Y., Ahn, J., Tamai, K., Taya, Y., and Prives, C. (2000). The human homologs of checkpoint kinases Chk1 and Cds1 (Chk2) phosphorylate p53 at multiple DNA damage-inducible sites. Genes Dev *14*, 289-300.

Shimizu, H., Burch, L. R., Smith, A. J., Dornan, D., Wallace, M., Ball, K. L., and Hupp, T. R. (2002). The conformationally flexible S9-S10 linker region in the core domain of p53 contains a novel MDM2 binding site whose mutation increases ubiquitination of p53 in vivo. J Biol Chem *277*, 28446-28458.

Shirvan, A., Ziv, I., Fleminger, G., Shina, R., He, Z., Brudo, I., Melamed, E., and Barzilai, A. (1999). Semaphorins as mediators of neuronal apoptosis. J Neurochem *73*, 961-971.

Shohat, G., Shani, G., Eisenstein, M., and Kimchi, A. (2002). The DAP-kinase family of proteins: study of a novel group of calcium-regulated death-promoting kinases. Biochim Biophys Acta *1600*, 45-50.

Stevens, C., Lin, Y., Sanchez, M., Amin, E., Copson, E., White, H., Durston, V., Eccles, D. M., and Hupp, T. (2007). A germ line mutation in the death domain of DAPK-1 inactivates ERK-induced apoptosis. J Biol Chem *282*, 13791-13803.

Suzuki, T., Nakagawa, M., Yoshikawa, A., Sasagawa, N., Yoshimori, T., Ohsumi, Y., Nishino, I., Ishiura, S., and Nonaka, I. (2002). The first molecular evidence that autophagy relates rimmed vacuole formation in chloroquine myopathy. J Biochem (Tokyo) *131*, 647-651.

Tanaka, Y., Kawahata, K., Nakata, T., and Hirokawa, N. (1992). Chronological expression of microtubule-associated proteins (MAPs) in EC cell P19 after neuronal induction by retinoic acid. Brain Res *596*, 269-278.

Tanida, I., Minematsu-Ikeguchi, N., Ueno, T., and Kominami, E. (2005). Lysosomal turnover, but not a cellular level, of endogenous LC3 is a marker for autophagy. Autophagy *1*, 84-91.

Tereshko, V., Teplova, M., Brunzelle, J., Watterson, D. M., and Egli, M. (2001). Crystal structures of the catalytic domain of human protein kinase associated with apoptosis and tumor suppression. Nat Struct Biol *8*, 899-907.

Tomasiewicz, H. G., and Wood, J. G. (1999). Characterization of microtubule-associated proteins in teleosts. Cell Motil Cytoskeleton *44*, 155-167.

Toulouse, G., Dehaene, S., and Changeux, J. P. (1986). Spin glass model of learning by selection. Proc Natl Acad Sci U S A *83*, 1695-1698.

Tucker, R. P. (1990). The roles of microtubule-associated proteins in brain morphogenesis: a review. Brain Res Brain Res Rev *15*, 101-120.

Tucker, R. P., Binder, L. I., and Matus, A. I. (1988). Neuronal microtubule-associated proteins in the embryonic avian spinal cord. J Comp Neurol *271*, 44-55.

Tucker, R. P., Garner, C. C., and Matus, A. (1989). In situ localization of microtubule-associated protein mRNA in the developing and adult rat brain. Neuron *2*, 1245-1256.

Tucker, R. P., and Matus, A. I. (1987). Developmental regulation of two microtubule-associated proteins (MAP2 and MAP5) in the embryonic avian retina. Development *101*, 535-546.

Tucker, R. P., and Matus, A. I. (1988). Microtubule-associated proteins characteristic of embryonic brain are found in the adult mammalian retina. Dev Biol *130*, 423-434.

Uchida, Y. (2003). Overexpression of full-length but not N-terminal truncated isoform of microtubule-associated protein (MAP) 1B accelerates apoptosis of cultured cortical neurons. J Biol Chem *278*, 366-371.

Velentza, A. V., Schumacher, A. M., Weiss, C., Egli, M., and Watterson, D. M. (2001). A protein kinase associated with apoptosis and tumor suppression: structure, activity, and discovery of peptide substrates. J Biol Chem *276*, 38956-38965.

Venter, J. C., Adams, M. D., Myers, E. W., Li, P. W., Mural, R. J., Sutton, G. G., Smith, H. O., Yandell, M., Evans, C. A., Holt, R. A., *et al.* (2001). The sequence of the human genome. Science *291*, 1304-1351.

Verhoef, P. A., Kertesy, S. B., Estacion, M., Schilling, W. P., and Dubyak, G. R. (2004). Maitotoxin induces biphasic interleukin-1beta secretion and membrane blebbing in murine macrophages. Mol Pharmacol *66*, 909-920.

Viereck, C., Tucker, R. P., and Matus, A. (1989). The adult rat olfactory system expresses microtubule-associated proteins found in the developing brain. J Neurosci *9*, 3547-3557.

Vouyiouklis, D. A., and Brophy, P. J. (1993). Microtubule-associated protein MAP1B expression precedes the morphological differentiation of oligodendrocytes. J Neurosci Res *35*, 257-267.

Wada, Y., Kitamoto, K., Kanbe, T., Tanaka, K., and Anraku, Y. (1990). The SLP1 gene of Saccharomyces cerevisiae is essential for vacuolar morphogenesis and function. Mol Cell Biol *10*, 2214-2223.

Waki, T., Tamura, G., Sato, M., Terashima, M., Nishizuka, S., and Motoyama, T. (2003). Promoter methylation status of DAP-kinase and RUNX3 genes in neoplastic and non-neoplastic gastric epithelia. Cancer Sci *94*, 360-364.

Walker, J. E., Saraste, M., Runswick, M. J., and Gay, N. J. (1982). Distantly related sequences in the alpha- and beta-subunits of ATP synthase, myosin, kinases and other ATP-requiring enzymes and a common nucleotide binding fold. Embo J *1*, 945-951.

Wang, Q. J., Ding, Y., Kohtz, D. S., Mizushima, N., Cristea, I. M., Rout, M. P., Chait, B. T., Zhong, Y., Heintz, N., and Yue, Z. (2006). Induction of autophagy in axonal dystrophy and degeneration. J Neurosci *26*, 8057-8068.

Wang, W. J., Kuo, J. C., Yao, C. C., and Chen, R. H. (2002). DAP-kinase induces apoptosis by suppressing integrin activity and disrupting matrix survival signals. J Cell Biol *159*, 169-179.

Warzocha, K., Bienvenu, J., Coiffier, B., and Salles, G. (1995). Mechanisms of action of the tumor necrosis factor and lymphotoxin ligand-receptor system. Eur Cytokine Netw *6*, 83-96.

Wyllie, A. H., Kerr, J. F., and Currie, A. R. (1980). Cell death: the significance of apoptosis. Int Rev Cytol *68*, 251-306.

Xu, Z. X., Liang, J., Haridas, V., Gaikwad, A., Connolly, F. P., Mills, G. B., and Gutterman, J. U. (2007). A plant triterpenoid, avicin D, induces autophagy by activation of AMP-activated protein kinase. Cell Death Differ.

Xue, L., Fletcher, G. C., and Tolkovsky, A. M. (1999). Autophagy is activated by apoptotic signalling in sympathetic neurons: an alternative mechanism of death execution. Mol Cell Neurosci *14*, 180-198.

Yamakawa, A., Ogata, H., Morita, K., Shibata, N., Andou, N., Sanuki, H., Yamada, K., Hioki, T., Ishii, T., and Higuchi, Y. (2004). Crystallization and preliminary X-ray analysis of two inhibitor complexes of the catalytic domain of death-associated protein kinase. Acta Crystallogr D Biol Crystallogr *60*, 764-766.

Yamamoto, M., Hioki, T., Ishii, T., Nakajima-Iijima, S., and Uchino, S. (2002). DAP kinase activity is critical for C(2)-ceramide-induced apoptosis in PC12 cells. Eur J Biochem *269*, 139-147.

Yamamoto, M., Takahashi, H., Nakamura, T., Hioki, T., Nagayama, S., Ooashi, N., Sun, X., Ishii, T., Kudo, Y., Nakajima-Iijima, S., *et al.* (1999). Developmental changes in distribution of death-associated protein kinase mRNAs. J Neurosci Res *58*, 674-683.

Yoshimori, T. (2007). Autophagy: paying Charon's toll. Cell *128*, 833-836.

Yukawa, K., Tanaka, T., Bai, T., Li, L., Tsubota, Y., Owada-Makabe, K., Maeda, M., Hoshino, K., Akira, S., and Iso, H. (2006). Deletion of the kinase domain from death-associated protein kinase enhances spatial memory in mice. Int J Mol Med *17*, 869-873.

Zaidi, A. U., McDonough, J. S., Klocke, B. J., Latham, C. B., Korsmeyer, S. J., Flavell, R. A., Schmidt, R. E., and Roth, K. A. (2001). Chloroquine-induced neuronal cell death is p53 and Bcl-2 family-dependent but caspase-independent. J Neuropathol Exp Neurol *60*, 937-945.

Zhang, L., Nephew, K. P., and Gallagher, P. J. (2007). Regulation of death-associated protein kinase. Stabilization by HSP90 heterocomplexes. J Biol Chem *282*, 11795-11804.